Fire Performance of Concrete Flat Slabs

Pasindu Thalpe Guruge

ORCID: 0000-0002-7288-690X

A thesis submitted in total fulfilment of the requirements for the degree of Doctor of Philosophy

Department of Infrastructure Engineering
Melbourne School of Engineering
The University of Melbourne

May 2020

Abstract

Concrete flat slabs are widely used, especially in multi-storey buildings, because of their resource efficiency and fast construction. The requirements for fire safety critically affect the overall design of these slabs. Fire design guidelines which are based on research carried out a few decades ago hinder the effective use of concrete flat slabs as they impose strict thickness and cover requirements. Since then, material properties of concrete have significantly changed, and construction methods have evolved considerably. Therefore, new research is needed to assess the fire performance of concrete flat slabs and provide a research base to improve the current fire safety design guidelines for concrete flat slabs.

Among the limited number of fire tests performed on concrete flat slabs, most of them were simply supported isolated specimens which did not take into account the continuity of the slab. Therefore, the author conducted a large-scale fire test on a laterally restrained flat slab specimen simulating the effect of adjacent slab panels in case of a fire. Recent studies emphasise the importance of capturing the behaviour during the cooling phase as there is a risk of failure also during that phase. Hence, the experiment was extended to measure the thermal and structural response during the cooling phase. Results indicate that the fire resistance level (FRL) of the restrained flat slab has been improved compared to the FRLs predicted by the design standards. The use of restrained support conditions which allows the development of membrane actions could be the reason for improved FRL.

Although fire tests provide vital information on the behaviour of flat slabs in fire, they are very expensive and time-consuming. As an alternative, numerical methods can be utilized to capture the effects of elevated temperatures on concrete flat slabs. Building upon the existing material models for concrete and steel at elevated temperatures, the author introduced the use of explicit coupled-temperature analysis technique in finite element software ABAQUS to determine the thermal and structural response of concrete flat slabs in fire. The models also account for the transient thermal creep of concrete when heated and change of material properties during the cooling

phase. The developed models were validated with the experimental results from the fire test carried out by the author, along with two more independent fire tests.

A validated numerical modelling technique was then employed in a parametric study to evaluate the influence of the thickness, the span between columns and the reinforcement arrangement on the FRL of concrete flat slabs. The aim of the study was to further understand the new design rules imposed by the latest Australian concrete design code. Outcomes of the analysis further validate some amendments incorporated in the design code while suggesting improvements to the critical distance rule.

The current construction industry prefers performance-based fire design over prescription-based fire design as it yields more optimized solutions on a case by case basis. In order to apply such methods to concrete flat slab fire design, a case study was conducted to model an actual fire scenario within a compartment in a multi-storey building and its effects on the flat slab. Fire Dynamics Simulator (FDS), a computational fluid dynamics based fire simulation software was implemented to capture the growth and decay of a compartment fire incorporating the combustible material characteristics of the furniture inside. Different fire scenarios were simulated, taking into account the different ventilation conditions. Critical temperature fields generated from the fire simulation were then applied to a FE model to assess the structural response. The predicted structural response for the actual fire scenario is significantly different from the response when the flat slab was subjected to standard design fire. This observation further highlights the importance of performance-based fire design approach, which takes building-specific parameters into account rather than generalized fire curves.

Publications related to thesis

No	Paper Title	Journal/Conference	Status	Type of Publication	Authors
1	Large-scale experiment on the behaviour of concrete flat slabs subjected to standard fire	Journal of Building Engineering	Published	Journal Article	Weerasinghe, P., Nguyen, K., Mendis, P., & Guerrieri, M.
2	Performance of modern building façades in fire: a comprehensive review	Electronic Journal of Structural Engineering	Published	Journal Article	Nguyen, K. T., Weerasinghe, P., Mendis, P., Ngo, T., & Barnett, J.
3	Fire performance of concrete flat slabs	The 10th International Conference on Structures in Fire, Belfast, UK	Published	Conference paper (peer reviewed)	Weerasinghe, P., Mendis, P., Nguyen, K. & Ngo, T.

Declaration

I certify that the thesis entitled

Fire Performance of Concrete Flat Slabs

Submitted for the degree of
Doctor of Philosophy

1. Is the result of my original work towards the PhD and due acknowledgement has been given in the text to all other material.
2. The thesis is less than 100,000 words in length, exclusive of tables, maps, bibliography and appendices

Pasindu Thalpe Guruge
Date: 30.04.2020

Acknowledgement

I would like to convey my sincere gratitude to all those who supported me during my journey as a graduate researcher. First and foremost, I would like to convey my gratitude to my supervisory committee: Prof. Priyan Mendis, Dr. Kate Nguyen, Prof. Tuan Ngo for their guidance, technical expertise, motivation and patience during my candidature. I would like to especially thank Prof. Priyan Mendis, my principal supervisor, for his continuous support and encouragement while sharing his expert knowledge in both academia and industry. I would like to acknowledge my co-supervisor Dr. Kate Nguyen, for her valuable inputs and enthusiasm, which paved me to enter the field of fire engineering. I would also like to thank Dr. Tharaka Gunawardena for chairing the review committee and giving constructive suggestions to improve my research.

Moreover, I would like to thank the ARC Centre for Advanced Manufacturing of Prefabricated Housing (CAMP.H) for providing a cohesive environment and exposing me to a globally recognized research culture. I convey my gratitude to the University of Melbourne, for granting me the Melbourne International Research Scholarship (MIRS) and other facilities during my candidature. I am also thankful to lecturers, research fellows, my colleagues, friends and the administrative staff at the Department of Infrastructure Engineering, The University of Melbourne for their continuous support. I would also like to acknowledge the research lab personnel at the Victoria University and RMIT University for their support rendered to me during my experiments.

Furthermore, I would like to take this opportunity to thank my former lecturers, staff and colleagues at the University of Moratuwa, Sri Lanka who laid the foundation for my career as a civil engineer and a researcher. I would also like to express my gratitude to the Sri Lankan education system, which provided me with an excellent primary and secondary education.

Finally, and most importantly, I would like to convey my heartfelt gratitude to my wife, my parents, brother and friends for being my strength and giving their unconditional love during both good times and bad times.

Table of Content

List of Figures

List of Tables

1 Introduction

1.1 BACKGROUND

Fire poses a significant risk for the structures and their occupants. Fires in structures could range from compartment fires within a confined space, façade fires on the exterior of the building, fires due to natural causes such as bush fires and fires due to explosions. The spread and the growth of fire affect the severity of the damage caused. The ignition source of a fire can be due to a simple mistake such as throwing away a cigarette bud near a combustible area, but the consequences can be devastating. Most construction materials tend to degrade in fire, and additional forces are generated due to thermal expansion at elevated temperatures. This could ultimately result in a total or partial collapse of the structure or minor damages that can be retrofitted. Therefore, a significant effort is put forward to ensure the fire safety of structures by designing them to withstand such catastrophic events.

Most of the modern-day buildings are multi-storey constructions. Scarcity of land, urbanisation and energy efficiency has driven the construction industry to move from traditional single-storey dwellings to high rise structures. A common form of a high-rise building is a frame with a core, columns, beams and slabs. Slabs are the horizontal structural elements which act as the floors. The most widely used materials in high-rise buildings are concrete and steel. Among them, slabs are usually constructed using concrete with embedded steel reinforcement. Concrete, which is a composite material consisting of cement and aggregates has a relatively high strength to weight ratio (compared to other common materials such as steel and timber), flowability in the early stage and durability which makes it an ideal construction material to be used to construct slabs. Steel reinforcement provides the tensile strength and the ductility required to prevent sudden failure. In favour of fire resistance, concrete is non-combustible and has low thermal conductivity and high specific heat. Hence, the thermal energy required to increase the temperature of concrete is significantly high. However, on the downside, some parts of the outer region of exposed concrete can disintegrate and detach from the structural element when subjected to fire. This phenomenon is defined as spalling of concrete. Also, the degradation of mechanical properties of both concrete and steel at elevated

temperatures is another critical problem encountered. Nevertheless, reinforced concrete slabs are widely used in high-rise buildings with certain measures taken to ensure the prolonged fire resistance allowing safe evacuation for the occupants while minimising the overall damage.

1.2 CONCRETE FLAT SLABS IN MULTI-STOREY BUILDINGS

Slabs support the weight of the occupants, goods and other permanent and live floor loads in a multi-storey building. Typical forms of slabs include slabs supported on beams (see Figure 1.1) and slabs supported directly on columns. The latter is defined as ‘flat slabs’ as the underneath of the slab is only one plane surface in the absence of beams. Flat slabs have many advantages over conventional slabs supported on beams. Quick and easy formwork, the capability to achieve lower storey heights which results in more stories within the total height and enhanced flexibility for partitioning are some of the key benefits of having flat slabs. As a result, many of the high-rise buildings incorporate flat slabs as the primary horizontal structural floor system (see Figure 1.2). However, on the downside, the connection between the flat slab and column poses a risk of brittle failure in the events of dynamic loading (i.e. earthquakes) and fire.

Figure 1.1: Conventional slabs supported by beams and columns

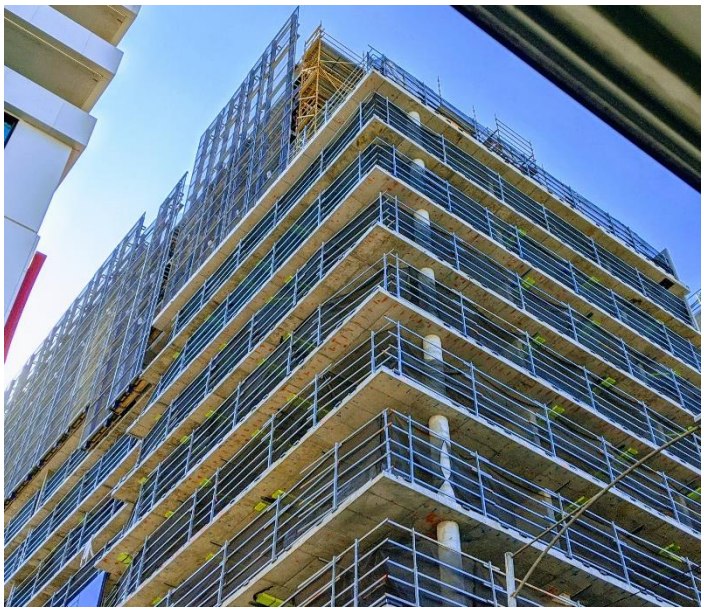

Figure 1.2: A multi-storey building constructed using concrete flat slabs

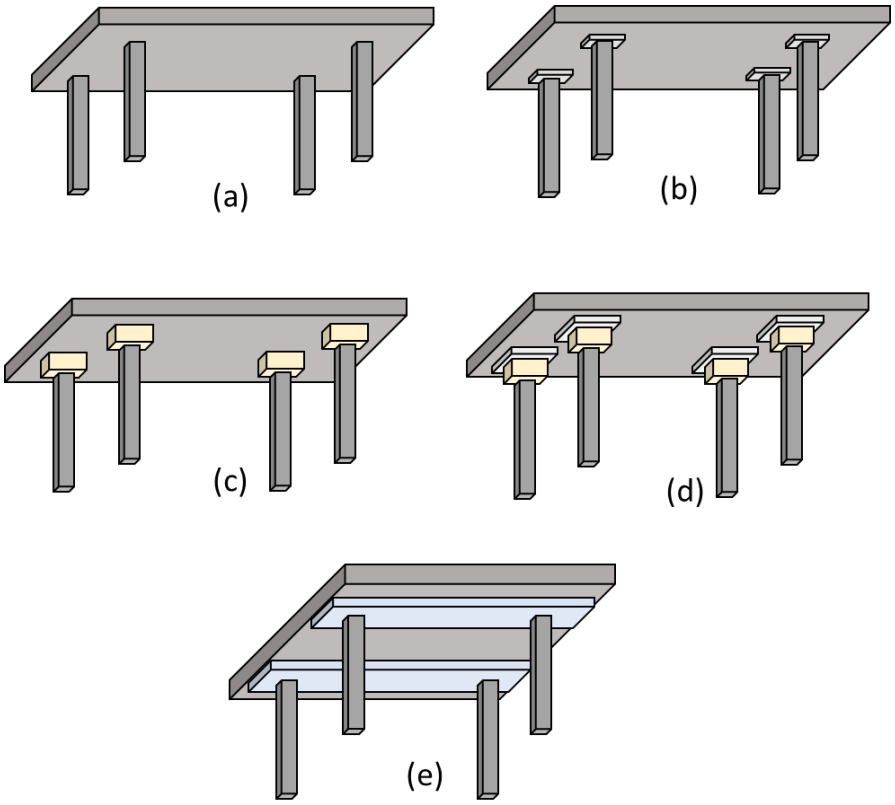

Figure 1.3: (a) Normal flat slab supported on columns, (b) Flat slab with drop panels, (c) Flat slab with column heads, (d) Flat slab with drop panel and column head, (e) Flat slab with band beams

Flat slabs can have different forms depending on the enhancement in the slab-column connecting region. Figure 1.3 illustrates such variations in structural arrangements commonly used. The thickness of the connection region is increased,

and these ‘drop panels’ improve the ductility of the slab-column connection. In some cases, these drop panels can take a conical shape, and they are called column heads. Band beams are also adopted as a strengthening technique.

Punching shear failure is one of the common failure patterns observed in buildings containing flat slabs. In the absence of beams, a hogging bending moment is generated near the slab-column connection, and due to that a tensile crack could start on the hogging surface and penetrate till the bottom layer. This type of shear failure is often catastrophic and can lead to the progressive collapse of the structure.

1.3 FIRE RELATED DISASTERS IN BUILDINGS WITH CONCRETE SLABS

It is worthwhile to get to know about the historical events that resulted in the collapse of concrete buildings due to fire. Some of the recent fire incidents [i.e. Grenfell tower fire in London (2017) and Lacrosse building fire in Melbourne (2014)] which are categorised as façade fires did not result in a complete collapse of the building although they resulted in many casualties and substantial financial losses. However, there are some reported incidents where partial or complete collapse have occurred in concrete multi-storey buildings.

Faculty of Architecture building at the Delft University of Technology in Netherland is one such example where partial collapse has happened due to fire in 2008 (see Figure 1.4). The fire started on the 6th floor of the 13-storey building, and it took 7 hours for firefighters to control the situation completely. No deaths were reported, but the building was demolished after the severe damages.

Figure 1.4: Partial collapse of the Architecture faculty building at Delft University of technology in 2008 (Kirk, 2010)

Another incident was reported in 2002 from Russia, where a nine-storey apartment building collapsed due to fire during ongoing reconstruction work (see Figure 1.5). The tragedy did cost a life, injured two and made more than 400 people homeless. In 2005, a 32-storey reinforced concrete high-rise building in Madrid, Spain partially collapsed due to a fire. The fire burned almost a day, and the upper ten floors collapsed, leaving the concrete core intact, which prevented the total collapse of the building. (see Figure 1.6)

Figure 1.5: Collapse of a 9-storey building in Russia (Beitel and Iwankiw, 2008)

Figure 1.6: Partially collapsed building in Madrid, Spain due to fire (Hellenic Cement Industry Association, n.d.)

A specific incident related to concrete flat slabs has occurred in 2004 where an underground car park in Gretzenbach, Switzerland collapsed due to fire. During that tragic incident, seven firefighters were killed, and the car park totally collapsed. (see Figure 1.7). Initially, a localised fire has started and then extended into a massive fire, ultimately resulting in failure of the roof slab (Annerel et al., 2013b). Investigations and analysis that followed the incident have claimed that the failure mode is punching shear near the slab-column connection due to increased axial loads of the column as a result of fire. Furthermore, the collapse sparked a discussion among the designers and authorities on the applicability and adequacy of the current design guidelines regarding fire resistance of concrete flat slabs.

Figure 1.7: Underground car park collapse in Gretzenbach, Switzerland in 2004 (Michael Noblett, n.d.)

These are only a few examples of compartmentation fires resulted in a partial or complete collapse of reinforced concrete buildings. However, in recent years many cases have been reported especially on high-rise building fires escalated by combustible cladding. Although the fire spread is external, it has caused damage to the internal slabs as well. Therefore, governments and authorities are very strict on making sure that building designers and contractors adhere to the fire safety design guidelines. Regulatory bodies who are responsible for building codes are also keen to regularly update and improve their design guidelines to ensure that the buildings are adequately fire-resistive.

1.4 RESEARCH PROBLEM, AIM AND OBJECTIVES

Concrete flat slabs are widely incorporated in multi-storey buildings owing to their efficiency in construction and economic benefits. However, the effects of fire on flat slabs are not well understood. Recent incidents question the reliability of the current design guidelines for fire safety design of concrete flat slabs. Some may argue that the rules are too strict and hinders the effective use of flat slabs, while others highlight the need to strengthen the requirements further. Only a limited number of small-scale experiments have been carried out to evaluate the behaviour of flat slabs in fire, and the current design guidelines are based on a series of fire tests carried out more than two decades ago. Since fire tests are generally expensive and time-consuming, the use of numerical methods to evaluate the fire resistance needs to be explored. There is also a need to compare the prescriptive code-based design approach for fire safety vs performance-based design approach to identify which yields the more efficient solution.

The main aim of the research is to critically evaluate the performance of concrete flat slabs and its failure mechanism in fire using both experimental and numerical methods and provide a research base to improve the current fire safety design guidelines for concrete flat slabs. This can be further broken down into a set of objectives.

- Identify and compare various design guidelines for fire safety design of concrete flat slabs.
- Conduct a large-scale fire test for a concrete flat slab to determine its behaviour when exposed to standard fire.
- Develop a numerical model to capture the effects of fire on concrete flat slabs.
- Validate the developed model with the experimentally measured thermo-mechanical performance.
- Study the influence of various parameters on the fire resistance level of flat slabs.
- Develop a model to predict the influence of an actual compartment fire on the structural performance of concrete flat slabs.

1.5 SIGNIFICANCE OF THE RESEARCH

The use of concrete flat slabs in multi-storey construction is increasingly getting popular due to its economic benefits and construction efficiency. However, the current fire design guidelines tend to hinder harnessing the full potential of the concrete flat slabs. Since fire-related disasters in high-rise buildings are occurring more frequently throughout the world, the building regulatory authorities impose strict guidelines related to fire safety. In order to obtain the approval, the building must meet the specified fire resistance criteria. For that, it needs to follow the design code requirements strictly. In the case of concrete flat slabs, most design codes in the world recommend a 200mm thickness or higher to achieve more than 1.5hrs of fire resistance. Furthermore, this thickness should be maintained throughout the whole floor area. As a result of that, the designer loses the freedom to even allocate a few centimetres of set-downs in slabs for adequate drainage in bathroom areas.

The current design guidelines and fire resistance predictions are based on a limited number of experiments on fire resistance of flat slabs carried out a few decades ago. It is important to note here that those fire tests were conducted on isolated, small-scale slab specimens without any lateral restraints. However, in the actual conditions of a building, the slab is a continuous element, and in the case of fire membrane actions can develop due to lateral restraints provided by the adjacent slab panel. Few researchers have argued that such membrane actions due to lateral restraint against thermal expansion could increase the fire resistance level. However, more evidence is needed, both experimentally and numerically, to establish that argument. This study, therefore, focuses on conducting a large-scale experiment on a laterally restrained concrete flat slab exposed to fire and developing numerical models to predict the fire resistance levels of flat slabs. The influence on different factors such as the span of the slab, thickness of the slab and reinforcement arrangement are also investigated using the developed numerical models. Chapter 3 describes the experiment conducted and the results while Chapter 4 and Chapter 5 focus on the numerical modelling of thermo-mechanical behaviour of concrete flat slabs in fire.

The behaviour of a structural element during the cooling phase is often overlooked assuming that the cooling down after a fire will not be crucial as much as heating during a fire. It is a known fact that the mechanical properties of both concrete and steel degrade at elevated temperatures. Degraded mechanical properties do not

totally recover during the cooling. In fact, material properties further degrade at a much slower pace than heating during the cooling phase. Incorporating such attributes to the structural model is pivotal when determining the fire resistance because the structure is vulnerable during the cooling phase too. This thesis presents a novel method to include the cooling phase material property changes and highlights the importance of using such an approach to improve the accuracy of the numerical models.

With performance-based approach overtaking the traditional prescription-based design for fire safety, both industry and academia need robust tools and methods to simulate a real fire scenario in buildings. In Chapter 6, the author describes the development of a compartment fire model which simulates the development of an actual fire inside an apartment and its growth, spread and decay. Fire-resistance of the floor slab is compared using the simulated fire against the standard code-prescribed fire to study the different structural performances. The use of such models will enable designers to optimise their design and provide more flexibility in case-specific solutions rather than solely relying on the design guidelines.

The scope of this study is limited to conventional concrete flat slabs supported only by rectangular columns. However, the methodologies developed can be used in any structural fire problem to derive its performance in fire.

1.6 STAGES OF THE RESEARCH

The overall methodology adopted in the research to achieve the aims and objectives laid out in Section 1.4 are presented in the following stages.

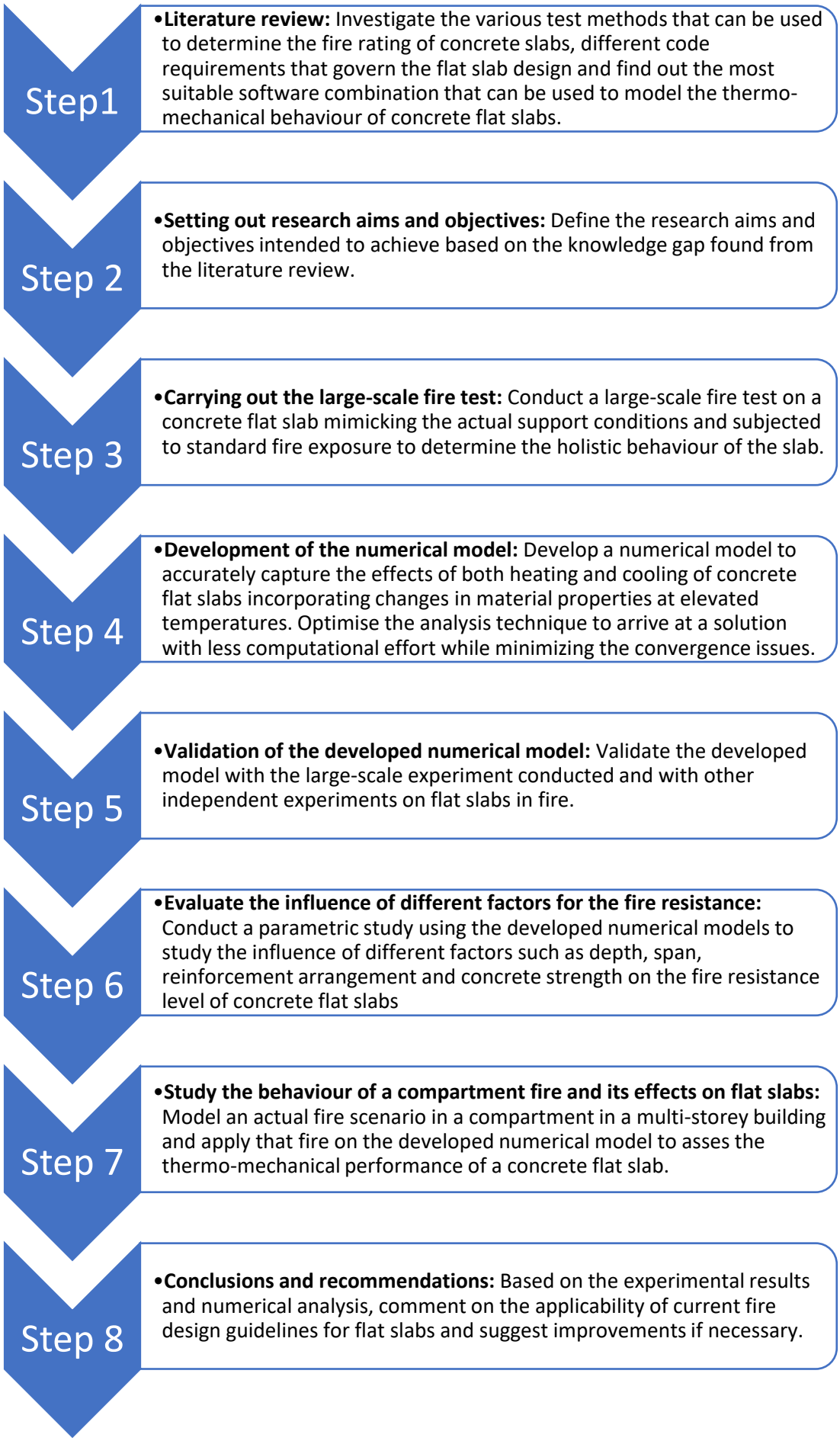
Step1
•Literature review: Investigate the various test methods that can be used to determine the fire rating of concrete slabs, different code requirements that govern the flat slab design and find out the most suitable software combination that can be used to model the thermo-mechanical behaviour of concrete flat slabs.
Step 2
•Setting out research aims and objectives: Define the research aims and objectives intended to achieve based on the knowledge gap found from the literature review.
Step 3
•Carrying out the large-scale fire test: Conduct a large-scale fire test on a concrete flat slab mimicking the actual support conditions and subjected to standard fire exposure to determine the holistic behaviour of the slab.
Step 4
•Development of the numerical model: Develop a numerical model to accurately capture the effects of both heating and cooling of concrete flat slabs incorporating changes in material properties at elevated temperatures. Optimise the analysis technique to arrive at a solution with less computational effort while minimizing the convergence issues.
Step 5
•Validation of the developed numerical model: Validate the developed model with the large-scale experiment conducted and with other independent experiments on flat slabs in fire.
Step 6
•Evaluate the influence of different factors for the fire resistance: Conduct a parametric study using the developed numerical models to study the influence of different factors such as depth, span, reinforcement arrangement and concrete strength on the fire resistance level of concrete flat slabs
Step 7
•Study the behaviour of a compartment fire and its effects on flat slabs: Model an actual fire scenario in a compartment in a multi-storey building and apply that fire on the developed numerical model to asses the thermo-mechanical performance of a concrete flat slab.
Step 8
•Conclusions and recommendations: Based on the experimental results and numerical analysis, comment on the applicability of current fire design guidelines for flat slabs and suggest improvements if necessary.

1.7 THESIS LAYOUT

The thesis comprises of seven chapters. A summary of the content of each chapter is presented below.

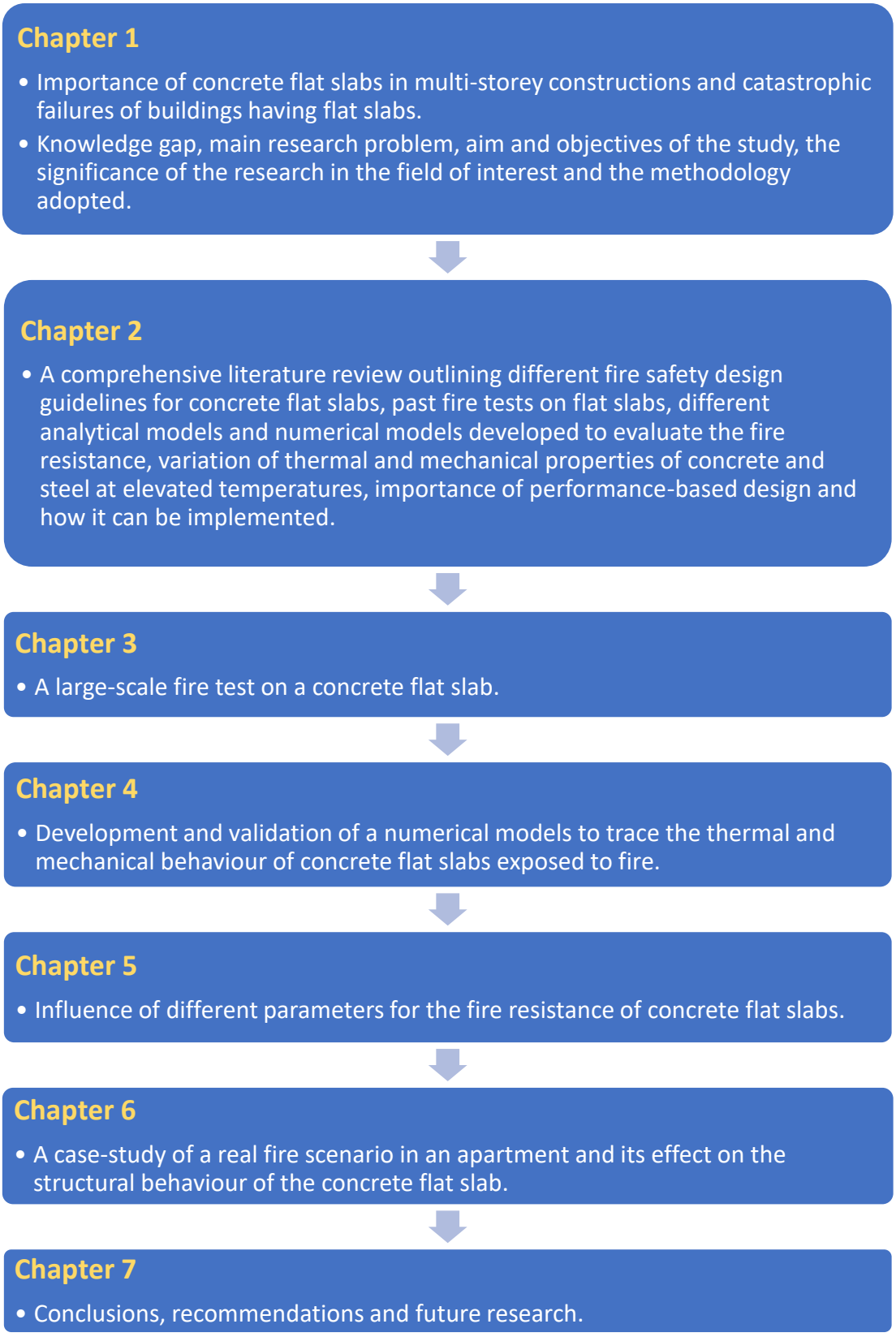

2 Literature Review

2.1 INTRODUCTION

This chapter aims to discuss the relevant research and current design practices related to fire resistive design of concrete flat slabs. In order to address the research problems discussed in Chapter 1, it is necessary to first understand the existing knowledge on concrete flat slabs and their fire resistance. A systematic approach was taken to identify the key research carried out over the years to study the performance of concrete flat slabs in fire. Current fire design guidelines which were based on these researches are also considered. The main aim was to identify the research gap pertaining to the fire-resistive design of concrete flat slabs.

A comprehensive literature review was conducted, and the findings are presented under several key topics. Importance of flat slabs in construction is highlighted, and then the current building code guidelines related to fire safety of flat slabs are compared. Then the experimental studies done on flat slabs in fire are reviewed, bringing out key outcomes and limitations. Analytical models developed to evaluate the fire resistance of concrete flat slabs are reviewed and discussed. The performance-based design approach and the use of structural fire modelling in the process were also in focus. Following sections will discuss the findings in detail.

2.2 IMPORTANCE OF FLAT SLABS IN CONSTRUCTION

Reinforced concrete slabs are the structural arrangement used in buildings which act as floors or platforms to support the dead and live loads in multi-storey buildings. Three main types of slabs are being used: one-way spanning slabs, two-way spanning slabs and flat slabs (see Figure 2.1). The significant difference between one-way and two-way spanning slabs with flat slabs is that the latter does not have any beams in the structural arrangement. Flat slabs are solely supported by columns and depending on the column configuration, different types of flat slabs can be identified (see Figure 2.2).

The origin of the use of reinforced concrete flat slab floors dates back to 1899, where George M. Hill is believed to have used this concept in the USA for the first time (Gasparini, 2002). C.A.P. Turner was instrumental in proving the reliability and

cost-effectiveness of flat slabs. By the end of 1909, the area of flat slabs used in the US was rapidly approaching a thousand acres (Gasparini, 2002).

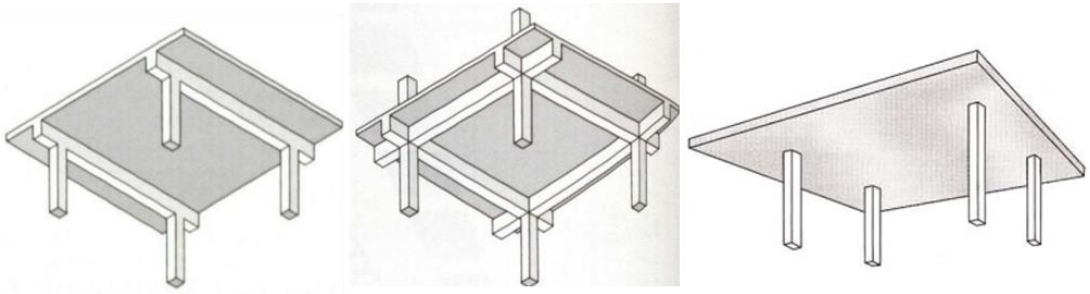

Figure 2.1 Slab types; a) one-way slab, b) two-way slab, c) flat slab (Portland Cement Association, 2005)

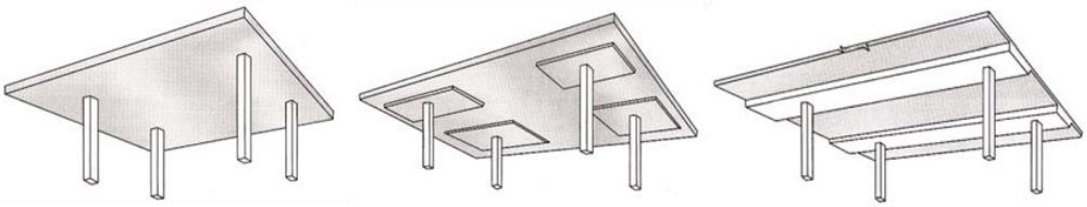

Figure 2.2 Types of flat slabs; a) Normal flat slab, b) Flat slab with drop panels, c) Flat slab with band beams (Portland Cement Association, 2005)

Many decades of research has shown the cost benefits and architectural gains of using flat slabs (Sahab et al., 2005).

- Quick and easy to build formwork compared to reinforced slabs with beams
- The architectural finishes can be directly applied to the underside of the slab
- In the absence of beams, lower story heights can be achieved which saves cost in vertical cladding, partition walls, mechanical systems and plumbing especially in multi-storey buildings
- More storeys can be accommodated within a restricted height of the building
- Provide more flexibility for partition locations
- Ability to extend windows up to the underside of the ceiling

As a result of these advantages, the use of flat slabs in high-rise buildings is increasingly getting popular. The behaviour of flat slabs at ambient conditions is a well-researched area for many decades, and the key focus was on the slab-column connection, which was considered to be critical in failure. The most common type of

failure observed is punching shear failure. Therefore, more emphasis is placed upon designing against the punching shear resistance of the flat slab. Design codes specify a concentration of reinforcement near the column to address this issue. However, one of the critical criteria in flat slab design is the design for fire resistance. The following will lay out the critical performance criteria considered in fire-resistive design and the current design code guidelines to meet those criteria.

2.3 FIRE RESISTANCE OF FLAT SLABS

Safety of a structure is ensured by designing it against certain catastrophic events. Fire in a building is such a catastrophic event, and it can cause severe damage to both the structure and its occupants. Therefore, it is essential to consider the effects of fire when designing any structure for fire resistance. Fire resistance is defined as the duration up to which the structural element can meet specific performance criteria. In general, there are three main performance criteria specified in design codes across the world. They are;

1. **Structural adequacy:** The ability of the structural element to carry the intended load without collapse. Generally, standards specify a limiting deflection or a rate of deflection for load-bearing tests to ensure the termination of the test before actual failure.
2. **Integrity:** The ability to prevent fire spread to another compartment from the origin. The element should not have any cracks or fissures which allow smoke, flame or hot gases to penetrate through.
3. **Insulation:** The ability to act as a barrier to contain the fire. The unexposed side temperature should not exceed a specific limit to prevent initiation of fire on the other side of the barrier.

For non-structural elements such as walls and partitions, only Integrity and Insulation criteria are considered whereas for flat slabs all three performance criteria apply. If one of the above three performance criteria are not met during a fire, the flat slab is considered as a failure. When exposed to fire, the duration that the flat slab could withstand while meeting these performance criteria is defined as the Fire resistance level (FRL).

In experiments related to flat slabs in fire, merely the time till failure is taken as the fire resistance of that particular slab. More details of this will be discussed in Section 2.6.

2.4 BUILDING CODES AND REGULATIONS ON FIRE RESISTIVE DESIGN OF CONCRETE FLAT SLABS

2.4.1 Code comparison for fire-resistive design in general

Fire resistive design of structural elements is carried out in accordance with the guidance given in the concrete design code of the respective country. Many of the modern-day codes follow a performance-based approach for fire design. In order to satisfy the performance requirement, either a prescriptive solution is proposed by the design code, or alternative design methods are allowed. This section will focus on the latest building regulations and guidelines given in Australia, Europe, America and New Zealand.

A summary of the comparison of fire design approach in general related to the countries mentioned above is given in Table 2.1.

Table 2.1 Comparison of fire-resistive design requirements of building codes

	AS 3600 (Standards Australia, 2009)	**NZC 3101 (Standards New Zealand, 2006)**	**BS EN 1992-1,2 (European committee for standardization, 2004b)**	**ACI 216.1-97 (American Concrete Institute, 2014)**
Basis of Design	Based on three main performance criteria; Insulation, Stability and Integrity			Based on two criteria; Barrier fire resistance and Maintaining structural fire resistance
	All four codes are performance-based			
Concrete types	Only considers a single type of concrete for all cases		Considers concrete made with siliceous and calcareous aggregates. Tabulated data are for normal-weight concrete, and 10% reduction is allowed for lightweight concrete. Special section for HSC.	Different concrete types considered - insulating concrete, lightweight, semi-lightweight, air-cooled blast furnace slag, carbonate aggregate, siliceous aggregate
Solutions Provided	Tabulated and graphical specifications for fire resistance of Beams, Slabs, Walls and Columns			

Alternative Methods	In cases other than using tables, calculation of fire resistance shall be done according to EC 2 (European committee for standardization, 2004b), using the load combinations in AS/NZS 1170.part0 (Standards Australia, 2002c)		Other than tables and graphs, a simplified calculation method to determine the structural sizes and an advance calculation method to verify simulations are included. **Simplified calculation** - Reducing the characteristic strength of concrete and steel according to the graphs provided. **Advance calculations**- Modelling thermal response (thermal actions & temp. dependent thermal properties of the material) and mechanical response (stress, strain, deformation etc.)	An analytical method was proposed to calculate the fire resistance and cover of flexural members. For calculations, concrete and steel temperature profiles were provided considering different widths, exposure times and concrete types.
Material properties of concrete	There is no mention of material properties for different temperatures		Strength of concrete at different temp. for different types of aggregates has been included in both compression and tension	Variation of concrete compressive strength for siliceous, carbonate and semi-lightweight aggregate types with temperature is given
Material properties of steel	There is no mention of material properties of r/f steel		Mechanical properties of r/f steel at elevated temp. are addressed. E.g., stress-strain graph, elongation, thermal conductivity	There's no mention about material properties of r/f steel
Beams	For a beam (supporting roof/floor or exposed to fire on all sides) (simply supported or continuous) - Minimum width and average axis distance (cover) specified. A graphical approach included too.	Same as Australian Standard, however, a minimum web thickness is specified for non-rectangular beams. No graphical approach.	Same as Australian Standard. Additionally, special attention is given regarding the area of top r/f over a cts. support for fire conditions. Differentiates for web thickness for different beam classes. (WA, WB, WC). Min. beam width specified to prevent concrete compression or shear failure of a cts beam at first intermediate support	No graphical or tabulated method. Instead, an analytical method is proposed to calculate the fire resistance and cover of flexural members.
Columns	Only applies braced columns comprise with certain restrictions the code applies. For other columns, alternative methods should be used.	Similar to Australian Standard but much less information. No emphasis on effective length, eccentricity or brace/unbrace. Generalised for all the columns.	Column design similar to AS. Buckling of columns under fire considered in Annex C.	Only one criterion to consider the minimum size and cover for all types of columns

	Considers the loading on column vs its ultimate strength and specifies the minimum axial distance and smaller cross-sectional dimension			
Slabs	For a slab (Simply Supported or Continuous/ 1 way or 2 way) - Minimum effective thickness and axis distance to lowest r/f are specified. For flat slabs and Ribbed slabs, different tables are provided.			A single value of min. thickness specified for all concrete floors, walls and roofs. The case having two layers of different types of concrete has been considered. Graphical representation of FR of slabs as influenced by the aggregate type, r/f steel type, moment intensity and cover. Temperature profiles for slabs made with different aggregate types during ASTM E 119 fire test are given
Walls	Effective thickness specified for Insulation and Min. axis distance and wall thickness specified for structural adequacy based on the load on walls	Same as Australian Standard. Additional section for external walls that could collapse outwards in fire.	Wall design is similar to Australian Standard. However, an allowance for calcareous aggregate concrete is made. Specification for firewalls are given	Same as slab and roof design. Additionally, fire resistance can be found for Insulated joints using ceramic fibre.
Insulating Coatings	Provision to increase fire resistance by means of insulating materials. Cement vermiculite, gypsum-vermiculite & gypsum-perlite are specified. For other materials, thickness shall be found with AS 1530.4.		Only mentioned that FR may be obtained by applying protective layers, but the properties and performance should be assessed using appropriate test methods.	Multiplying factor for different types of finishes on the non-fire exposed side and a specific time assigned to finish materials on fire exposed side. Fire-resistance of concrete roofs with board insulation considered
Spalling	Not mentioned under design for fire resistance		Explosive spalling, falling of concrete, joints and protective layers are addressed	Under prestressed beams - Adequate provisions against spalling shall be provided by U-shaped or hooped stirrups spaced not to exceed the depth of the member, and having a cover of 1 in.

Annexes	-	-	Annexes provide information on; • Temperature profiles • Alternative calculation methods • Buckling of columns under fire • Calculation of shear, torsion r/f and anchorage	-

In summary, all four codes are based on performance-based design criteria. All codes contain tables or figures to specify prescriptive design guidelines in the form of element dimensions and concrete cover required to meet a certain performance level. Specific alternative methods are also proposed which can be used instead of prescribed dimensions. Different concrete types are considered in some design codes to account for the differences in concrete properties at elevated temperature. Regarding slabs, ACI code (American Concrete Institute, 2014) does not differentiate between normal slabs with beams and flat slabs. It provides a typical thickness and cover requirement for floors, walls and roofs in general. However, the other three codes specify a different thickness and cover requirements for flat slabs and the values prescribed are higher than that of regular slabs with beams. Therefore, it indicates that the behaviour of flat slabs in fire could be different from that of regular slabs with beams.

2.4.2 Performance requirements for concrete flat slabs fire design

Fire resistive design of flat slabs in both AS 3600 (Standards Australia, 2009) and NZC 3101 (Standards Newzealand, 2006) are based on the European guidelines which specify a minimum thickness and cover to reinforcement in order to satisfy the performance criteria. According to Figure 2.3 and Figure 2.4, it is evident that both AS 3600 (Standards Australia, 2009) and BS EN 1992-1-2 (European committee for standardization, 2004b) use the same thickness and cover for flat slabs. For an FRL of 90 min and upwards it specifies the same thickness of 200 mm and the concrete cover increases. Background document to EN 1992-1-2 describes the research work which the slab thicknesses in Figure 2.4 are based on (Anderberg et al., 2004). According to the report, the research carried out by Kordina (1993) on flat slabs under fire is the only basis for these thicknesses. More details of this study are presented in Section 2.6.1.

FIRE RESISTANCE PERIODS (FRPs) FOR STRUCTURAL ADEQUACY FOR FLAT SLABS INCLUDING FLAT PLATES

FRP for structural adequacy (min)	Minimum dimensions (mm)	
	Slab thickness	Axis distance (a_s)
30	150	10
60	180	15
90	200	25
120	200	35
180	200	45
240	200	50

NOTES:

1 a_s = axis distance to the reinforcement in the lowest layer.

2 For prestressing tendons, the axis distance shall be increased as given in Clause 5.3.3.

Figure 2.3 Fire resistive design requirements for flat slabs as specified by AS 3600 (Standards Australia, 2018)

Standard fire resistance	Minimum dimensions (mm)	
	slab-thickness h_s	axis-distance a
1	2	3
REI 30	150	10*
REI 60	180	15*
REI 90	200	25
REI 120	200	35
REI 180	200	45
REI 240	200	50
* Normally the cover required by EN 1992-1-1 will control.		

Figure 2.4 Fire resistive design requirements for flat slabs as specified by EN 1992-1-2 (European committee for standardization, 2004b)

The thicknesses and covers specified in these design codes should be used with an FRL specified for a particular type of construction. Usually, the building regulation authority of that country specifies these fire resistance levels based on the importance and use of a building type. In Australia, the National Construction Code (NCC) (The Australian Building Codes Board, 2016) layout the performance requirements for each construction type. According to NCC, class A construction (Buildings over four stories fall into class A fire-resistive construction) require a minimum fire rating level (FRL) of 120 min or above for floors. Therefore, according to Figure 2.3 and Figure 2.4, the flat slab thickness should always be higher than 200 mm for high-rise buildings.

Another issue that has been raised due to this 200 mm thickness limit is when there is a requirement for a set down in slabs. Set downs are placed on slabs in bathroom areas to have proper drainage of water. Typical set downs can be 20 mm-30 mm. However, even a 20 mm set down in a 200 mm thick flat slab would violate the concrete code and NCC requirement to achieve a 120 min FRL. Increasing the total slab thickness by 20 mm would prove to be uneconomical when costs accumulate for many floors throughout the height of a multi-storey building. However, the latest revision of AS 3600 (Standards Australia, 2018) has addressed this issue by specifying a certain distance from the column (which is considered to be a critical failure zone) where this thickness requirement should be maintained. If the span between two columns is taken as 'l', according to the code, the thickness requirement specified in Figure 2.4 should be maintained for a distance of 'l/16' from the column face. Beyond this distance, only the thickness requirement for insulation criteria needs to be satisfied. However, there is no mention of the research basis for such a limiting distance. Furthermore, Eurocode (European committee for standardization, 2004b) still requires to adopt the specified thickness for the whole floor area. Therefore, it is essential to conduct more studies to find out the validity of the latest revision to the code.

2.4.3 Standard fire testing

Fire tests are conducted to determine the fire rating of a structural component experimentally. The structural component or the system is loaded to simulate the actual conditions it will undergo during a fire. A prescribed thermal load is then applied to the test specimen by means of a burner. Fire load is usually applied to the bottom surface of concrete slabs. The main reasons being the behaviour of a fire where heat tends to propagate upwards, and underside of the slab is the most vulnerable as there is no protection from finishes. There are standards which specify the methodology for fire testing. Some of the widely used ones are;

- **International standard ISO 834** (International Organization for Standardization, 1999) - Fire resistance tests: Elements of building construction.
- **Australian standard AS 1530** (Standards Australia, 2014d) - Methods for fire tests on building materials, components and structures Part 4: Fire-resistance tests for elements of construction

- **American standard ASTM E119** (ASTM International, 2016) - Standard test methods for fire tests of building construction and materials
- **British standard BS 476** (British Standard Institute, 1987) - Fire tests on building materials and structures
- **Canadian standard CAN/ULC-S101-14** (Standards Council of Canada, 2014) - Standard methods of fire endurance tests of building construction and materials

In the case of testing of concrete slabs, standard fire curve specified by ISO 834 (also in AS 1530.4) has been used in most tests. Equation (2.1) gives variation of temperature (T) with time (t).

$$T = 345log_{10}(8t + 1) + T_o \tag{2.1}$$

where t is time in minutes and T_0 is ambient temperature (^oC).

ASTM E 119 (ASTM International, 2016) defines the temperature variation with time (T) according to equation (2.2).

$$T = 750\left[1 - e^{-3.79559\sqrt{t_h}}\right] + 170.41\sqrt{t_h} + T_o \tag{2.2}$$

where t_h is time in hours and T_0 is ambient temperature (^oC).

Both ASTM E 119 and ISO 834 fire curves are very similar (see Figure 2.5). However, different fire curves, such as hydrocarbon fire and external fire are used for different scenarios. Hydrocarbon fire curve is much more severe compared to the standard fire, and it is usually used to test components of a structure vulnerable to a severe fire. For example, a car park contains high amounts of fuel which increase the severity in case of a fire. Most widely used fire curve for slabs in normal buildings is the standard fire curve in accordance with ISO 834.

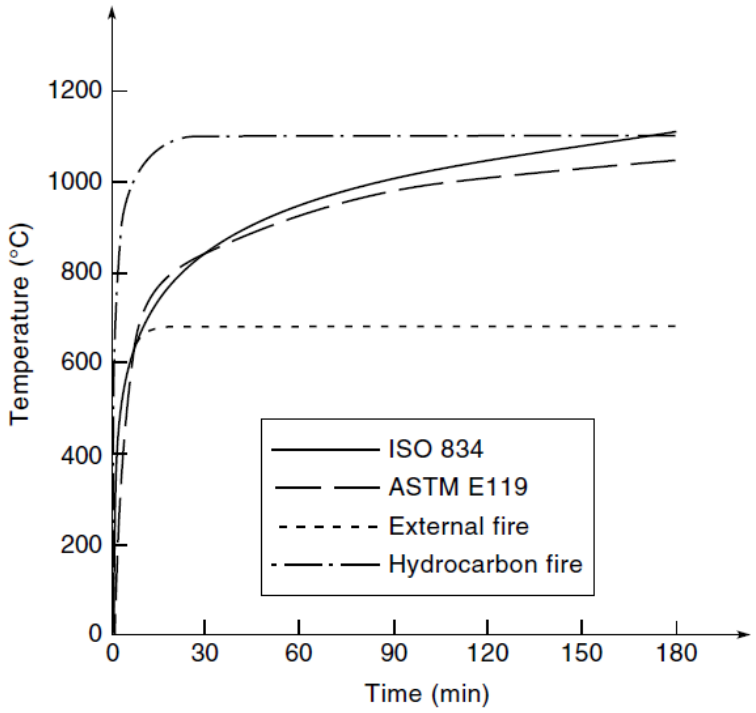

Figure 2.5 Some standard design fire curves (Buchanan and Abu, 2017)

2.5 STUDIES ON CONVENTIONAL SLABS IN FIRE

Compared to studies on fire behaviour of flat slabs, more research has been carried out to investigate the fire behaviour of regular, prestressed and post-tensioned concrete slabs. It is worthwhile to understand the critical findings of those studies which can lead the way to a better understanding of fire behaviour of flat slabs. Some of the key outcomes of those studies are presented here.

2.5.1 Reinforced concrete slabs supported on beams

Bailey and Toh (2007) have conducted studies on small scale unrestrained reinforced concrete slabs at elevated temperatures. A total number of 44 small-scale (1.7 m x 1.1 m) slab specimens were tested at ambient and elevated temperatures. Slabs were made out of 40-50 MPa concrete and subjected to a furnace specific time-temperature history having a maximum temperature of around 975^{o}C. Results show that the failure mode is predominantly due to the membrane action by fracture of reinforcement across the shorter span (see Figure 2.6)

Later, Wang et al. (2013), Yang et al. (2013) and Zhang et al. (2014) have conducted full-scale tests (on a three-storey steel frame building with concrete slabs) to investigate the fire behaviour of continuous concrete slabs. Wang et al. (2013) highlight that the deformation of a concrete slab subjected to fire depends on two

critical factors: restraints and number & location of heated panels. After observing the cracking pattern, the authors make further observations that cracking pattern in heated panels depends on the boundary restraints whereas in un-heated panels it depends on the number and location of heated panels. Full-scale tests conducted by Yang et al. (2013) focus more on the different effects on interior panels and corner panels due to fire. Results showed that two types of panels behaved differently, which provides substantial evidence that the restraints have effects on the failure mode. The authors conclude that the interactions between adjacent elements have significant effects on the structural fire behaviour which is different from that observed in isolated member tests.

Figure 2.6 Failure mode of a simply supported RC slab at elevated temperatures (Bailey and Toh, 2007)

Another set of full-scale tests were carried out by Zhang et al. (2014) on simply supported two-way slab subjected to ISO fire curve. Despite the large deflections, the slabs did not collapse, and the author concludes that this is due to the tensile membrane action in slabs. This also agrees with the previous research done by Lim et al. (2004). They observed that the typical failure mode is fracture of reinforcement in the long span.

2.5.2 Other types of slabs

Apart from normal reinforced concrete slabs, research has been done on the fire behaviour of prestressed, post-tensioned and hollow-core slabs under fire. Aimin et al. (2013) have conducted studies on unbounded prestressed concrete slabs, and the results reveal that the failure mode is due to plastic hinges at internal supports and

cracking at internal mid-span. Experiments carried out by Hou et al. (2013) on the same type of slabs suggest that reinforcement layout and effective prestress has effects on the failure mode. The authors conclude that by extending the negative reinforcement, fire resistance can be improved. Also, the paper highlights that for high effective prestress, the stress reduction in prestress steel wire will be high in fire. Both authors (Aimin et al., 2013, Hou et al., 2013) along with Zheng et al. (2010) present proof that higher degrees of prestressing can increase the risk of spalling.

Bailey and Ellobody (2009) have conducted experimental investigations on fire behaviour of bonded post-tensioned slabs. The findings highlight that restrained slabs performed better in fire. The authors observed cracks directly inline and parallel to the tendons, which are due to thermal stresses at relatively low tendon temperatures. Gales et al. (2011) have observed a similar behaviour and go on to conclude that the localised heating of UPT tendons induces premature tendon rupture during fire.

The behaviour of hollow-core slabs was studied by Shakya and Kodur (2015). They have found that the slabs can sustain a fire exposure up to 2 hours under service loads. Furthermore, it points out that the axial restraints increase fire resistance by about 30 min.

A key finding from these studies is that axial restraint in slabs which could be due to restrained support conditions or prestress tendons has improved the fire resistance. This observation is important when analysing the results from fire tests on flat slabs. More details will be discussed in the following section.

2.6 EXPERIMENTAL INVESTIGATIONS ON FLAT SLABS IN FIRE

Compared to the number of studies on conventional slabs in fire, there are only a limited number of studies conducted to evaluate the behaviour of flat slabs in fire. Among those, certain experiments were the basis for the guidelines laid out in design codes related to fire design of flat slabs. This section will discuss the test methodology, key findings, limitations and the development of fire tests on flat slabs.

2.6.1 Test by Kordina (1993)

A series of fire tests conducted by Kordina (1993) is the basis for the fire design guidelines related to flat slabs. Minimum thickness specification for fire-resistive design of concrete flat slabs in BS EN 1992-1-2 (European committee for

standardization, 2004b) and AS 3600 (Standards Australia, 2009) is based on these tests.

The tests utilized a slab panel (2.5m x 2.5m) connected to a single central column with loading applied via a ring to the slab panel to simulate uniformly distributed load (see Figure 2.7). This setup would not allow for any catenary actions to be considered between columns. Ten slabs with a thickness of 200 mm and 4 slabs with a thickness of 150 mm were subjected to standard ISO 834 fire on the compression side. The failure mechanism observed for all the cases was punching shear failure with time to failure varied from 17 min to 120 min. With such a loading arrangement for a slab supported on a single column, it is clear that failure mechanism can only be punching shear after top reinforcement has yielded. The angle of the failure cone averaged 32^0. Some test specimens showed signs of spalling as well.

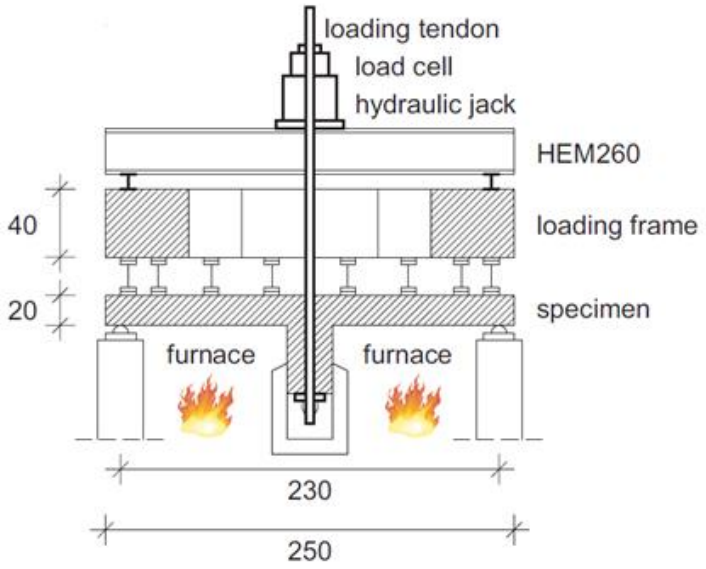

Figure 2.7 Test set-up used by Kordina (1993) as represented by Bamonte et al. (2012)

The test load applied to the specimens were different in all the cases. The load was increased during the first 30 mins of fire exposure to simulate the expected redistribution of internal forces during a fire. Six out of 14 specimens have failed during this first 30 mins while the load is still being increased. Since the level of loading is different for all the cases, it is difficult to establish a correlation between the fire resistance period and other parameters such as thickness, concrete strength and reinforcement ratio. However, in all the cases, failure load was greater than the design punching shear capacity (V_{Rd}). In the design codes, the load in the case of a fire is considered as 70% of the ambient design loads. Although at the beginning, the load

was similar to that level, the increase of load during the initial phase resulted in a load higher than V_{Rd}. Therefore, derived fire resistance durations can be conservative.

The specimens employed in the experiment were simply supported and free to expand in the lateral direction. A critical comment made by the Eurocode code committee (Anderberg et al., 2004) due to such arrangement is that it would not capture the membrane effect during a fire. In a real building floor arrangement, the flat slab is continuous, and due to this continuity, adjacent slab panels will resist against the lateral expansion. That will create a membrane action, and it is speculated that this would reduce the amount of deformation, thus increasing the fire resistance. More details about the membrane action will be given in Section 2.7. Without this action, fire resistance obtained by isolated member tests without lateral restraints can be conservative.

2.6.2 Test by Salem et al. (2012)

Salem et al. (2012) conducted a series of fire tests on 14 flat slab specimens of 1.1 m x 1.1 m having a thickness of 100 mm. Instead of applying the load while being heated, they exposed the tension side of the slabs to a furnace specific fire (max. temp 180^{o}C – 420^{o}C) for a duration of 1, 2, and 3hrs. After they have cooled down the load was applied through the column stub until failure. Two cooling methods were implemented, gradual cooling in air and sudden cooling with the spraying of water. Residual punching shear capacity was determined in this case instead of a fire-resistance level.

The study concluded that the exposure of slabs to fire has resulted in a reduction of 18.3% to 43% of ultimate punching shear strength in ambient conditions. Furthermore, sudden cooling has resulted in reducing the punching shear strength by 25% more than the gradually cooled specimens. A fundamental limitation of this study is that no loading was applied when heating and therefore, coupled thermally induced and load-induced deformation is not taken into account. Moreover, the loading arrangement was isolated simply supported specimens which do not account for the membrane action. Small-scale specimens used in the study may not capture the full effect of punching shear, as the size effect directly influences the punching shear behaviour (Bažant and Cao, 1987).

2.6.3 Test by Liao et al. (2013)

Another series of fire tests were carried out by Liao et al. (2013) using 12 flat slab specimens of 1.8 m x 1.8 m and 1.2 m x 1.2 m, all having a thickness of 120 mm. Six of them were tested at ambient temperature to determine the punching shear strength, and six of them were tested for fire resistance. 4 specimens were subjected to heat on their tension side and the other 2 on their compression side. Slabs were exposed to the Standard ASTM E119 time-temperature curve (ASTM International, 2016). Applied load during fire was determined using the punching shear strength tests at ambient conditions rather than relying on the design shear strength calculated according to codes. 54% of the ultimate punching shear strength was applied during heating. The study aimed to find the influence of concrete strength (normal strength 32 MPa and high strength 58 MPa), tensile steel ratio (0.92% and 1.43%) and heated surface (tension or compression) on the fire resistance level.

Results show that the slabs subjected to heat in the compression side did not fail up to 8hrs, whereas slabs heated on the tension side failed at 4hrs. Slabs made using high strength concrete has spalled during heating, and their fire resistance was worse than that of normal strength concrete slabs. The failure angles reported were 33^{o}-38^{o}. Specimens having higher steel reinforcement ratio had slightly lower fire resistance. Authors concluded that this is due to higher thermal conductivity of steel. Support conditions used in these tests were also similar to previous tests with no restrains against lateral expansion.

2.6.4 Test by Annerel et al. (2013a)

First and the only instance where large-scale flat slab specimens (3.2 m x 3.5 m) were exposed to fire while being loaded is during the test series conducted by Annerel et al. (2013a). A total of 6 slabs having a thickness of 250 mm were tested, two at ambient temperature and 4 at elevated temperatures. Shear reinforcement was placed at some specimens to find out whether it will have any effect for fire resistance. Test arrangement was very similar to that of Kordina's (1993) tests, and slabs were exposed to standard ISO 834 fire for 120 mins. 70% of the ambient punching shear capacity calculated according to design codes were applied during fire.

It was found that shear reinforcement had no significant impact on fire resistance. Punching angle was found to be in the range of 17^{o} – 39^{o}. Although normal

strength (25 MPa) concrete was used and specimens were cured until moisture content dropped down to 3.5% - 4%, spalling was observed in the compression side. Two slabs which were loaded up to full service load (0.7 of V_{rd}) did not fail up to 2hrs of standard fire exposure. However, due to a technical fault, the load on the other two specimens were increased to 1.5 -2 times the full service load, and they failed after just 20 mins of standard fire exposure. The authors highlight the danger of potential brittle failure of flat slabs due to this increase of load. Support conditions for this test were also similar to previous tests which did not provide any lateral restraints.

2.6.5 Test by Ghoreishi et al. (2015)

Ghoreishi et al. (2015) have conducted a series of tests on 6 small-scale specimens of 1m x 1m having a thickness of 120 mm. They were exposed to a furnace specific time-temperature history and the maximum temperature reached was in the range of 250^{o}C – 320^{o}C which is far less than the temperature of the standard fire curves. Slabs were subjected to heat, and when the furnace test has reached a stable value, the load was applied to the column stub until failure. Such test configuration gives the punching shear strength at a particular temperature rather than capturing the complete behaviour of a slab in fire to determine the fire resistance level. The loads were compared with the failure load predicted by design codes. Design failure load at elevated temperature was simply calculated by accounting for the degradation of material properties in the ambient punching shear strength equation.

2.6.6 Test by Smith et al. (2014)

Smith et al. (2014) conducted the most recent series of fire tests on flat slabs at the University of Edinburgh fire lab. A total number of 15 specimens of 1.4 m x 1.4 m having thicknesses of 50 mm, 75 mm and 100 mm were exposed to a furnace specific fire having a maximum temperature around 550^{o}C. Three different reinforcement ratios (0%, 0.8% and 1.5%) were used for each thickness. 5 specimens were tested at the ambient conditions to find out the punching shear strength. 70% of the ambient capacity was applied on the column stub and maintained while heated. The main difference of this study compared to all other previous experiments is that it has used both unrestrained and restrained support conditions while loading. In the restrained specimens, both lateral translation and rotation were prevented. The same load was maintained during the cooling phase too, in order to evaluate the punching shear behaviour during cooling down.

Based on the results of these tests, some critical observations can be made. Fire resistance duration of the restrained specimens was higher than that of unrestrained specimens. This further strengthens the argument which states membrane action developed due to restrained support conditions could enhance the fire resistance of flat slabs. Another important finding is that some of the restrained specimens failed during the cooling phase. This is significant, as most of the fire tests considered only the heating regime and the fire resistance level is determined only during this heating regime. However, in an actual fire scenario in a building, the continuous flat slab (which is closely represented by the restrained specimens in this test) is subjected to both heating and cooling down. Often the firefighters underestimate the danger during this cooling down phase after extinguishing a fire, therefore, as future studies authors elaborate the importance of detailed studies during the cooling regime to find out the behaviour and residual capacity of flat slabs.

In summary, among the limited number of fire tests conducted on concrete flat slabs, they especially looked at the punching shear behaviour at elevated temperature as it was deemed to be the critical failure mode found in flat slab failures under fire. Majority of the experiments were conducted using small scale tests, and therefore, size effect on punching shear behaviour can be influential. Some are exposed to a furnace-specific time-temperature history while the others are exposed to standard fire conditions. Load levels and the application of loading is different from each test method. Therefore, it is difficult to compare all the results together in order to make persuasive arguments about fire resistance levels. Key outcomes from the analysis of different experiments are as follows.

- Isolated specimen tests having simply supported boundary conditions are not capable of capturing the membrane action on slabs. Thus, the fire resistance levels predicted are conservative. Only recently a test has been conducted on restrained slab specimens, and it showed that the restrained support conditions enhance the fire resistance. Such boundary conditions can closely represent the condition of a continuous flat slab in an actual building.
- Fire resistance of normal strength concrete specimens was better than that of high strength concrete specimens which were more susceptible for spalling.

- Shear reinforcement has little or no influence on the punching shear resistance at elevated temperatures.
- Reinforcement ratio has an impact on fire resistance, and slabs with higher steel reinforcement ratios have slightly lower fire resistance.
- Cooling phase can be critical as well, especially in restrained specimens as failure can occur during cooling down phase too.

2.7 MEMBRANE ACTION IN SLABS

Membrane action of slabs is due to the development of in-plane forces within the depth of the concrete slab (Bailey, 2004). This could be either tensile membrane action or compressive membrane action. The slab perimeter should be vertically supported and restrained against the horizontal movement for membrane action to occur. A slab exposed to fire on its bottom surface could induce large vertical displacements in the slab span (Burgress et al., 2013). This could result in tensile membrane action in the centre, and compressive membrane action around the perimeter of the slab, as shown in Figure 2.8, given that horizontal restraints are not provided at supports. When supports are restrained against the horizontal movement, only tensile membrane action occurs.

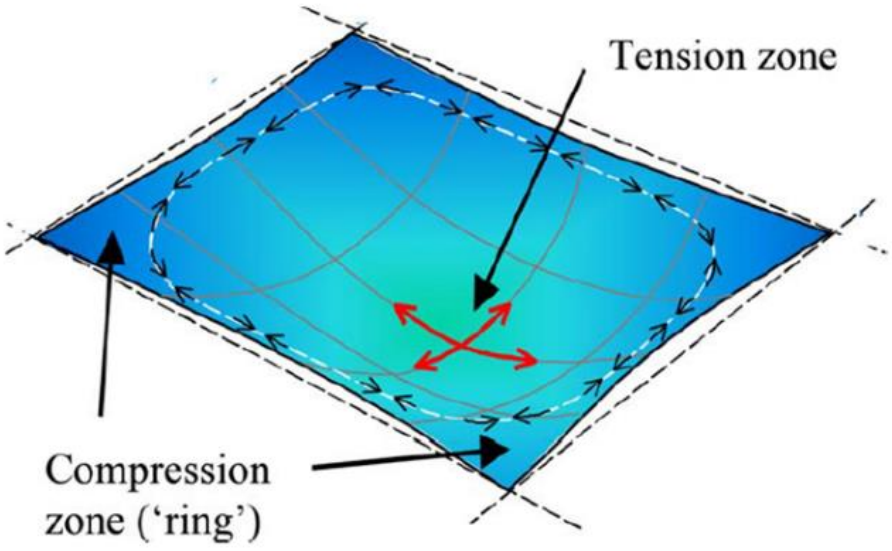

Figure 2.8 Membrane action of a floor slab with no horizontal restraint (Bailey, 2004)

It has been found that this membrane actions improve the flexural stiffness and load capacity of slabs in ambient conditions as well as in heated conditions (Gillie et al., 2002, Vecchio and Tang, 1990). Especially in fire scenarios which induce large vertical displacement both horizontally restrained and unrestrained slabs have performed better (Bailey, 2004). However, these studies were on slabs which have beams to support the edges. It is crucial to consider the applicability of this concept for flat slabs as well because it could significantly affect the resistance against fire.

A recent study carried out by Moss et al. (2008) describes a numerical model to analyse the fire behaviour of multi-bay two-way flat slabs. The author has used two fire scenarios; the standard ISO 834 fire for 4 hours and a parametric fire based on ISO 834 for one hour. Results showed that due to restraint conditions by adjacent slab panels and membrane action, 200mm thick slab has not failed during the test duration of 4 hours. Different types of behaviour were observed for a fire with a decay phase and a fire without a decay phase. The authors conclude that designers must ensure sufficient anchorage of top steel into edge beams to resist the tensile membrane forces. Although experimental investigations have not been carried out to prove the argument, the contrasting behaviour observed urges to reconsider the conservative approach in isolated element testing found in most of the experiments related to flat slabs in fire.

2.8 ANALYTICAL MODELS TO ASSESS THE FIRE PERFORMANCE OF CONCRETE FLAT SLABS

When a flat slab is subjected to fire, two phenomena occur. First, the material strength of both concrete and reinforcing steel degrades as a result of the elevated temperature. Secondly, the axial load induced in the columns supporting the slab increases as a result of the moment redistribution occurring due to thermal deformations (see Figure 2.9). As a result of that, the most common failure mechanism reported is the punching shear failure near the slab -column connection. Analytical models to assess the fire performance of flat slabs are basically evaluating the punching shear resistance at elevated temperature. These models are extensions of the ambient punching shear capacity models incorporating material degradation and additional effects due to thermal deformations.

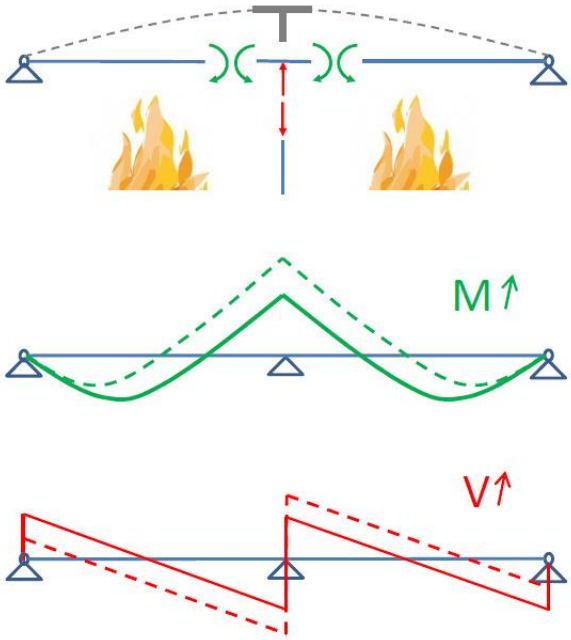

Figure 2.9 Increase of moment and shear due to fire as illustrated by Annerel and Taerwe (2015)

2.8.1 Effective section method

The effective section method is based on the 500°C isotherm method proposed in Eurocode 2; EN 1992-1-2 (European committee for standardization, 2004b). According to this method, a section of the structural element where the temperature is more than 500°C is considered to have no strength at all, and the remaining section where the temperature is lower than 500°C is considered to have full strength similar to ambient conditions. The capacity of the structural element is then calculated considering this remaining section below 500°C.

Bamonte et al. (2009) further developed this method specifically for punching shear in flat slabs by incorporating the reduction of the critical perimeter. Critical perimeter is the area around the column which is considered to contain the punching shear cone during punching shear failure. The dimensions of this critical shear perimeter depend on the effective depth. Due to fire, the effective depth of the slab section reduces in accordance with the 500°C isotherm method, and therefore it affects the critical perimeter as well. Bamonte et al. (2009) incorporated that using following equations [eqn. (2.3) and eqn. (2.4)].

$$D(t) = d(0) - w(t) \tag{2.3}$$

$$U_1(t) = u_1(0) - \alpha w(t) \tag{2.4}$$

Where d(0) and $u_1(0)$ are the effective depth and critical perimeter at the ambient conditions, respectively. D(t) and w(t) are the effective depth and fully damaged depth at elevated temperature. Critical perimeters given by EC2 and ACI 318 are different and therefore depending on the use of code, α is 24 (if using EC2) and 12 (is using ACI) for a rectangular section. Punching shear strength ($V_R(T)$) at a temperature T with relative to shear strength at ambient conditions ($V_R(20)$) is expressed using equation (2.5) according to the proposed method.

$$\frac{V_R(T)}{V_R(20)} = \left[1 - \frac{\alpha w(T)}{u_1}\right] \times \left[1 - \frac{w(T)}{d}\right] \tag{2.5}$$

This method is one of the simplest in its form and is based on the assumption that material strength does not degrade if the temperature is below 500°C, which is not valid. Therefore, this method is a good approximation of the punching shear strength at elevated temperature but should be used with caution.

2.8.2 Extended critical shear crack theory

Muttoni (2008) proposed the Critical Shear Crack Theory (CSCT) to evaluate the punching shear strength near the column-slab connection in ambient conditions. In this method, the punching behaviour is explained by a shear crack which penetrates the complete depth of the section (defined as the critical crack), and the subsequent rotation of the section beyond the crack. More details of the derivation can be found in Muttoni (2008). Failure load is determined by the intersection point of the load-rotation curve and the shear capacity vs rotation curve (failure criterion) as illustrated in Figure 2.10.

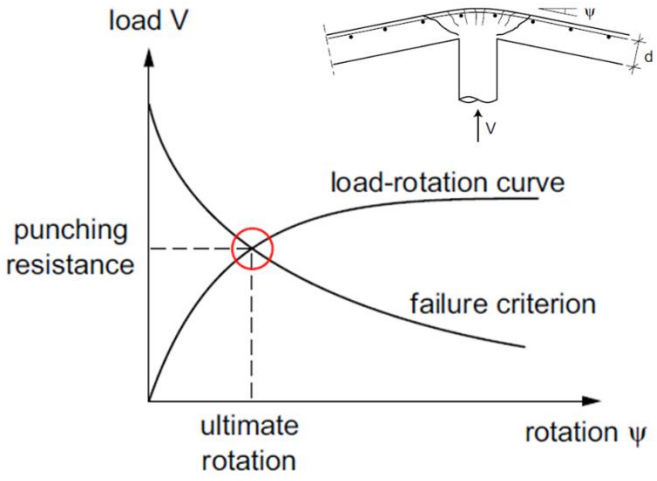

Figure 2.10 Punching shear resistance according to CSCT as illustrated by Bamonte et al. (2012)

Muttoni (2008) proposed the following equation [eqn. (2.6)] to be used to derive the failure criteria. It is based on the assumption that the shear strength depends on the size of the critical crack and the aggregate interlock within the cracked zone.

$$V_R = \frac{0.75\ (u_1 \times d \times \sqrt{f_c'}}{1 + 15 \times \left[\frac{\varphi \times d}{16 + d_g}\right]} \tag{2.6}$$

u_1 – critical perimeter

d – effective depth

d_g – maximum size of aggregate

f_c'- concrete strength

V_R- punching shear strength

φ- rotation

A relationship for the load rotation curve was developed considering the equilibrium of forces acting on the outer rigid radial section beyond the cracked zone, and the relationship is as follows [eqn. (2.7)].

$$\varphi = 1.5 \times \frac{r_s}{d} \times \frac{f_y}{E_s}\left[\frac{V_R}{V_{flex}}\right]^{3/2} \tag{2.7}$$

Where; $V_{flex} = 2\pi \times m_R \times \frac{r_s}{(r_q - r_c)}$

f_y – flexural reinforcement yield strength

m_R – nominal moment capacity per unit width

E_s- flexural reinforcement Young's modulus

However, this equation (2.7) was derived for an axisymmetric circular slab, whereas most of the flat slab specimens tested were square ones. In order to use the same equation r_s and r_q values need to be derived for a square slab according to the following equations [eqn. (2.8) and eqn. (2.9)].

$$r_s = \frac{4}{\pi} \cdot \frac{r_q - r_c}{a - c} \cdot \frac{a^2 - (a.c) - \frac{c^2}{4}}{[a + b_1 - 2(c + b_2)]} \tag{2.8}$$

$$r_q = \sqrt{\left(\frac{a}{2} - b_2\right)^2 + \frac{b_1^2}{4}} \tag{2.9}$$

All parameters are illustrated in Figure 2.11.

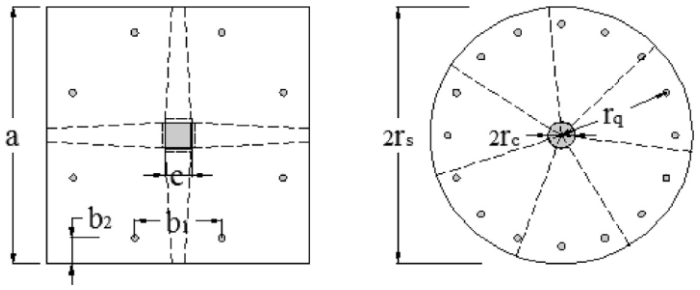

Figure 2.11 Parameters for equations 8 and 9 Arna'ot et al. (2017)

Bamonte et al. (2012) modified this CSCT to be used in elevated temperatures incorporating the material degradation and additional rotation and thermal displacement induced due to thermal strains of the slab. Critical perimeter (u_1) and effective depth (d) was reduced in the failure criterion [eq. (2.3) & (2.4)] to implicitly account for the reduction in compressive strength at elevated temperatures. For the load- rotation curve, two components of displacements were taken into account. Displacement due to load (δ_{load}) and thermal sagging (δ_{th}). The principle of superposition was used to find the total effect of both these components on the load rotation curve, as illustrated in Figure 2.12.

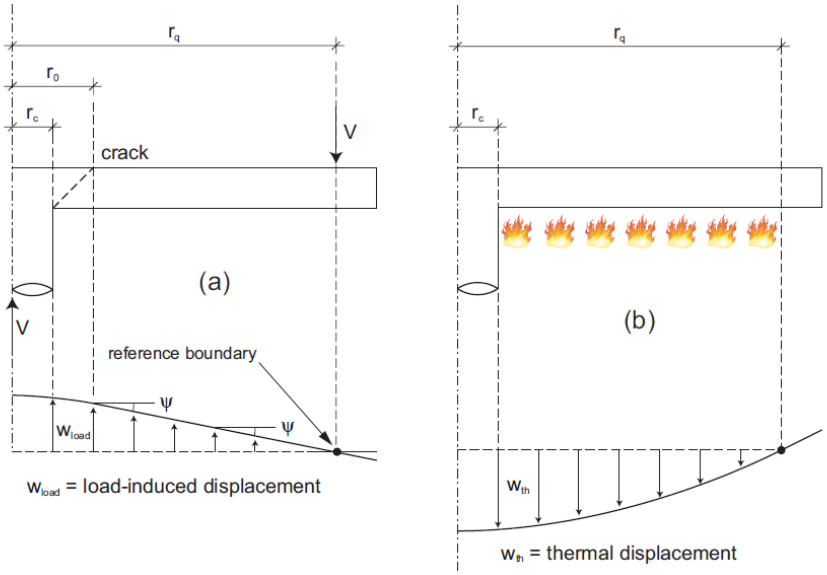

Figure 2.12 Deformation due to loading and thermal effect (Bamonte et al., 2012)

The use of this method can be found in the literature by Smith et al. (2015) to compare the failure loads predicted by modified CSCT with their experimental results. A reasonable agreement was found between the predicted capacities and experimentally measured values. Figure 2.12 illustrates the effect of elevated temperature on the load-rotation curve and the failure criterion curve, which ultimately results in a reduction of punching shear strength.

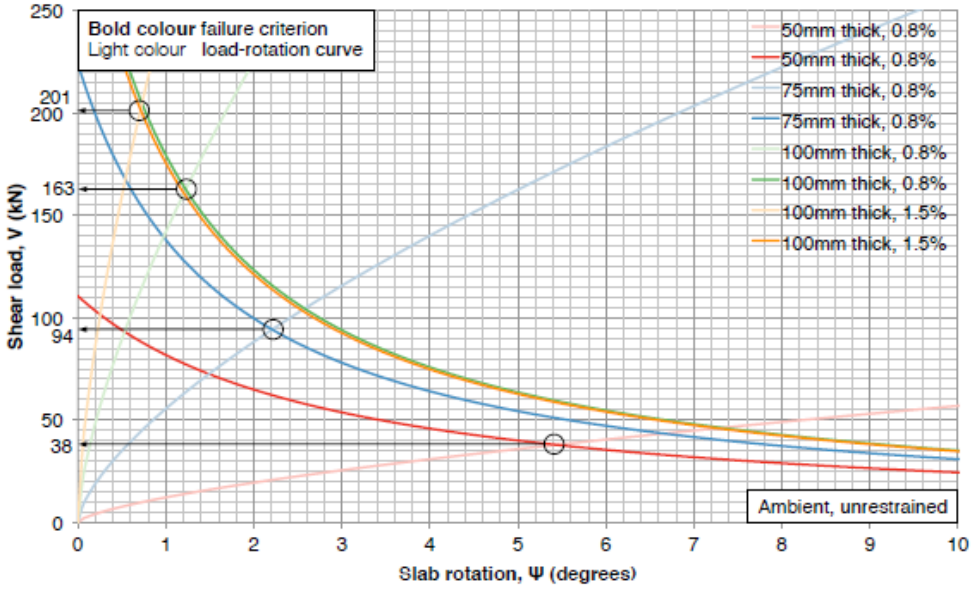

(a) Ambient temperature

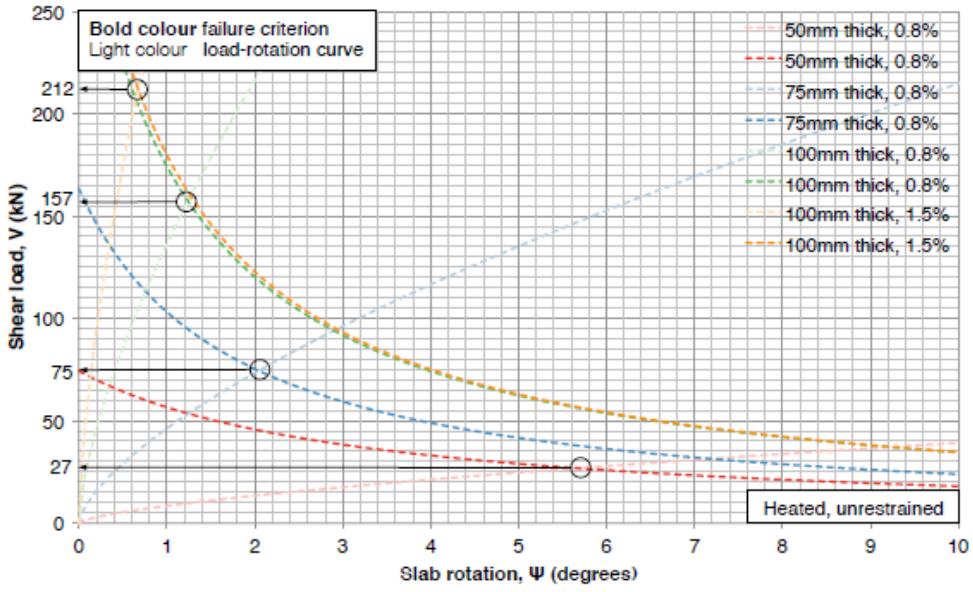

(b) Elevated temperature

Figure 2.13 Application of CSCT at (a)ambient and (b)elevated temperature conditions (Smith, 2016)

One crucial assumption in this calculation by Smith et al. (2015) is that the material strength values were degraded considering the maximum temperature experienced by the slab specimen, not the average temperature across the whole thickness. As Arna'ot et al. (2017) point out this assumption can be valid for relatively thin slabs (50 – 100 mm) tested by Smith et al. (2014), however, may not be valid for thick slabs (in the order of 200 – 250 mm). Practically, the exposed surface temperature could be much higher than the temperature within the slab. Therefore, based on this assumption, calculations would consider a much lower strength for concrete, which

ultimately could yield a very low punching shear strength than the experimentally measured value. Therefore, using the averaged temperature across the depth of the slab could yield more accurate results.

2.8.3 Modified Theordorkapoulos Model

A shear strength model proposed by Theodorakopoulos and Swamy (2002) was modified by Ghoreishi et al. (2015) to be used in the case of fire. The original model proposed by Theordorkapoulos et al. is as follows [eqn. (2.10) & (2.11)].

$$V_R = u_1 \times X \times cot\emptyset \times f_{ct} \tag{2.10}$$

Where;

$$\frac{1}{X} = \frac{1}{2X_f} + \frac{1}{2X_s} \tag{2.11}$$

u_1- critical perimeter according to BS 8110 (British Standard Institute, 1985)

Ɵ - Crack angle assumed to be 30^o

x_s – 0.25 of the effective depth d

f_{ct} – tensile strength from indirect splitting test

Following assumptions were made during the modification of the above theory for elevated temperature case.

- Critical perimeter is 1.43d distance away from the column face
- $f_{ct} = 0.323f'^{2/3}_c$ where f'_c is the concrete cylinder strength
- Reduction of concrete strength is assumed according to EC2 (European committee for standardization, 2004b)
- X_f is computed in accordance with Canadian Concrete Standards CSA A23.1 (Canadian Standard Association, 2014)

With the proposed modifications the punching shear strength at elevated temperature (V_R) is given by equation (2.12);

$$V_R = 2.238(c + 2.86d) \times X \times (f'_c)^{2/3} \tag{2.12}$$

c – column size

d – effective depth

Apart from Ghoerieshi, Arna'ot et al. (2017) have used this model to compare 10 different experimental results and found reasonable agreement with the predicted

values. Given the simplicity of the model, it can be used with caution to estimate the punching shear resistance at elevated temperatures.

2.9 THERMO-MECHANICAL MODELLING OF STRUCTURES EXPOSED TO FIRE

Simulation of behaviour under a fire scenario is twofold. The model should accurately predict the thermal behaviour, which describes the temperature variation and heat transfer across the element with time when exposed to fire. Apart from that, the model should be able to determine the deformation and stresses occur, and the overall structural behaviour as a result of the elevated temperature. Some computer programs have been developed specifically for this purpose (structural fire modelling), and on the other hand, general-purpose finite element modelling packages can be used to incorporate the effects of fire in the structure. Table 2.2 provides an overview of the software and their capabilities which have been utilized to study the thermal and structural behaviour of assemblies under fire.

Table 2.2 Software packages commonly used for fire modelling

Software	Used by	Analysis type	Outputs	Limitations/ Advantageous
SAFIR	Lim et al. (2004) Moss et al. (2008)	Integrated thermal and structural analysis program for performing non-linear 2D and 3D analyses of steel, concrete and composite structures in fire	▪ Temperature distribution ▪ Deformation ▪ Stresses	Difficult to model a complex assembly
ANSYS	Shakya and Kodur (2015)	Accounts for geometric and material nonlinearities, support conditions and temperature-dependent thermal and mechanical properties of concrete and steel.	▪ Temperature distribution ▪ Deformation (displacement and rotation) ▪ Stresses (bending, shear)	General-purpose FE analysis program with a user-friendly GUI. Capable of modelling any structural arrangement.

ABAQUS	George and Tian (2012) Sangluaia et al. (2013) Ellobody and Bailey (2009) Kodur and Alogla (2017)	Non-linear 2D and 3D thermal and structural analysis.	▪ Temperature distribution ▪ Deformation (displacement and rotation) ▪ Stresses (bending, shear)	General-purpose FE analysis program with a user-friendly GUI. Possible to model any structural arrangement. Visualisation of time dependant results is promising
VULCAN	Huang et al. (1999)	Three-dimensional analysis of the structural behaviour of composite steel-framed buildings in fire	Deflection and Stresses only	More of a numerical procedure with less involvement of a GUI. Difficult to model a complex assembly
PC Temp		1-D thermal analysis	Temperature distribution across the thickness with time or position Stresses	Limited to plate like shapes only Does not generate temperature or stress contours.
TASEF	Thomas et al. (1995) Thomas (2010)	A special-purpose program for calculating temperatures in structures exposed to fire.	Time-temperature curves for different nodes, isothermal lines, temperature fields	Limited only to thermal analysis
Pyrosim/ FDS	Nguyen et al. (2013) Rajendram et al. (2015)	Simulates fire scenarios using computational fluid dynamics (CFD) optimized for low-speed, thermally driven flow.	The spread of smoke temperature distribution Spread of carbon monoxide, and other substances during fires	A comprehensive fire dynamic simulator but limited to thermal and smoke analysis only

According to the comparison, some programs are only capable of thermal analysis, while others are capable of both thermal and mechanical analysis. Some have a graphical user interface (GUI) which makes it more user-friendly whereas some

programs require the user to input data in the form of a programming language. Another critical aspect is the diverse and meaningful outputs that can be easily visualised. Considering all these criteria, FE package ABAQUS was chosen as a versatile program which is well equipped with different types of elements and material models to simulate the behaviour of structures in fire. It has the capability of capturing the effect of the non-linear behaviour of material properties when the temperature changes. Furthermore, it can couple both thermal and mechanical analysis together to calculate the structural response. The ability to create complex 3-D geometries and visualise the results in a user-friendly manner is an added advantage. It has an inbuilt GUI and also allows for user-defined subroutines depending on the requirements of the analysis.

Another vital computer program in fire modelling is the Fire Dynamic Simulator (FDS). FDS is based on computational fluid dynamics (CFD), and it is widely used by both researchers and industry to model the behaviour of fire. Pyrosim, which is a separate GUI developed to be used in the case of compartment fires (fires in buildings), can be used to generate the input code for FDS. In FE packages such as ABAQUS, a predefined temperature or heat flux can be applied as a boundary condition to the structure for the thermal analysis. That temperature field or heat flux can be derived from standard fire curves in the design codes. However, the fire in a real building could depend on various factors such as the combustible fuel load within the building, the ventilation, building geometry and etc. Such parameters cannot be incorporated in an FE package explicitly. Therefore, CFD based programs such as FDS which are capable of taking into account the aforementioned parameters and generate the temperature fields and heat fluxes becomes very useful. With the tendency to go for performance-based design approach, the use of FDS provides more realistic fire resistance levels. Coupling the fire characteristics predicted by FDS with structural fire models in ABAQUS is the way forward in simulating structures exposed to fire.

2.9.1 Concrete Damage Plasticity (CDP) model in ABAQUS

It is crucial to incorporate the appropriate constitutive model to represent the behaviour of concrete at elevated temperatures accurately. Mainly, ABAQUS has three models to represent concrete: a) Brittle crack concrete model, b) Smeared crack concrete model and c) Concrete Damaged Plasticity (CDP) model. Numerous studies (Al Hamd et al., 2018, Albrifkani and Wang, 2016, Ellobody and Bailey, 2009, George

and Tian, 2012, Kodur and Agrawal, 2016, Wahalathantri et al., 2011) have used the CDP model to simulate the concrete performance in fire. Compression crushing and tensile cracking failure of concrete are accurately captured by the CDP model. The yield function [eqn. (2.13)] proposed by Oliver et al. (1989) and modified by Lee and Fenves (1998) is implemented in the model.

$$F = \frac{1}{1-\alpha}[\bar{q} - 3 \propto \bar{p} + \beta(\tilde{\epsilon}^{pl})\langle\hat{\sigma}_{max}\rangle - \gamma\langle-\hat{\sigma}_{max}\rangle] - \bar{\sigma}_c(\tilde{\epsilon}_c^{pl}) \qquad (2.13)$$

Where,

$$\propto = \frac{(\sigma_{b0}/\sigma_{c0}) - 1}{2(\sigma_{b0}/\sigma_{c0}) - 1}$$

σ_{b0} – Biaxial compressive strength

σ_{c0} – Uniaxial compressive strength

$(\sigma_{b0}/\sigma_{c0})$ – Usually taken as 1.16

$\bar{q}$ – Misses equivalent effective stress

$\bar{p}$- Hydrostatic pressure stress

$\beta(\tilde{\epsilon}^{pl}) = \frac{\bar{\sigma}_c(\tilde{\epsilon}_c^{pl})}{\bar{\sigma}_t(\tilde{\epsilon}_t^{pl})}(1-\alpha) - (1+\alpha)$; shows up only when $\hat{\sigma}_{max}$ is positive

And, $\bar{\sigma}_c(\tilde{\epsilon}_c^{pl})$ – Effective cohesion stress for compression

$\bar{\sigma}_t(\tilde{\epsilon}_t^{pl})$ - Effective cohesion stress for tension

$\gamma = \frac{3(1-K_c)}{2K_c-1}$; where K_c is the ratio of the tensile to compressive meridian, which defines the shape of the yield surface in deviatory plane as shown in Figure 2.14. K_c = 2/3 corresponds to Rankine formulation. γ is active when $\hat{\sigma}_{max}$ is negative. (i.e. Triaxial compression)

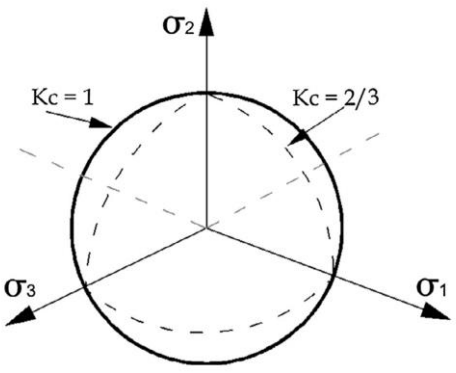

Figure 2.14 Yield surface in the deviatory plane (Genikomsou and Polak, 2015)

The CDP model includes the following flow potential function, which is a non-associated Drucker-Prager hyperbolic function [eqn. (2.14)].

$$G(\sigma) = \sqrt{(\varepsilon\sigma_{t0}\tan\psi)^2 + \bar{q}^2} - \bar{p}\tan\psi \tag{2.14}$$

Where,

ψ- Dilation angle measured in at high confining pressure.

ε- Eccentricity; Default value 0.1 (Dassault Systèmes, 2014)

Figure 2.15 schematically represents dilation angle ψ and eccentricity ε in the meridian plane

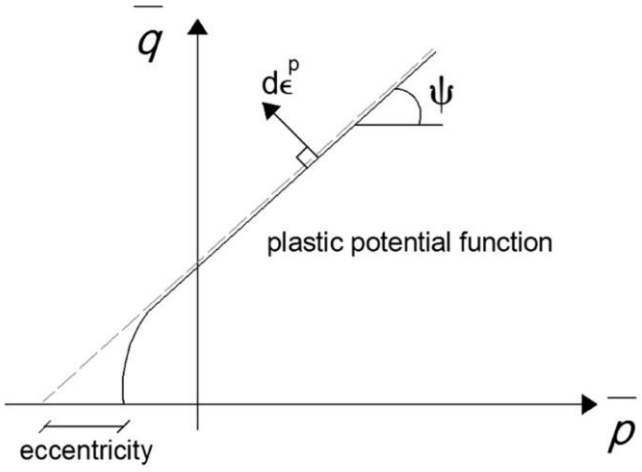

Figure 2.15 Dilation angle and eccentricity in meridian plane (Genikomsou and Polak, 2015)

Damage is introduced to the model by two parameters; d_t (damage in tension) and d_c (damage in compression). With the inclusion of damage, the effective tensile ($\bar{\sigma}_t$) and compressive ($\bar{\sigma}_c$) cohesion stresses are as follows [eqn. (2.15) & (2.16)] (Dassault Systèmes, 2014).

$$\bar{\sigma}_t = \frac{\sigma_t}{(1-d_t)} = E_0(\varepsilon_t - \tilde{\varepsilon}_t^{pl}) \tag{2.15}$$

$$\bar{\sigma}_c = \frac{\sigma_c}{(1-d_c)} = E_0(\varepsilon_c - \tilde{\varepsilon}_c^{pl}) \tag{2.16}$$

Where,

E_0- Initial(undamaged) elastic stiffness

ε_t and ε_c- Total tensile and compressive strain

$\tilde{\varepsilon}_t^{pl}$ and $\tilde{\varepsilon}_c^{pl}$- Equivalent plastic strains

Damage in CDP accounts for the irrecoverable inelastic strain when concrete is loaded and then unloaded (cyclic loading). Damage is also important to formulate the energy balance equation which consists of elastic and inelastic components. However, in monotonic loading if formulation is done based on total energy or force balance, damage parameters will not be incorporated. Therefore, the damage parameter is omitted in some studies (Genikomsou and Polak, 2015) on punching shear behaviour as the loading is static and loaded only once until failure. However, if the slab undergoes progressive failure, there is a possibility of stress redistribution, hence unloading will occur in localized regions. Therefore, the choice of using the damage parameter will depend on many factors.

Viscoplastic regularization can be introduced to the model by defining the viscosity parameter μ. This technique is used to overcome convergence difficulties. While small values of μ produce more accurate results, it can significantly increase the analysis time and more vulnerable to convergence issues. A viscosity of 0.000t is recommended for analysis at high temperature (Wahid et al., 2019a), where t is the duration of the analysis in seconds or minutes. However, if damage parameters are omitted then there is no requirement of having a viscosity parameter. This explains why some studies has used μ=0 (see Table 2.3)

Table 2.3 summarises the values of the key parameters of CDP model used by several researchers (Al Hamd et al., 2018, Albrifkani and Wang, 2016, Ellobody and Bailey, 2009, Genikomsou and Polak, 2015, Genikomsou and Polak, 2017, Wahalathantri et al., 2011) to represent concrete behaviour at elevated temperatures accurately.

Table 2.3: Parameters used in the CDP model in ABAQUS

Dilation angle (ψ)	Eccentricity (ε)	σ_{b0}/σ_{c0}	K_c	Viscosity parameter (μ)
30^o – 40^o	0.1	1.16	0.667	0 - 0.001

2.9.2 Material properties at elevated temperature

Defining the correct material properties that account for the change of temperature is vital in structural fire models. With relevant to flat slabs, material properties of concrete and reinforcing steel at elevated temperatures will be discussed in this section. Material properties can be divided into two main categories. Thermal

properties of the material which are utilized for the heat transfer model in thermal analysis and, Mechanical properties of the material which are utilized for the structural analysis in fire. Under thermal properties, conductivity and specific heat will be explained, and under mechanical properties stress-strain behaviour, Young's modulus, creep and thermal elongation will be considered.

2.9.2.1 Thermal properties

Three-dimensional heat transfer in the slab is governed by the thermal conductivity and specific heat of the constituent materials. Density is an important property as well because it is related to thermal diffusivity. However, it is acceptable to assume that the density of concrete and steel remains the same at elevated temperatures. However, thermal conductivity and specific heat vary with increasing temperature.

Several trends proposed by a few researchers and design codes for concrete are presented in Figure 2.16. Thermal properties of concrete depend on the type of aggregate used. Therefore, thermal conductivity is defined for two main aggregate types; carbonate/calcareous and siliceous aggregates. With the increasing temperature, the thermal conductivity decreases non-linearly due to degradation of the material. Among these models, the most widely used values are from the EC2 (European committee for standardization, 2004b). It has namely two limits; upper limit and lower limit. EC2 suggests using the lower limit for modelling as it is based on experimental data.

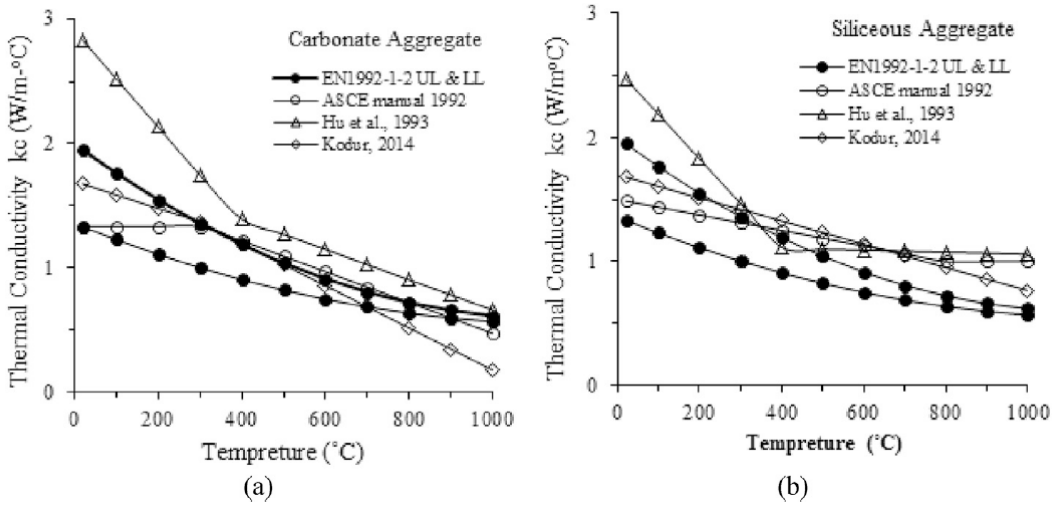

Figure 2.16 Thermal conductivity models for concrete (Arna'ot et al., 2017)

For reinforcing steel, most widely used thermal properties for fire design can be found in Eurocode 3. The variation of thermal conductivity at elevated temperatures according to the relationships in EC3 (European committee for standardization, 2005a) is presented in Figure 2.17. From ambient temperature up to 800^{o}C thermal conductivity reduces linearly from 54 W/mK to 27.3 W/mK and remains constant after 800^{o}C.

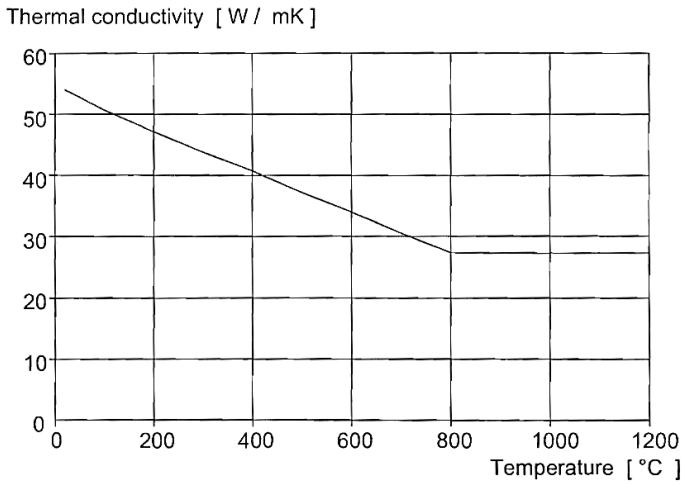

Figure 2.17 Variation of thermal conductivity of steel (European committee for standardization, 2005a)

Specific heat of concrete remains more or less at a constant value with increasing temperature. However, specific heat is artificially increased at 100^{o}C to explicitly account for the effect of the moisture trapped within the concrete in heat transfer. (see Figure 2.18). The amount of increment will depend on the moisture content percentage. The effect of this is useful to accurately capture the temperature plateau, which occurs at around 100^{o}C in a time-temperature history measured during experiments. Although EC2 (European committee for standardization, 2004b) does not differentiate between carbonate and siliceous aggregates for specific heats, some other models in literature have proposed two separate models considering the type of aggregate.

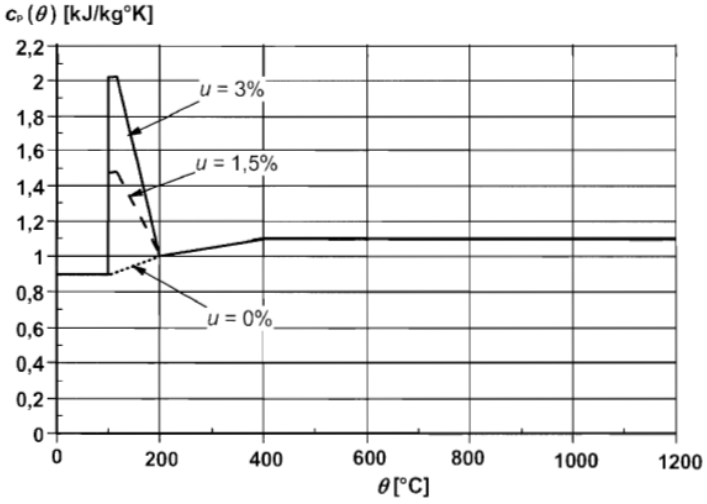

Figure 2.18 Variation of specific heat capacity of concrete with temperature (European committee for standardization, 2004b)

Variation of specific heat of reinforcing steel at elevated temperatures can be derived from the relationships given in EC3 (European committee for standardization, 2005a) as follows (see Figure 2.19). There is a sudden increase in specific heat at around 730^{o}C, which is due to a metallurgical change. Apart from that, the values hover around 550 – 650 J/kg K. Some suggest that for simple calculations, specific heat can be taken as 600 J/kg K for all the temperatures (Buchanan and Abu, 2017).

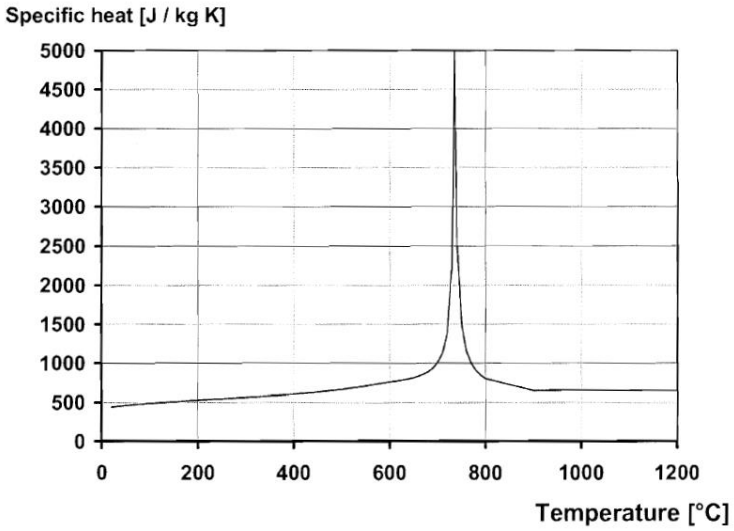

Figure 2.19 Variation of specific heat capacity of r/f steel with temperature (European committee for standardization, 2005a)

In summary, conductivity and specific heat of both concrete and steel vary with the increasing temperature. It is essential to incorporate these variabilities in the heat transfer model in order to predict the variation of temperature within the section accurately.

2.9.2.2 Mechanical properties

Mechanical properties, such as strength and stress-strain behaviour, Young's modulus and thermal elongation are the main inputs for the mechanical model. It simulates the structural behaviour of the slab according to the temperature variation predicted by the thermal analysis. Variation of these properties with temperature is mostly non-linear. Therefore, these values need to be cautiously implemented in numerical models.

Strength of concrete degrades with increasing temperature. Both compressive strength (f_c) and tensile strength of concrete (f_t) reduce with increasing temperature. The decay in tensile strength is much faster than the decay of compressive strength. Figure 2.20 shows the trend in decay proposed by several researchers and design codes. When the temperature exceeds 900ºC – 1000ºC concrete completely loses its compressive strength. Stiffness of concrete significantly degrades when heated. It can be represented from the decay of the Young's modulus, as shown in Figure 2.21.

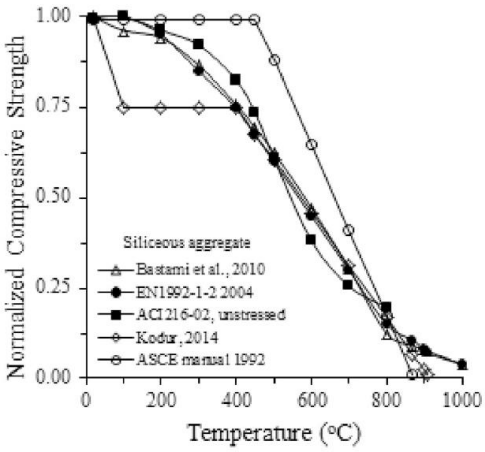

Figure 2.20 Decay of concrete compressive strength at elevated temperature (Arna'ot et al., 2017)

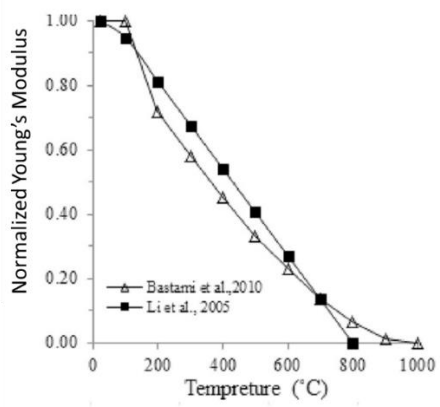

Figure 2.21 Decay of Young's Modulus of concrete at elevated temperature (Arna'ot et al., 2017)

After 600°C concrete loses all of its tensile strength according to the most widely implemented EC2 model (European committee for standardization, 2004b) for tensile strength degradation at elevated temperatures (see Figure 2.22). However, this can lead to convergence errors in numerical models. As a remedy, Dwaikat and Kodur (2009) have proposed a relationship for concrete tensile strength (f_{tT}) beyond 600^0C (eqn. (2.17)). In some models, tensile strength at elevated temperature is completely neglected and only the compressive strength considered.

$$f_{tT} = \begin{cases} f_t, & T \leq 100^0C \\ f_t\left(\frac{600-T}{500}\right), & 100^0C < T \leq 550^0C \\ f_t\left(\frac{1200-T}{6500}\right), & 550^0C < T \leq 1200^0C \\ 0, & T > 1200^0C \end{cases} \quad (2.17)$$

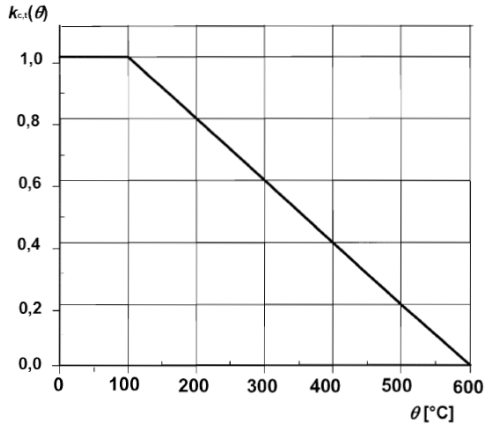

Figure 2.22: Coefficient $k_{c,t}(\Theta)$ allowing for the decrease of the tensile strength of concrete at elevated temperatures (European committee for standardization, 2004b)

Tensile behaviour of concrete can be represented using several approaches in CDP model in ABAQUS. It can be expressed using either cracking strain, crack displacement or fracture energy. The selection of the appropriate method heavily influences in achieving a convergent solution for the non-linear numerical analysis. By evaluating the available literature, it was found that the tensile cracking strain based on the fracture energy has yielded accurate results avoiding convergence issues (Ellobody and Bailey, 2009, Genikomsou and Polak, 2015, Wahid et al., 2019a). Therefore, a similar method is adopted in this study and the derivation of tensile properties at elevated temperatures are as follows (Genikomsou and Polak, 2015).

a) The stress-strain relationship of concrete in tension increases linearly from 0 to tensile strength (f'_t) according to Figure 2.23. The gradient of that part is the corresponding Young's modulus (E_0) at that temperature.

b) The softening phase after cracking is represented by a bilinear stiffening response until the ultimate strain (ε_u) is reached.

c) To determine ε_1 and ε_u, the crack widths w_1 and w_u were calculated according to Figure 2.24.

d) The fracture energy (G_f) is defined by the following equation (eqn. (2.18)) proposed by CEB-FIP model code (Comite Euro-International Du Beton, 1993).

$$G_f = G_{fo}(f_{cm}/f_{cmo})^{0.7} \qquad (N/mm) \tag{2.18}$$

Where, G_{fo} is the base fracture energy of 0.0026N/mm corresponding to a maximum aggregate size of 10mm. f_{cmo} is equal to 10 MPa and f_{cm} is the mean compressive strength of concrete given by, $f_{cm} = f_{ck} + 8$ (f_{ck}- characteristic compressive strength).

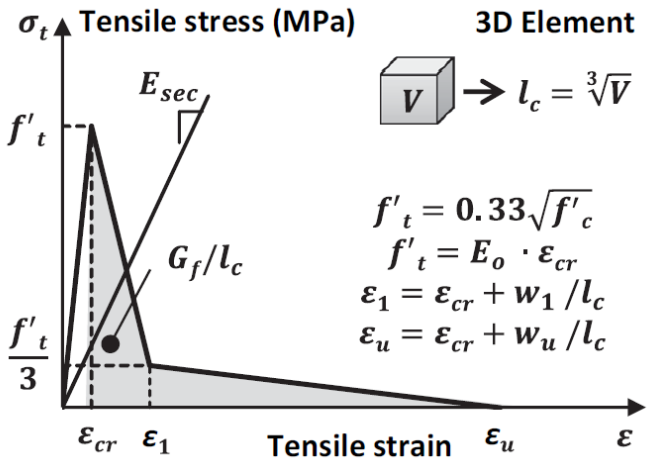

Figure 2.23: Tensile stress-strain relationship for concrete (Genikomsou and Polak, 2015)

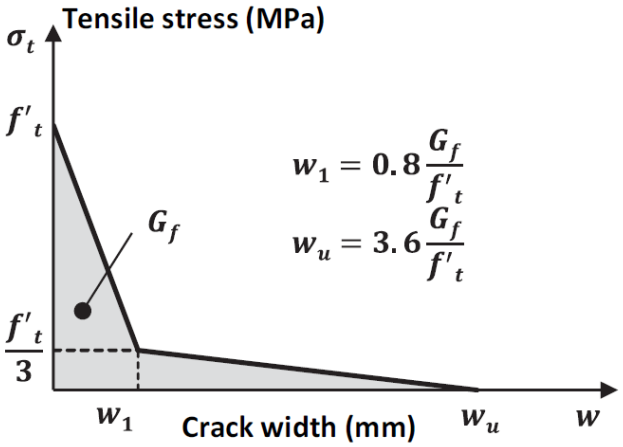

Figure 2.24: Tensile stress-crack width relationship for concrete (Genikomsou and Polak, 2015)

Relationships that explain the compressive stress-strain behaviour of concrete at ambient conditions can be further extended to represents its performance at elevated temperature. Key parameters affected by heating are the compressive strength, strain at ultimate strength and fracture strength. Several key models proposed by different studies and design codes are as follows (see Table 2.4).

One of the most commonly used models is the relationships proposed by EC2 (European committee for standardization, 2004b). The latest version of the stress-strain model for concrete accounts for creep explicitly whereas the previous version did not. Figure 2.25 illustrates the variation of stress and strain at different temperatures according to the EC2 model. It allows the use of linear or parabolic softening branch after yielding of concrete.

Table 2.4: Different stress-strain relationships for concrete at elevated temperatures

Reference	**Stress-strain relationship at elevated temperatures**
Kodur (2014)	$\sigma_{cT} = f'_{cT}\left[1 - \left(\frac{30(\varepsilon_{cT} - \varepsilon_{max}}{\varepsilon_{max}(130 - f'_c)}\right)^2\right]$, $\varepsilon_{cT} > \varepsilon_{max}$ $\sigma_{cT} = f'_{cT}\left[1 - \left(\frac{(\varepsilon_{max} - \varepsilon_{cT})}{\varepsilon_{max}}\right)^2\right]$, $\varepsilon_{cT} \leq \varepsilon_{max}$
Bastami et al. (2010)	$\sigma_{cT} = f'_{cT}\left[\frac{(a + bt + c).(\varepsilon_{cT}/\varepsilon_{max})}{a + bt + c - 1 + (\varepsilon_{cT}/\varepsilon_{max})^{a+bt+c}}\right]$, $\varepsilon_{cT} > \varepsilon_{max}$ $\sigma_{cT} = f'_{cT}\left[\frac{c.(\varepsilon_{cT}/\varepsilon_{max})}{c - 1 + (\varepsilon_{cT}/\varepsilon_{max})^{c}}\right]$, $\varepsilon_{cT} \leq \varepsilon_{max}$ Where, $a = 2.7(12.4 - 1.66 \times 10^{-2} f'_{cT})^{-0.46}$ $b = 0.83\exp(-911/f'_{cT})$ $c = [1.02 - 1.17(E_p/E_c]^{-0.74}$

EC2 EN 1992-1-2 (European committee for standardization, 2004b)	$\sigma_{cT} = f'_{cT}\left[\frac{3\varepsilon_{cT}}{\varepsilon_{max}\left(2+\frac{\varepsilon_{cT}}{\varepsilon_{max}}\right)^3}\right], \varepsilon_{cT} \leq \varepsilon_{cu}$

** σ_{cT} – stress at temperature T, f'_{cT}- compressive strength at T, f'_c- compressive strength at room temperature ε_{cT}- compressive strain at T, ε_{max}- ultimate strain

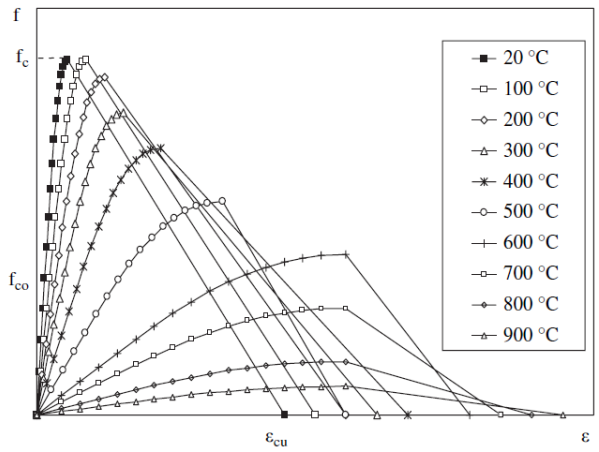

Figure 2.25 Typical stress-strain behaviour at different temperatures according to EC2 model (Ellobody and Bailey, 2009)

Similar to concrete, reinforcing steel also undergoes significant decay of strength when heated. Figure 2.26 shows the trend for reduction of yield strength and Young's modulus with temperature, according to Buchanan and Abu (2017). Note that there is a slight difference in the rate of decay for reinforcing steel vs structural steel.

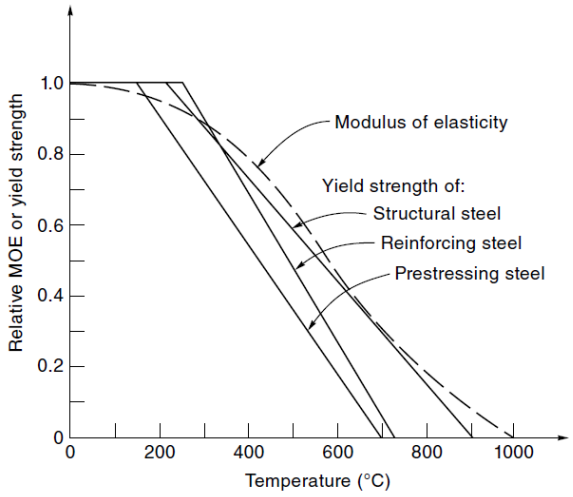

Figure 2.26 Decay of yield strength and Young's modulus of steel at elevated temperatures (Buchanan and Abu, 2017)

BS EN 1992-1-2 (European committee for standardization, 2004b) provides tabulated values for strength reduction factors for two classes of reinforcing steel;

namely class N and class X. Class N is generally recommended over class X when there is no experimental evidence available. The general stress-strain relationship is also given in the same code and for different temperatures. (see Figure 2.27).

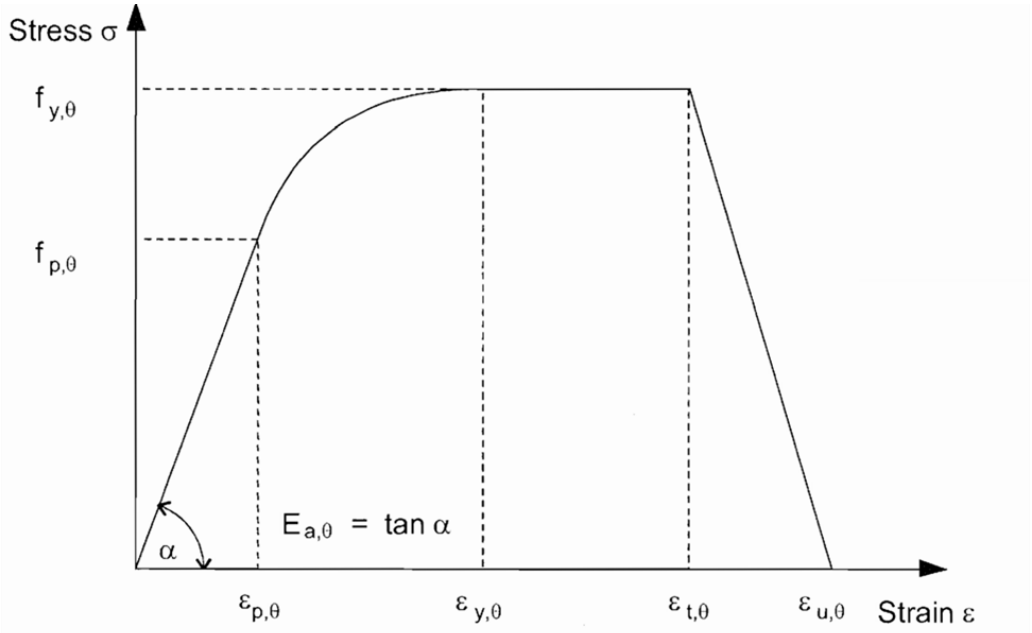

Strain range	Stress σ	Tangent modulus
$\varepsilon \le \varepsilon_{p,\theta}$	$\varepsilon E_{a,\theta}$	$E_{a,\theta}$
$\varepsilon_{p,\theta} < \varepsilon < \varepsilon_{y,\theta}$	$f_{p,\theta} - c + (b/a)\left[a^2 - \left(\varepsilon_{y,\theta} - \varepsilon\right)^2\right]^{0.5}$	$\frac{b\left(\varepsilon_{y,\theta} - \varepsilon\right)}{a\left[a^2 - \left(\varepsilon_{y,\theta} - \varepsilon\right)^2\right]^{0.5}}$
$\varepsilon_{y,\theta} \le \varepsilon \le \varepsilon_{t,\theta}$	$f_{y,\theta}$	0
$\varepsilon_{t,\theta} < \varepsilon < \varepsilon_{u,\theta}$	$f_{y,\theta}\left[1 - \left(\varepsilon - \varepsilon_{t,\theta}\right)/\left(\varepsilon_{u,\theta} - \varepsilon_{t,\theta}\right)\right]$	-
$\varepsilon = \varepsilon_{u,\theta}$	0,00	-
Parameters	$\varepsilon_{p,\theta} = f_{p,\theta}/E_{a,\theta}$ $\varepsilon_{y,\theta} = 0{,}02$ $\varepsilon_{t,\theta} = 0{,}15$ $\varepsilon_{u,\theta} = 0{,}20$	
Functions	$a^2 = (\varepsilon_{y,\theta} - \varepsilon_{p,\theta})(\varepsilon_{y,\theta} - \varepsilon_{p,\theta} + c/E_{a,\theta})$ $b^2 = c\left(\varepsilon_{y,\theta} - \varepsilon_{p,\theta}\right)E_{a,\theta} + c^2$ $c = \frac{(f_{y,\theta} - f_{p,\theta})^2}{\left(\varepsilon_{y,\theta} - \varepsilon_{p,\theta}\right)E_{a,\theta} - 2(f_{y,\theta} - f_{p,\theta})}$	

Figure 2.27 Stress-strain relationship for steel at elevated temperature as per the EC3 model (European committee for standardization, 2005a)

Thermal elongation is one of the critical input parameters for structural fire models which governs the overall behaviour of the slab. In most cases, the thermal deformation is much higher than the load-induced deformation. Thermal deformation is directly characterized by thermal elongation. Usually, the input variable will be the coefficient of thermal expansion (α) instead of thermal elongation. Therefore, the accuracy of the model is highly sensitive to thermal expansion input properties.

Thermal elongation of concrete also depends on the type of aggregates used. Figure 2.28 shows the thermal elongation relationship given by EC2 (European committee for standardization, 2004b) and other researchers for different types of concrete.

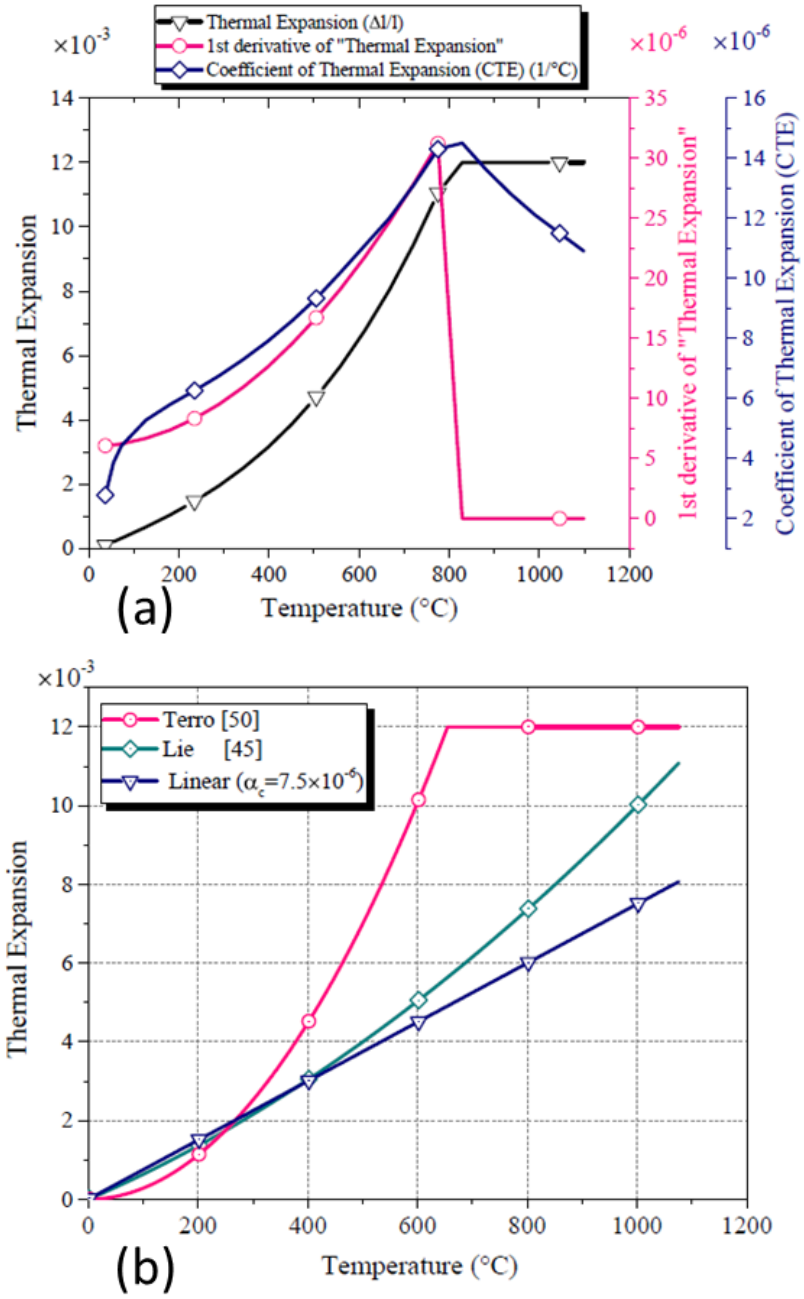

Figure 2.28 Thermal expansion models for concrete (a) EC2 model (b) Models by others (Hajiloo and Green, 2019)

In a fire, different layers across the slab are heated to different temperatures. Due to this, thermal deformation varies non-linearly across the depth of the slab as the thermal coefficient of expansion varies across the slab. In non-linear finite element

analysis, this could result in over predicting the deformation, or it could easily give conversion errors which may result in early termination of the analysis. To avoid this, some models have used a constant value for α such as 8.1 x 10^{-6} for concrete with limestone aggregates and 13.2 x 10^{-6} for concrete with Thames gravel aggregates (Ellobody and Bailey, 2009).

Thermal elongation of steel varies linearly with the temperature for most regions according to the relationship given in BS EN 1992-1-2 (see Figure 2.29). In the region 750^{o}C – 860^{o}C, it has a fixed thermal elongation. This is due to the metallurgical change occurring during that temperature range, which can also be seen from the specific heat variation (Figure 2.19). EC3 (European committee for standardization, 2005a) recommends a linear coefficient of 14 x 10^{-6} /^{o}C for normal design purposes. Some authors point out that it is not necessary to take into account the effects of thermal strain in steel for the design of simple members, such as single beams and columns (Buchanan and Abu, 2017). The reason being that thermal restraint forces developed in beams could actually be beneficial to the fire performance. However, that will result in an increase of axial loads in columns.

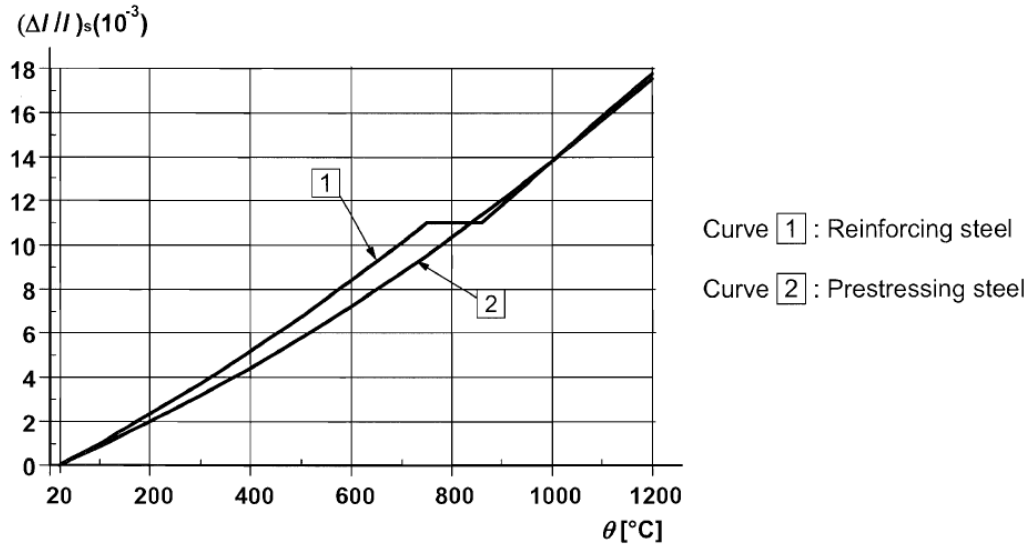

Figure 2.29 Thermal elongation for steel (European committee for standardization, 2004b)

2.10 PERFORMANCE-BASED FIRE DESIGN APPROACH

Performance-based fire protection mainly revolves around three key attributes according to SFPE handbook for fire engineers (Hurley et al., 2015). First one is the desired level of fire safety of a building in fire. Depending on the importance and use of the building, the fire safety level agreed upon can be different. Secondly, the

definition of the design basis of the building which involves identification of the design fire scenarios. It takes into account occupant characteristics and building characteristics. Finally, the importance of an engineering analysis to evaluate the adequacy of proposed strategies to provide the intended level of safety in the design fire scenarios, is noted.

Many countries in the world have moved or moving towards the performance-based design approach for fire safety. Multi-level hierarchical performance-based format, as shown in Figure 2.30, is adopted when developing these building codes.

Goals, functional objectives and performance requirements which should be met by the buildings are defined in the top level. Lower level spells out the means of meeting the above goals. It could be either an acceptable solution which prescribes specific predefined rules to be adopted in the building. Alternatively, it could be by means of an approved calculation method to show that the required performance level is achieved by the building. The third avenue is by satisfying the specified goals by an alternative design which is based on comprehensive fire engineering design from first principles.

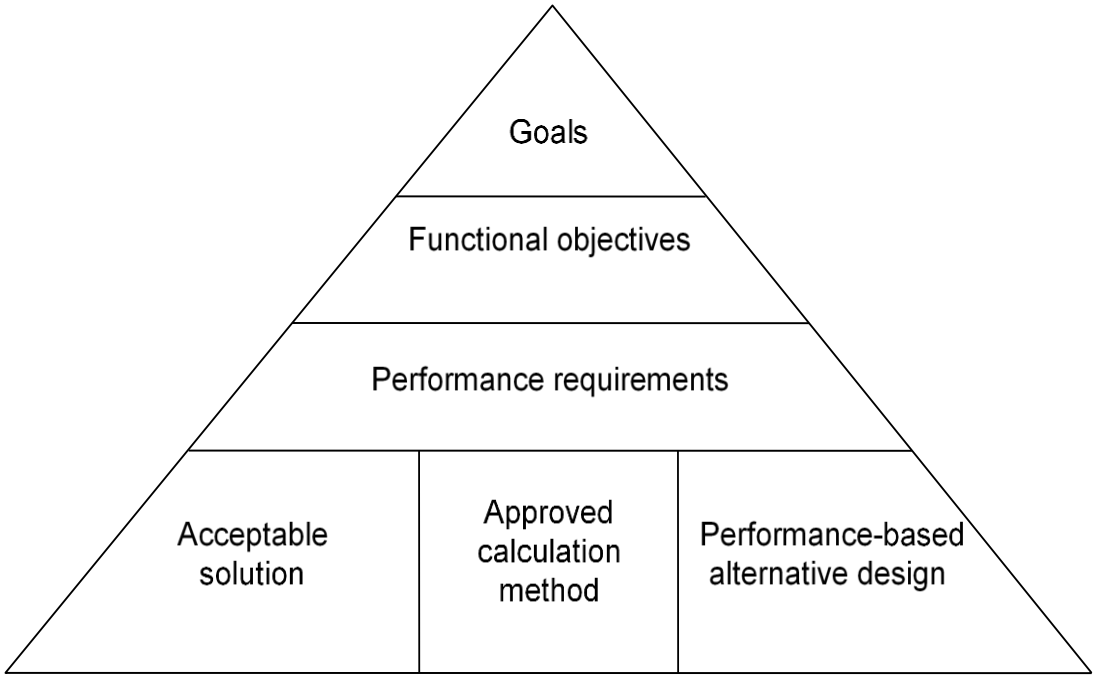

Figure 2.30 Typical hierarchical relationship for performance-based design (Buchanan and Abu, 2017)

There are both advantages and disadvantages of using a performance-based approach over conventional prescription-based design. One benefit is that the designer can optimise and go for a cost-effective design, based on the use and features of the building. For example, specific locations of the building may contain more fuel, and therefore, the risk of fire damage is high. More fire protective features can be incorporated in such risky areas individually rather than considering the same level of risk for the whole building. Since performance-based design requires a careful engineering analysis of different fire scenarios, it improves the understanding of how a building would perform in a fire. Conventional design rules will not allow such case-specific details as they are intended for more general cases.

On the downside, such alternative analysis can only be carried out by competent professionals, such as qualified fire engineers. It can consume more time and resources in the design stage than just following prescriptive guidelines. Also, the outcome is based on the expertise of the fire engineer involved. Another disadvantage is that the conditions and the use of the building can change with time. In such a scenario, the goals and performance requirements specified in the initial fire design may not be valid anymore. Sensitivity to such changes should be carefully assessed in the performance-based approach in order to maintain the same level of fire safety.

SFPE handbook illustrates the performance-based design process, as shown in Figure 2.31.

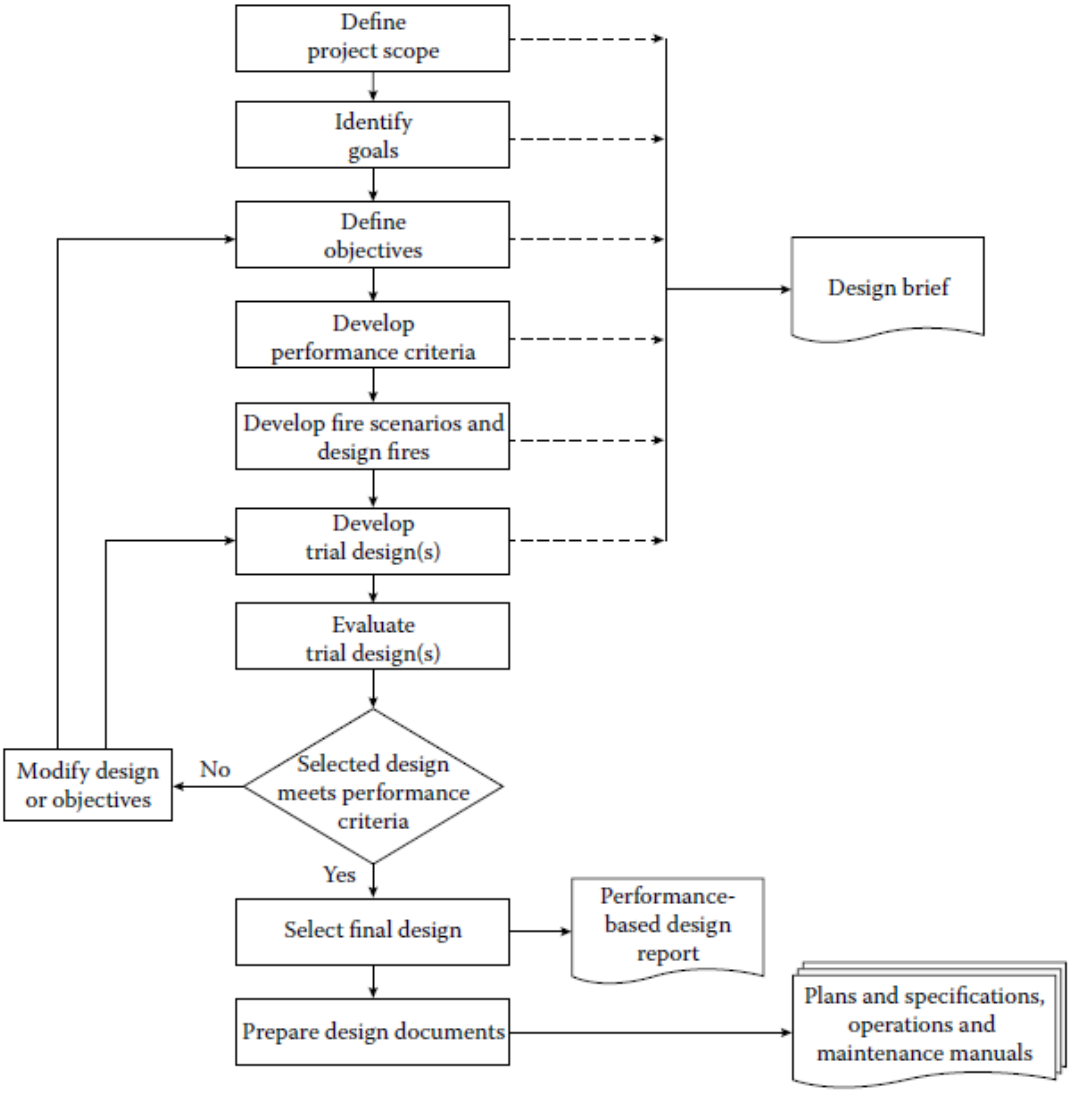

Figure 2.31 Performance-based design process (Hurley et al., 2015)

Key steps in this process are developing fire scenarios and design fires. Next few sections will discuss the current state-of-the-art approach for developing such design fire curves.

2.10.1 Compartment fires, influencing factors and modelling

A fire enclosed within a building is categorised as a compartment fire as it is confined between the walls and floor slabs of the building. In a compartment fire, the effect of radiative feedback is more pronounced than an open fire, promoting the further release of fuel and fire growth (Pierce and Moss, 2007). The stages of development of a compartment fire can be categorised into four phases, the incipient phase, growth phase, fully developed phase, and decay phase (Nyman, 2002). Figure 2.32 graphically represents the fire development stages with respect to time and rate

of heat release. Note that the transition between the growth and fully developed fire is known as the flashover, while the broken line represents the depletion of fuel prior to flashover or poorly ventilated conditions (Drysdale, 2011). In the absence of fire suppression, the fire will rapidly grow from a small incipient fire to a maximum size that is restricted by either the amount of fuel present (fuel-controlled fire) or the amount of air available for combustion through ventilation openings (ventilation-controlled fire) (Quintiere, 2006). When all the fuel load has combusted, the heat release rate begins to diminish, and the fire undergoes the decay phase (Bwalya et al., 2003).

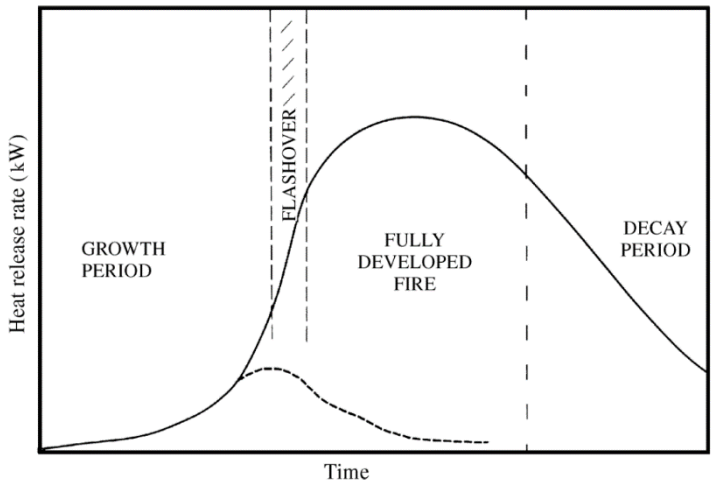

Figure 2.32 Stages of development of a compartment fire (Drysdale, 2011)

2.10.1.1 Compartment size

The development of a compartment fire is affected by the size and shape of the compartment, the fuel load contained in the compartment, the ventilation through the compartment, and the form and type of construction materials (Quintiere, 2006). Studies have shown that the average temperature of fire in a smaller compartment is higher than the temperature observed from a larger compartment (Węgrzyński and Konecki, 2018). A smaller compartment is better at retaining heat as there is a smaller boundary area at which convective heat transfer occurs (Węgrzyński and Konecki, 2018).

2.10.1.2 Ventilation

Under well-ventilated conditions, a compartment fire has enough oxygen within the compartment to combust all the fuel vapours present. Under this situation, the fire is defined as fuel-controlled, where the maximum development of the fire is dependent

on the fuel present within the compartment (Ingason et al., 2014). On the other hand, when a compartment fire occurs under limited ventilation, the oxygen concentration available within the compartment is limited. Several different scenarios may occur depending on the volume of air supply from the vents. If the compartment fills up with smoke and the vent supplies insufficient air to sustain enough oxygen concentration, the flame will be extinguished. Besides that, the flame could experience oscillation where it cycles between the brink of extinction and its original size. If there is enough air supply to sustain steady burning, the fire burns until the fuel is exhausted. However, the fire will burn at a slower rate than a well-ventilated fire, resulting in a lower heat release rate and lower maximum temperature within the compartment (Utiskul et al., 2005).

2.10.1.3 Fuel Load

The fire load in a compartment fire varies depending on the material properties and size of the furnishing. As stated by Yuen et al. (2014), the material properties that are important when simulating a fire are specific heat capacity (C), thermal conductivity (k), density (ρ), the heat of combustion (ΔH_c), emissivity (ε) and heat of reaction.

Thermogravimetric analysis (TGA) is a common method used to determine the combustion properties of a sample (Xu et al., 2007). The method analyses changes in the mass of a sample as the sample temperature are varied, producing a TGA curve showing the mass of the sample at varying temperatures, and the derivative curve (DTG) showing the rate of change of the sample mass at different temperatures (Vyazovkin, 2002). This enables the estimation of other material properties of, such as the threshold temperature at which the material ignites, the reference temperature at which the rate of mass change is the greatest, the heat of reaction, the percentage of the sample remaining after combustion, and the burn-out temperature (Xu et al., 2007).

2.10.1.4 Modelling a compartment fire

It is evident that the fire scenario inside a building is influenced by the compartment size, ventilation and fuel load. These factors are inter-dependent, and concurrently affect the development and decay of a compartment fire. To capture the wholistic behaviour, experiments can be conducted, but they are expensive and time-consuming. Since many parameters are involved, it is difficult to conduct experiments

for all the different scenarios. Therefore, analytical or numerical models need to be developed to determine the characteristics of a compartment fire.

Time-temperature history is one of the main outputs which can describe a fire event. Several realistic time-temperature histories have been developed, taking into account the influential factors for a compartment fire. Those will be discussed in Section 2.11.

With the advancement of the use of computational fluid dynamics in fire spread, numerical modelling of compartment fire can be conducted using software, such as Fire Dynamic Simulator (FDS). It has a solid phase solver which accounts for the pyrolysis and combustion of solid material, and the gas phase solver uses CFD to model the spread of fire, heat transfer, smoke movement and CO_2 yield. It can capture the influence of compartment size on fire spread, the effect of ventilation for the development and decay of fire and the role of fuel load for the severity of the fire and fire spread. The advantage of such a model is that the influencing parameters can be changed to simulate different fire scenarios for different building configurations and uses. That would be significantly cost-effective than carrying out experiments. However, the limitation of this type of modelling is that in most cases, there won't be any experimental results to validate the model. The accuracy of the model is governed by the accuracy of the input data and the knowledge of the user on fire dynamics. Therefore, the building codes highlight the importance of competency of the people involved in performance-based design and the correct usage of accurate material properties from reliable sources (Dutta et al., 2019b, Kim and Bhattacharyya, 2016, Kim et al., 2019) .

2.11 PARAMETRIC FIRE CURVES

Representation of a real fire is characterised by a parametric fire curve, which gives the time-temperature history depending on the fuel load, ventilation and wall lining materials. One of the most widely used parametric fire curves is published in BS EN 1991-1-2:2002 (European committee for standardization, 2002). The gas-phase temperature (θ_g) in the heating phase of the fire compartment according to the Eurocode parametric fire curve is given by eqn. (2.19);

$$\theta_g = 20 + 1325(1 - 0.324e^{-0.2t^*} - 0.204e^{-1.7t^*} - 0.47.2e^{-19t^*}) \qquad (2.19)$$

where; $t^* = t.\Gamma$ with t being the time in hours and Γ accounts for the ventilation and material characteristics.

$$\Gamma = \frac{[O/b]^2}{(0.04/1160)^2} \tag{2.20}$$

$$\text{O – Opening factor} = \frac{A_v\sqrt{h_{eq}}}{A_t} \tag{2.21}$$

where; A_v is the total area of vertical openings on all walls, h_{eq} is the weighted average of window heights on all walls and A_t is the total area of the enclosure including walls, ceiling and floor and openings.

$$\text{b - } \sqrt{thermal\ inertia} = \sqrt{\rho c \lambda} \tag{2.22}$$

where $\rho, c\ and\ \lambda$ are the density, specific heat and thermal conductivity of boundary of enclosure respectively.

If the boundary is made up of two layers of materials the thermal inertia of those materials can be calculated separately (b_1 and b_2) and the code gives instructions on how they can be incorporated in the fire model.

Duration of the burning period (heating phase) depends on the fuel load and ventilation. Therefore, burning period (t_{max}) is given by;

$$t_{max} = \frac{0.002.q_{t,d}}{O} \tag{2.23}$$

where; $q_{t,d}$ is the design value of the fire load density (MJ/m^2) related to the total surface area, and O is the opening factor. More guidelines to calculate the fire load density is given in Annex E of BS EN 1991-1-2 (European committee for standardization, 2002).

According to the proposed model in Eurocode (European committee for standardization, 2002), the decaying phase of the fire depends on the duration of the burning period. Therefore, three different decaying rates are given for fires with a burning phase of less than 30 min, between 30 min and 2 hrs and more than 2 hrs. More details can be found in (European committee for standardization, 2002). Figure 2.33 shows parametric time-temperature curves derived from Eurocode (European committee for standardization, 2002) equation by Buchanan and Abu (2017) for a 5 m x 5 m room of 3 m high. Four different ventilation scenarios are considered, and for

each case, time-temperature history is plotted for 3 different fuel loads and 2 different material types. However, the decaying rate is slightly modified from the Eurocode (European committee for standardization, 2002) relationship. Regardless, it shows how the different fuel loads and ventilation can make significant changes to the fire curve compared with the standard ISO 834 fire.

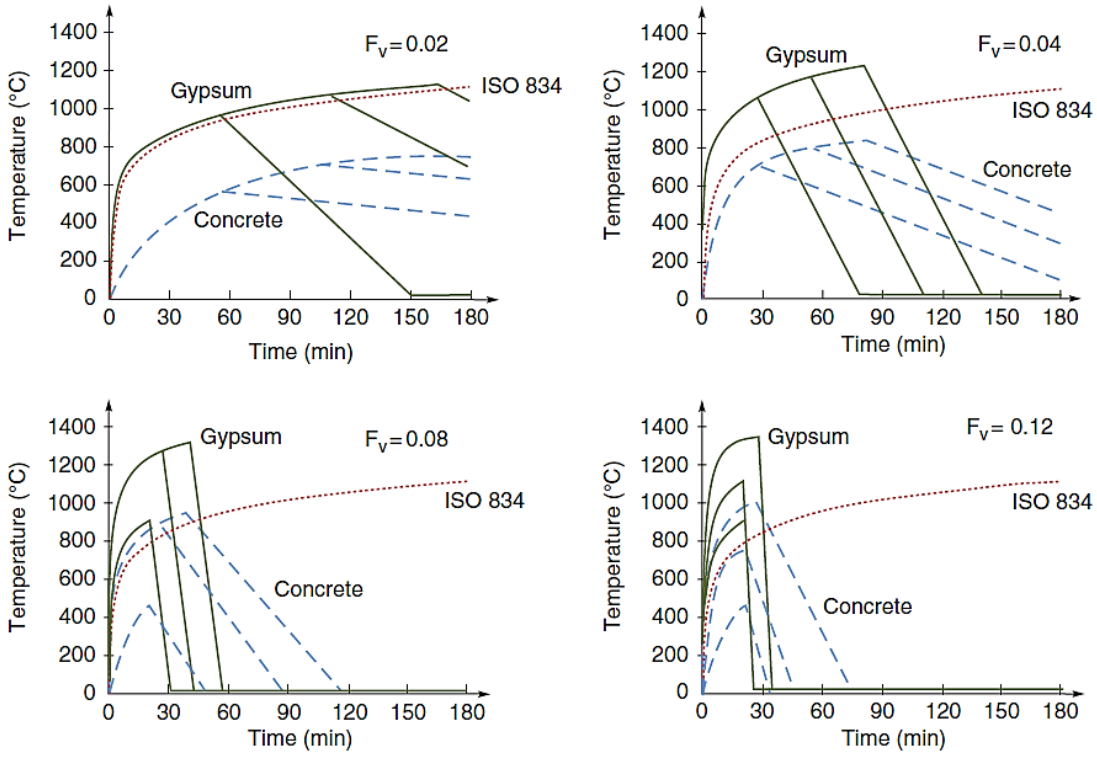

Figure 2.33 Parametric time-temperature curves (Buchanan and Abu, 2017)

However, limitation of these parametric models is that it is valid only for fire compartments smaller than 500m^2 without openings in the roof. Maximum compartment height is 4m. It also does not account for the partitions inside a compartment and how fire will spread in such a situation. Therefore, advanced fire models using CFD can be used to simulate realistic conditions of a compartment fire. Rather than just a time-temperature history, such advanced models can generate heat flux variation, the spread of smoke and identify localised effects of fire as well (Dutta et al., 2019a, Feenstra et al., 2018). Those outputs then can be used as input data for structural fire models to predict the behaviour of the building in fire (Chen et al., 2018, De Boer et al., 2019). Such an approach would be a more comprehensive and holistic way of getting the full benefits of performance-based fire design.

2.12 SUMMARY

A comprehensive literature review was carried out to explore the existing knowledge on concrete flat slabs in construction and their performance at elevated temperatures. Concrete flat slabs are beneficial in many ways for multi-storey construction, but it was identified that the current fire design guidelines hinder the effective use of this construction technique.

To further understand the basis for these guidelines, the limited number of experimental investigations on flat slabs in fire were reviewed. Some of the limitations that stood out were the use of small-scale unrestrained specimens for testing, which does not represent the actual continuous boundary conditions of flat slabs in buildings. Therefore, more effort is needed to carry out large-scale fire tests on restrained specimens to investigate the fire resistance of concrete flat slabs.

Several analytical models which were developed to assess the flat slab behaviour in fire were discussed, and as indicated, the use of these methods is only limited for research purposes. The industry mostly relies on the design charts and tables provided in design codes. The complexity of some of the models may have been a reason for this.

Most of the international building regulatory bodies allow the use of performance-based design techniques to evaluate the fire resistance of structures. The approach is mainly two-fold; Modelling the fire scenario in the building and structural effects due to the modelled fire. Some of the commonly used structural fire modelling software packages are compared to select a suitable methodology to be used in this research. The importance of material properties for the structural fire model is highlighted with a focus on critical parameters that are important for concrete and reinforcing steel.

Finally, compartment fire development and influencing factors were discussed in detail. The use of realistic fire curves is depicted by introducing parametric fire curves commonly used. The limitations of those parametric curves were identified and stressed on the importance of fire simulation software that can be used to generate case-specific time-temperature histories.

3 Large-scale experiment on the behaviour of concrete flat slabs subjected to standard fire

3.1 INTRODUCTION

The use of concrete flat slabs in buildings is getting popular due to numerous reasons. Flat slabs require a simple formwork system compared to conventional slabs which involve beams and therefore, it is fast and resource-efficient. In multi-storey buildings, more floors can be accommodated within a specific height in the absence of beams. Due to strict design guidelines and building regulations, fire-resistive design of concrete flat slabs has been one critical factor that governs the overall design of the slab. These guidelines are based on a limited number of punching shear tests on flat slabs at elevated temperatures. This chapter presents a large-scale fire test carried out to investigate the punching shear behaviour of flat slabs in fire.

The current code-based approach to structural fire design of concrete flat slabs specifies a minimum thickness and a minimum cover to withstand a particular fire duration. Most codes follow a performance-based approach where fire resistance is defined using three main performance criteria; structural adequacy, integrity and insulation. Thicknesses specified for flat slabs are considerably higher than thicknesses specified for conventional slabs with beams. Reason for that is the different failure mechanisms observed in two types of slabs. Flat slabs under fire failed due to punching shear (Annerel et al., 2013b, Bamonte et al., 2009) whereas conventional slabs failed due to flexural failure (Bailey and Toh, 2007).

Australian concrete code AS 3600 (Standards Australia, 2018) which is based on Eurocode 2(EC2) part 1-2 (European committee for standardization, 2004b) for fire design rules, adopts a similar approach. Australian building code (The Australian Building Codes Board, 2016) requires buildings having four or more stories to have a minimum fire rating of 2 hours. To achieve that, the concrete code recommends a minimum slab thickness of 200 mm and a cover of 35 mm. It should be noted that for a fire rating of 1.5-4 hrs, the minimum thickness remains the same at 200 mm, and the minimum cover requirement is increased. Before the amendment to AS 3600 in 2018

(Standards Australia, 2018) , a major limitation of these guidelines was that since it enforced this minimum thickness throughout the floor, the designer could not allocate set-downs without increasing the thickness of the whole floor. Slab set-downs are used, especially in bathroom areas, to allow for proper drainage and are usually between 20-50 mm. Although it seems like increasing the slab thickness will not have a significant effect for that particular floor, this additional use of material can accumulate throughout the height of the building (especially in a high-rise building). It uses more material, and the increase of dead weight of the building will lead to strengthening other structural elements as well. Although the latest version of Australian concrete code addressed this issue by specifying this thickness requirement only within a certain distance from the column, current Eurocode 2 (European committee for standardization, 2004b) still specifies to use the recommended thickness throughout the floor slab.

3.1.1 Fire tests on Concrete flat slabs

To further understand the values specified in the code, it is vital to investigate the background as into how these values were defined. AS 3600 (Standards Australia, 2018) flat slab requirements were directly based on EC2 (European committee for standardization, 2004b) and the EC2 values are based on a series of experiments carried out by Kordina (1993). As illustrated in Figure 3.1(a), they tested a total number of 14 slabs having thicknesses of 200mm and 150mm and the fire resistance period of the majority of them were less than 70min. All the slab specimens showed a punching shear failure (Kordina, 1993). It is evident that the loading arrangement, as shown in Figure 3.1(b), would cause a punching shear failure, as illustrated in Figure 3.1(c).

There are few other experimental investigations on flat slabs under fire conducted by Annerel et al. (2013a), Liao et al. (2013), Salem et al. (2012), Ghoreishi et al. (2015) and Smith et al. (2014), and all those specimens have failed due to punching shear. More details of these experiments were given in Chapter 2. Some studies have shown that flat slabs in actual buildings can experience membrane forces and moment redistribution when exposed to fire compared to the isolated specimens being tested (Bailey, 2004, Vecchio and Tang, 1990, Wang et al., 2013). When the slab perimeter is vertically supported and restrained against the horizontal movement, compressive membrane forces will occur at small vertical displacements. The

development of such in-plane forces within the depth of the slab is called membrane action (Bailey, 2004). Most of the aforementioned studies used simply supported test specimens which did not allow such membrane actions to develop.

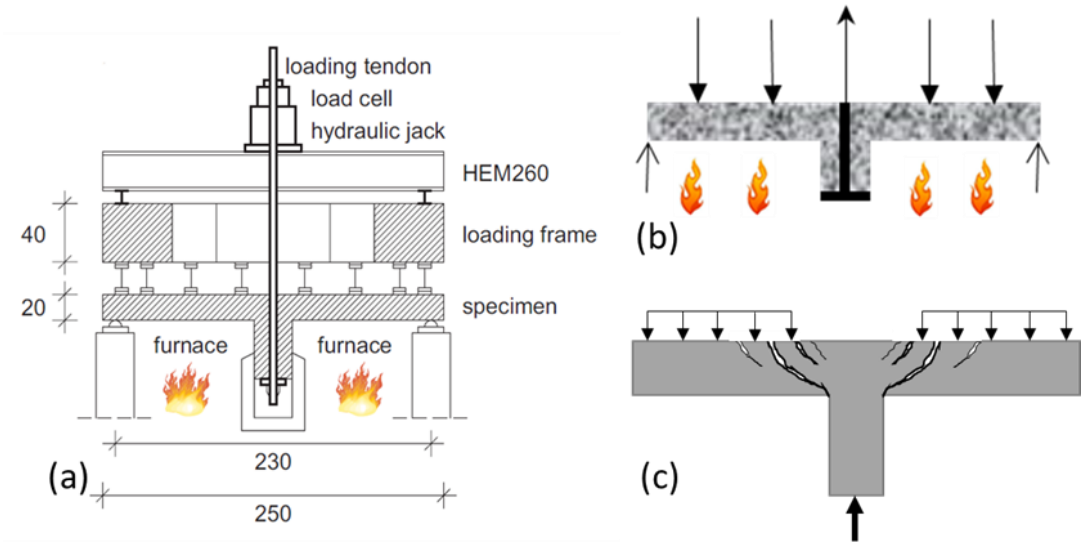

Figure 3.1: a) Test set-up by Kordina (1993) as represented by Bamonte et al. (2012) b) Illustration of the loading arrangement (c) A typical punching shear failure of a flat slab

Smith et al. (2014) have recently conducted fire tests on restrained flat slab specimens and their results show that punching shear resistance is improved by having such restrained supports. Lim et al. (2004) have numerically shown that compressive membrane forces developed during a fire can significantly increase the fire resistance period. Punching shear initiates as result of crack propagation from the tensile surface as explained in section 2.8.2. If there are compressive membrane forces, they will act against this crack propagation which in return increase the punching shear resistance. As the current design guidelines are based on fire tests conducted on simply supported isolated specimens, they can be conservative because the actual behaviour under fire can deviate from what has been predicted by the tests. EC2 committee also agrees with this view as they state that Kordina's tests (which the EC2 is based on) are on the safe side because there was no restraint for longitudinal expansion, and therefore no membrane effects (Anderberg et al., 2004). However, collapses due to fire in buildings having flat slabs confirm the fact that punching shear failure will be critical in fire.

Among the limited number of fire test data available for flat slabs, most test specimens (Ghoreishi et al., 2015, Liao et al., 2013, Salem et al., 2012, Smith et al., 2014) are smaller than 1.5 m in size. Since the failure shear stress is influenced by the

size effects (Bažant and Cao, 1987), it is crucial to have data on real scale specimens subjected to fire. Furthermore, only Smith et al. (2015) have previously performed a fire test on restrained concrete flat slabs and results indicate that the fire resistance level is significantly improved by having restrained supports. That study also emphasises the importance of capturing the behaviour during the cooling, as some specimens failed during the cooling phase (Arna'ot et al., 2017, Smith et al., 2014). However, the slabs were exposed to a furnace specific fire curve instead of the standard fire curve. The cooling phase characteristics have an impact on the residual material properties as well (dos Santos and Rodrigues, 2016, Reddy and Ramaswamy, 2017). The fire test presented in this chapter was conducted on a full-scale specimen subjected to standard ISO 834 fire (International Organization for Standardization, 1999) which was laterally restrained against longitudinal expansion and measurements were also taken during the cooling phase.

3.2 EXPERIMENTAL INVESTIGATION

3.2.1 Test specimen

Size of the test specimen was chosen according to the large-scale furnace available at the Victoria University, Werribee. Slab size was 3.78 m x 4.75 m having a thickness of 180 mm and have a column stub of 0.25 m x 0.25 m x 0.4 m connected at the centre. The concrete cover was 29 mm, which corresponds to an axis distance of 35 mm. The thickness was taken as 180 mm as it was needed to find out the fire-resistant duration of a slab below 200 mm thickness as specified by EC2 part 1-2 (European committee for standardization, 2004b) for a FRL of 90 min and above. Figure 3.2 presents the size and reinforcement detailing of the slab specimen.

For the flexural reinforcement at the bottom, 12 mm diameter deformed bars were positioned in two orthogonal directions with a spacing of 100 mm, which corresponds to a reinforcement ratio (ρ) of 0.9%. A 200 mm x 200 mm spaced square rebar mesh having 10 mm diameter bars were used as top reinforcement (ρ = 0.3%) (see Figure 3.2). Eight bars of 20 mm diameter were positioned in the column along with stirrups of 6 mm diameter along the height of the column with 80mm spacing.

To measure the temperature of the slab surfaces as well as inside the slab, a total of 21 K-type thermocouples were embedded at different locations, as shown in Figure 3.3. Each location had 5 TCs grouped together where two were for the exposed (A)

and unexposed (E) surfaces while others were 45 mm (B), 90 mm (C) and 135 mm (D) from the exposed slab surface. At location 3, one TC was placed touching the bottom reinforcement to record the temperature of the steel reinforcement during the test. Exposed surface TCs were placed 2-4 mm above the slab bottom level to avoid the formation of a localised passageway for flames to penetrate to the slab through TC tips.

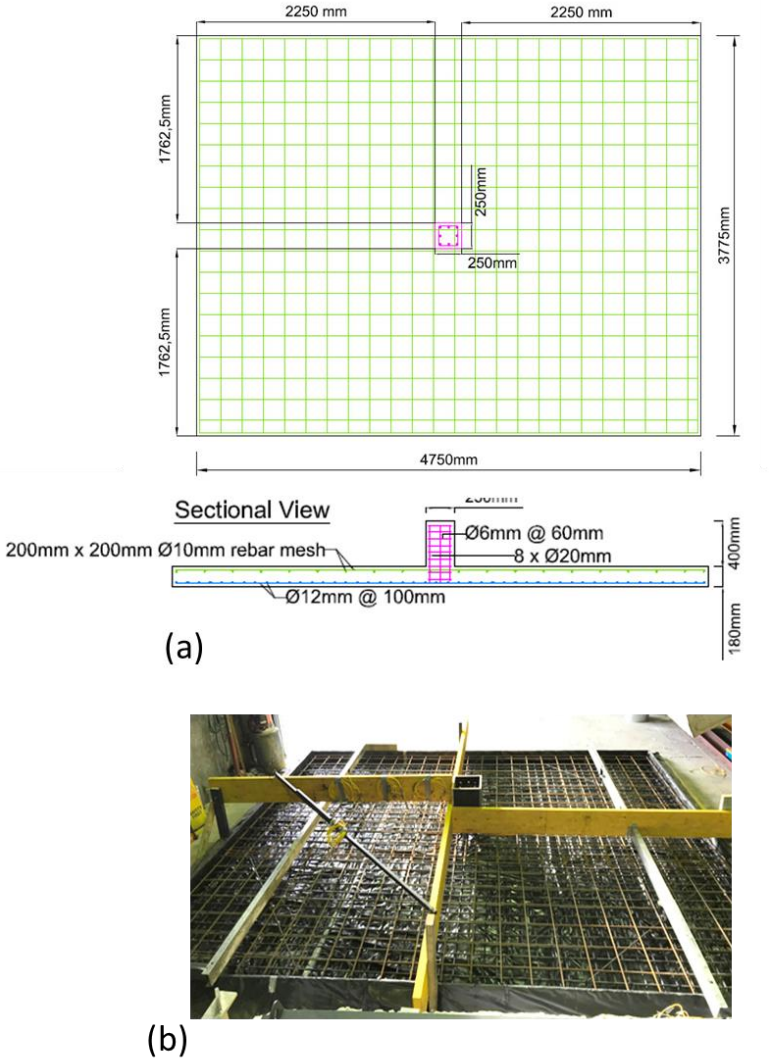

Figure 3.2: a) Geometry and the reinforcement detailing of the slab specimen, b) Reinforcement layout of the slab

Deflections were measured using string pots and laser transducers. A total number of 11 string pots were placed along two orthogonal directions, as shown in Figure 3.3. D1 to D7 measured the deflection along the short span 50 mm away from the column face where D 8 – D11 measured the deflection along half of the long span.

Laser transducers were placed at D4, D5, D6, D7 and D11 coinciding with the string pot locations to verify the measurements recorded by string pots.

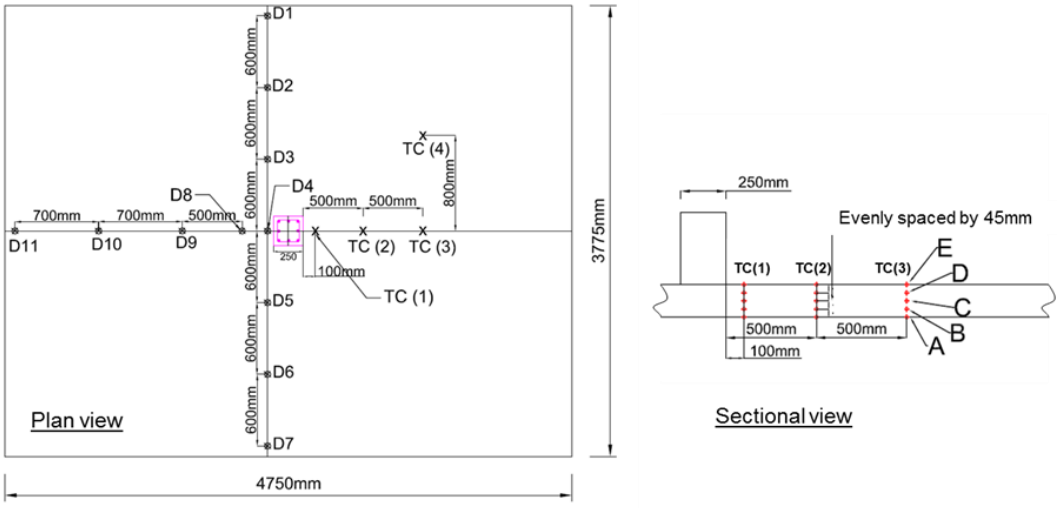

Figure 3.3: Thermocouple and displacement measurement locations

3.2.2 Concrete mix details

The slab was cast under laboratory conditions, and the concrete was ordered from a ready mixed concrete plant. A mixture of 20 mm and 14 mm siliceous type aggregates were used sourced from local quarries. Water cement ratio was kept at 0.38 with added water-reducing admixture to achieve a slump of 100 mm. 2 kg/m^3 of poly fibres were added to increase the resistance against spalling in fire (Kalifa et al., 2001, Müller et al., 2019). Table 3.1 presents the details of the concrete mix used.

Table 3.1: Concrete mix details and slump

Boral Cement, Berrima SL	203 kg/m^3
Boral Cement, Maldon GGBS	147 kg/m^3
Siliceous aggregates 20 mm	475 kg/m^3
Siliceous aggregates 14 mm	550 kg/m^3
Calcareous sand	840 kg/m^3
Poly fibre	2 kg/m^3
Water reducing admixture	1500 ml/m^3
Total water	165 kg/m^3
W/C	0.38
Slump	100 mm

3.2.3 Mechanical properties of concrete at ambient conditions

Tests were conducted to determine the compressive strength, tensile strength, Young's modulus, and Poisson's ratio of concrete at ambient conditions which will be useful in future studies in order to develop any numerical or analytical models to simulate the behaviour of the slab during the experiment. Ø100 mm x 200 mm cylinders were tested according to AS 1012.9 (Standards Australia, 2014a) at 7 days and 28 days to determine the compressive strength. Splitting tensile strength was performed on Ø150 mm x 300 mm cylinders in accordance with AS 1012.10 (Standards Australia, 2014b) to find out the tensile strength of concrete (see Figure 3.5). Young's modulus and Poisson's ratio were determined according to AS 1012.17 (Standards Australia, 2014c) using Ø100 mm x 200 mm cylinders (see Figure 3.4).

Table 3.2 summarises the results obtained from these tests.

Figure 3.4: Splitting tensile test set-up and a failed specimen after the test

Figure 3.5: Test specimen for Young's modulus test with deformation measurement rig

Table 3.2: Mechanical properties of concrete at ambient temperature

Compressive strength (7 days)	26 MPa
Compressive strength (28 days)	39 MPa
Tensile strength (28 days)	3.7 MPa
Young's modulus (28 days)	28600 MPa
Poisson's ratio (28 days)	0.29

3.2.4 Sample Preparation and Test Procedure

After preparing the formwork and laying out reinforcement, as shown in Figure 3.3, thermocouples were embedded, and the slab was cast with the concrete as specified in Table 3.1. After concrete got hardened slab was covered with burlap and sprayed water for curing. After 28 days of curing, the test was conducted. Table 3.3 summarises the key features of the current test, along with some previous flat slab tests in fire for comparison.

The test was conducted by applying the ISO 834 fire (International Organization for Standardization, 1999). At the time of testing, the specimen was first fitted to the supporting frame with column stub facing upwards, as shown in Figure 3.6 and then frame and specimen were placed on top of the furnace. The supporting frame provided vertical restraint against loading by means of the bottom plate of the supporting frame, as shown in Figure 3.7 and also lateral restraint against thermal expansion when heating. Load cell and the hydraulic actuator for loading were then connected to the top of the column stub, as shown in Figure 3.8. To measure the displacement, a series of string pots were connected across the two orthogonal directions, as shown in Figure 3.3. Figure 3.7 presents the overall arrangement of the test set-up. More realistic support conditions were used in the test compared to previous tests with simply supported conditions. Although the restraint conditions provided by the adjacent slabs may slightly change during the fire, for practical reasons, the same fixity had to be kept in the test. The author could not place any load-cells on the side of the frame, as that location will be heated during the test and load cells would have malfunctioned. This has previously happened in the small-scale test conducted by Smith et al. (2014).

Table 3.3: Comparison of key features of the current test with previous tests on flat slabs in elevated temperatures

	Smith et al. (2014)	Annerel et al. (2013a)	Kordina (1993)	Liao et al. (2013)	Current Test
Slab size and thickness	1400 x 1400 thickness = 50,75,100	3200 x 3500 thickness = 250	2500 x 2500 thickness = 200,150	1220 x 1220 1800 x 1800 Thickness = 120	4750 x 3775mm Thickness 180mm
Column size *c – column width, d- effective depth	120x120, 100 mm height c/d = 1.4 to 4	300 x 300, 650 mm height c/d = 1.4	250 x 250, 400 mm height c/d = 1.6 to 2.3	180 x 180, 400 mm height c/d = 2	250x 250, 400 mm height c/d = 1.7
Ambient Concrete Strength	51 MPa	32 MPa (Requested C25/30)	35 to 51 MPa	32MPa (NSC) and 58MPa (HSC)	39 MPa
Steel Strength	F_y = 550MPa – 571MPa	F_y = 500 MPa	F_y = 504 to 590 MPa	F_y = 420 MPa	F_y = 550 MPa
Aggregate size and type	Max. size 10mm Siliceous	Max. size 14mm Siliceous and calcareous sand Calcareous aggregates	No information regarding the mix properties	Siliceous	Siliceous
Curing and conditioning	16 months in a dehumified environment	Cured up to 120days.	88 to 178 days old	Covered with burlap for 28 days and stored in open space for 250 days	Cured for 28 days
Heating surface and loading arrangement	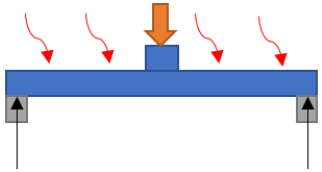	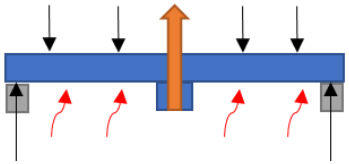	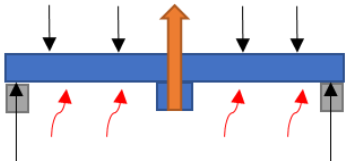	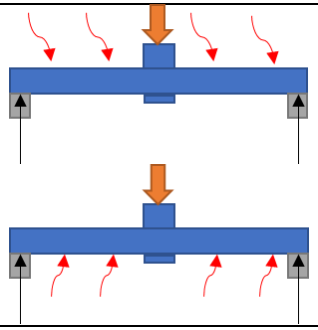	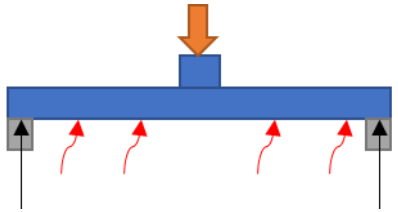
Fire curve	Furnace specific. Max. temp. 510^{0}C	ISO 834 fire curve	ISO 834 fire curve	ASTM E119 curve	ISO 834 fire curve
Fire duration	2 hours of heating and cooling down till 150^{0}C in slabs	2 hrs	2 hrs	Up to 8 hrs	3.5 hrs and cooling down up to 12 hrs

Support conditions	Restrained and Unrestrained	Unrestrained.	Unrestrained.	Unrestrained	Partially restrained
Flexural r/f ratio	0.8% and 1.5%	0.6%	0.56% and 1.54%	0.92% and 1.43%	0.9%
Load applied	50 kN – 250 kN	580 kN – 620 kN		116 kN – 260 kN	225 kN – 275 kN
Load calculation	EC2 design calculation(European committee for standardization, 2004a) Critical shear crack theory(Fernández Ruiz and Muttoni, 2010)	EN 1992-1-1 service load(European committee for standardization, 2004a) Belgian standards NBN B15-002(Belgian Standards Institution (BIN), 1999)	P_{test} = 70% of ultimate shear strength ($V_{Rd,l}$ calculated according to EC2(European committee for standardization, 2004a))	P_{test} = 54% of ultimate shear strength (by doing ambient tests until failure)	P_{test} = 50% of ultimate shear strength ($V_{Rd,l}$ calculated according to EC2(European committee for standardization, 2004a))
Test methodology	Loaded at a displacement rate of 2 mm/min until the required load had been reached. The load was held constant and slabs were heated. For slabs that didn't fail after 2 hrs, the applied load was maintained whilst slabs cooled down to 150C.	First, loaded the slab until service load. Load remained constant during heating for 2 hrs, after which the load was increased up to failure	Initial load (0.7 $V_{Rd,l}$) was increased during the first 30 mins of fire exposure. Some slabs failed during this period and for others, the load was kept constant after 30 mins	The load was first applied and maintained for 30-50min until deformation stabilized. Then specimens were heated while maintaining the load until the deformation rate exceeded 7mm/s or until 8hrs	The load was first applied at room temperature and maintained until deformation stabilized. Then the specimen was heated while maintaining the load
Measurements	Deflection – Using DIC In-plane forces – Strain gauges bonded to the reaction frame Temp – 15 TCs, 3 sets of 5 across the depth placed 150 mm outside the expected punching shear perimeter	Displacement – Using LVDTs TCs- Inside column stub and 0.5m and 1m away from the centre on top and bottom face	Deformation and temperature. (Instrumentation used, and locations of measurements are not clear)	Temp – 3 layers of K-type TCs at 30,60 and 90 mm beneath the heated surface Displacement – 5 non-contact laser displacement meters and 2 LVDTs	Temp – 4 locations, 5 TCs across the depth at each location Displacement – 5 non-contact laser displacement meters and 11 string pots.

Figure 3.6: Slab specimen with the supporting frame prior to mounting on the furnace

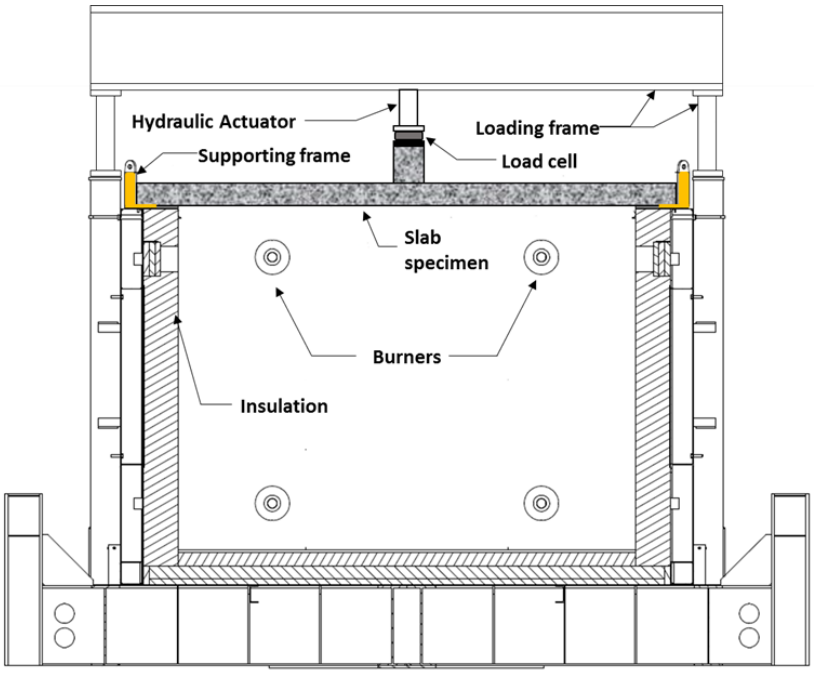

Figure 3.7: Test set-up

Figure 3.8: TCs, String pots and hydraulic actuator fixed to the specimen

The load applied to the column stub was determined based on the design punching shear capacity at ambient conditions ($V_{rd,c}$) calculated according to the following equation [eqn. (3.1)] from EC2 (European committee for standardization, 2004a).

$$V_{rd,C} = [C_{Rd,C}.k(100\rho_1 f_{ck})^{1/3} + k_1\sigma_{cp}]U.d \quad (3.1)$$

Where;

$C_{Rd,c}$ taken as 0.18

k = 1 + (200/d)0.5 taken as 2

ρ_1 tensile reinforcement ratio taken as 0.9%

f_{ck} characteristic compressive strength taken as 39 N/mm2

$k_1\sigma_{cp}$ component accounting the axial loading and/or prestressing; neglected for this calculation

U punching shear perimeter taken as 3320mm

d effective depth taken as 145mm

Calculated punching shear capacity at ambient conditions ($V_{rd,c}$) was 530 kN, and 50% of that value was used in the test. First, the specimen was gradually loaded from 0 – 265 kN and then allowed 8-10 minutes for the deformation to stabilize. After that, the furnace was turned on, and the heat was applied underneath the slab (tension side) while maintaining the load at the same level. The main aim was to find out whether the specimen would resist up to 2 hrs of ISO 834 standard fire exposure. It was decided to stop the test if the slab reached the failure deflection limit of $L^2/400d$ as specified by AS 1530.4 (Standards Australia, 2014d) or if cracking was observed visually. If it did not fail until 2hrs, then heating was continued beyond 2 hrs until failure or heating was stopped after 3.5 hrs. Then the behaviour during the cooling phase was observed as well, which could be a critical phase according to recent studies by Smith et al. (2014).

3.3 TEST RESULTS AND DISCUSSION

3.3.1 The behaviour of the slab

The tension side of the slab specimen was exposed to ISO 834 standard fire. Figure 3.9 gives the measured time-temperature relationship of the furnace compared with the ISO 834 standard fire curve (International Organization for Standardization, 1999). Furnace temperature closely matches with the standard fire curve.

With the downward deformation due to heat, the pressure of the hydraulic actuator was dropping as the test started. In order to maintain the same load, continuous pumping was done to maintain the pressure while monitoring the load level. The load level was managed to be kept within the range of 225 - 275 kN for 120 mins with only a small drop, as shown in Figure 3.10. However, the length of the piston reached the limit at 120 mins, and therefore the load could not be maintained beyond this point.

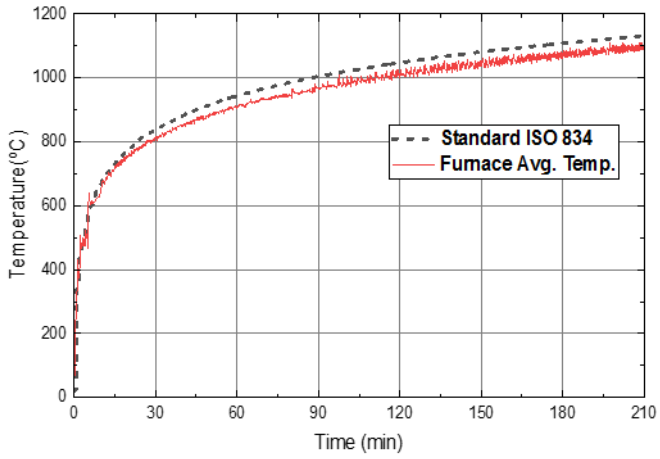

Figure 3.9: Temperature inside the furnace

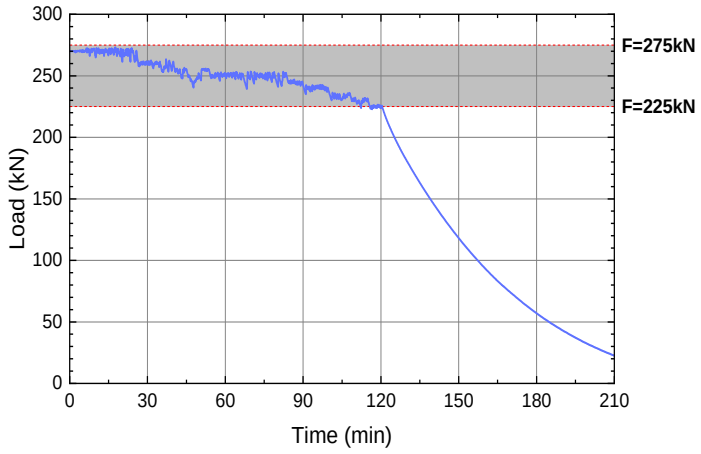

Figure 3.10: Applied load on the slab

The slab did not fail for 2 hrs, and at that point, the piston of the hydraulic actuator was close to reaching its limit due to continuous pumping carried out to maintain the initial load. At that point, it was decided not to increase the pressure further, and therefore after 2 hrs, the load gradually dropped. (see Figure 3.10). However, the heating continued until 3.5 hrs, and the deflection of the slab did not exceed the limit while there were no cracks observed visually. After 3.5 hrs it was

decided to stop heating, but the measurements were continuously taken during the cooling phase too.

3.3.2 Temperature Variation

Temperature readings were taken at 4 locations, as shown in Figure 3.3 on the exposed side, across the depth of the slab at 45 mm, 90 mm and 135 mm from the exposed side and the unexposed side. Figure 3.11 shows the readings obtained during the heating phase and the cooling phase at each depth. Apart from the readings on the exposed surface, other 4 locations have similar temperature readings which suggest that the heating was uniformly applied throughout the slab area.

It can be seen from the graphs that the exposed surface has reached a maximum temperature of 1000^{o}C at 3.5 hrs, but the temperature of the unexposed surface is only 55^{o}C. It shows the good insulation characteristic of concrete, and importantly the unexposed surface temperature is well below the 180^{o}C limit specified by AS1530.4 (Standards Australia, 2014d), which is the failure criteria for insulation. Furthermore, the measured temperatures are in close agreement with the temperature profiles for slabs given in EC2 part 1-2 Annex A (European committee for standardization, 2004b).

A temperature plateau can be observed around 100^{o}C limit from the readings on 90 mm and 135 mm away from the exposed surface. This could be due to the reason that a significant amount of thermal energy is required to evaporate free water trapped inside the concrete. Therefore, when that depth reaches 100^{o}C, the temperature did not increase for a certain period, and after the plateau, the temperature started to increase at a steady rate.

During the cooling phase, the exposed surface temperature drops as soon as the heating was stopped. However, temperature increases for a while across the depth and then start to decrease. The trapped thermal energy within the slab transfers from the exposed surface towards the unexposed surface, which results in this behaviour. In fact, the maximum temperature of the unexposed surface (80^{o}C) is reached during this cooling phase. This increase in temperature across the depth further degrades the strength (and other material properties) of concrete even after heating ceased, which could explain why some punching shear failures were observed during the cooling phase.

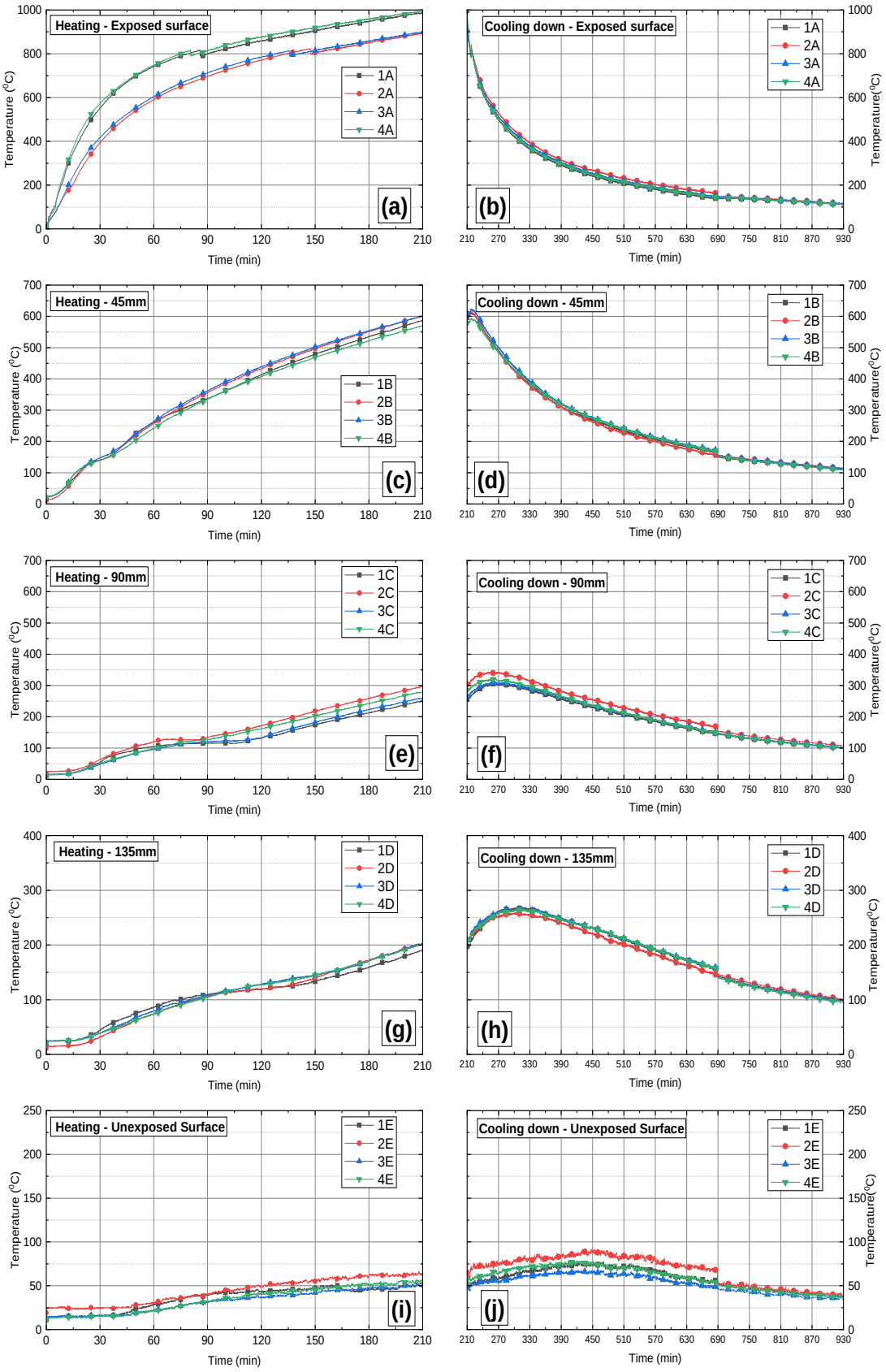

Figure 3.11: Temperature variation of the slab during heating and cooling down. (a)exposed surface – heating, (b)exposed surface-cooling, (c)At 45mm-heating, (d) At 45mm-cooling, (e)At 90mm-heating, (f)At 90mm-cooling, (g)At 135mm-heating, (h)At 135mm-cooling, (i)Unexposed surface-heating, (j)Unexposed surface-cooling

There was one TC installed in close contact with the bottom steel reinforcement at location 3, and the readings indicate that a maximum temperature around 500°C was reached during the heating phase. During the cooling phase, this was increased to around 520°C within the first 30 mins and then gradually decreased (Figure 3.12). A concrete cover of 35 mm provided was sufficient to keep the temperature of the steel reinforcement to an acceptable level.

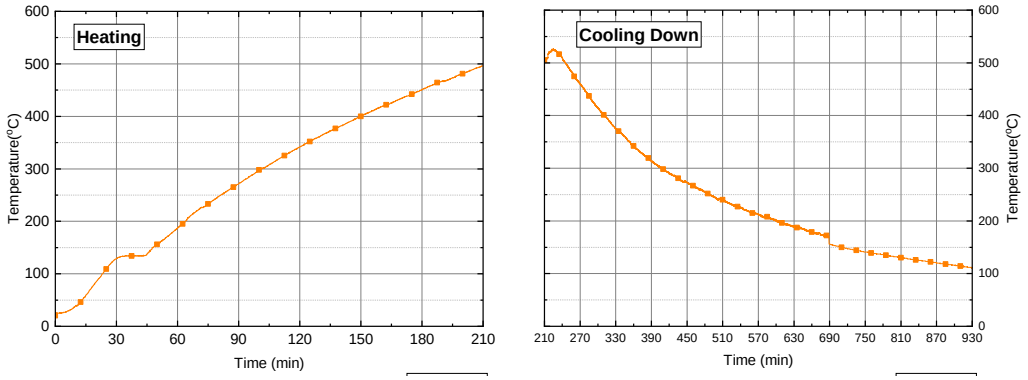

Figure 3.12: Temperature variation close to the bottom reinforcement

3.3.3 Deflection

The deflection was measured using string pots connected to the slab at 11 locations in two orthogonal directions (see Figure 3.3). Figure 3.13 shows the deflection along the short span, and Figure 3.14 shows the deflection along the half of the long span. Data recorded by laser transducers in addition to string pots are not presented here as they were taken at the same locations, only as a verification method for string pot measurements. Starting time of the furnace was taken as t=0 min, and downward deflection was considered positive when presenting the results. As described earlier, the load was applied before heating and kept constant for about 15 minutes, and the measurements indicate that the deformation was stabilized during this period. D1, D7 and D11 string pots measured the deformation close to the supporting frame. Those showed a very small downward deflection about 5mm when the load was applied. This was due to the squeezing of insulation wool underneath the supporting frame between the frame and the furnace (see Figure 3.7), which was placed to prevent the leakage of flames and hot air. After 120 mins when the loading was gradually reduced (see Figure 3.10), D1, D7 and D11 showed a very small upward deflection. This may be due to the squeezed insulation subjected to relaxation. This may have also led to the formation of some marks at the underneath of the specimen (see Figure 3.15).

After heating commenced, downward deflection started to increase considerably, although the applied load was kept constant. This implies that the deflection towards the fire was due to the thermal strain as a result of elevated temperature. Deflection at the centre was higher, and it decreases as it goes away from the centre as expected. Initial load was maintained until 2 hrs and the maximum deflection at that time was 85mm which is much less than the deflection limit (L^2/400d) for structural adequacy failure criteria specified by AS 1530.4 (Standards Australia, 2014d). The fire resistance period of the specimen is further discussed in next Section (3.3.4).

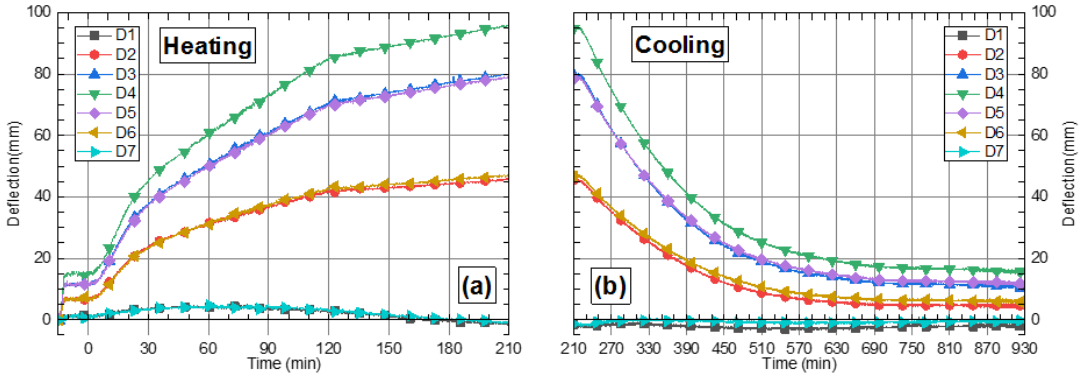

Figure 3.13: Deflection along the short span during (a)heating and (b)cooling

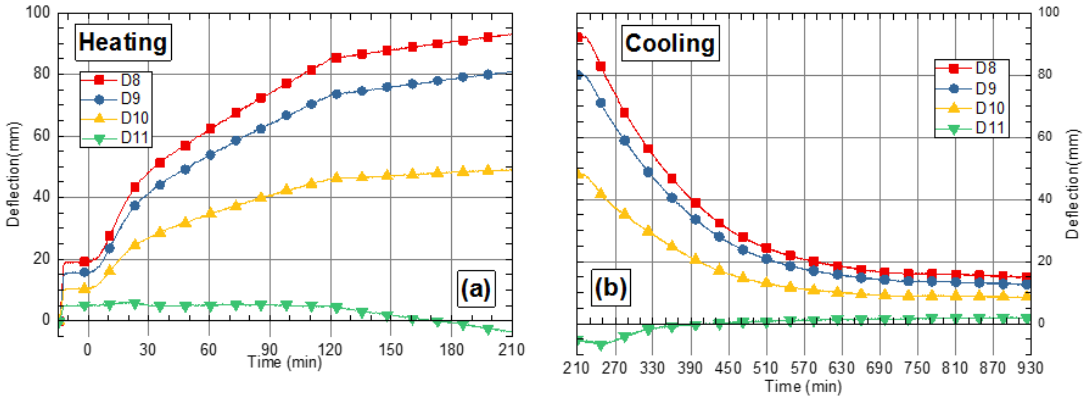

Figure 3.14: Deflection along the long span during (a)heating and (b)cooling

After 2hrs of heating, the load was allowed to drop (see Figure 3.13 and Figure 3.14), but even during that period, the deflection was increasing. This implies that the thermal strain is dominant than the load-induced strain in this case. The rate of increase of deflection is, however, lowered after 2 hrs. After 3.5 hrs of fire exposure, the maximum deflection of the slab was 95 mm, which is still less than the failure criteria.

The load was completely removed during the cooling phase, and it is reflected in the deformation measurements where deflection gradually decreased and reached a stable value after about 10 hrs of cooling. However, it did not reach the initial value indicating that the elevated temperature has caused permanent plastic deformation in the slab.

3.3.4 Fire resistance

Fire resistance is defined as the time until the slab reaches one of the failure criteria for structural adequacy, integrity and insulation. The maximum deflection of 95mm reached during the heating phase is well below the $L^2/ 400d$ failure criteria for structural adequacy. There were no visible cracks during that period. Some wrinkles can be seen in Figure 3.15, which were due to the polythene laid underneath the reinforcement prior to casting of the slab, as shown in Figure 3.2(b). Although the slab was cured only for 28 days, there was no spalling during the complete test (see Figure 3.15). Therefore, it is evident that the slab has passed the structural adequacy and integrity criteria during the heating phase.

Figure 3.15: The exposed surface of the specimen after the test

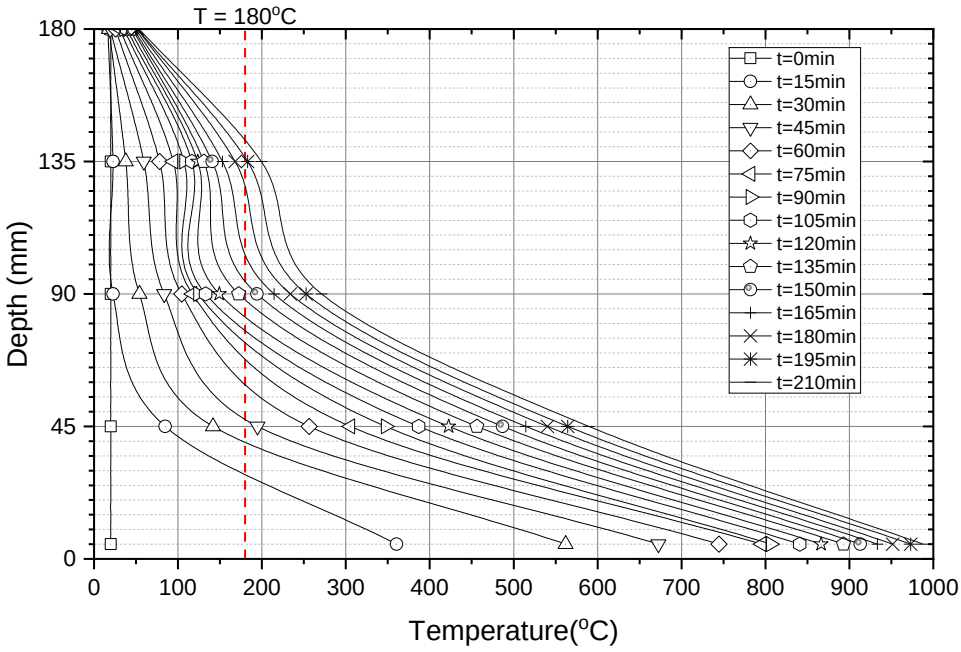

Figure 3.16: Temperature profiles across the slab during heating

According to the temperature profiles presented in Figure 3.16, the maximum temperature recorded of the unexposed surface during heating was 55°C which is below 180°C limit specified by AS 1530.4 (Standards Australia, 2014d) for insulation failure criteria. Therefore, according to the results, the slab has reached a fire resistance of 3.5 hrs.

In contrast to the guidelines specified by the design codes which requires to have a 200 mm thick slab with 35 mm axis distance to have a 2 hr FRL, the 180 mm thick slab used in the experiment with 35 mm axis distance has survived more than 2 hrs of standard fire exposure. Due to the lateral restraints against expansion, membrane action is allowed to develop during fire, and this could have influenced the enhancement in fire performance in this particular case. It closely represents the actual conditions in a building as the flat slab is continuous and adjacent slab panels could provide lateral restraint against heating; hence, membrane actions will be developed.

3.4 SUMMARY

Majority of fire tests conducted on flat slabs have used simply supported isolated specimens, and current design guidelines are based on these tests. Such arrangements could not capture the effect of membrane action during fire, and it was speculated that this membrane action could increase the fire resistance level. To address this issue, a large-scale flat slab specimen was tested against standard fire exposure with partially restrained supports to evaluate its fire performance. This is the first instance where a large-scale partially restrained flat slab was subjected to standard fire.

Based on the fire test, the following conclusions and recommendations can be made;

- The concrete mix contained poly fibre, and the specimen was cured only for 28 days. No spalling was observed during the total duration of the test.
- The 180mm flat slab specimen did not fail for 3.5 hrs of ISO 834 standard fire exposure in contrast to the fire resistance levels specified by the standards
- The use of restrained support conditions which closely represent the actual condition of a flat slab in a building has increased the fire resistance level. Membrane action developed during fire could have improved the punching shear resistance.
- Data were recorded during the cooling phase as well due to the tendency of failure in the cooling phase, especially in restrained specimens. This data is incorporated in work reported in next chapter to validate finite element models to predict the behaviour of flat slabs in fire.
- Further testing on laterally restrained specimens is recommended to capture the effect of membrane action on the fire resistance level of concrete flat slabs.

4 Thermo-Mechanical Modelling of Concrete Flat Slabs in Fire

4.1 INTRODUCTION

Experimental investigation on structural elements under fire provides vital information to study the performance of those in fire. However, to apply fire and to test and then collect data under such an environment requires expensive test equipment, and it can be time-consuming and challenging. Numerical analysis is a widely accepted method which could overcome that to a certain extent. Material properties of structures exposed to fire undergo significant changes in both mechanical and thermal properties which incur many non-linearities to the model. Therefore, modelling under fire can be complicated, and convergence issues are reported in many cases (Earij et al., 2017, Ellobody and Bailey, 2009, Albrifkani and Wang, 2016, George and Tian, 2012). This chapter focuses on the use of finite element (FE) modelling to simulate the behaviour of flat slabs in fire. The models will be validated using the results from the experimental investigation described in the previous chapter and also two other experiments conducted on flat slabs exposed to fire.

Several finite element packages have been used in other studies to capture the effects of fire in a structure. The different capabilities and shortcomings of those widely used software packages have been discussed in Chapter 2, Section 2.9. After evaluating them, FE package ABAQUS was chosen to develop the numerical models. A structural fire model is basically two-fold, a heat-transfer model to predict the variation of temperature across the structural element and a mechanical model to predict the deformation, stress variation and failure of the structural element. ABAQUS has the capability to carry out both heat transfer analysis and mechanical analysis concurrently (coupled-temperature displacement analysis) or heat transfer analysis followed by structural analysis (sequential analysis). The use of both these methods is discussed in this chapter. Furthermore, it has also got the capability to use temperature-dependent material properties, which is vital as both mechanical and thermal properties of material undergo significant changes at elevated temperatures. Concrete damage plasticity (CDP) model in ABAQUS can accurately capture the

compression crushing and tensile cracking failure in concrete, and it has been widely used in other studies as well in both ambient and elevated conditions (Albrifkani and Wang, 2016, Ellobody and Bailey, 2009, Genikomsou and Polak, 2015, Kodur and Alogla, 2017, Wahalathantri et al., 2011). Reinforcement can also be incorporated with concrete and provides more freedom to assign non-linear material properties for the steel as well. Another benefit is that the improved capabilities of visualisation of the output with time-history plots, field outputs, temperature contours, etc. Considering all the information summarised, it was decided to use the FE package ABAQUS to develop the numerical models to capture the behaviour of concrete flat slabs in fire.

4.2 MODELLING APPROACH IMPLEMENTED IN ABAQUS

Two main components of a thermo-mechanical model; heat transfer analysis and mechanical analysis can be either coupled together or sequentially analysed in ABAQUS. Both implicit and explicit solvers can be used for both these cases. All of these different approaches, their benefits and drawbacks will be discussed.

In the sequential analysis, first, a heat transfer model is developed incorporating thermal properties such as conductivity and specific heat of concrete and steel. Fire is applied as a temperature boundary condition taking into account the temperature time-history of the exposed surface of the slab. Thermal boundary conditions are applied to account for the convective and radiant heat transfer from the unexposed surfaces to the external environment. Then a transient state heat transfer analysis is conducted to obtain the temperature variation with time throughout the slab. Temperatures are recorded as a nodal output. A separate model (having the same mesh characteristics as the heat transfer model), is created with temperature-dependent mechanical properties of concrete and steel. Load and specific boundary conditions are applied to this model and the nodal output generated from the previous heat transfer analysis is applied as a pre-defined field. During the analysis, the program will take into account the nodal temperature, and corresponding material properties to that temperature will be taken into account. Both standard and the explicit solver can be used for this type of analysis. One of the significant drawbacks of the standard implicit solver is that there is a high chance of getting convergence errors due to both material and geometric nonlinearities.

The explicit solution procedure can overcome this issue because no global tangent stiffness and mass matrices need to be assembled (Albrifkani and Wang,

2016). However, the computational time for explicit analysis can be significantly high as the duration of the fire is on the scale of hours. The explicit analysis is more suitable to simulate quick, transient events in the scale of seconds.

In the coupled temperature displacement analysis, both temperature variation and mechanical loading can be applied at the same time. It was mainly developed for the purposes of simulating concise events with interdependent material properties with temperature (i.e., A steel plate is subjected to friction. Friction causes the steel to generate heat, and as a result of that, the mechanical properties of steel are altered. Moreover, it affects friction co-efficient in return). Coupled temperature-displacement analysis can account for such thermal and mechanical mutual effects. This method is seldom used for any structural fire problem. However, with certain improvisations, the possibility of using this type of analysis is described as well. The explicit solver is more suitable for this method as the implicit solver can encounter convergence issues since the material model contains both thermal and mechanical non-linear material properties.

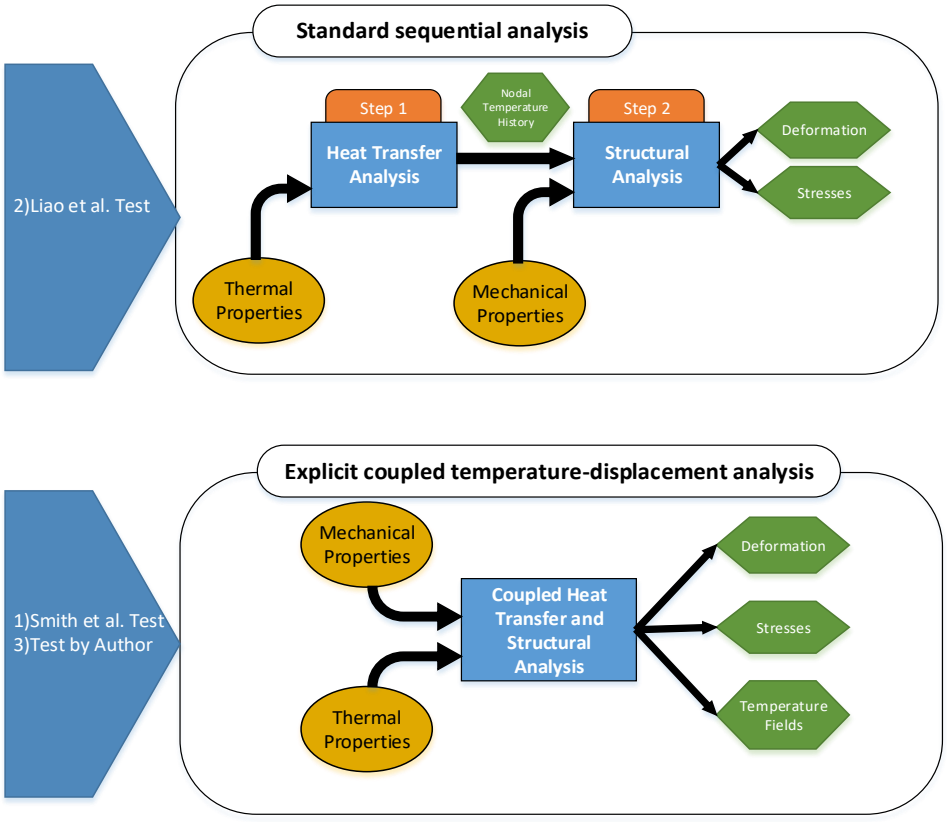

Figure 4.1: Different analysis approaches used for the numerical analysis

The following section describes the use of these different techniques validated with three independent experimental investigations on concrete flat slabs at elevated temperatures. Figure 4.1 illustrates the use of the different types of analysis for each case. Smith et al. test (2014) and authors large scale test described in Chapter 3 were modelled using the explicit coupled approach whereas Liao et al. (2013) experiment was modelled using the standard approach. Pros and cons of both approaches will be discussed in later sections based on the analysis.

4.3 MATERIAL PROPERTIES

4.3.1 General

Key to an accurate, comprehensive numerical model is the correct input of material data. In thermo-mechanical modelling, there are two main types of material properties used; thermal properties and mechanical properties. Under thermal properties, conductivity and specific heat are employed to conduct the heat transfer analysis. Under mechanical properties, stress-strain behaviour, elasticity and thermal coefficient of expansion are utilized to predict the structural behaviour at elevated temperatures. Among several material models proposed, EC2 constituent models were implemented in this study. They provide detailed material properties and their variation with temperature for both concrete and steel. Chapter 2 contains a detailed review of different material models available in the literature for concrete and steel. More specific details on the input material properties related to each model will be discussed in the following sections which describe the numerical models in detail.

4.3.2 Transient Creep

Concrete strain mainly consists of four main components. Mechanical strain, Thermal strain, Transient strain and Creep strain. Mechanical and Thermal strain components are represented by the stress-strain behaviour and thermal expansion of concrete, respectively. Creep is defined as the deformation under sustained loading, which depends on the load level and the duration of the sustained loading. At ambient conditions, it takes a significantly long duration for creep effects to develop. However, at elevated temperatures, the creep effects are amplified, and during an event of a fire, the amplified effects of creep strain significantly influence the overall deformation of the structure. Creep strain and Transient strain are combined and referred to as the

transient-creep strain or load-induced thermal strains (LITS) in fire engineering (Al Hamd et al., 2018).

Transient creep effects in fire are predominant when the temperature in concrete is more than 500^0C and stress level is more than 50% as found by Kodur et al. (Alogla and Kodur, 2018, Kodur and Alogla, 2017). It has been mentioned that the latest EC2 stress-strain relationship for concrete implicitly accounts for transient creep strains at elevated temperatures. However, several studies have shown that implicit inclusion would not accurately capture the additional creep induced deformation, especially when the load level and temperature within the concrete are high (Al Hamd et al., 2018, Alogla and Kodur, 2018, Kodur and Alogla, 2017). Therefore, if the temperature is higher than 500^0C and the structural element is heavily loaded, it is recommended to incorporate the transient creep effects explicitly in the numerical model.

Among the different models proposed to explain the creep of concrete at elevated temperatures, Anderberg and Thelandersson's creep and transient models (Anderberg and Thelandersson, 1976), Schneider's transient creep model (Schneider, 1986), Diederichs's transient creep model (Li and Purkiss, 2005), Terro's transient creep model (Terro, 1998) and Nielsen et al. transient creep model (Nielsen et al., 2002) are important. Researchers (Alogla and Kodur, 2018, Kodur and Alogla, 2017) studied the applicability of these models and Nielsen et al. model have yielded results that closely matches with the experimental results for Kodur and Alogla (2017). They have used the inbuilt CREEP function in ABAQUS to include the transient creep component. However, it should be noted that this function only works with the standard implicit solver and not applicable for the explicit solver. In the current study, both the implicit and explicit solvers are being used, and therefore, a more versatile creep model is required. Al Hamd et al. (2018) have recently proposed and validated the use of Anderberg and Thelandersson's creep models directly incorporated to the stress-strain behaviour of concrete. They have used the stress-strain relationship of the previous version of the EC2 – ENV 1992-1-2 (British Standards Institution, 1996) where the creep was not accounted for and then added the additional transient creep strain calculated following Anderberg and Thelandersson's creep model [Eqn. (4.1) & (4.2)]. Figure 4.2 further illustrates the procedure. The same method is adopted in this study as well since it does not require a separate CREEP function which only works with the standard implicit solver.

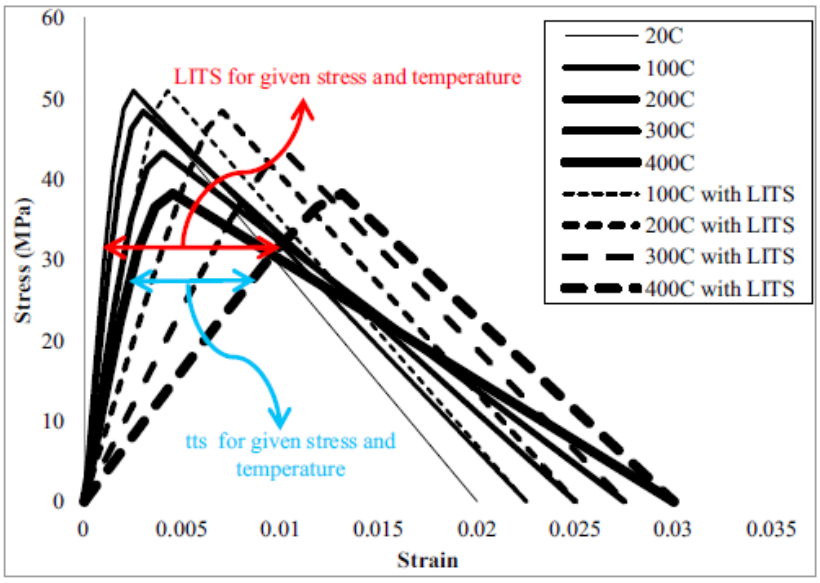

Figure 4.2: Stress-strain behaviour of concrete with and without LITS as illustrated by Al Hamd et al. (2018)

$$\varepsilon_{ts} = -k_{tr}\frac{\sigma}{\sigma_{u0}}\varepsilon_{th} \quad for\ T \leq 550^0C \tag{4.1}$$

$$\frac{\partial \varepsilon_{ts}}{\partial T} = -0.0001\left(\frac{\sigma}{\sigma_{u0}}\right) \quad for\ \ T > 550^0C \tag{4.2}$$

Where ε_{ts} is the transient creep strain, k_{tr} is a material parameter, σ_{u0} is the compressive strength of concrete at ambient temperature and T is temperature.

Incorporation of transient creep effects is further discussed under each case in the following sections.

4.3.3 Material properties during the cooling phase

Most of the fire tests which were carried out using concrete flat slabs have focused on the behaviour only during the heating phase. Either the slab has failed before the end of the test, or the slab has survived the entire duration of heating, and the test was terminated at that moment. As discussed in Chapter 2, the standard fire curves only contain increasing temperatures with time. However, the real fires are much different from that. The fire gradually dies when the fuel runs out, resulting in a drop of temperatures, which is known as the cooling phase. Strength of concrete and steel further degrades during this phase and the remaining strength when the element cools down to room temperature is called the residual strength. It is crucial to incorporate this strength degradation in a numerical model as few recent fire tests on flat slabs have also shown that they could fail during this cooling phase.

The trend of strength degradation in concrete during the cooling phase is not as severe as the strength degradation during the heating phase. The residual strength of concrete is influenced by the maximum temperature experienced during the heating phase, the time allowed for recovery after fire and the method of cooling used for quenching the fire (Kodur and Agrawal, 2016). Some studies have shown that concrete heated up to 220^0C or more has dropped its strength up to 20% from its original value($f_{c,20c}$), immediately after concrete has cooled down to room temperature (Drysdale et al., 1990). Annex C of the EC2 composite structures design code (European committee for standardization, 2005b) presents a relationship for the reduction of strength during cooling down. According to that when the maximum temperature (Θ_{max}) experienced by concrete is more than 300^0C, the residual strength of concrete at 20^0C: $f_{c,\Theta,20C}$ (after cooling down to room temperature) is 90% from the strength at maximum temperature ($f_{c,\Theta\ max}$). Strength at any temperature between Θ_{max} and 20^0C during the cooling phase can be linearly interpolated between $f_{c,\Theta\ max}$ and $f_{c,\Theta,20C.}$ Figure 4.3 will further illustrate this relationship. This model is adopted in the numerical models to represent the strength degradation of concrete during the cooling phase.

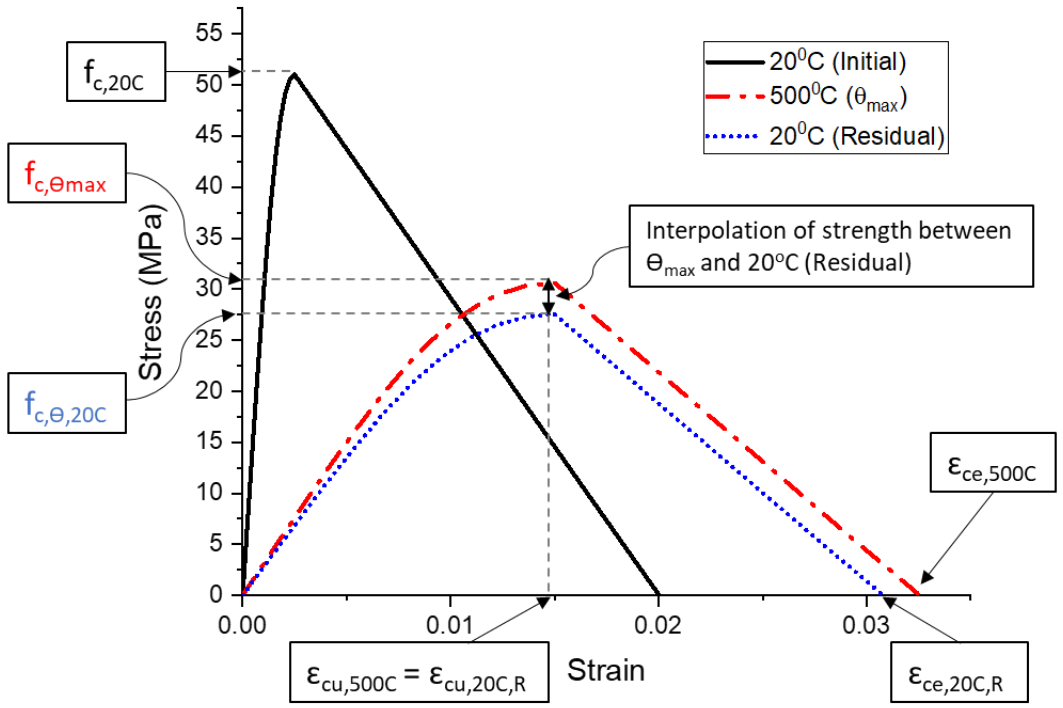

Figure 4.3: Determination of the stress-strain relationship of concrete during the cooling phase

The strength degradation of reinforcing steel is only influenced by the temperature reached during the heating phase. It has been shown that there is no strength degradation if the maximum temperature reached is below 500^0C (Neves et al., 1996). If the temperature reached during heating is between 500^0C and 800^0C residual strength ratio lies between 1 and 0.7, and after 800^0C it remains at 0.7, as shown in Figure 4.4 below. Strength ratio between the ambient strength before heating and remaining strength after heating and subsequent cooling down to ambient conditions again, is defined as the residual strength ratio.

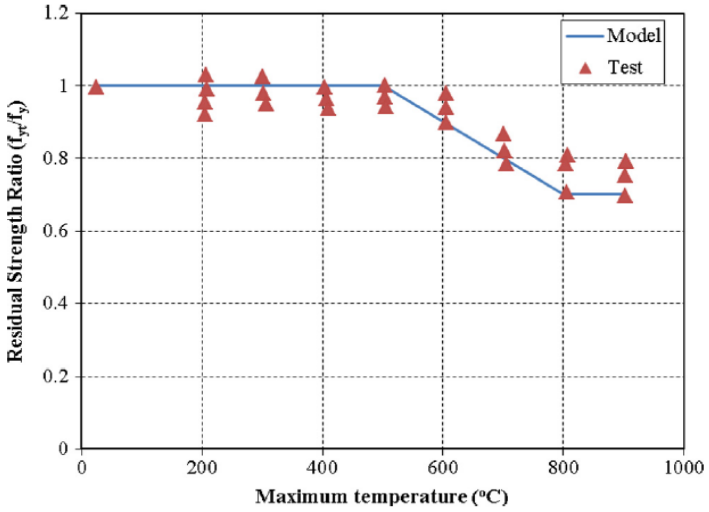

Figure 4.4: Normalized residual strength of hot rolled reinforcing steel as illustrated by Kodur and Agrawal (2016) and Neves et al. (1996)

Assigning the cooling phase material properties in ABAQUS is not straight forward. Although it has the option to define the change of material properties with temperature, the trend in changes during heating and cooling are different. The analysis can be broken down to 'steps' in ABAQUS, and the program does not allow to change the material properties from one step to another. To overcome this challenge, the 'FIELD VARIABLE' function was used. Material properties during the heating phase were assigned with one field variable (FV=x) and the properties during the cooling phase were assigned with another field variable (FV=y). Then the input Python code of the numerical model is modified to change the field variable from 'x' to 'y' when the analysis changes from heating phase to the cooling phase. That way, the program identifies the change of field variable in nodes and assign the corresponding material properties under that specific field variable. More details of this implementation will be discussed during the upcoming sections.

4.4 NUMERICAL MODELLING OF CONCRETE FLAT SLABS SUBJECTED TO FIRE

This section will discuss the numerical models developed to predict the behaviour of concrete flat slabs during fire. Models were validated using two independent experiments carried out on small-scale flat slabs and the large-scale fire test discussed in Chapter 3. Following sections will layout the methodology adopted for each test and the comparison of modelled results with the experimentally measured results.

4.4.1 Test by Smith et al. (2014)

4.4.1.1 Experimental set-up

The experiment by Smith et al. (2014), which involved restrained support conditions were used to develop the finite element model of the flat slab. The study consisted of a total of 15 slab specimens (50, 75 and 100mm thick) which were tested at ambient temperature and elevated temperature under restrained and unrestrained support conditions. Details of the experiment can be found in Smith et al. (2014) and explained in Chapter 2. Figure 4.5 shows the specimen size, loading arrangement, fire exposure and support conditions along with the reinforcement arrangement of flat slab specimens used in the test. A 100mm thick, 0.8% reinforced, restrained slab specimen was selected to illustrate the modelling technique. The load was applied to the column stub as shown in Figure 4.5 at ambient conditions. When the load reached a value of 162kN (which is 70% of the punching shear capacity at room temperature), it was maintained for a few minutes until the deformation stabilised. Then the slab was heated from the compression side, as shown in Figure 4.5 for a duration of 2 hrs while maintaining the load at 162kN. The applied fire was a non-standard furnace specific fire having a maximum temperature of around 500^0C. (see Figure 4.6). Exposed surface temperatures were calculated based on the readings of the thermocouples embedded inside the slab to measure temperature across the depth. More details of the experiment can be found in Smith (2016). Deformation and the temperatures across the depth of the slab were measured during the test. Since the slab did not fail having exposed to a 2 hr fire duration, the heating was stopped, and the slab was allowed to cool down for another two hours while maintaining the same load.

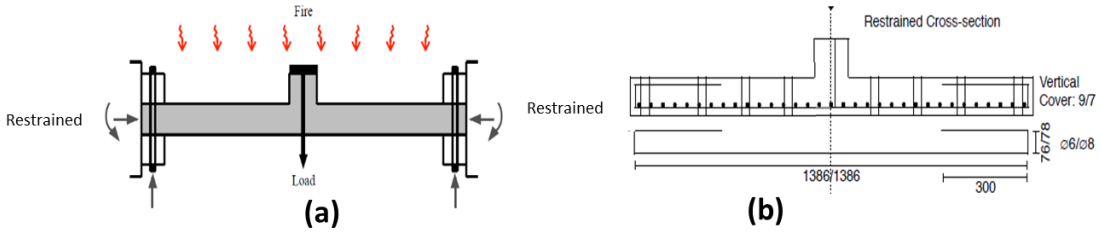

Figure 4.5: Test set up used by Smith et al. (2014) a) Support conditions, loading and fire exposure; b) Reinforcement arrangement (Specimen size – 1.4m x 1.4m x 0.1m, 0.25m x 0.25m x 0.1m column at the middle)

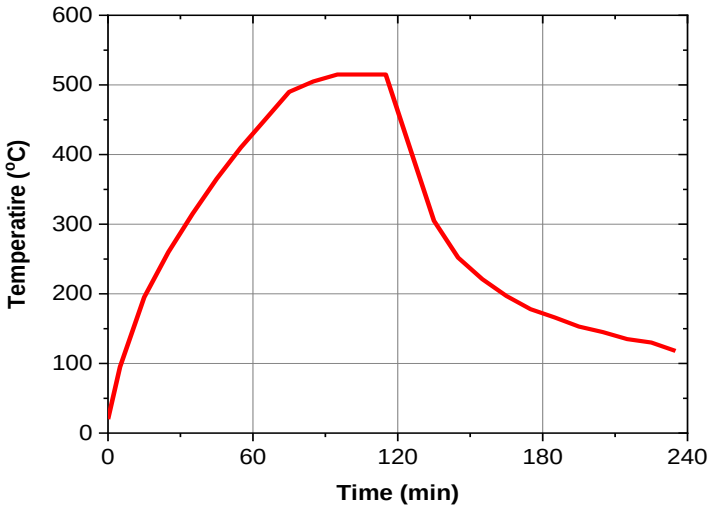

Figure 4.6: Exposed surface temperature of the slab

4.4.1.2 Material data and other parameters used in the FE model

Concrete damage plasticity model was selected to represent concrete as discussed previously. Convergence was reported as a common issue related to modelling behaviour under fire as it contains both material nonlinearities and geometric nonlinearities (George and Tian, 2012). Temperature dependence of material properties makes it even more challenging to converge on a solution. As a remedy in standard implicit modelling, the time increment of an iteration can be made very small. However, the computational cost of such models is very high as the usual duration of the applied fire in an analysis can be 1 to 4 hours. Therefore, the explicit dynamic solver was used in this analysis to simulate the quasi-static behaviour with some improvisations. The techniques used will be discussed in detail in the following sections.

Concrete damage plasticity (CDP) model in ABAQUS uses concepts of isotropic damaged elasticity in combination with isotropic tensile and compressive plasticity to

represent the inelastic behaviour of concrete (Dassault Systèmes, 2014). The main two failure mechanisms assumed are tensile cracking and compressive crushing in concrete. More details regarding this were presented in Chapter 2. General parameters considered for the CDP model are the dilation angle (ψ) 30^o, the eccentricity 0.1, the stress ration (f_{bo}/f_{co}) 1.16, the shape factor (K_c) 0.667 and the viscosity parameter 0.005 which have been also used in other similar studies (Albrifkani and Wang, 2016, Genikomsou and Polak, 2015, George and Tian, 2012).

Stress-strain behaviour of concrete in compression and tension at elevated temperatures were calculated in accordance with the guidelines given in Table 3.1 of EN 1992-1-2 (European committee for standardization, 2004b). Concrete compressive strength (f_{cu}) and tensile strength ($f_{ck,t}$) were determined experimentally as 51 MPa and 4MPa, respectively (Smith, 2016). Based on that, a linear elastic behaviour was assumed up to $0.4f_{cu}$ for compressive stress-strain behaviour of concrete. It was followed by a parabolic variation until it reaches the ultimate strength according to the relationship given in EN 1992-1-2 (European committee for standardization, 2004b). The softening behaviour of concrete is represented through a linear descending branch (see Figure 4.7). For this model, the transient creep effect was not considered as the exposed temperatures were low, and the maximum temperatures reached within the depth were below 500^{0}C. Previous studies have shown that transient creep effects are critical when the concrete temperature has exceeded 500^{0}C (Alogla and Kodur, 2018, Kodur and Alogla, 2017).

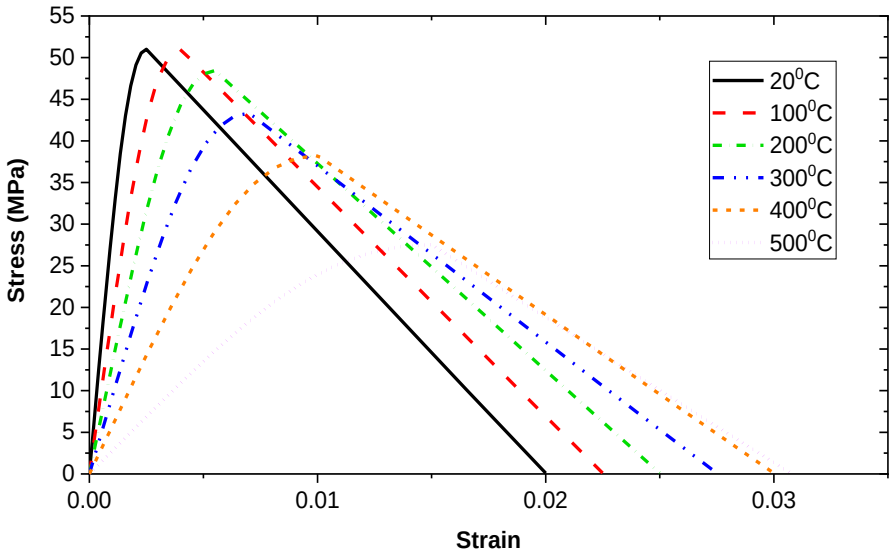

Figure 4.7: Stress-strain behaviour of concrete in compression at elevated temperatures

For the stress-strain response of concrete in tension, a linear elastic behaviour was assumed up to its tensile strength followed by a bilinear softening response. The area under the softening branch was determined based on the fracture energy (G_f), which is assumed to be 0.25 N/mm for this model. More details of this method can be found in Ellobody and Bailey (2009) and Genikomsou and Polak (2015) and discussed in Chapter 2. As seen from Figure 4.8, the tensile stress of concrete reaches zero at the ultimate strain at the end of the softening branch. However, ABAQUS manual (Dassault Systèmes, 2014) states that this could lead to convergence errors and therefore, it recommends keeping the stress at ultimate strain to be at least 10% of the tensile strength. This recommendation was followed when inputting these stress-strain values to ABAQUS. Note that in Figure 4.8 both 20°C and 100°C curves are overlapped as tensile strength in concrete does not degrade up to 100°C as shown in Figure 2.22.

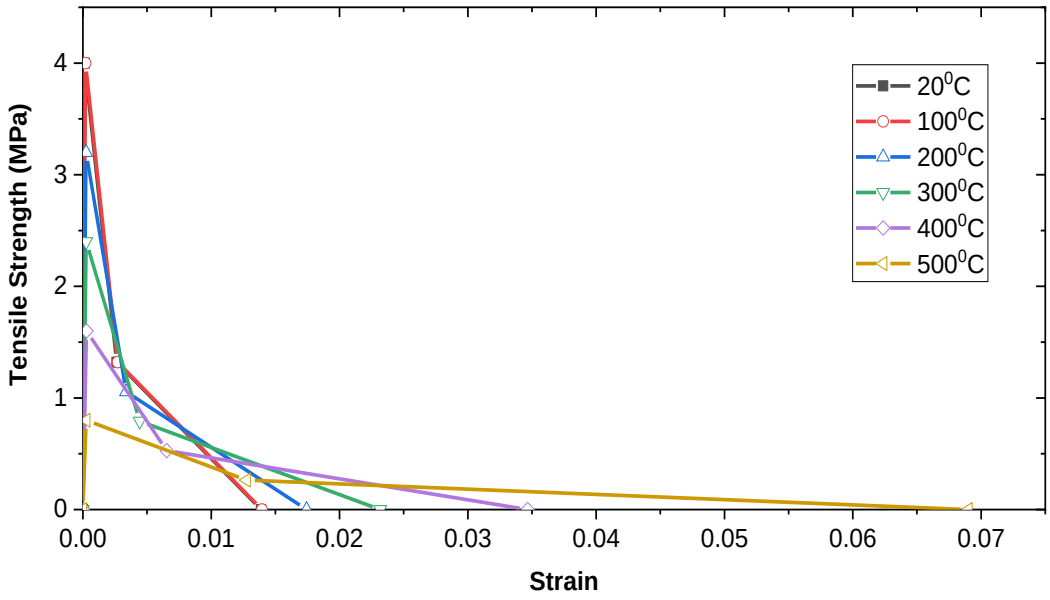

Figure 4.8: Stress-strain behaviour for concrete in tension at elevated temperatures

The stress-strain relationship for reinforcing steel at elevated temperatures was determined according to Table 3.2b of EN 1992-1-2 (European committee for standardization, 2004b) having a yield strength of 549MPa and Young's modulus of 200GPa (Smith, 2016) (see Figure 4.9). Stress and strain values given in the design code are engineering stresses and strains, whereas, for the accuracy of the numerical model, it requires true stress and strain values. Therefore, the code stresses and strains

were converted to true stresses and strains using the following two equations [Eqn. (4.3) & (4.4)].

$$\sigma_n = \sigma(1 + \varepsilon) \tag{4.3}$$

$$\varepsilon_n = ln(1 + \varepsilon) \tag{4.4}$$

Where σ_n and ε_n are true stress and true strain respectively. σ and ε are engineering stress and strain provided by European design codes (European committee for standardization, 2004b).

General plasticity model in ABAQUS was used to input the non-linear behaviour of steel at elevated temperatures.

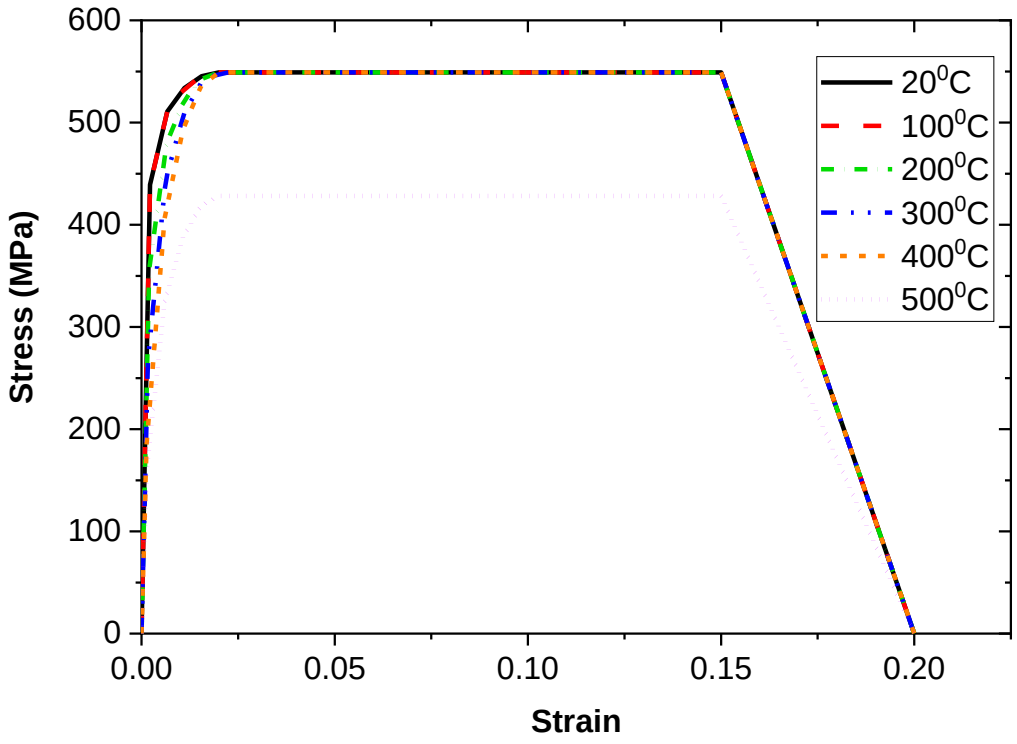

Figure 4.9: Stress-strain relationship for reinforcing steel at elevated temperatures

Thermal properties of concrete (specific heat and conductivity) were also derived from relationships given in EN 1992-1-2 (European committee for standardization, 2004b) for siliceous concrete (Smith, 2016). The lower limit of thermal conductivity was selected as it gives more realistic temperatures for concrete structures than the upper limit (European committee for standardization, 2004b) (see Figure 4.10). Thermal elongation and coefficient of thermal expansion for siliceous concrete were determined in accordance with section 3.3.1 in EN 1992-1-2 (European

committee for standardization, 2004b)(see Figure 4.11). Thermal properties of steel were not taken into account as the element types used in the FE model for reinforcing steel did not participate in the heat transfer analysis. Wang (2006) has shown that the temperature across the depth with and without reinforcing bars was very similar and therefore, the effect from steel for the heat transfer can be negligible. However, the temperature of the reinforcement can be indirectly found by relating to the temperature of the concrete at the same depth.

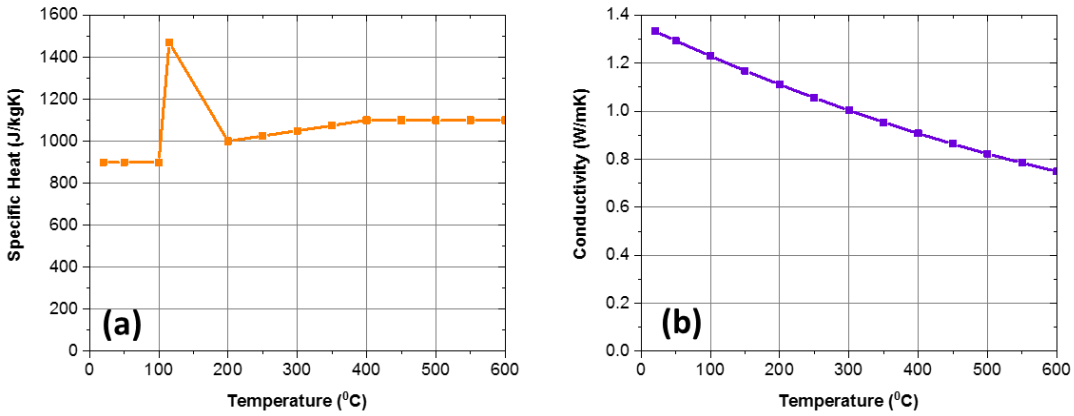

Figure 4.10: Thermal properties for concrete (a) Specific heat and (b) Conductivity

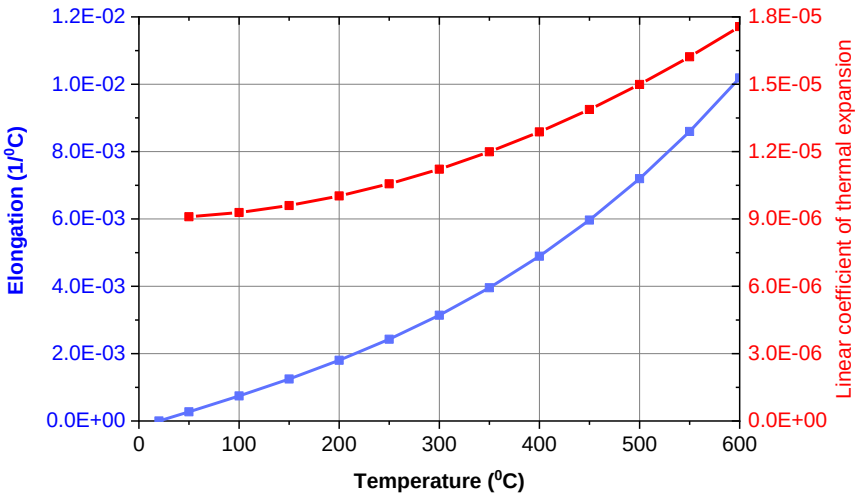

Figure 4.11: Thermal elongation and coefficient of thermal expansion for concrete

Based on the symmetricity of loading and boundary conditions, only a quarter of the slab (0.7 m x 0.7m x 0.1m) was modelled to save the computational time. C3D8RT (An 8-node thermally coupled brick) elements were used to model concrete whereas reinforcement was modelled using T3D2 (A 2-node linear 3-D truss.) elements. Truss elements representing reinforcement were embedded using the embedded region constraint, assuming a perfect bond between concrete and

reinforcement. This assumption is also made in several other studies (Genikomsou and Polak, 2015, Kodur and Agrawal, 2016), and it has yielded accurate results.

Slab specimen in the experiment was restrained along the perimeter against both translation and rotation. (See Figure 4.12). In the model, the bottom edge was restrained, and axial spring elements were used along the side surfaces to represent the lateral restraints (see Figure 4.12). Genikomsou and Polak (2017) used a similar approach to investigate the compressive membrane action in flat slabs at ambient conditions. The advantage of using spring supports in this particular case is further explained in the results section. The explicit solver in ABAQUS only allows having node-to-node spring elements in the model. Hence, all the nodes in a particular side are assigned to one reference point, and the spring element was assigned to that specific reference point with spring stiffness defined along the lateral direction.

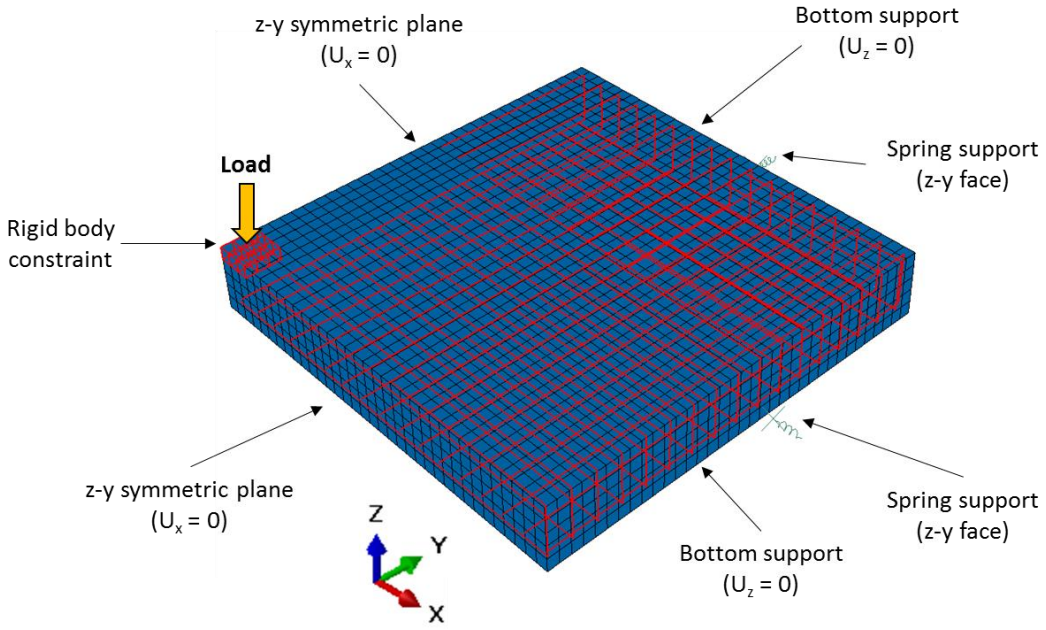

Figure 4.12: Boundary conditions, loading and constraints used in the FE model

4.4.1.3 Analysis procedure

The analysis was carried out in two different steps. First, loading was applied using a dynamic explicit step. Although ABAQUS/Explicit uses a dynamic solution procedure, it can be used for quasi-static analysis with a low rate of loading (Genikomsou and Polak, 2015). In the experiment, the slab was cast along with a short column where the loading was applied through a hydraulic jack to the column. However, in the analysis, only the slab was modelled and to simulate the effect of the column, a rigid body constraint was applied to the location of loading. (See Figure

4.12). Then, the dynamic explicit coupled temperature displacement step in ABAQUS was used to carry out the thermo-mechanical analysis. In this step, the load (P) applied in the first step was kept constant while the temperature measured in the experiment was applied to the top surface of the slab as a boundary condition. The use of explicit solver avoids the convergence issues encountered in a standard static implicit analysis.

The total duration of the test was 4 hours; 2 hours of heating followed by 2 hours of cooling. For the heating step, the convective coefficients were taken as 25 W/m^2K and 9 W/m^2K for exposed surface and unexposed surface, respectively (European committee for standardization, 2004b). In the cooling step, a convective coefficient of 9 W/m^2K was assigned for all the surfaces. Concrete emissivity was taken as 0.7 and Stefan-Boltzmann constant to be 5.67×10^{-8} W/m^2K^4 to simulate the radiative heat transfer in both steps.

Generally, an explicit step is particularly well-suited to simulate brief transient dynamic events (Dassault Systèmes, 2014). However, it can be used for an analysis consisting of long duration with some improvisations. Explicit time integration algorithm uses a very small time increment. It can be increased by either artificially increasing the mass of the structure (mass scaling) or by artificially increasing the loading speed (load factoring) (Albrifkani and Wang, 2016). Mass scaling can cause large inertia forces which can deviate the solution from quasi-static state to a dynamic state. Therefore, load factoring method was applied in this model. It should be noted that load factoring in this study refers to the thermal load. Although the duration of heating is 2 hours, it has been scaled down to 2 seconds in the coupled temperature displacement step with modifications to the units involving time. i.e. conductivity, specific heat, coefficient of convection and Stefan-Boltzmann constant for radiation.

4.4.1.4 Results and Discussion

Numerical models were validated comparing the thermal and structural response predictions from the analysis. Thermocouples (TCs) in the experiment were placed 200 mm away from the column surface across the depth (at 10mm, 33mm, 65mm, 82mm and 101mm). TC which was used to measure the exposed surface temperature was located 10mm inside the slab depth as described by Smith (2016). Therefore, measured temperatures were extrapolated to calculate the applied temperature to the exposed surface. Nodal temperature results from 200 mm away from the column surface across the depth were compared with the measured temperature values. It

should be noted that temperatures at 20mm intervals across the depth were determined using the temperature profiles at 10min intervals from Smith (2016). Figure 4.13 shows the temperature variation across the slab depth during the heating and cooling phases of the experiment and model. Modelled temperatures are in good agreement with the measured data.

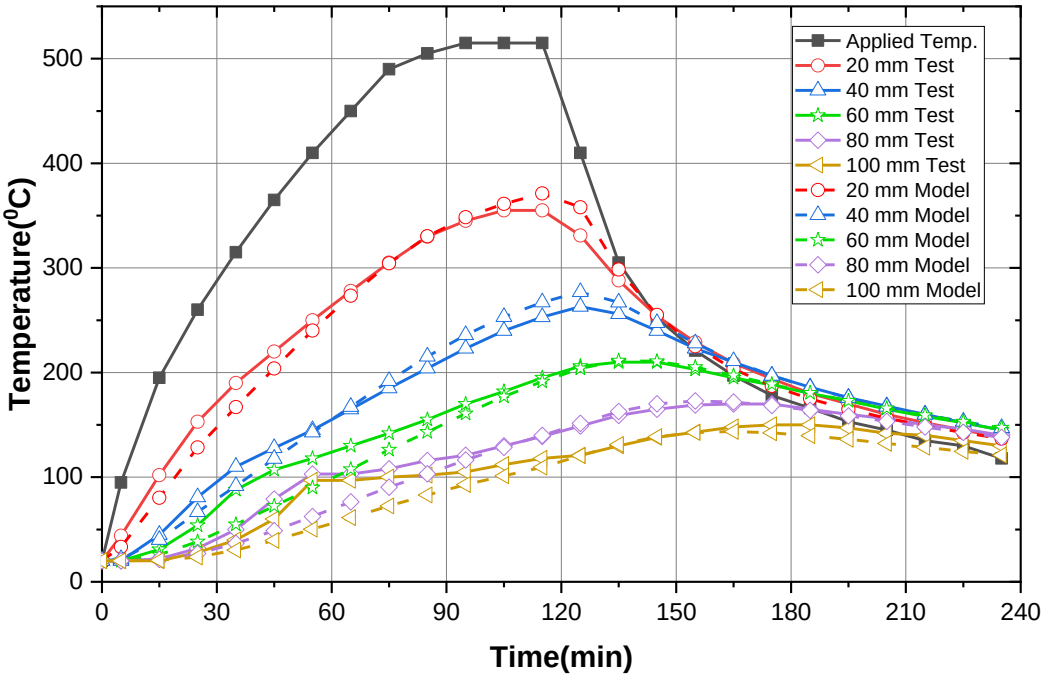

Figure 4.13: Experimental and modelled temperature variation across the slab depth

Deflection criteria was considered to validate the structural response of the FE model. Downward displacement was determined using two methods in the experiment. Employing a displacement transducer (LP) connected to the loading rod which goes through the column and using digital image correlation (DIC). However, it was concluded that the DIC measurements were more accurate than LP as the localised crushing of the concrete around the column stub and extension of the loading rod due to the elevated temperature can artificially increase the LP measurements (Smith, 2016). Therefore, DIC measurements were taken to compare the modelled displacement with experimental displacement.

Figure 4.14 presents the results, and it should be highlighted that when the perimeter is fully fixed, the modelled deflections are much lower than the measured deflections. Releasing the restraints increase the deflection but make the model more flexible. Therefore, spring supports were used as discussed before and a spring

stiffness of 30,000 N/mm used in the model as suggested by Genikomsou and Polak (2017) to represent the membrane action due to lateral restraints. With the use of spring supports a close match between measured and modelled deflections has been achieved.

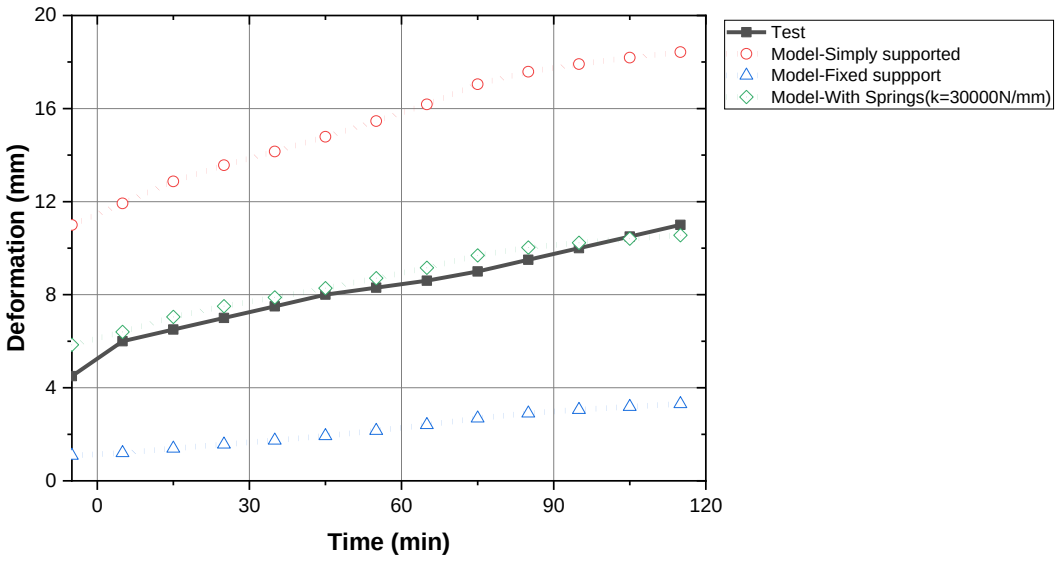

Figure 4.14: Experimental and modelled deflection of the slab during the heating phase

It should be noted that if the same material properties were used for the cooling phase, the deformation reduces after heating stops. This is due to the unrealistic strength gain of concrete when the temperature drops down. As per the properties assigned in accordance with the stress-strain relationship given in EC2 (Figure 4.7), when the temperature drops down gradually from 600^0C across the depth, the strength and Youngs modulus of concrete increase. This results in a reduction of deflection, as shown in Figure 4.15. However, in the experiment, the deformation further increased during the cooling phase as well, indicating further strength and stiffness degradation. To account for that, the residual material properties proposed by EC2 composite code(European committee for standardization, 2005b) as discussed in Section 4.3.3 were applied to the model employing the field variable.

When assigning the inelastic strains of concrete for CDP in ABAQUS, the heating phase properties were given the field variable value 1, and the cooling phase properties were given the field variable value 2. Similar field variables were assigned for the Young's modulus as well. Then the input FORTRAN code was modified so that the field variable for the whole node-set was assigned 1.0 during the heating step,

and in the cooling step, it was changed to 2.0. This has yielded a deformation which closely resembles the experimentally measured values, as shown in Figure 4.15.

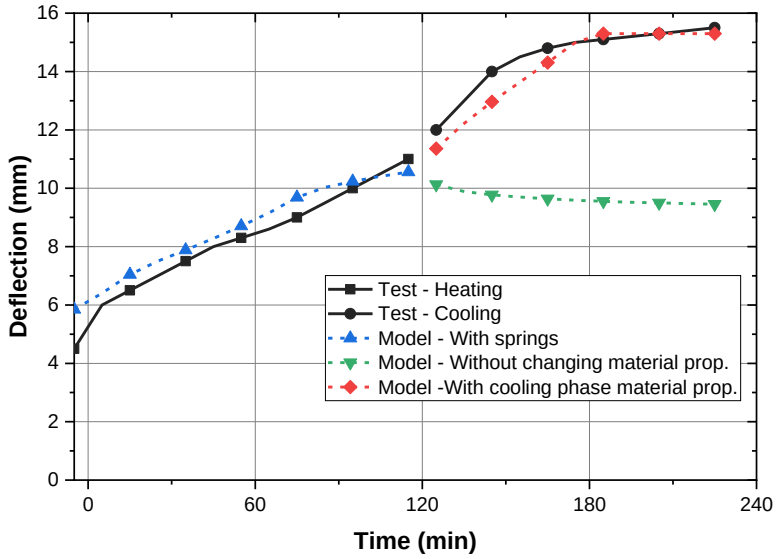

Figure 4.15: Comparison of modelled deformation during the cooling phase

To further ensure that the analysis was in a quasi-static state, the kinetic energy (KE) and the total internal energy (IE) of the model was compared. KE is negligible compared to IE as depicted from Figure 4.16. Therefore, it can be assured that the analysis was in a quasi-static state throughout the simulation.

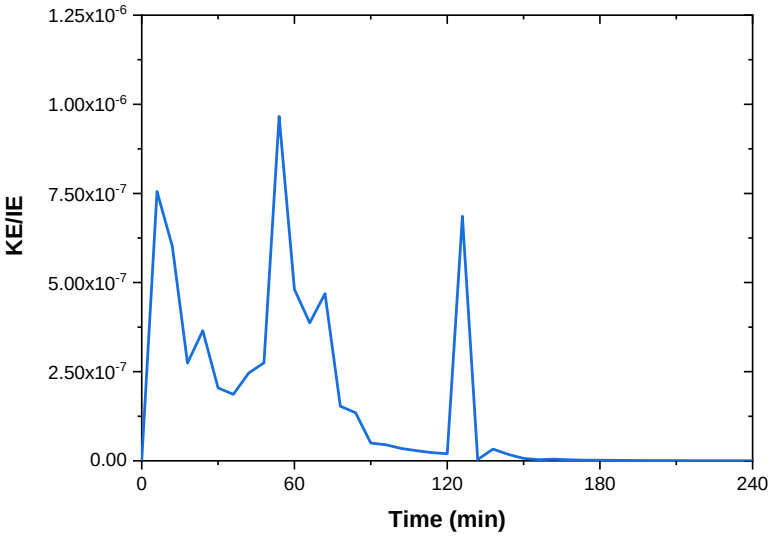

Figure 4.16: Ratio between Kinetic Energy and Internal Energy of the model throughout the analysis

4.4.2 Test by Liao et al. (2013)

4.4.2.1 Experimental set-up

Liao et al. (2013) conducted small-scale fire tests on simply supported concrete flat slabs. A total number of 6 specimens were tested at elevated temperature, and fire was applied to both compressive and tensile faces of the slab. Figure 4.17 shows the experimental set-up and the details of the specimen. The numerical model discussed in Section 4.4.1 focused on fire on the compression side of the flat slab, and therefore, in this section, a numerical model will be developed to represent a specimen heated on the tension side. Slabs which used normal strength concrete was chosen for the model as high strength concrete specimens showed spalling at high temperatures and modelling spalling would be out of the scope of this study. Also, slabs are usually constructed using normal strength concrete.

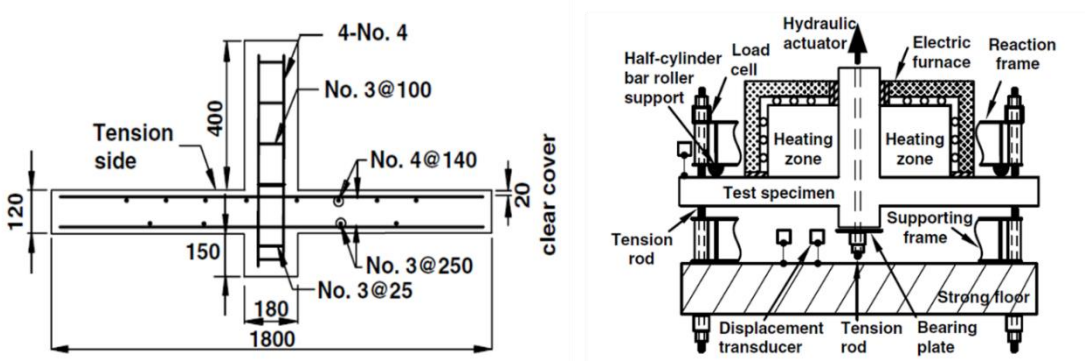

Figure 4.17: Test set-up and details of the slab specimen used in the experiment (Liao et al., 2013)

Test load was taken as 54% of the ultimate punching shear strength at ambient conditions. For the specimen selected, a load of 116kN was applied to the column stub and maintained for 30-50 mins until deformation stabilised. Then the slab was subjected to heating which closely matches the ASTM E119 standard time-temperature curve (ASTM International, 2016) as shown in Figure 4.18. Deformation and temperature were measured at different locations during the test. The test was conducted only for a heating regime until the failure of the slab.

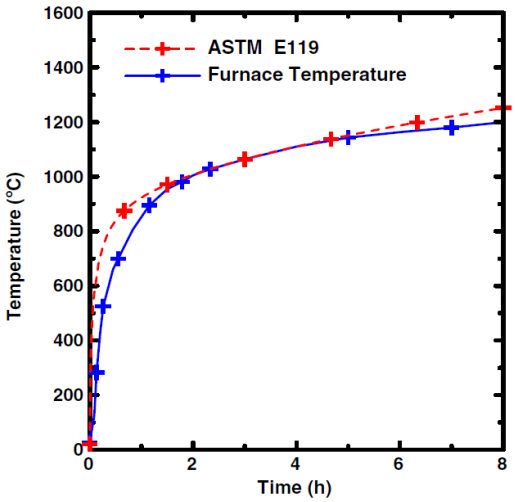

Figure 4.18: Furnace temperature vs the ASTM E119 standard temperature (Liao et al., 2013)

4.4.2.2 Material data and other parameters used in the FE model

EC2 material properties (European committee for standardization, 2004b) were employed for both concrete and steel at elevated temperatures. The lower limit of thermal conductivity for siliceous concrete was used (Figure 4.10(b)) as it yields more accurate results (European committee for standardization, 2004b). Specific heat for concrete having a moisture content of 1.5% is considered (Figure 4.10(a)).

Ambient concrete strength was measured to be 32MPa, and stress-strain behaviour at elevated temperature was determined based on that and EC2 Table 3.1 (European committee for standardization, 2004b). Several researchers have highlighted (Al Hamd et al., 2018, Kodur and Alogla, 2017) the importance of incorporating load-induced thermal strain (or transient creep strain) into numerical models as discussed in Section 4.3.2. Therefore, the method proposed by Al Hamd et al. (2018) was used where LITS is added to the stress-strain curve it-self. As it is mentioned that transient creep is explicitly included in EC2 (European committee for standardization, 2004b), preceding code stress-strain behaviour proposed in ENV 1992-1-2 (British Standards Institution, 1996) was selected to add LITS. Andelberg's creep model was utilized to determine the transient creep strain at elevated temperatures. With transient creep strain added, the stress-strain relationship adopted in the model is shown in Figure 4.19.

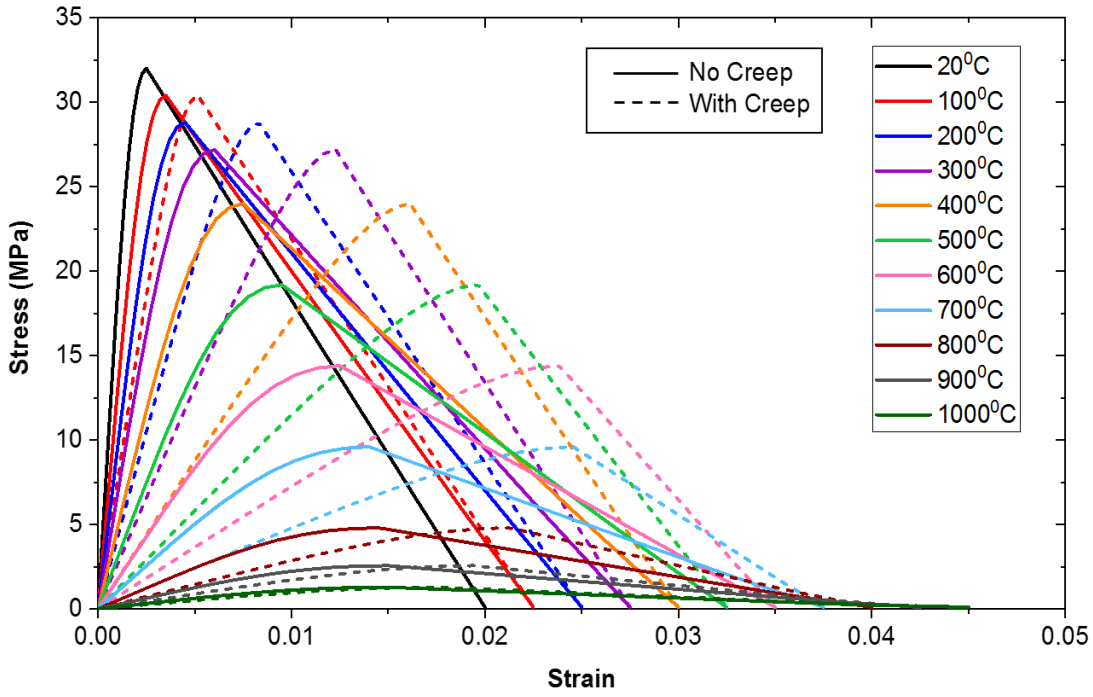

Figure 4.19: Stress-strain curve for concrete in compression including transient creep strain

Tensile strength of concrete is not mentioned in the study, and it is assumed to be 10% of compressive strength (Ellobody and Bailey, 2009). A linear elastic behaviour was assumed until it reaches the tensile strength followed by a bilinear softening response. The area under the softening branch was determined based on the fracture energy (G_f), which is assumed to be 0.25 N/mm for this model (see Figure 4.20). Note that in Figure 4.20 both 20°C and 100°C curves are overlapped as tensile strength in concrete does not degrade up to 100°C as shown in Figure 2.22.

At 600°C, the tensile strength of concrete becomes negligible or zero. To avoid this problem, the equation proposed by Dwaikat and Kodur (2009) has been followed to represent tensile behaviour of concrete beyond 600°C, as discussed in Chapter 2. Figure 4.21 presents the tensile behaviour beyond 500°C. General parameters considered for the CDP model are the dilation angle (ψ) 30°, the eccentricity 0.1, the stress ratio (f_{bo}/f_{co}) 1.16, the shape factor (K_c) 0.667 and the viscosity parameter 0.005 which have been used in other similar studies as well.

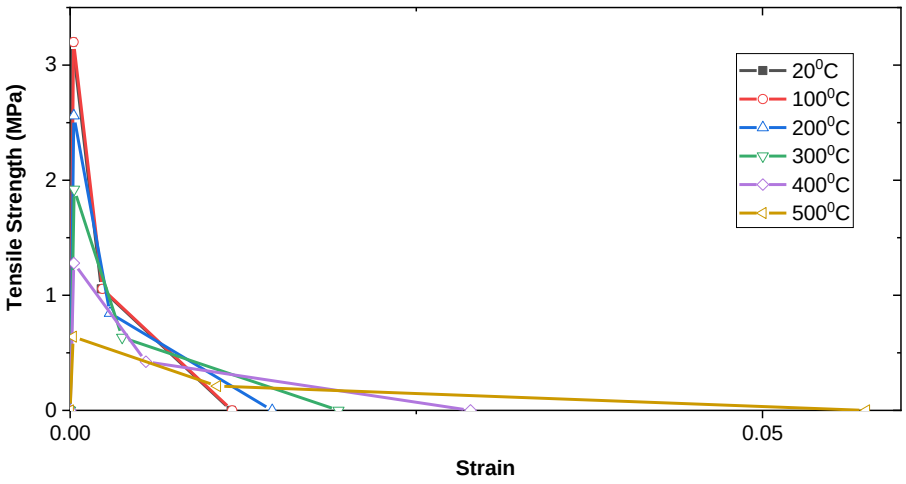

Figure 4.20: Stress-strain behaviour of concrete in tension until 500^{0}C

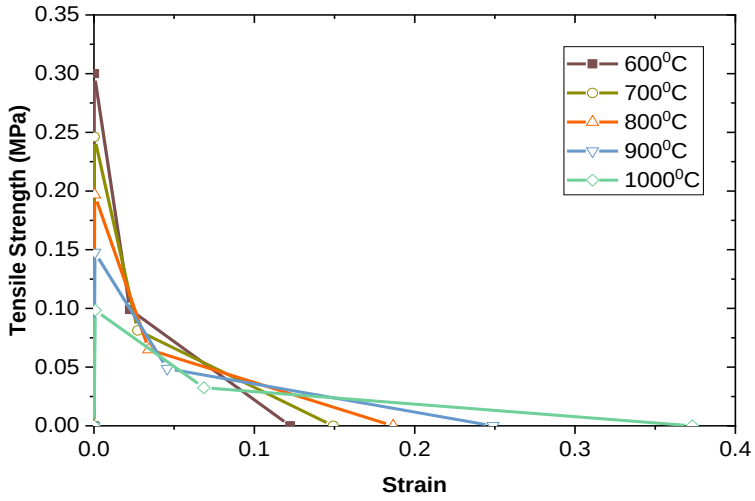

Figure 4.21: Stress-strain behaviour of concrete in tension beyond 500^{0}C

The stress-strain relationship for reinforcing steel at elevated temperatures was determined according to Table 3.2b of EN 1992-1-2 (European committee for standardization, 2004b) having a yield strength of 420MPa and a young's modulus of 200GPa (Liao et al., 2013) (Figure 4.22). General plasticity model in ABAQUS was implemented to input the non-linear behaviour of steel at elevated temperatures.

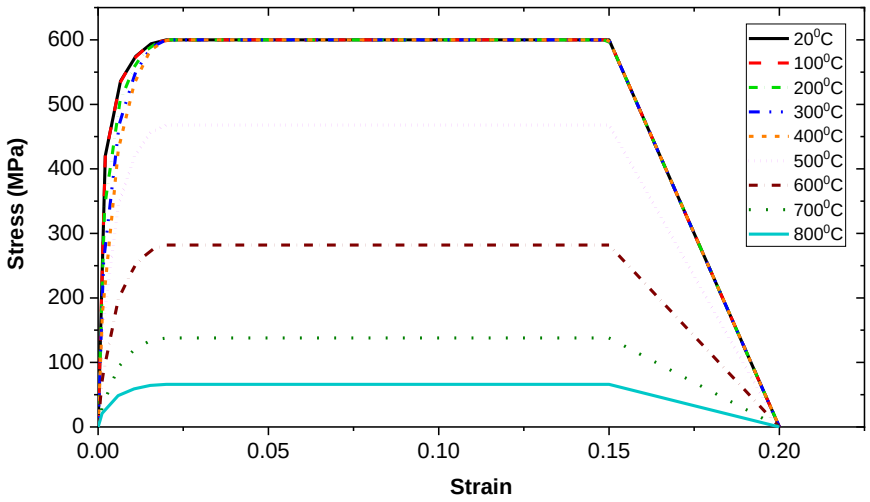

Figure 4.22: Stress-strain behaviour of steel at elevated temperatures

Thermal elongation is one of the most critical input parameters when modelling under fire. The output of the model is highly sensitive to these values (Ellobody and Bailey, 2009). EC2 provides thermal elongation for both concrete and steel at elevated temperatures. These values were converted into linear thermal expansion coefficients (α) taking the reference temperature as 20°C and inserted into ABAQUS. Thermal expansion properties of concrete adopted is similar to shown in Figure 4.11 previously, whereas for steel properties given in EC2 are used (see Figure 4.23).

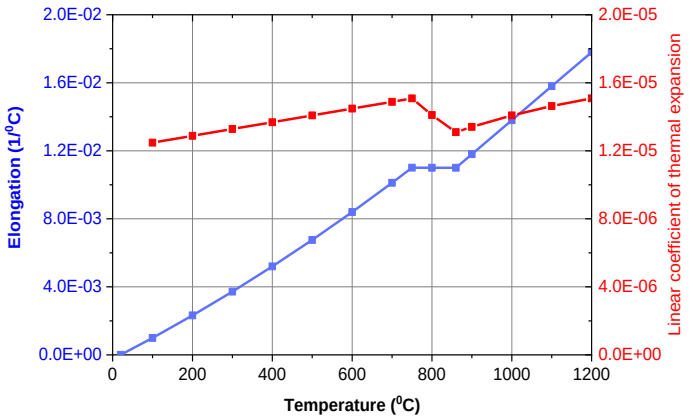

Figure 4.23: Thermal expansion of reinforcing steel

Thermal properties of concrete utilized during the heat transfer analysis were similar to that of Figure 4.10 used previously. Since this model adopted the sequential approach, it allowed the heat transfer between concrete and steel reinforcement. Therefore, the following thermal properties for reinforcing steel were implemented in accordance with EC2 (European committee for standardization, 2004b). (see Figure 4.24).

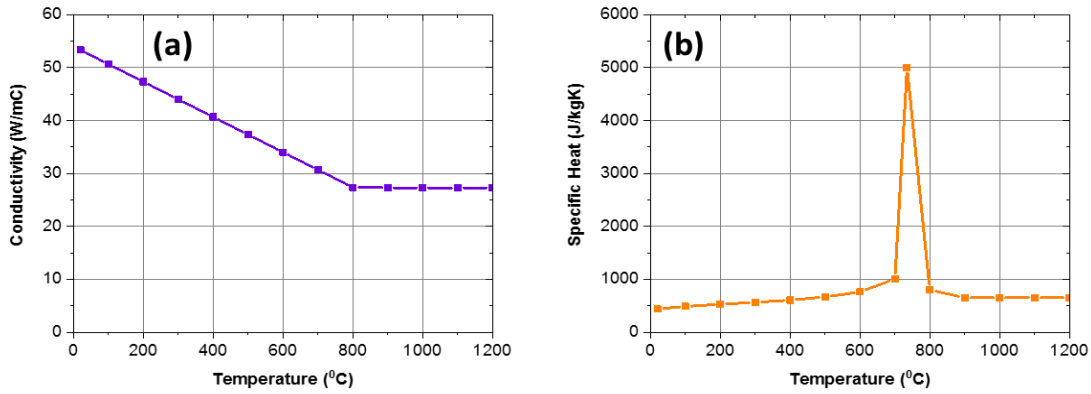

Figure 4.24: (a) Conductivity and (b)Specific heat of reinforcing steel

Since this model has adopted the sequentially coupled thermo-mechanical analysis, two different types of elements and boundary conditions were employed during heat transfer analysis and mechanical analysis. In the heat transfer analysis step, DC3D89(An 8-node linear heat transfer brick) elements represented concrete and steel was represented by DC1D2 (A 2-node heat transfer link) elements. Embedded region constraint was assigned to simulate the connection between reinforcement and concrete. This has been used in several other studies as well (Kodur and Alogla, 2017, Hawileh and Kodur, 2018), assuming a perfect bond between concrete and steel, which has yielded accurate results. The heated portion of the slab is shown in Figure 4.25, which agrees with the heated area during the experiment.

After the heat transfer step, a standard implicit step was used to model the behaviour of the slab under fire. Concrete was represented by C3D8R (An 8-node linear brick with reduced integration) elements whereas steel was represented by T3D2 (A 2-node linear 3-D truss) elements. Simply supported boundary conditions were assigned, as shown in Figure 4.25 following the experimental arrangement. Vertical direction (z) was restrained against translation to match with the positioning of the supporting frame around the specimen. X and Y translations were also restrained only along the outer surface of the slab (as shown in Figure 4.25) to prevent the lateral translation of the slab during the loading. Since it was only restrained on the outer surface, the poison effect and the thermal expansion was allowed during loading and heating, which is similar to the experiment.

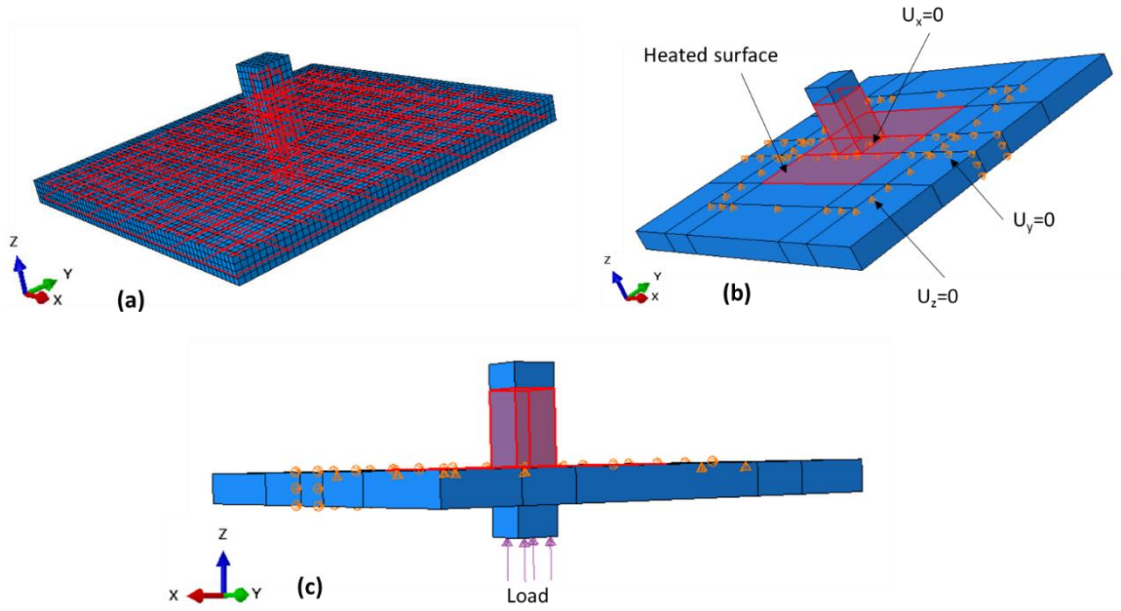

Figure 4.25: (a) Meshed FE model with embedded rebar, (b) Heated surface and boundary conditions applied, (c) External load applied to the model

4.4.2.3 Analysis procedure

The standard sequential approach was adopted in this study, where a heat transfer analysis is conducted as the first step to apply the fire, and the resulted temperature distribution across the sample is recorded. In the subsequent step, the temperature history output of the heat transfer analysis and the external load was applied to the structure until the failure or termination of the test. Convection heat transfer coefficients of 25W/m^{2}K and 9W/m^{2}K were used for the exposed and unexposed surfaces, respectively during the heat transfer analysis. Emissivity was taken as 0.7. Nodal temperature output of the heat transfer step was recorded for the whole model, which is later used as an input for the mechanical analysis.

After the heat transfer step, a static general step was conducted to model the behaviour of the slab under fire. Initially, the load was applied and kept constant for a period of 30 minutes as it was done in the experiment. Then fire load was applied in the form of a predefined field which was imported from the nodal output of the previous heat transfer analysis. It should be noted that the overall mesh of the two models (heat transfer and mechanical) should be identical to apply the nodal temperature for the subsequent mechanical analysis correctly.

4.4.2.4 Results and Discussion

Thermal response of the model was validated by comparing the obtained temperature variation across the depth with the measured temperature during the experiment. Figure 4.26 shows the locations of the TCs chosen for the validation. Among them, T3 and T7 locations showed a similar trend, whereas the temperatures in location T1 are lower than them. Comparison of the measured vs modelled time-temperature histories is shown in Figure 4.27 and Figure 4.28. A close match to the experimental results was achieved in the model. It should be noted that there is a temperature plateau around 100^0C in the measured temperature trends. That is a result of the thermal energy being used to evaporate the trapped water within the specimen. However, it was challenging to achieve that from the heat transfer model, although the EC2 specific heat definition artificially increases the heat capacity around 100^0C to account for this. Apart from that, the temperature trend and the final temperature distribution closely matches the experimental results.

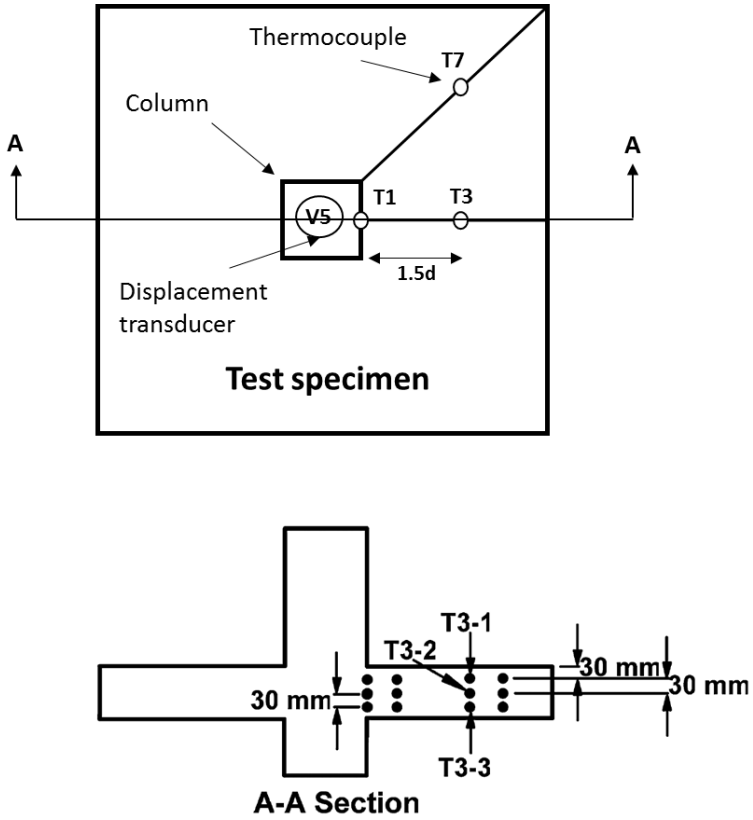

Figure 4.26: Thermocouple and Displacement transducer locations in the experiment which have been used to validate the numerical models

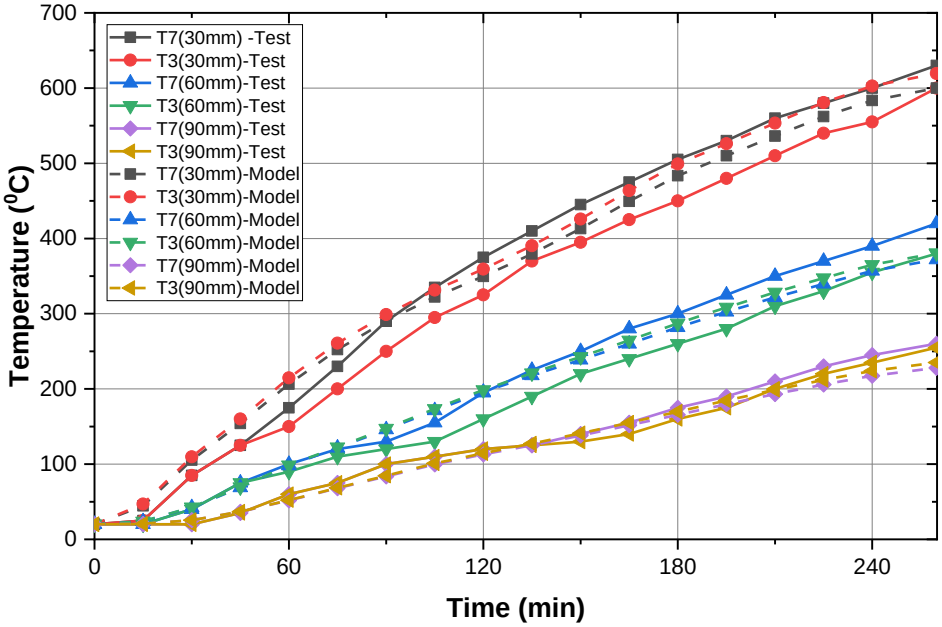

Figure 4.27: Measured vs Modelled time-temperature histories across the slab depth; T3 and T7

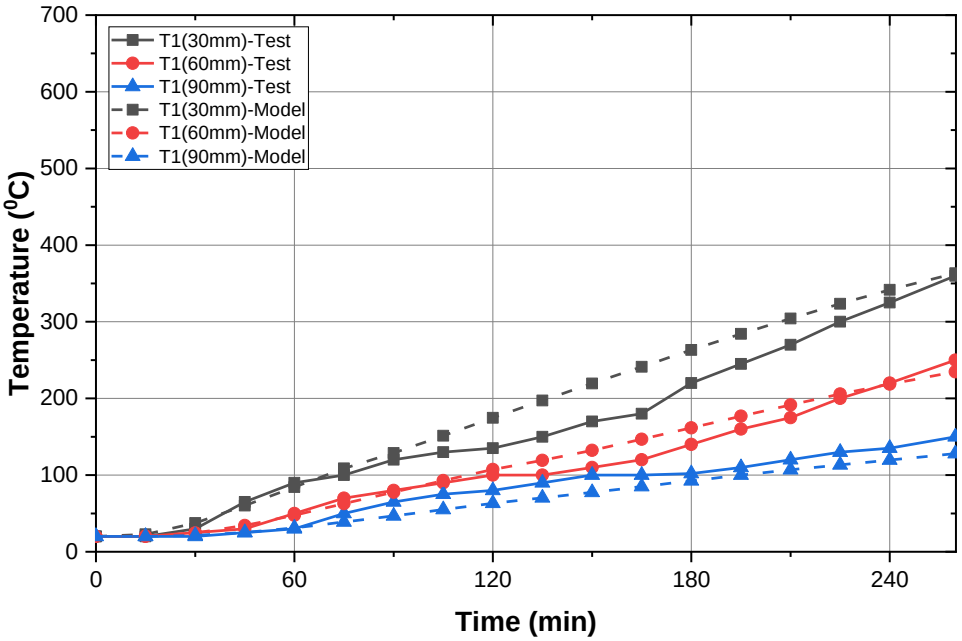

Figure 4.28: Measured vs Modelled time-temperature histories across the slab depth; T1

To validate the structural response, the measured deformation at the column centre (V5 in Figure 4.26) and the time to failure were compared with the modelled deformation at the same location and the time to failure in the model. Figure 4.29 shows the comparison of the measured and modelled deformations. The numerical model accurately traced the measured displacement trend. The failure time in the experiment was 4.33 hrs (260 min), and in the model, the failure was at 4.5 hrs (270 min), showing a very close match.

Achieving a close match for the thermal response and structural response suggests that the numerical models developed can predict the behaviour of the flat slab specimen in fire with reasonable accuracy. The inclusion of LITS and the use of sequential thermo-mechanical analysis technique is, therefore validated in this case.

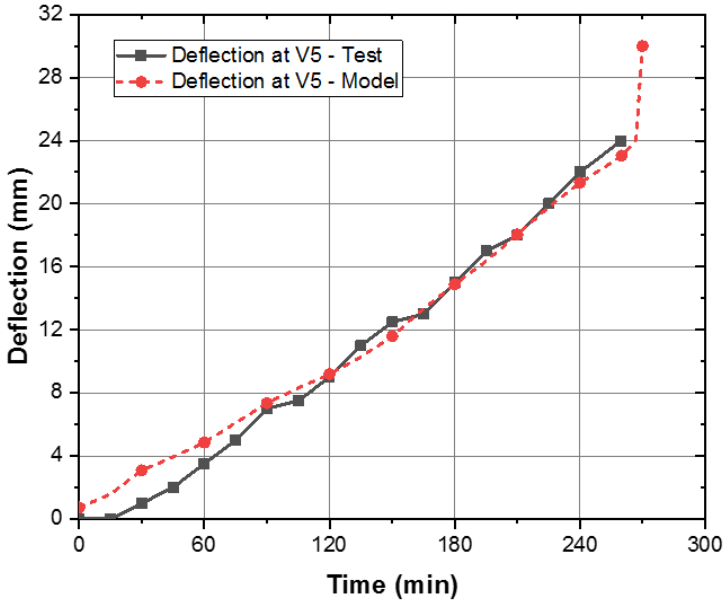

Figure 4.29: Modelled vs Measured deflection at V5

4.4.3 Large-scale experiment

4.4.3.1 Experimental set-up

The large-scale experiment discussed in Chapter 3 was considered to develop the numerical model in this section. The experiment was discussed in detail in the previous chapter. The experimental set-up, instrumentation, loading and the applied heat were presented in Figure 3.2 & 3.3 and Section 3.2 in Chapter 3.

4.4.3.2 Material data and other parameters used in the FE model

As discussed in Chapter 3, laboratory-scale tests were conducted to find the compressive strength and tensile strength of concrete at ambient conditions. They were 39MPa and 3.7MPa, respectively. Young's modulus at ambient conditions was found to be 28600MPa. Based on those values the variation of strength, Youngs's Modulus and stress-strain behaviour for different temperatures were assumed to follow the model given in ENV 1992-1-2 (British Standards Institution, 1996) which is similar to the previous model discussed in Section 4.4.2. Hence, the following figure (Figure 4.30) illustrates the stress-strain relationship for different temperatures utilized in the numerical model. The slab was subjected to the standard ISO 834 fire exposure

(International Organization for Standardization, 1999) and the temperatures within the cross-section are well above 500^{0}C. Therefore, the load-induced thermal strains (LITS) were explicitly included when developing the stress-strain curve, using the approach discussed in Section 4.3.2.

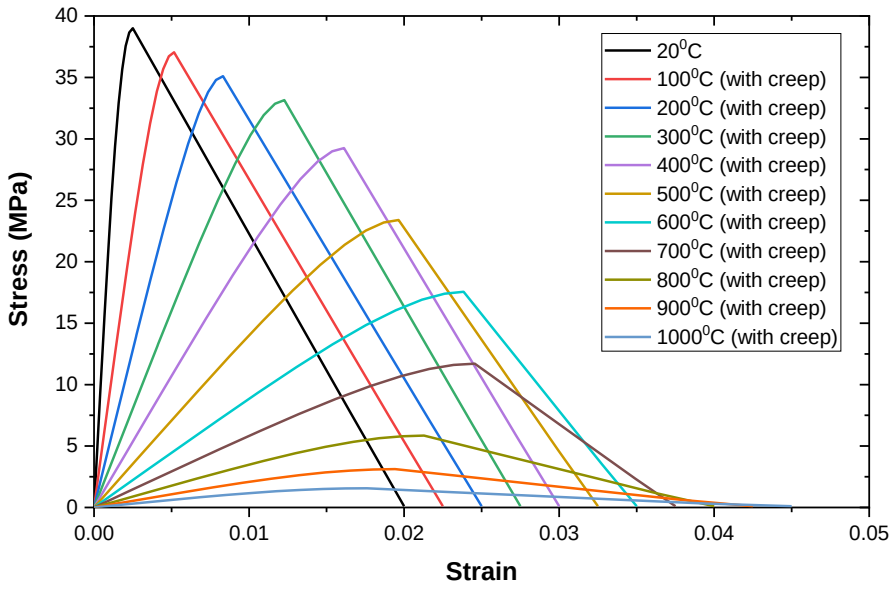

Figure 4.30: Stress-strain behaviour of concrete in compression at elevated temperatures – including transient creep effect

Figure 4.31 and Figure 4.32 depict the tensile behaviour of concrete at different temperatures which are similar to the relationships discussed in Section 4.4.1.2.

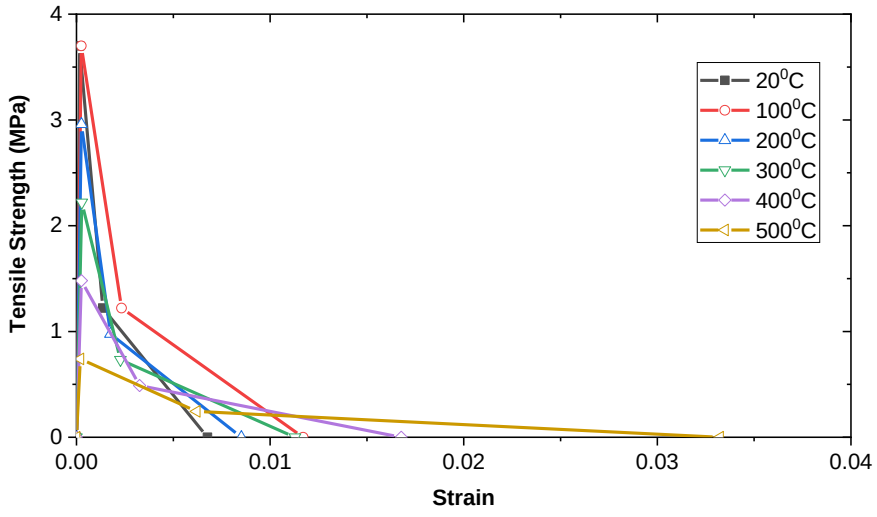

Figure 4.31: Stress-strain behaviour of concrete in tension until 500^{0}C

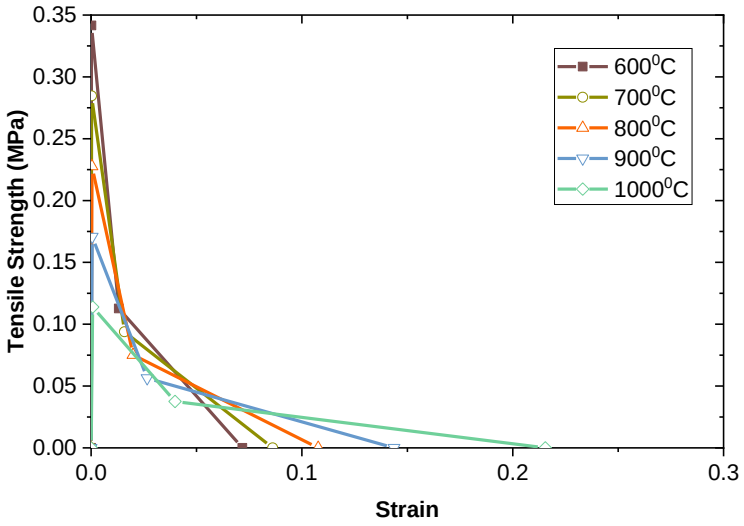

Figure 4.32: Stress-strain behaviour of concrete in tension beyond 500^0C

The other parameters used for the CDP model in ABAQUS are similar to the ones used in previous two models; the dilation angle (ψ) 30^o, the eccentricity 0.1, the stress ration (fb_o/fc_o) 1.16, the shape factor (K_c) 0.667 and the viscosity parameter 0.005.

As per the data provided by the steel manufacturer, the reinforcing steel has a yield strength of 550MPa and an ultimate strength of 627MPa. Based on those values, the stress-strain behaviour and the deterioration of Young's modulus of reinforcing steel were determined in accordance with EC2 (European committee for standardization, 2004b) (see Figure 4.33).

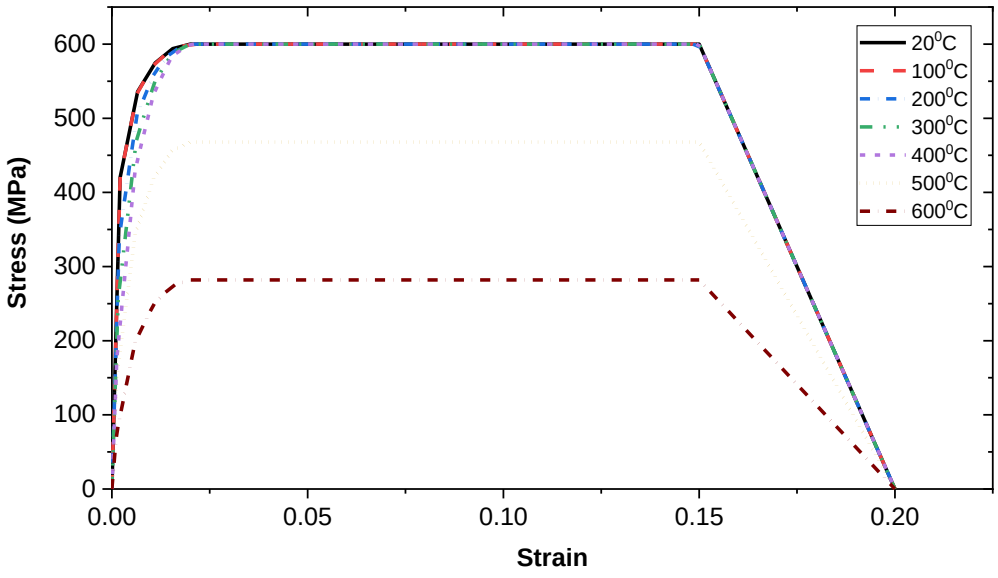

Figure 4.33: Stress-strain behaviour of steel at elevated temperatures

A siliceous type of aggregates was incorporated in the concrete mix for the experiment. Therefore, the variation of thermal conductivity was similar to the one used in the previous model, as shown in Figure 4.10. However, the moisture content in the slab specimen could be higher than that of previous experiments because this slab specimen was cured only for 28 days using wet burlaps whereas the previous slabs were cured for 16 months and 278 days respectively. Although the moisture content was not measured during the experiment, the highest value given (3% m.c) in EC2 to determine the specific heat was assumed in this case. Figure 4.34 shows the variation of the specific heat for concrete considered in this model.

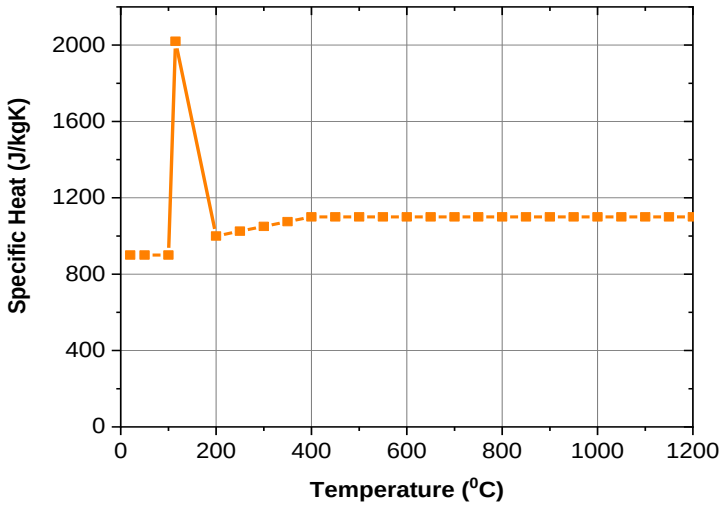

Figure 4.34: Variation of specific heat of concrete with 3.5% m.c.

Thermal properties of reinforcing steel (thermal conductivity and specific heat) are similar to the ones used in the previous model. (see Figure 4.24). Thermal elongation and coefficient of thermal expansion for concrete and steel are also similar to the values shown in Figure 4.11 and Figure 4.23.

Since a cooling phase of 12 hours follows the heating phase of the experiment, it is crucial to incorporate the material properties of concrete during the cooling phase. The methodology discussed in Section 4.3.3 was used here with the following steps.

a) Since the element size used in the mesh is 45mm, the slab was divided into four layers.

b) From the heat transfer analysis, the maximum average temperature (T_{max}) reached at mid-depth of each layer during the whole test was determined.

c) Depending on the T_{max} the residual strength and residual stress-strain curve for each layer were determined, as discussed in Section 4.3.3, following Annex C of the EC4 composite structures design code (European committee for standardization, 2005b).

d) Material properties (stress-strain behaviour and Young's modulus) during the heating phase for the whole model was entered to ABAQUS along with 'Field Variable' = 1.

e) Cooling phase material properties for each layer was entered to ABAQUS with different Field Variables. (i.e. 2 for the top layer, 3 for 2^{nd} layer etc.)

f) During the heating phase, the whole model was assigned with Field Variable (FV) 1. So that the ABAQUS uses only the material properties with FV = 1 during heating.

g) When the cooling phase begins, the exposed layer starts to cool down first while the temperatures of the layers beneath are still increasing. Therefore, only the FV of the top layer (exposed layer) was changed to '2' whereas the other layers still have the FV =1. By doing that the program assigns the cooling phase material properties (materials assigned with FV 2) to that particular layer and the other layers still have got the heating phase material properties.

h) When the 2^{nd} layer starts to cool down (i.e. t= 270min), the FV of that layer each changed to '3' in the FORTRAN code. Then the program takes into account the cooling phase material properties corresponding to that layer.

i) Similarly, when each of the layers starts to cool down, FV of that layer can be changed at that particular time of the analysis to assign the cooling phase material properties.

In this particular experiment, the bottom two layers (90 mm and beyond from the exposed surface) have not reached a maximum temperature more than 300^0C. Therefore, it is reasonable to assume that the strength at T_{max} remains after it cools down to room temperature. Hence, the same stress-strain relationship at T_{max} is maintained during the cooling phase of each layer. Figure 4.35 illustrates the layers

considered, T_{max} for each layer and the cooling phase material properties used for each layer.

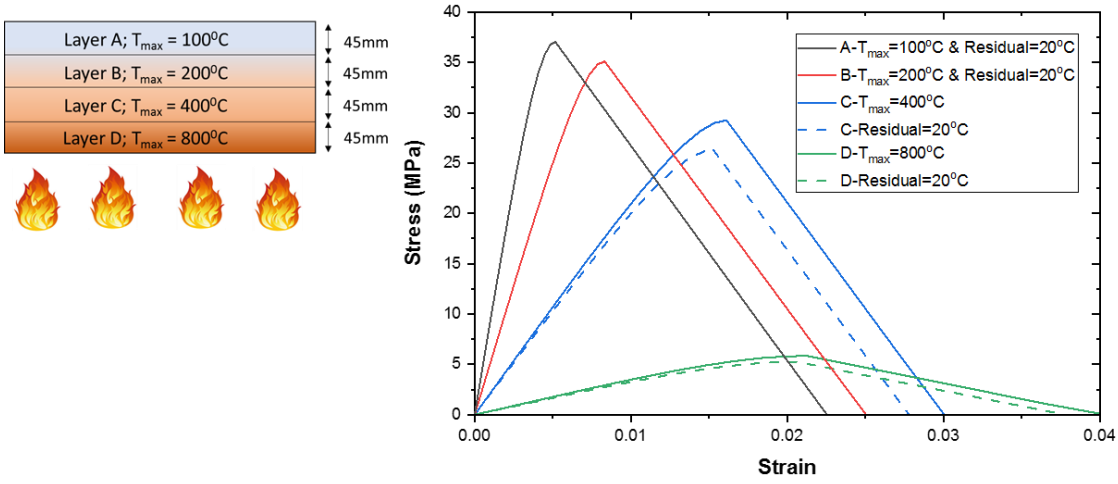

Figure 4.35: Average maximum temperature reached at each layer and the corresponding cooling phase stress-strain curves used in the analysis

ABAQUS/Explicit solver was implemented for the coupled temperature-displacement analysis. To align with that, concrete was represented by C3D8RT (An 8-node thermally coupled brick) elements whereas reinforcement was modelled using T3D2 elements (A 2-node linear 3-D truss). The connection between the reinforcement and concrete was modelled using the 'Tie constraint' available in ABAQUS. Unlike the embedded constraint, Tie constraint allows the heat transfer between concrete and steel. Therefore, the thermal properties of steel and variation of mechanical properties of steel also can be accounted for during the analysis.

The perimeter of the underside of the slab was restrained against translation against z-direction, as shown in Figure 4.36. As the slab was laterally restrained against thermal expansion during the test, spring elements were used for side surfaces in the model. A similar approach has been used in a previous study and also yielded accurate results in the model described in Section 4.4.1. Side surfaces were assigned to reference points by 'rigid-body constraint' and then a node-to-node spring element was assigned between the two reference points, as shown in Figure 4.36.

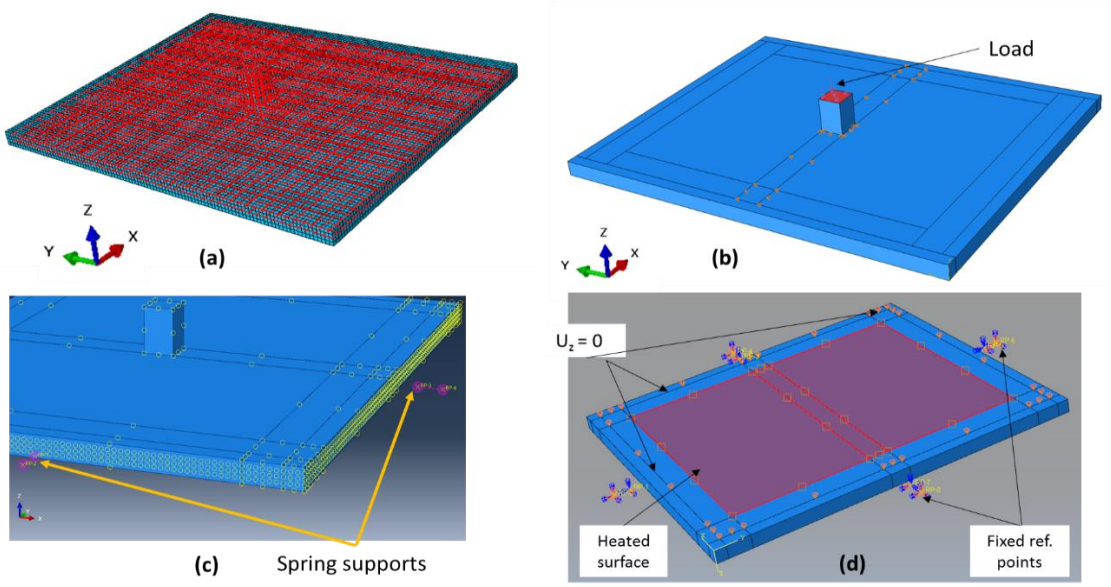

Figure 4.36: (a) Meshed slab with 'tie' reinforcement, (b) Application of the load on the column stub, (c) Spring supports on the side surfaces, (d) $U_z = 0$ along the perimeter of the underside, heated surface and reference points

4.4.3.3 Analysis procedure

The coupled temperature displacement analysis was followed in this model. For the heat transfer from the external surfaces, convection coefficients of 25 W/m^{2}K and 9 W/m^{2}K were used for exposed and unexposed surfaces, respectively, as suggested by BS EN 1991-1-2 (European committee for standardization, 2002). The emissivity of concrete was taken as 0.7 with Stefan-Boltzmann constant of 5.67 x 10^{-8} W/m^{2}K^4. During the cooling phase, the convective coefficient for all the surfaces was considered to be 9 W/m^{2}K. Since the average furnace temperature during the cooling phase was measured during the experiment, the same values were assigned as the boundary conditions of the exposed surface during cooling.

Table 4.1: Parameters associated with time scale in the explicit step

Parameter	**SI Unit**	**Compatible unit for general ABAQUS analysis**	**Units when 3600s = 1s in explicit step**
Conductivity	W/m.K	mW/mm.K	(mW/mm.K) x 3600^3
Specific Heat	J/kg.K	mJ/T.K	(mJ/T.K) x 3600^2
Convective coefficient	W/m^2.K	mW/mm^2.K	(mW/mm^2.K) x 3600^3
Stefan-Boltzmann constant	W/m^2.K^4	mW/mm^2.K^4	(mW/mm^{2}K^4) x 3600^3

Since the explicit solver is used, the duration of fire exposure should be scaled down to a few seconds. As discussed in Section 4.4.1, the units of the following parameters were changed taking 3600s of real fire exposure condensed to 1s in the explicit analysis step (see Table 4.1).

The load factoring may sometimes artificially induce kinetic energy to the structural system. Therefore, it is crucial to damp out such additional kinetic energy during the analysis in order to maintain the quasi-static state. ABAQUS/Explicit solver has the capability to introduce a small amount of damping to avoid such numerical instabilities arising from load factoring. Rayleigh damping described by the following equation is incorporated during the analysis [Eqn. (4.5)].

$$C = \alpha M + \beta K \tag{4.5}$$

Where, C – viscous damping, M – mass inertia, K – stiffness matrix. α is the mass proportional damping factor, whereas β is the stiffness proportional damping factor.

$$\xi_i = \frac{\alpha}{2\omega_i} + \frac{\beta\omega_i}{2} \tag{4.6}$$

Equation (4.6) describes the damping ratio (ξ_i) for corresponding values of α and β where ω_i is the natural frequency of the model. The stable time increment is significantly reduced by the influence of stiffness proportional damping factor (β), which results in significant increase in the computational time. Albrifkani and Wang (2016) suggest using only the mass proportional damping factor (α) assuming β=0 which still yields accurate results. The recommended damping ratio (ξ_i) is in the range between 25% to 35% (Albrifkani and Wang, 2016).

In order to determine α, the natural frequency (ω_i) of the structural model needs to be calculated. Linear perturbation analysis step in ABAQUS can be utilized to derive the modal shapes of the structure, and hence natural frequency can be calculated. The natural frequency of the aforementioned model is found to be 215 rad/s (34.15 Hz) by conducting a linear perturbation analysis. The corresponding mass proportional damping factor (α) is calculated to be 129 for a damping ratio (ξ_i) of 30%.

During the explicit analysis, first, the load was applied and maintained for 1s. The applied load is maintained for the first 2 hrs (2 s in the explicit step) of heating according to the trend shown in Figure 3.10 Chapter 3. After 2 hrs, the load was reduced according to Figure 3.10, and at cooling phase load was entirely removed.

4.4.3.4 Results and Discussion

The first step of the validation was to match the modelled thermal response with the measured thermal response of the slab. Thermocouple locations and their depths are presented in detail in Chapter 3. Comparison of the temperatures was presented separately for heating phase (Figure 4.37) and cooling phase (Figure 4.38). A good match between the measured and the modelled temperatures has been achieved in the numerical model. However, there is only one difference between the modelled exposed surface temperature and the measured average temperature. Exposed surface temperature for the model was taken following the average temperature measured inside the furnace (which is similar to the ISO 834 standard fire exposure). As mentioned in Chapter 3, the exposed surface TCs were 2-4 mm above the slab bottom level to avoid the formation of a localised passageway for flames to penetrate to the slab through TC tips. Hence, they measured a relatively lower temperature than the actual exposed surface temperature.

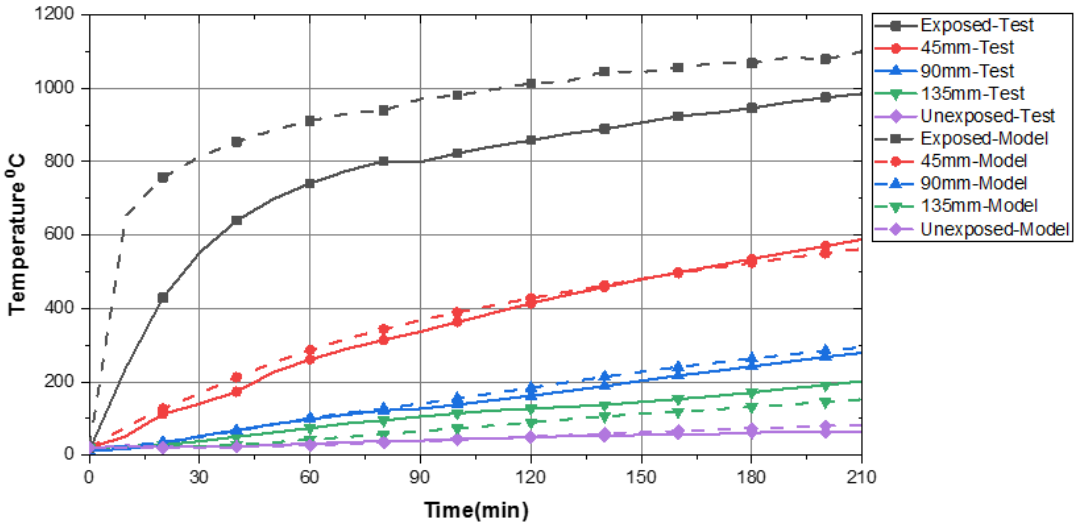

Figure 4.37: Measured vs Modelled temperature variation during the heating phase

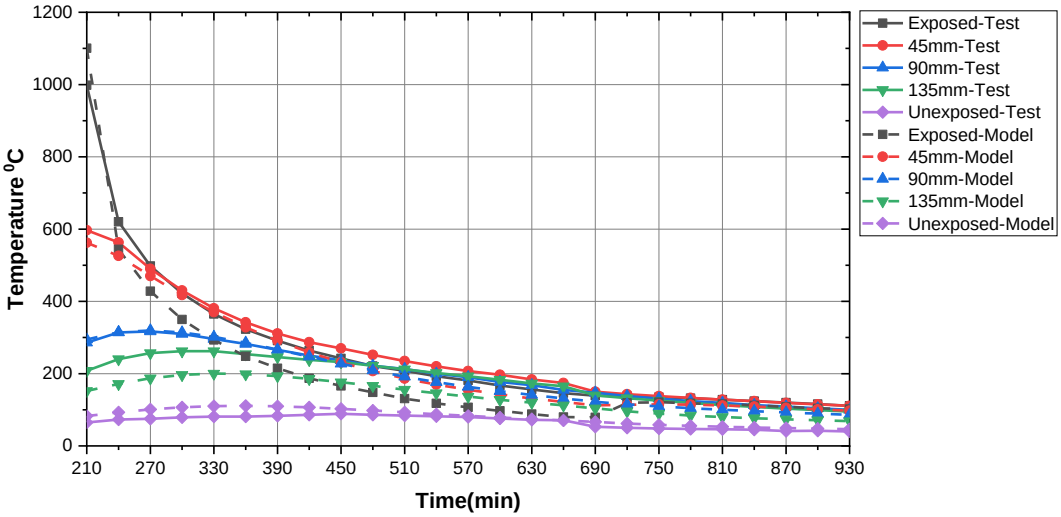

Figure 4.38: Measured vs Modelled temperature variation during the cooling phase

Figure 4.39 presents the measured and modelled deflections at the centre of the slab specimen. A close match has been achieved by using the correct material properties during cooling phase. Therefore, the developed numerical method can be validated and utilized to investigate the overall behaviour of concrete flat slabs subjected to fires having both heating and cooling phases.

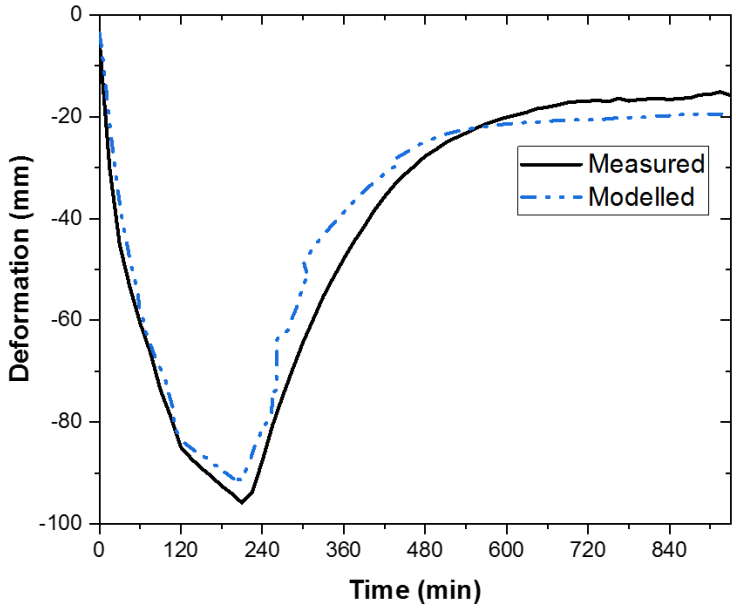

Figure 4.39: Structural response: Measured vs Modelled deformation at centre

4.5 SUMMARY

Thermo-mechanical modelling of concrete flat slabs subjected to fire is discussed in detail in this chapter. Real scale experiments of structures in fire require a vast amount of resources both financially and timewise. Alternatively, numerical simulations can be utilized to overcome such challenges. However, such models require to be validated first, with results from an actual fire test before they are to be used with reasonable accuracy.

Among the several options available, the general-purpose finite element package ABAQUS was implemented to develop the numerical models. Capability to capture the variation of material properties with temperature, the availability of widely used material models to simulate concrete and steel, the ability to conduct both heat transfer and mechanical analysis concurrently or sequentially and the enhanced capabilities to visualise the outputs were main drivers to select ABAQUS software. Two different analysis approaches were studied in particular; sequential analysis with standard implicit solver and coupled temperature-displacement analysis with the dynamic explicit solver. Three independent experiments on concrete flat slabs subjected to fire were selected to validate the numerical models using both approaches. The use of standard implicit solver can often encounter non-convergence issues due to the numerous material non-linearities present owing to temperature variations. To overcome such issues, the explicit solver was implemented with some improvisations. Results have shown that it can predict the thermal and structural response with reasonable accuracy without having non-convergence issues.

Load induced thermal strains (LITS) or transient thermal creep strains play a vital role in the structural response, especially in elevated temperatures (more than 500^0C). Therefore, it is crucial to include these effects in the numerical models developed. Transient creep effects are incorporated in the latter two models which were subjected to significantly high temperatures. The use of LITS has assisted in achieving a matching structural response with the experimental results.

The cooling phase of a fire is often overlooked due to the lack of understanding of the critical effects during cooling down. Both concrete and steel further degrade during the cooling phase, and therefore, structural failure could occur during cooling down. If the same material properties used during heating are also prescribed in the cooling phase, the numerical model will provide an incorrect structural response. A

method to incorporate the cooling phase material properties in ABAQUS is discussed in detail, and it has yielded realistic deformation trends during the cooling phase.

Developed numerical models were validated against three independent fire tests on flat slabs. Both thermal and structural responses were validated separately. Hence, the modelling technique and the material models adopted can be confidently utilized to conduct a parametric study to determine the influencing factors for the fire resistance of concrete flat slabs.

5 Parametric Study

5.1 INTRODUCTION

The previous chapter explained in detail on the development and validation of thermo-mechanical modelling of concrete flat slabs in fire. In this chapter, these validated models are utilized to study the influence of several key parameters on the fire resistance levels of flat slabs. Conducting fire tests on several specimens to determine these factors would be significantly costly and would require a lot of working hours. Alternatively, the use of numerical modelling is fast and resource-efficient.

Priority is given to find the influence of specific parameters prescribed in fire design codes in order to achieve a specific fire resistance level (FRL). Most design codes specify a certain thickness and cover requirement for this purpose while some design codes specify additional rules regarding the top reinforcement of the slab. In the latest version of the Australian concrete structures standard (Standards Australia, 2018), amendments are included for flat slabs in fire. According to the previous version of the standard (Standards Australia, 2009), the thickness requirement specified for flat slabs should be maintained throughout the whole floor. Usually, the thicknesses specified for flat slabs are higher than the thicknesses specified for conventional slabs supported on beams. The vulnerability of flat slabs for punching shear in fire is the main reason behind specifying additional thickness. However, the latest version of the code states that this thickness requirement needs to be maintained only for a distance of 0.16L from the column face, where L is the longest span between the two columns. For the remaining floor area, only the thickness requirement for insulation failure criteria (which is less than the thickness limit for flat slabs) needs to be satisfied. Therefore, the thickness of the slab and the span between the two columns are selected as variables for the parametric study.

Another rule that changed was the requirement of continuing top reinforcement of the column strip within the span of the slab. Column strip is defined as the critical area in the vicinity of the column where additional top reinforcement should be introduced in order to strengthen against punching shear failure. Usually, it is taken as

one-quarter of the span for each side of the column. The previous version of the concrete standard specified that when required FRL is 90 min or above, at least 20% top reinforcement included in the column strip should continue over the full span. However, in the latest version of the standard, this clause is omitted. In order to find out the effect of this alternation, continuity of the top reinforcement within the column strip is taken as a variable in the parametric study. Following sections will present the parametric study in detail.

5.2 DETAILS OF THE PARAMETRIC STUDY

5.2.1 General details

As discussed previously, the thickness of the flat slab, the span between two columns supporting the flat slab and the continuation of top reinforcement within the column strip are considered as the main variables in this study. For an FRL of 1.5hrs or more, the design standard specifies a thickness of 200 mm. The large-scale experiment conducted by the author had a 180 mm thick flat slab which survived 2 hrs of fire with loading. Therefore, thicknesses considered here are 200 mm, 180 mm and 160 mm. Usually, the span between two columns in a multi-storey building is around 6m. Two other spans were selected, a short span of 4m and a long span of 8m. For all the cases, the strength of concrete is taken as 40 MPa, which is being widely used to construct concrete flat slabs. Table 5.1 summarises the different models considered and their characteristics.

Table 5.1: Characteristics of different cases considered

Name	Thickness (mm)	Span (m)	Continuation of top reinforcement	Concrete strength (MPa)	Axis distance (mm)	Top r/f	Bottom r/f
D_160_4	160	4	Discontinuous	40	40	Φ12mm @240mm	Φ16mm@ 200mm
D_180_4	180	4	Discontinuous	40	40	Φ12mm @200mm	Φ16mm@ 160mm
D_200_4	200	4	Discontinuous	40	40	Φ16mm @240mm	Φ20mm@ 240mm
D_160_6	160	6	Discontinuous	40	40	Φ12mm @240mm	Φ16mm@ 200mm
D_180_6	180	6	Discontinuous	40	40	Φ12mm @200mm	Φ16mm@ 160mm
D_200_6	200	6	Discontinuous	40	40	Φ16mm @240mm	Φ20mm@ 240mm
D_160_8	160	8	Discontinuous	40	40	Φ12mm @240mm	Φ16mm@ 200mm

D_180_8	180	8	Discontinuous	40	40	Φ12mm @200mm	Φ16mm@ 160mm
D_200_8	200	8	Discontinuous	40	40	Φ16mm @240mm	Φ20mm@ 240mm
C_160_4	160	4	Continuous	40	40	Φ12mm @240mm	Φ16mm@ 200mm
C_180_4	180	4	Continuous	40	40	Φ12mm @200mm	Φ16mm@ 160mm
C_200_4	200	4	Continuous	40	40	Φ16mm @240mm	Φ20mm@ 240mm
C_160_6	160	6	Continuous	40	40	Φ12mm @240mm	Φ16mm@ 200mm
C_180_6	180	6	Continuous	40	40	Φ12mm @200mm	Φ16mm@ 160mm
C_200_6	200	6	Continuous	40	40	Φ16mm @240mm	Φ20mm@ 240mm
C_160_8	160	8	Continuous	40	40	Φ12mm @240mm	Φ16mm@ 200mm
C_180_8	180	8	Continuous	40	40	Φ12mm @200mm	Φ16mm@ 160mm
C_200_8	200	8	Continuous	40	40	Φ16mm @240mm	Φ20mm@ 240mm

Specified axis distance for an FRL of 2 hrs is 35 mm. A value of 40 mm was selected as it will match with the mesh size used in the numerical models. When selecting the reinforcement for each case, the non-dimensional parameter ρ (reinforcement ratio) is kept constant for all the models to avoid the different influences of reinforcement for the FRL. 'ρ' is defined as the ratio between the area of reinforcement in flexure or compression within the section and concrete area of the section. For top reinforcement, ρ is taken as 0.4%, and for bottom reinforcement, ρ is taken as 0.85%. These values are in line with the nominal reinforcement ratios used in flat slabs (Liao et al., 2013). The slabs are subjected to ISO 834 standard fire curve (International Organization for Standardization, 1999), which only has a heating regime.

5.2.2 Material properties

A detailed description of the different material models incorporated in numerical modelling can be found in Chapter 4, which contains the development and validation of thermo-mechanical models for flat slabs in fire. In this section, an overall summary of the mechanical and thermal properties of concrete and steel, employed in the analysis will be presented.

Concrete damage plasticity model in the finite element package ABAQUS was implemented to represent concrete. Compressive and tensile behaviour of concrete at elevated temperatures, as presented in Figure 5.1 and Figure 5.2 was applied for the model. Note that in Figure 5.2 (a) both 20°C and 100°C curves are overlapped as tensile strength in concrete does not degrade up to 100°C as shown in Figure 2.22. Transient creep of concrete at elevated temperatures was explicitly included in the compressive behaviour, as explained in Section 4.3.2 of Chapter 4. Other parameters for concrete damage plasticity model such as the dilation angle (30^0), the eccentricity (0.1), the stress ratio (1.16), the shape factor 0.667 and the viscosity (0.01) are the typical values used in Chapter 4 validation exercise.

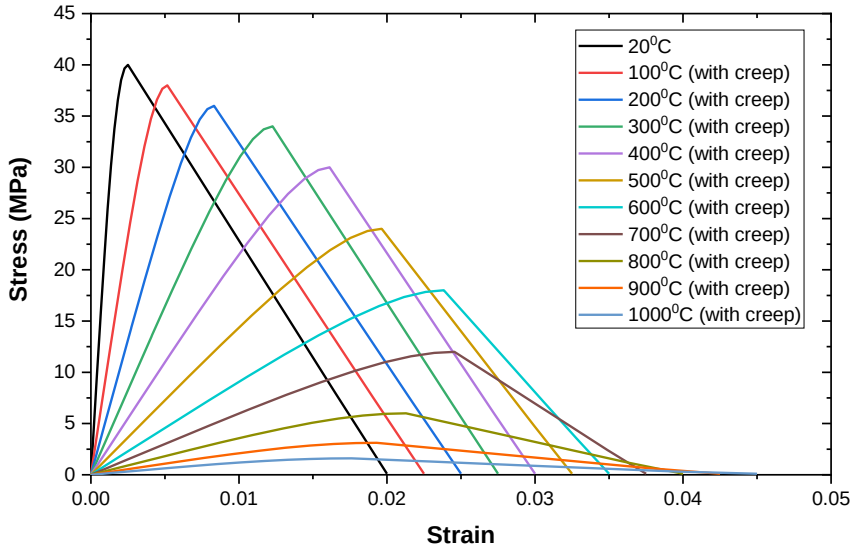

Figure 5.1: Compressive behaviour of 40MPa concrete with transient creep included

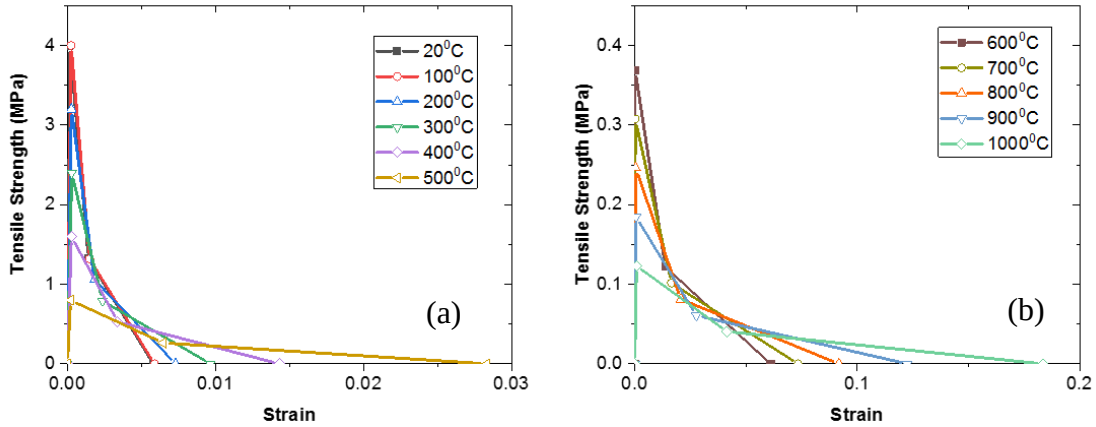

Figure 5.2: Tensile behaviour of 40MPa concrete (a) from 20°C to 500°C , (b) from 600°C to 1000°C

Thermal elongation and the coefficient of thermal expansion of concrete follows the trend, as shown in

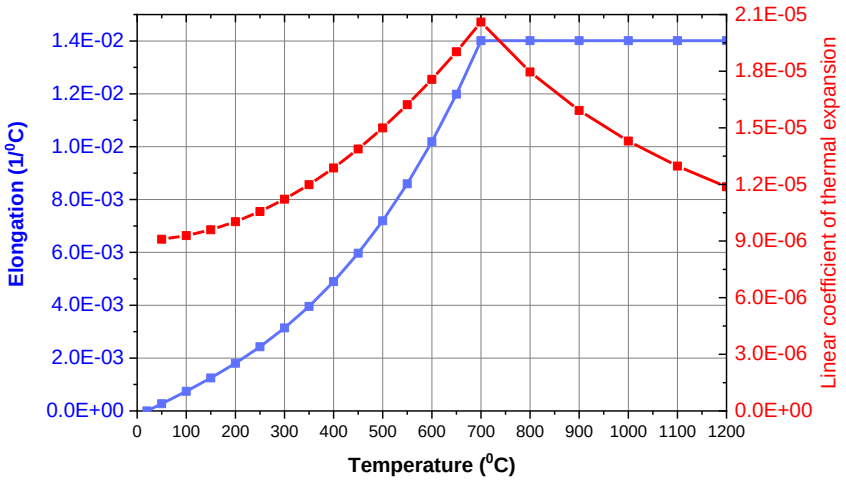

Figure 5.3. For conductivity and specific heat, the values illustrated in Figure 5.4, and Figure 5.5 are considered. The properties are determined based on EN 1992-1-2 (European committee for standardization, 2004b), similar to the method discussed in Chapter 4 and Chapter 2 in detail.

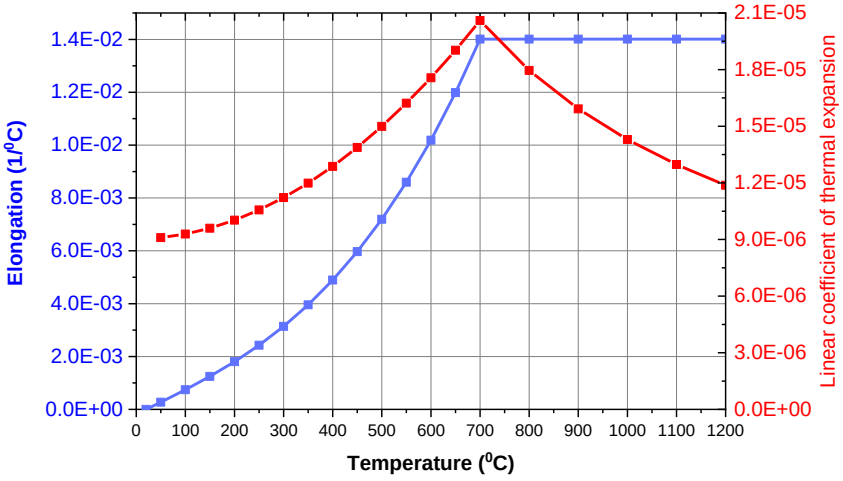

Figure 5.3: Thermal elongation and the coefficient of thermal expansion for concrete

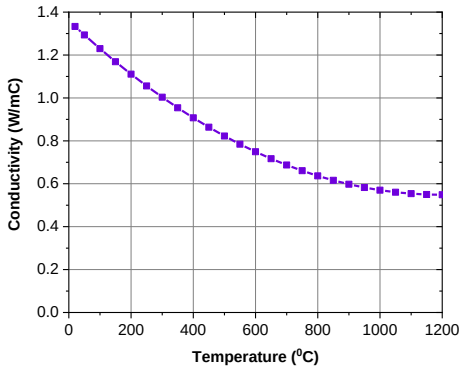

Figure 5.4: Thermal conductivity of concrete

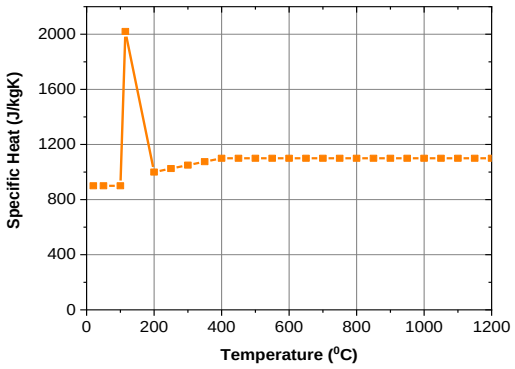

Figure 5.5: Specific heat of concrete

Reinforcing steel having a proportional strength of 550MPa and a yield strength of 627 MPa was considered for the study. The stress-strain relationship for steel at elevated temperatures is presented in Figure 5.6. Thermal expansion, conductivity and specific heat of steel employed in the models are illustrated in Figure 5.7, Figure 5.8 and Figure 5.9, respectively.

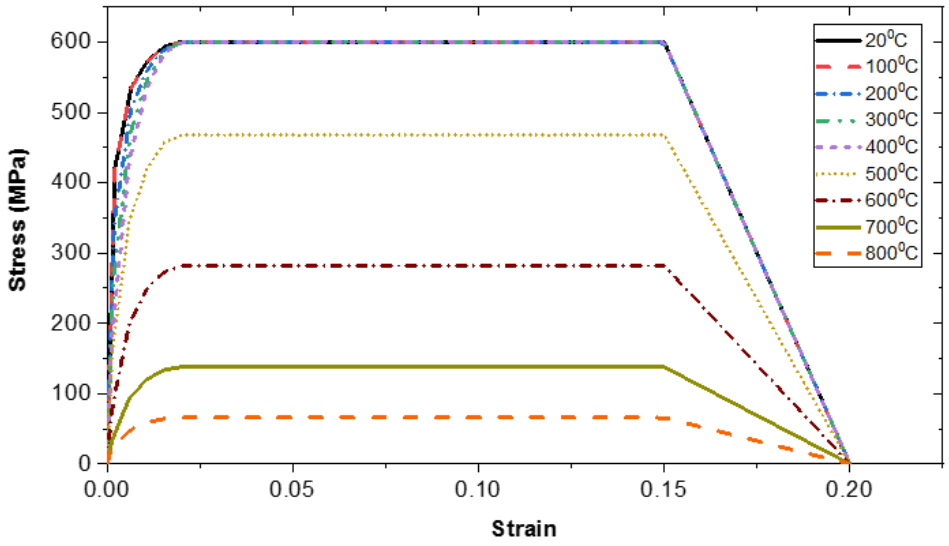

Figure 5.6: Stress-strain behaviour of steel

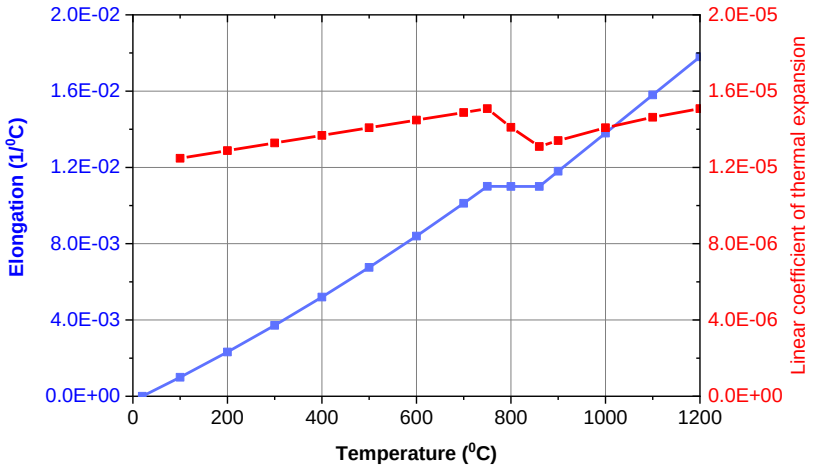

Figure 5.7: Thermal elongation of expansion of thermal co-efficient of steel

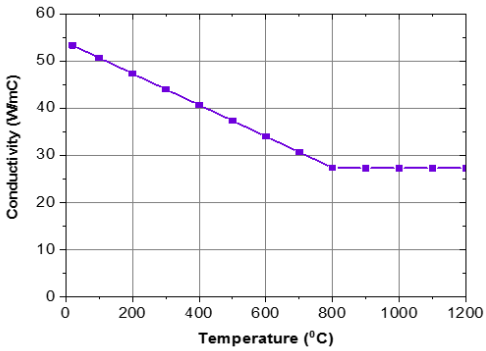

Figure 5.8: Thermal conductivity of steel

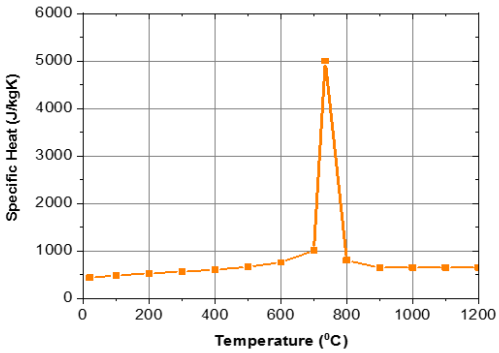

Figure 5.9: Specific heat capacity of steel

5.2.3 Boundary conditions and other model input parameters

Figure 5.10 illustrates the basic shape of the specimen under consideration. The span(l) between the columns and the thickness (t) of the slab are changed accordingly.

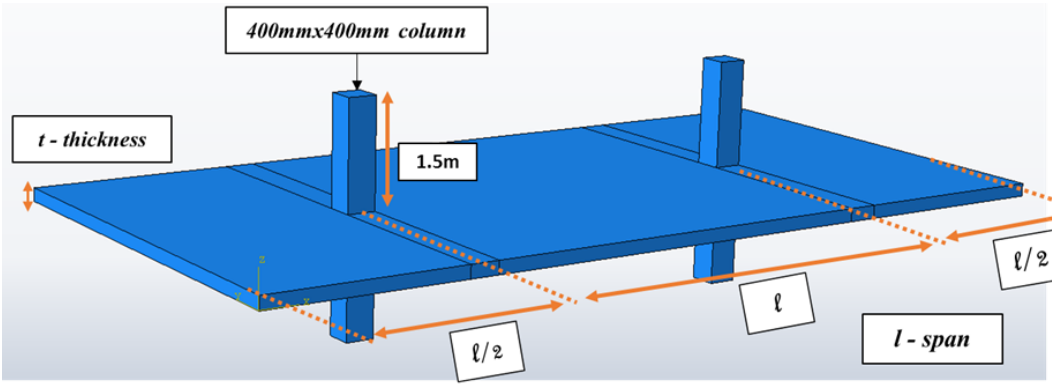

Figure 5.10: Shape of the slab column assembly

For all the cases, a column size of 400mm x 400mm was selected. For a multi-storey building assumed to be having a floor to floor height of 3m, the column was extended up to half of the floor height (1.5m) from both top and bottom as shown in Figure 5.10. The bottom end was pinned, and the top end was allowed to expand only in the z-direction. When the span between two columns is 'l', the slab was extended up to l/2 distance for each side. To represent the continuity of slab, spring elements having a spring stiffness of 30000 N/mm were assigned to each side surface (see Figure 5.11). This method has proven to be successful in representing the lateral restraints provided by the adjacent slab (as validated in Chapter 4); hence the compressive membrane action will be accounted for during the simulation. Reinforcement arrangement inside the slab is illustrated in Figure 5.12.

Typically, in a compartment fire, the flames and heat propagate upwards, and therefore, the underside of the slab will be considered as the exposed surface. Hence, the temperature boundary condition corresponding to ISO 834 standard time-temperature curve (as shown in Figure 5.13) for a duration of 5 hrs was applied to the bottom surface of the slab. To account for the heat loss to the surrounding environment through the unexposed top surface by means of convection and radiation, a convective film coefficient of 4 W/m^2K and an emissivity of 0.7 was implemented as suggested by clause 3.1 in BS EN 1991-1-2 (European committee for standardization, 2002).

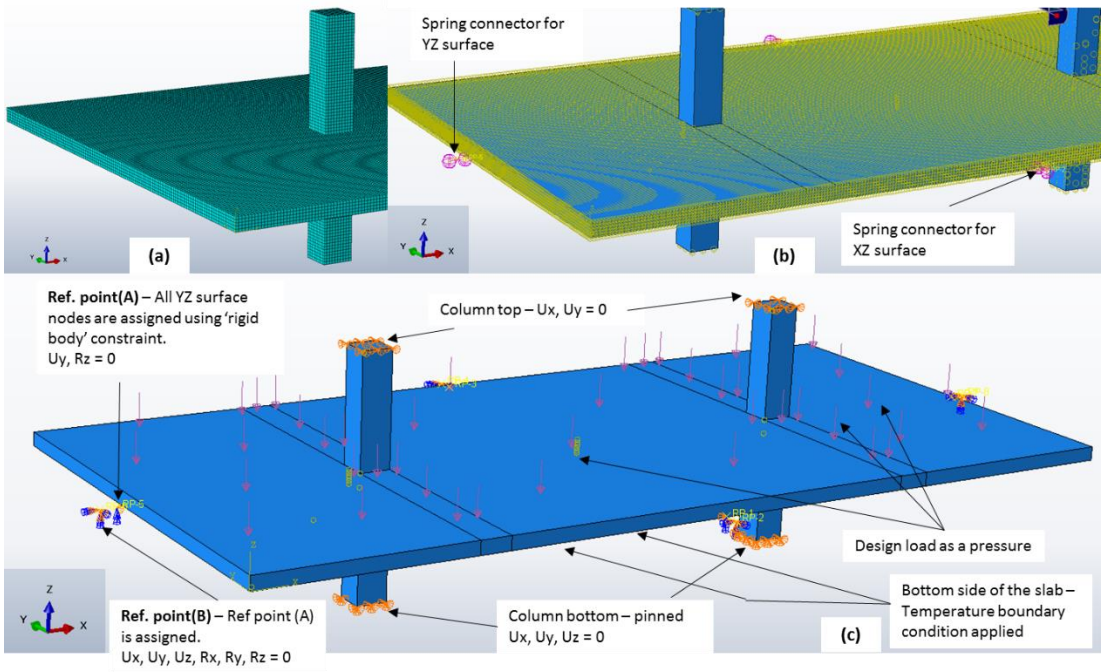

Figure 5.11: (a) Meshed model, (b) Spring assignment for side faces, (c) Loading and boundary conditions utilized

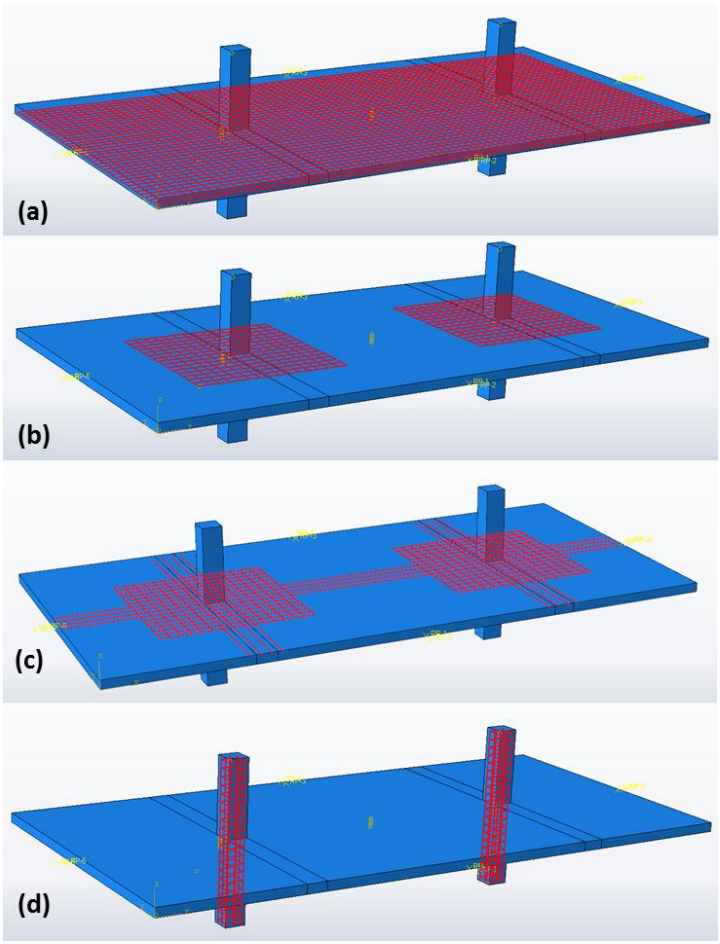

Figure 5.12: Reinforcement included; (a) Bottom layer, (b) Top layer (Discontinuous), (c) Top layer (20% of r/f continuous in the column strip), (d) Column r/f

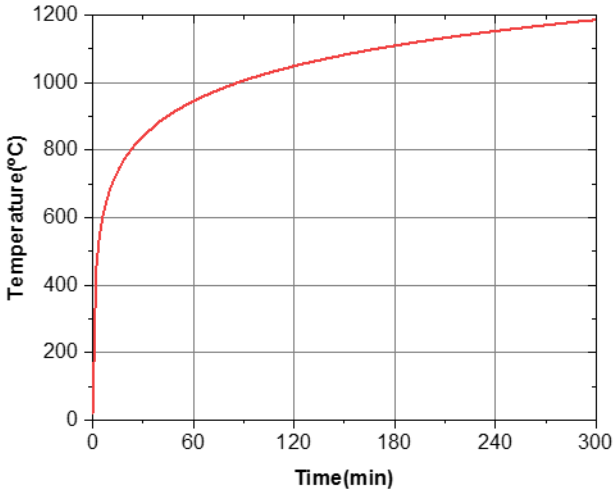

Figure 5.13: ISO 834 standard time-temperature curve for 5 hours of heating

AS1170.0 (Standards Australia, 2002a) and AS1170.1 (Standards Australia, 2002b) guidelines were followed to determine the design fire load acting on the slab. The calculation for a 200 mm slab is as follows.

- Dead loads (G_k) = self-weight of the slab + finishes and partitions

  = (0.2m x 25 kN/m^3) + 1.5 kN/m^2

  = 6.5 kN/m^2

- Imposed load (Q_k) = 4 kN/m^2 ; (Conservatively assumed)

- Design fire load = $G_k + \psi Q_k$; ψ is taken as 0.7 (Standards Australia, 2002a)

  = 6.5 + 0.7 x 4

  = <u>9.3 kN/m^2</u>

Similarly, the design load for other depths can be calculated and they change slightly. To be conservative with the analysis and for consistence, a design fire load of 10 kN/m^2 was assumed for all the cases. Calculated design load was applied as a pressure on the top surface of the slab, as shown in Figure 5.11(c).

5.2.4 Analysis procedure

The validation exercise explained in Chapter 4 implies that the coupled temperature-displacement analysis step module in ABAQUS combined with the explicit solver is the most efficient method to follow in the thermo-mechanical

analysis. Therefore, the same procedure introduced by the author is implemented for this parametric study.

Concrete was represented using C3D8RT (An 8-node thermally coupled brick) elements whereas reinforcement was represented using T3D2 elements (A 2-node linear 3-D truss). The connection between the concrete and reinforcement was accounted for by means of the 'Tie constraint' option available in ABAQUS. That will ensure both deformation and temperature transfer from concrete to reinforcement during loading and heating. A mesh size of 40mm was selected for 160mm and 200mm thick slabs whereas a mesh size of 36mm was selected for 180mm thick slabs. That ensured the requirement of having at least four elements through the thickness to avoid hour-glass effects as suggested by Sun (2006) and implemented for flat slabs by Wahid et al. (2019b).

As discussed in Chapter 4, in order to maintain the quasi-static state of the analysis, it is vital to include damping to the model by means of the Rayleigh mass proportional damping factor (α). 'α' depends on the natural frequency of the structure, and therefore, a linear perturbation analysis step was carried out in ABAQUS for all the models to determine the modes of vibration. Results are summarised in Table 5.2, which spells out the damping factors employed in each case.

Table 5.2: Damping employed during analysis

Model name	**Natural frequency (f_i in Hz)**	**Damping ratio ξ_i**	**Damping factor $\alpha = 4\pi f_i \xi_i$**
D_160_4 C_160_4	13.19	30%	49.7
D_180_4 C_180_4	14.14		53.3
D_200_4 C_200_4	14.77		55.7
D_160_6 C_160_6	5.35		20.2
D_180_6 C_180_6	5.8		21.9
D_200_6 C_200_6	6.12		23.1
D_160_8 C_160_8	2.84		10.7
D_180_8 C_180_8	3.1		11.7
D_200_8 C_200_8	3.28		12.4

The design load, as calculated above, was first applied to the slab in ambient conditions using a smooth step amplitude to ensure the loading does not cause any dynamic effects. In the subsequent step, the load was maintained at the same level while the fire was applied to the model as a temperature boundary condition to the bottom of the slab. In order to minimise the computational cost, the load factoring technique explained in Chapter 4; Section 4.4.3.3 was utilized here as well. As such, 1 hour of fire exposure is scaled down to 1s of analysis time during the explicit step for heating. The analysis was continued until failure or the duration of fire reaches 5 hrs in case it did not fail. Total internal energy and total kinetic energy of the model was recorded throughout the procedure to find out whether the analysis remained in the quasi-static state. Thermal and Structural response was captured by recording the temperature across the depth, deformation in the span and the vicinity of the columns and plastic strain development around the critical area near the slab-column connection.

5.3 RESULTS

The analysis aimed to find out the influence of different factors for the fire resistance level (FRL) of the flat slab. Failure could be either structural failure due to excessive deformation or thermal failure due to the unexposed surface getting heated for more than 180^0C. Structural failure can be identified either from the kinetic energy (KE) history of the model or from the deformation of the model during heating. At failure, there is a sudden spike in the KE graph (a default output in ABAQUS which records the kinetic energy for the whole model due to deformation, as a time-history plot), which indicates a sudden deformation corresponding to structural failure. This may also be visible from the deformation history showing a sudden increase in the rate of deflection. Thermal failure can be identified from the nodal temperature history of the unexposed surface. Apart from that, the type of failure and in case of punching failure, the punching angle and critical area is determined using the plastic strain output.

Above all, the analysis should be in the quasi-static state in order to yield accurate predictions. This was determined by comparing the total internal energy (IE) and total kinetic energy (KE) histories of the model. If the KE is insignificant compared to IE, then it can be confidently stated that the analysis remained quasi-static throughout the duration. Figure 5.14 and Figure 5.15 illustrate the KE and IE graphs

for a typical model and KE history for the same model, which was utilized to identify the failure. The remaining energy graphs can be found in Appendix A.

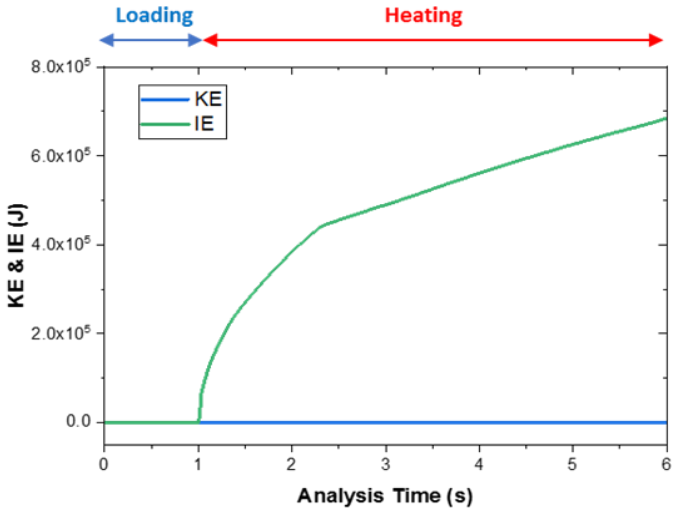

Figure 5.14: Kinetic energy and Internal energy variation with time for C_160_4

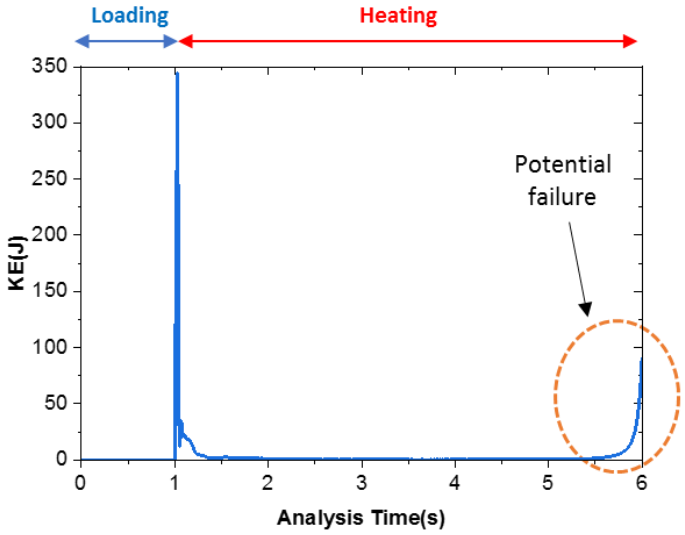

Figure 5.15: Kinetic energy variation with time for C_160_4

There is a sudden increase in KE when analysis time t=1s. This is the point where heating starts and the rise in KE at that moment is due to the initiation of thermal expansion. However, when comparing with IE (see Figure 5.14), it is evident that the analysis is still in the quasi-static state.

In some cases, the span of the slab has reached the limiting deflection of span(L)/30 as proposed by Buchanan and Abu (2017) without distinctly showing a sudden rise in the kinetic energy. In those cases, the fire resistance was taken as the time until the deflection reaches the limiting criterion (L/30).

Table 5.3 presents a summary of the key outputs for all the models.

Table 5.3: Summary of the results from the parametric study

Model name	FRL	Type of failure	Punching angle	*Def. at mid-span at failure (mm)	*Def. of the column at failure (mm)	Temp. of the unexposed surface at failure (°C)
D_160_4	4 hrs 50min	Insulation criteria		-33	+5.8	180
D_180_4	No failure for 5Hrs			-7.2	+5.6	146
D_200_4	No failure for 5Hrs			-6	+5.4	116
D_160_6	3 hrs	Punching shear	16°	-200	+2.1	114
D_180_6	No failure for 5Hrs			-126.7	+4.2	146
D_200_6	No failure for 5Hrs			-71.2	+4	116
D_160_8	32 min	Punching shear	18.4°	-266	-1.8	23
D_180_8	2 hrs	Punching shear	14°	-266	-1.6	60
D_200_8	No failure for 5Hrs			-247	+3.1	116
C_160_4	4hrs 45min	Punching shear	12.5°	-45	+5.4	177
C_180_4	No failure for 5Hrs			-12.7	+5.5	148
C_200_4	No failure for 5Hrs			-6.4	+5.3	118
C_160_6	2 hrs 50min	Punching shear	16°	-200	+1.85	107
C_180_6	No failure for 5Hrs			-138	+3.8	148
C_200_6	No failure for 5Hrs			-83.6	+1	118
C_160_8	32 min	Punching shear	18.4°	-266	-0.6	23
C_180_8	1hrs 58 min	punching shear	14°	-266	-1.7	58
C_200_8	No failure for 5Hrs			-253.8	+3	118

*Upward displacement regarded as positive

Deformation was measured in the mid-span between two columns and in the middle of the column. Figure 5.16 illustrates the time history of deformation for different cases.

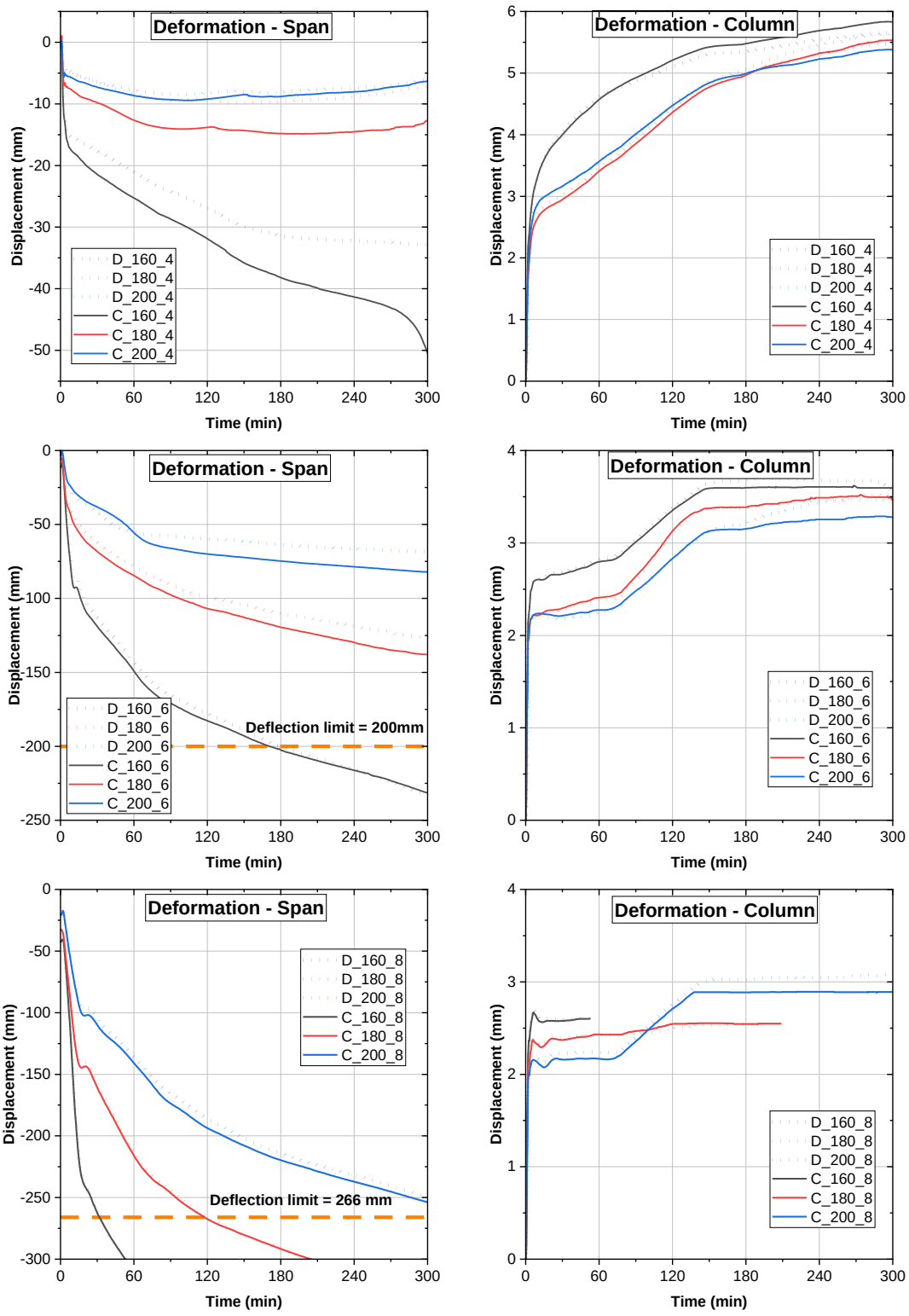

Figure 5.16: Deformation time-history of mid-span and column for different cases using the numerical models

The temperature history obtained across a typical model is presented in Figure 5.17 Temperature histories for other models can be found in Appendix A.

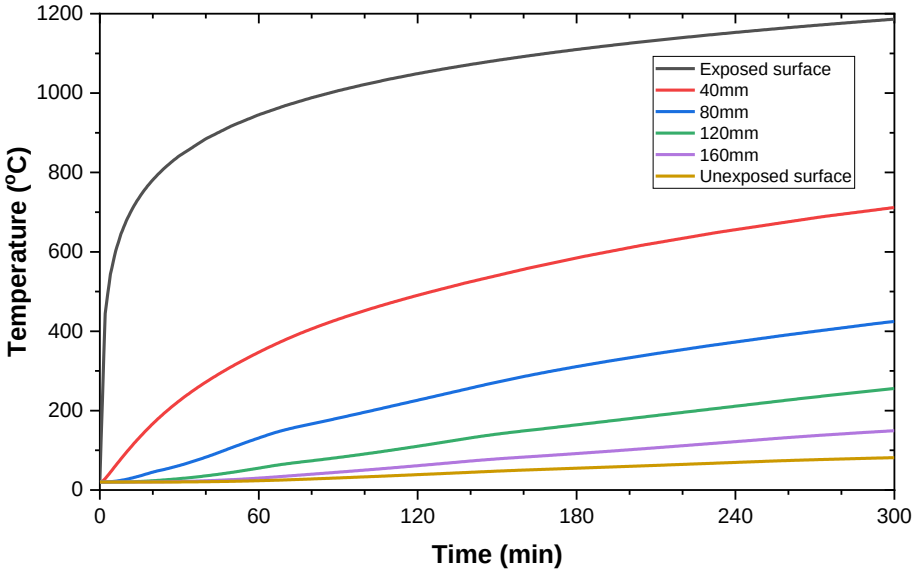

Figure 5.17: Temperature history predicted by numerical model for D_200_8

The punching angle for the cases where slab failed in punching shear was determined from the plastic strain distribution across the cross-section of the slab-column connection as illustrated in Figure 5.18.

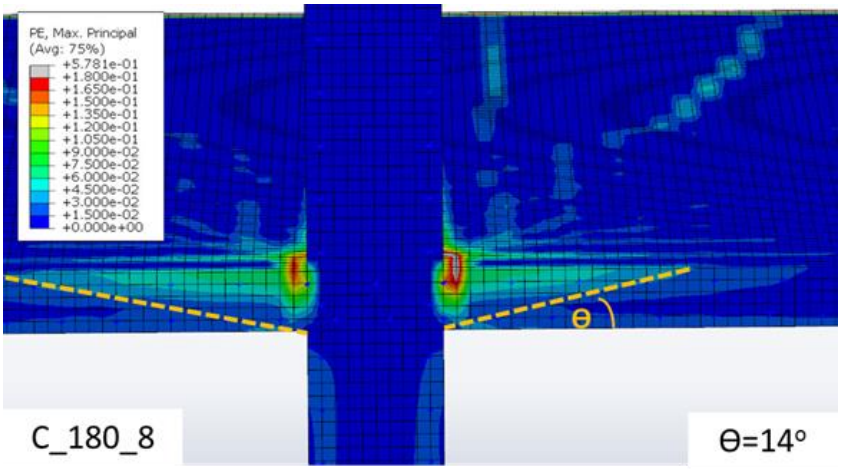

Figure 5.18: Shape of the punching cone developed for C_180_8 when it reaches the deflection limit

Deformation at the failure of a typical case is presented in Figure 5.19 and Figure 5.20. The span is deflecting towards the fire, whereas the columns are extending upwards due to the thermal expansion. There is a slight sideways movement of the column near the slab-column connection, which is due to the lateral thermal expansion of the slab portion.

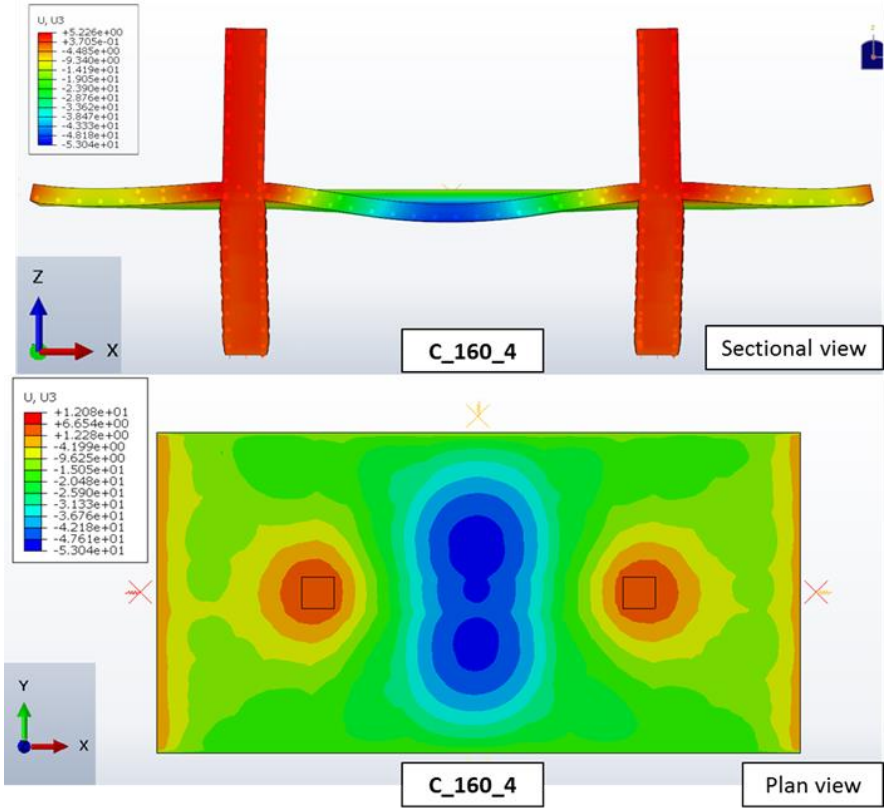

Figure 5.19: Shape of the deformed slab at the failure of C_160_4

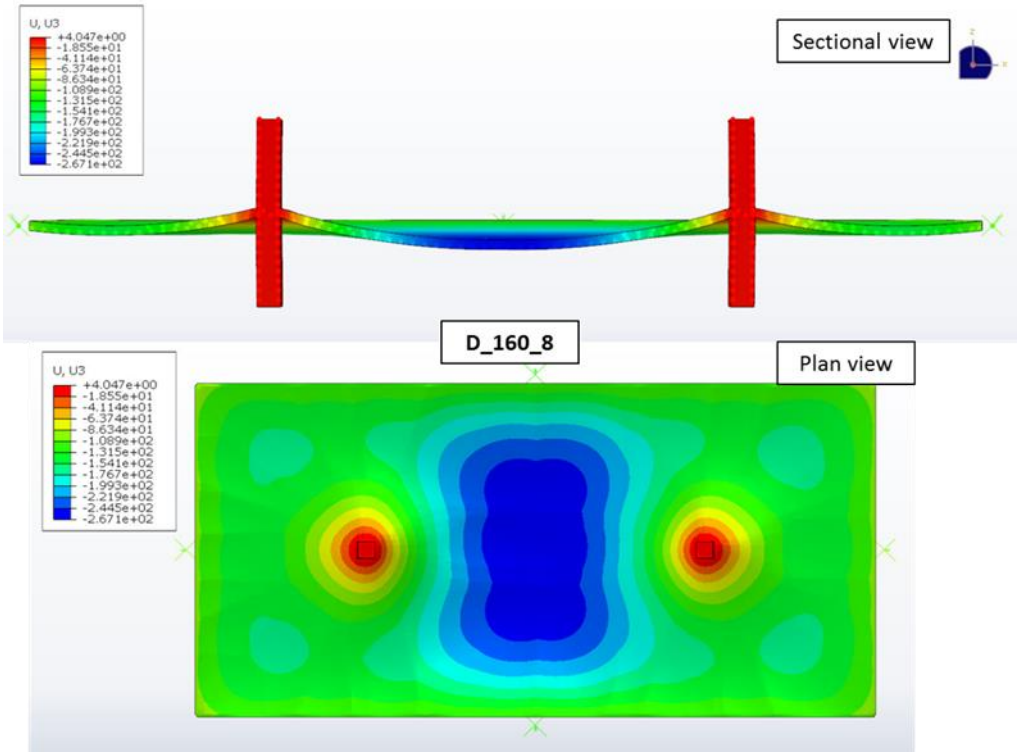

Figure 5.20: Shape of the deformed slab at the failure D_160_8

5.4 DISCUSSION

The results indicate that out of the three failure criteria in fire (structural adequacy, integrity and insulation), all the cases which failed were due to excessive deformation violating the structural adequacy criterion except 160mm thick slab without continuous top reinforcement having a 4m span. That particular slab failed after 290 min due to insulation criterion, as the unexposed surface temperature exceeded 180^0C. Out of 18 cases considered, 8 cases failed (marked in light red and red in Figure 5.21), and all other specimens survived 5 hours of standard fire exposure. For the comparison, the specimens failed due to structural adequacy criterion will be considered here after.

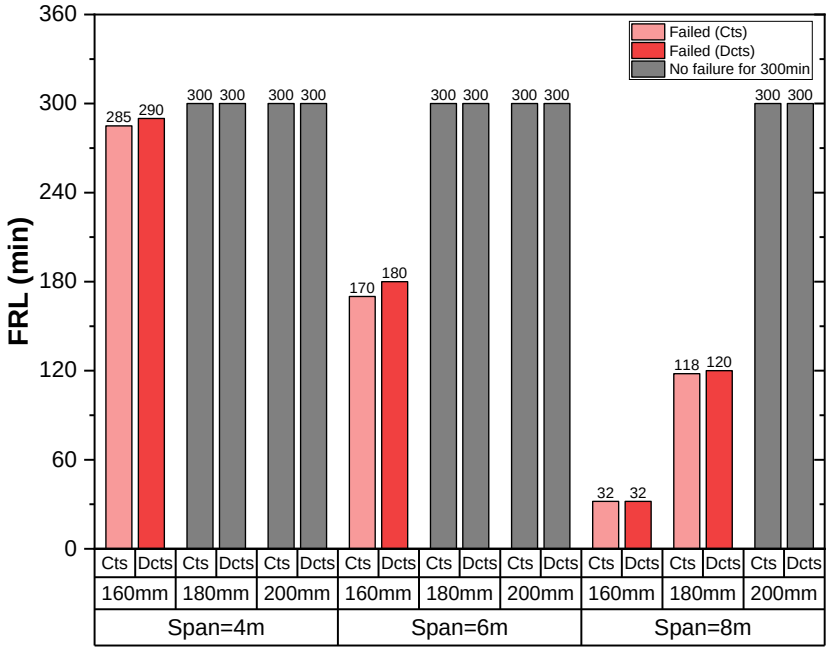

Figure 5.21: Fire resistance levels (FRLs) for different cases analysed

160mm thick slab specimen having a column span of 4m and continuous reinforcement (C_160_4) showed a sudden increase in the rate of deflection at around 4 hrs and 45 mins after heating. The failure of other specimens was determined when the deflection reached the limit of span/30. Looking at the FRLs, it is evident that the FRLs of the specimens having at least 20% of reinforcement continuing over the span in the column strip area are slightly less than the FRLs of specimens without such continuity of reinforcement. Although having more reinforcement increases the stiffness of the slab, the addition of more steel within the cross-section can increase the overall thermal conductivity of the slab.

Furthermore, the thermal expansion coefficient of steel is higher than the thermal expansion coefficient of concrete. Therefore, specimens having more reinforcement can deform more due to thermal strain, which reduces the FRL. The deformation in span (see Figure 5.16) also supports this argument. Material degradation at elevated temperatures can also affect this behaviour as the specimen will deform more when the concrete and steel get weakened. Liao et al. (2013) had similar observations during a series of small-scale punching shear tests at elevated temperatures. i.e. the specimens having higher reinforcement ratios exhibited poor fire resistance. The trend, as mentioned above in FRL further validates the decision to remove the clause 5.5.2 (b)(ii) from Australian Concrete Standard (AS 3600). It previously stated that at least 20% of total top reinforcement is required in each direction over intermediate supports, continuous over the full span and should be placed in the column strip.

Another crucial trend to notice here is that when the span is increasing, FRL is significantly decreasing for the same thickness of the slab and same design fire load. For example, the 160mm thick slab with continuous reinforcement has a FRL of 285 mins when the span is 4m. For the same loading, the FRL is reduced to 32 mins when the span is increased to 8m. FRLs of 180mm thick slabs are also reduced from 3hrs to 2hrs when the span was increased from 6m to 8m.

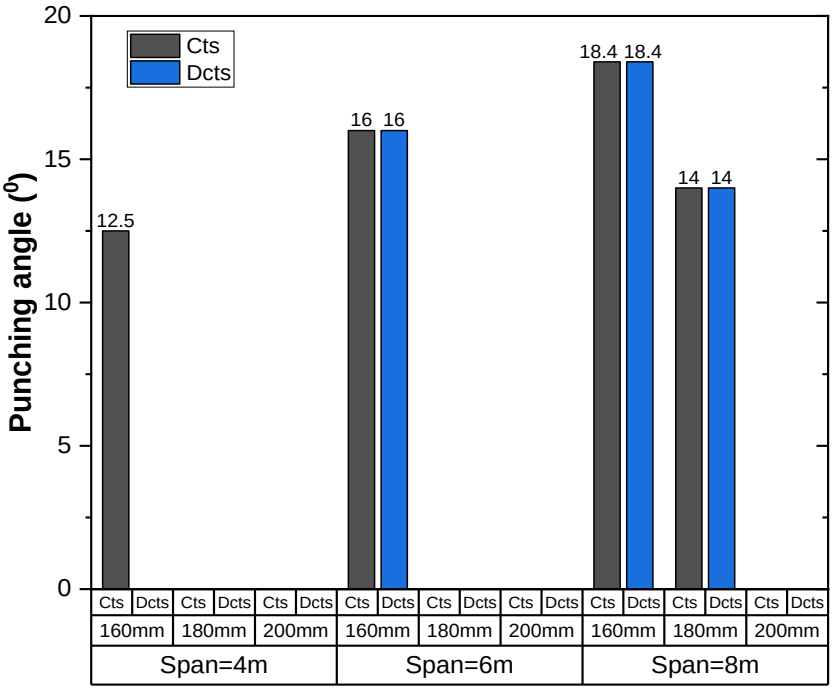

Figure 5.22: Punching angle for failed specimens

Figure 5.22 summarises the punching angles developed in the failed specimens. According to the results, the continuity of reinforcement does not have any effect on the punching angle. However, when the span increases for the same slab thickness, the punching angle also increases. When the punching angle increases, the critical distance from the column face decreases. For the same span, when the thickness of the slab increases, the punching angle decreases. That will increase the critical distance from the column face. To further illustrate this phenomenon, the critical distances determined based on the aforementioned punching angles are presented in Figure 5.23.

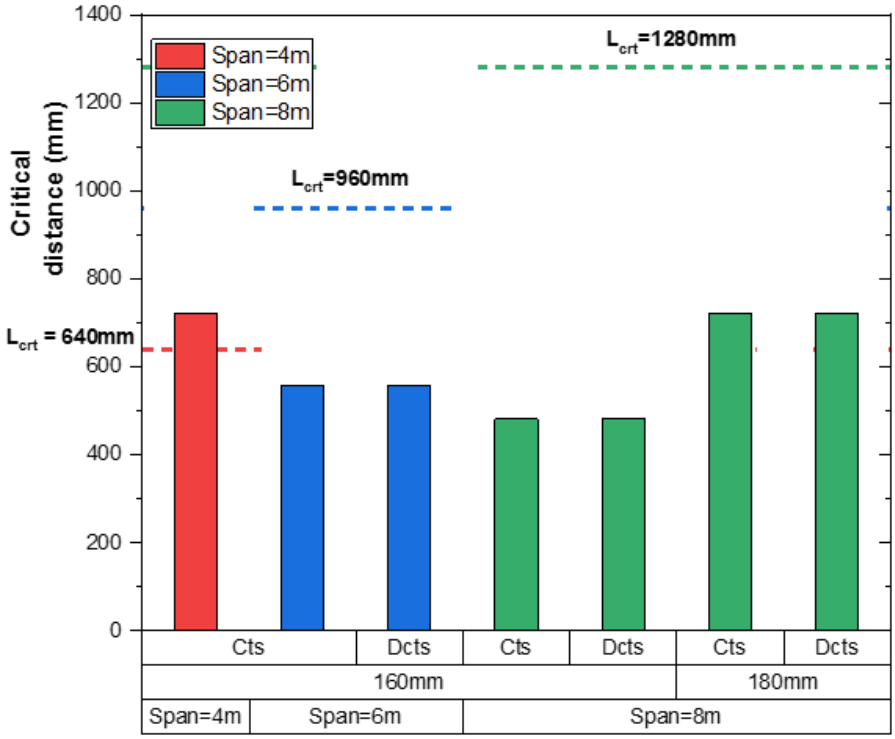

Figure 5.23: Critical distance from column face determined based on the punching angles

In Figure 5.23, dashed lines represent the limit of critical length (0.16 x span) proposed by the latest version of AS 3600 (Standards Australia, 2018). As stated earlier in the previous version, the thickness specified by the standard to achieve a certain FRL had to be maintained throughout the whole floor area. However, with the latest amendment, that thickness can be reduced beyond the L_{crt} limit. When the span is 6m and 8m, the punching cone developed is well within the L_{crt} limit. Therefore, reducing the slab thickness beyond this critical area poses less risk. However, when the span is 4m, the punching cone extends beyond this L_{crt} limit. In such a scenario,

reducing the slab thickness further within the punching cone could increase the risk of punching shear failure. Therefore, the study indicates the need to carefully asses this 0.16L value proposed by AS3600 (Standards Australia, 2018), for smaller spans.

5.5 SUMMARY

Numerical modelling technique validated in Chapter 4 was implemented in this parametric study to determine the influence of critical factors such as span between the columns, thickness of the slab and continuity of top reinforcement for the fire resistance level (FRL). Typical spans used in buildings were selected, a short span of 4m, a medium span of 6m and a long span of 8m respectively. The idea of changing the span was to investigate further the 0.16L (where L is the span) critical length proposed by the latest version of AS3600. According to the amendment, the thickness specified for flat slabs is required only within that distance from the column face and all the other areas, the thickness can be reduced according to the values specified for insulation criteria. A thickness of 200mm was selected as that is the thickness currently specified by most design standards to achieve a FRL of 1.5 hrs or more. In addition to that, thickness values of 180mm and 160mm were chosen in order to evaluate how thicknesses lower than the prescribed value from design standards will behave during fire. In the previous version of AS3600, there was a requirement of at least 20% of top reinforcement within the column strip continuing over the full span. However, the code committee has removed that clause from the latest version of the standard. Therefore, the continuity of the top reinforcement over the full span was taken as another parameter to determine the validity of the latest amendment.

Nominal values of 0.85% and 0.4% for the bottom and top reinforcement respectively, were adopted as the reinforcement ratio (a non-dimensional value) in slab specimens. Validated material models for concrete (40 MPa) and steel (627 MPa) at elevated properties, as described in Chapter 4 were utilized. A design vertical load of 10 kN/m^2 (including self-weight) relevant to fire was applied in all scenarios. A total number of 18 cases were simulated to investigate the behaviour of different cases when the slab is exposed to standard ISO 834 fire for 5hrs.

Results indicate that when the span increases, FRL reduces. Since the same design load per unit area is applied, the load supported by the column increases when the span increases. Therefore, the slab-column connection becomes heavily stressed,

and as a result, risk of failure is increased. Another observation is that for the same span, when the thickness of the slab increases, the FRL increases. Increasing the thickness makes the slab stiffer and as a result, decreases the risk of failure. The continuity of top reinforcement also has an effect on FRL. It is interesting to note that from the slabs which failed, slabs having 20% top reinforcement continuing over the full span have failed before the slabs that do not have such an arrangement. Although having more reinforcement is beneficial in ambient conditions, in case of a fire, more reinforcement increases the overall conductivity of the slab as the conductivity of steel is greater than the conductivity of concrete. Having a higher thermal expansion for steel compared to concrete also contributes to more deformation in the slabs having more reinforcement. Hence, the latest amendment in AS 3600 to remove the requirement to continue top reinforcement for the full span can be further validated from the results.

Plastic strain outputs suggest that the most heavily stressed area is near the slab-column connection when heated. The shape of stress distribution can be utilized to determine the angle of punching failure. By analysing the punching angles of the failed slabs, it can be observed that the punching angle is increased when the span is increasing. That results in a reduction of the critical length from the column face. For the same span when the thickness increases, punching angle decreases which result in increasing the critical length. The main outcome, however, is that when the span is 6m and 8m, the critical length (0.16L) as specified by the latest amendment to AS 3600 lies well above the critical length calculated based on the punching angle. However, when the span is 4m, the critical length calculated is higher than the critical length proposed by the design standard. Therefore, the author suggests that it is safer to prescribe a critical length, considering the punching angle and thickness rather than specifying a single limit for all the cases based on the span.

6 Performance-based design of a concrete flat slab subjected to fire: A case study

6.1 INTRODUCTION

Fire resistance levels prescribed in design codes were based on fire tests where the structure was exposed to a standard time-temperature curve. Usually, these fire curves only have an indefinitely increasing heating phase. However, a fire in a multi-storey building will have an initial development phase, burning phase and a decay phase where ultimately the fire will self-distinguish when fuel runs out, or ventilation is blocked. The severity of such natural fires will depend on various factors such as the compartment size, the amount of fuel from the combustible material within the compartment and the ventilation provided by openings at different locations. With the latest design codes allowing the use of computational methods in order to determine the FRLs, it is worthwhile to investigate how a flat slab will behave under standard fire exposure and natural fire exposure. This chapter will, therefore, describe a case-study on the approach to model an actual fire scenario in an apartment in a multi-storey building. Different modelling techniques and software commonly used will be compared to arrive on a suitable methodology to be used. Setting up the model will be discussed in detail, and the application of temperature output from the developed fire model into the structural model will be explained.

6.2 IMPORTANCE OF PERFORMANCE-BASED DESIGN

Buildings codes around the world have shifted from prescription-based to performance-based codes due to technological advancements made in fire safety design. This enables the use of the latest fire models and tools to optimise designs that meet the fire safety requirements, allowing for improved safety and design functionality at a reduced cost (Hadjisophocleous and Mehaffey, 2016).

Traditionally, fire resistance testing involves exposing the building element to a standard fire time-temperature curve which originated back to the 1900s, where wood-burning furnaces were used (Babrauskas and Williamson, 1978). At present, buildings contain modern furniture made out of synthetic and thermoplastic materials which

have higher heat release rates than wood, resulting in more severe fire scenarios than as encompassed by the standard fire curve (Ariyanayagam and Mahendran, 2014). Full-scale tests at Cardington have proven that the standard fire curve can underestimate the fire severity in both maximum temperature and duration (Lennon and Moore, 2003). This means the actual fire resistance of a building element when exposed to a real fire scenario can be less than expected, leading to unsafe evacuation times for building occupants. In some scenarios, the severity of the fire can be lower than that of predicted by the standard time-temperature curve (International Organization for Standardization, 1999) as propagation and duration of fire is mainly influenced by the fuel load, ventilation and compartment characteristics. The standard time-temperature curve only has a heating regime, whereas a real fire gradually dies down due to low fuel or low ventilation.

The adaptation of performance-based codes means that the fire resistance of a structural element can be determined more accurately by exposing the material to a more realistic fire curve, which takes into account important parameters such as the fuel load, ventilation, size and material properties of the compartment (Ma and Mäkeläinen, 2000). It gives more freedom to the designer to use resources more efficiently while satisfying the same safety requirements. Hence, the trend towards the performance-based design of structural elements for fire safety can be regarded as a good prospect.

6.3 MODELLING AN ACTUAL FIRE IN A BUILDING

6.3.1 Fire in compartments

A fire enclosed within a multi-storey building can be categorised as a compartment fire, given that the fire is confined between the walls and floor slabs of the building. The different stages of a compartment fire and the influencing factors such as the compartment size, ventilation and fuel load were discussed in detail in Chapter 2, Section 2.10.1. The critical issue here is that the compartment fire does not always follow the trend prescribed by the standard time-temperature curve. Therefore, an attempt has been made to model a compartment fire in a building having concrete flat slabs and determine the structural performance of the slab having exposed to the modelled fire.

6.3.2 Different approaches and software for fire modelling

Fire modelling is frequently used in fire research and performance-based design to formulate the time-temperature relationship for differing fire scenarios. It serves as a supplement or alternative to expensive full-scale fire tests. Tools used for fire modelling can be classified in three different categories as discussed below.

6.3.2.1 Empirically based calculations

Empirically based calculations provide approximate solutions calculated by hand using algebraic equations formed within a limiting set of assumptions (Walton et al., 2016b). Examples include Method of Babrauskas; Method of Law; Swedish Method; Japanese Method (Walton et al., 2016b); and the BFD curve (Barnett, 2002). The expressions can predict only average temperatures, but not the temperatures of specific locations (Walton et al., 2016b).

6.3.2.2 Zone Modelling

Zone models divide the modelled space or compartment into several large zones or control volumes, and then it solves the equations of conservation of mass and energy for these control volumes (Walton et al., 2016a). The two-zone model commonly used in zone modelling software divides the space into the hot upper layer containing combustion products and a cooler bottom layer bearing clean, fresh air (Tavelli et al., 2014). Examples of zone modelling software include Consolidated Model of Fire and Smoke Transport (CFAST); FireWind; BRANZfire; and FPETool Fire Simulator. Zone modelling requires less computational duration and power than CFD models to simulate (Tavelli et al., 2014). However, application of zone modelling is unsuited for compartments with complex geometries or analysis where detailed spatial resolution is required (Hadjisophocleous and Mehaffey, 2016), nor it is suitable for determining the temperature profile at selected locations (Jain et al., 2008).

6.3.2.3 Computational Fluid Dynamic Modelling

Computational fluid dynamics (CFD) modelling implements a series of partial differential equations to solve for the Navier-Stokes continuity equation, conservation of mass, momentum, and energy. The partial differential equations are simultaneously applied to millions of small control volumes within the modelled space, providing much higher spatial resolution than zone modelling but requiring more considerable computational time to simulate (McGrattan and Miles, 2016).

The two main approaches for turbulence modelling used in CFD fire modelling are Reynolds-Averaged Navier-Stokes (RANS) method and Large Eddy Simulation (LES) method (McGrattan and Miles, 2016). These two methods are applied to minimise the computational requirement compared to direct numerical simulation (DNS), wherein the partial differential equations are computed without any simplifications (McGrattan and Miles, 2016).

The Reynolds-Averaged Navier-Stokes (RANS) approach is suitable for studies where details of instantaneous flow are unessential, and only the steady-state flow is of importance (Zhiyin, 2015). The approach only solves for the time-averaged flow results while all instantaneous turbulent flow effects (both large and small scale) are approximated by a turbulence model. This leads to the approach being ill-suited for predicting the transient flow behaviour (Zhiyin, 2015). Examples of CFD modelling software that apply the RANS approach includes SMARTFIRE and Kameleon FireEx (KFX) (McGrattan, 2005).

The Large Eddy Simulation (LES) approach directly computes large scale turbulence motions (eddies) and models small-scale motions using a sub-grid scale (SGS) model (Zhiyin, 2015). Given that most of the turbulent energy, causing momentum transfer and turbulent mixing are contained within large eddies, the LES approach produces greater accuracy compared to the RANS approach. However, this requires a higher computational power than the RANS approach (Zhiyin, 2015).

6.3.2.4 Evaluation of LES CFD software

Examples of CFD software utilising the LES approach and a comparison between them are shown below in Table 6.1.

In a review by Vinocour (1989), Vinokur identified that finite-difference discretisation might suffer from imprecision due to truncation errors when calculating for position vectors, derivatives, and treatment of boundary points. By comparison, finite-volume discretisation avoids such truncation errors in its calculation by forgoing calculations for the precise location of the average point (Vinocour, 1989).

Based on a comparison by Diskin et al. (2010) on node-centred (vertex-centred) and cell-centred finite-volume discretisation schemes for the simulation of inviscid flow (such as fire), cell-centred schemes are better at simulations using rectangular

geometries and curved geometries. They also offer lower complexity and less second-order discretisation errors compared to vertex-centred schemes (Diskin et al., 2010).

Table 6.1: Comparison of different CFD software capable of simulating fire

	Fire Dynamic Simulator (FDS) (Binbin, 2011, Yang et al., 2018)	**ANSYS FLUENT (ANSYS Inc., 2009, Binbin, 2011, Yang et al., 2018)**	**ANSYS CFX (ANSYS Inc., 2011, Yang et al., 2018)**	**PHOENICS (Greenshields , 2018)**	**FireFOAM(Chen et al., 2011, OpenCFD Ltd., 2018)**
Discretizati-on Method	Cell-centred finite-volume method	Cell-centred finite-volume method	Node-centred finite-volume method	Hybrid-difference scheme finite-difference method	Cell-centred finite-volume method
Meshing	Only cuboids can be selected which forms rectilinear meshing	Various cell shapes can be selected to form meshing that accurately models object	Various cell shapes can be selected to form meshing that accurately models object	Cartesian, Cylindrical-Polar or Body-Fitted grids to form meshes	A variety of shapes for the meshing to form structured and unstructure d meshes.
Pyrolysis Model	Solid phase pyrolysis model	Solid state pyrolysis not accounted for	Solid state pyrolysis not accounted for	Solid phase pyrolysis model	Pyrolysis is treated as a region model
Combustion Model	Single step, mixing-controlled chemical reaction using three lumped species	Multiple physical models included	Multiple of physical models included	Multi-fluid model (MFM)	Eddy dissipation concept (EDC)
Turbulence Model	Large Eddy Simulation (LES) or Direct Numerical Simulation (DNS)	k-ε model, k-ω model, LES model, DES model	k-ε model, k-ω model, LES model, DES model	k-ε model, k-ω model, LES model, Reynolds-stress model	Large Eddy Simulation (LES)
Application	A tool specifically for fire dynamics studies	General-purpose	General-purpose	General-purpose	Tool developed explicitly for fire

From comparative research by Binbin (2011), ANSYS FLUENT produces more accurate meshing than FDS. Despite this, Binbin (2011) finds that FDS simulation

results corresponded more closely with actual temperature and smoke thickness measurements than FLUENT. From a study by (Maragkos et al., 2012), it was concluded that FireFOAM obtained better agreement for mean cross-stream velocities and entrainment rates. However, FDS, with the use of the sub-grid scale (SGS) model, produced a more accurate simulation of a turbulent helium plume.

In summary, CFD modelling using LES provides the highest degree of accuracy to the fire model among the methods explored. Among the software options explored in Table 6.1, FDS appears to be the most optimum tool for the fire modelling requirements of the research project.

Based on the analysis, Fire Dynamic Simulator (FDS) is selected as the most suitable modelling tool for the modelling requirements of the research. It produces the most accurate simulation results among the different software evaluated (Binbin, 2011, Maragkos et al., 2012). However, this is obtained at the expense of greater computational time and power. To reduce the time needed to construct and simulate the computer models and enable the integration of parallel processing, PyroSim, a graphical user interface for FDS simulation developed by Thunderhead Engineering Consultants, was adopted for the research (Thunderhead Engineering, 2014). PyroSim is only used to create the input file for FDS and hence it does not affect the simulation time. However, significant time-saving is achieved by the graphical method of creating the input file using PyroSim.

FDS numerically solves the following governing equations [eq. (6.1) to (6.4))] using a finite-difference technique with specified initial and boundary conditions (Nguyen et al., 2014).

Mass conservation;
$$\frac{\partial \rho}{\partial t} + \nabla . \rho u = \dot{m}_b^m \tag{6.1}$$

Momentum equation;
$$\frac{\partial}{\partial t}(\rho u) + \nabla . \rho u u + \nabla p = \rho g + f_b + \nabla . \tau_{ij} \tag{6.2}$$

Energy conservation;
$$\frac{\partial}{\partial t}(\rho h_s) + \nabla . \rho h_s u = \frac{Dp}{Dt} + \dot{q}^m - \dot{q}_b^m - \nabla . \dot{q}^n + \varepsilon \tag{6.3}$$

Equation of state;
$$p = \frac{\rho R T}{\bar{W}} \tag{6.4}$$

where,

ρ – material density

u - velocity vector

p - pressure

$\dot{m}_b^m$ - production rate of species by evaporating particles
f_b - external force
τ_{ij} - stress tensor
h_s - sensible enthalpy
$\dot{q}^m$ - heat release rate per unit volume from a chemical reaction
$\dot{q}_b^m$ - energy transferred to the evaporating droplets
$\bar{W}$ - molecular weight of the material mixture of different species
R - Gas law constant

A second-order accurate finite-element approximation is applied to the aforementioned equations to solve for the six unknowns, density (ρ), velocity components $(u_x, u_y, u_z)^T$, temperature T and the pressure p. Fine rectangular grid cells are utilized to represent the domain where scalar quantities (such as density) are assigned at the centre of each cell, and vector quantities (such as velocity) are associated with the cell surfaces (McGrattan et al., 2010).

6.3.3 Model set-up

An arbitrary multi-storey apartment is required as the basis of the simulation. The floor plans from a typical level of the mixed-use development project Colombo City Centre, Sri Lanka were obtained for the project. A 2-bedroom, 2-bathroom unit was recreated in PyroSim for the layout of the modelled compartment. The unit measures 12.2 m width at its widest, 10.4 m width at its narrowest, has a depth of 8.4 m, and a floor to ceiling height of 2.8 m (floor to floor height 3m). The floor plan of the apartment unit is shown below in Figure 6.1, while the created PyroSim model of the apartment unit is shown below in Figure 6.2 and Figure 6.3.

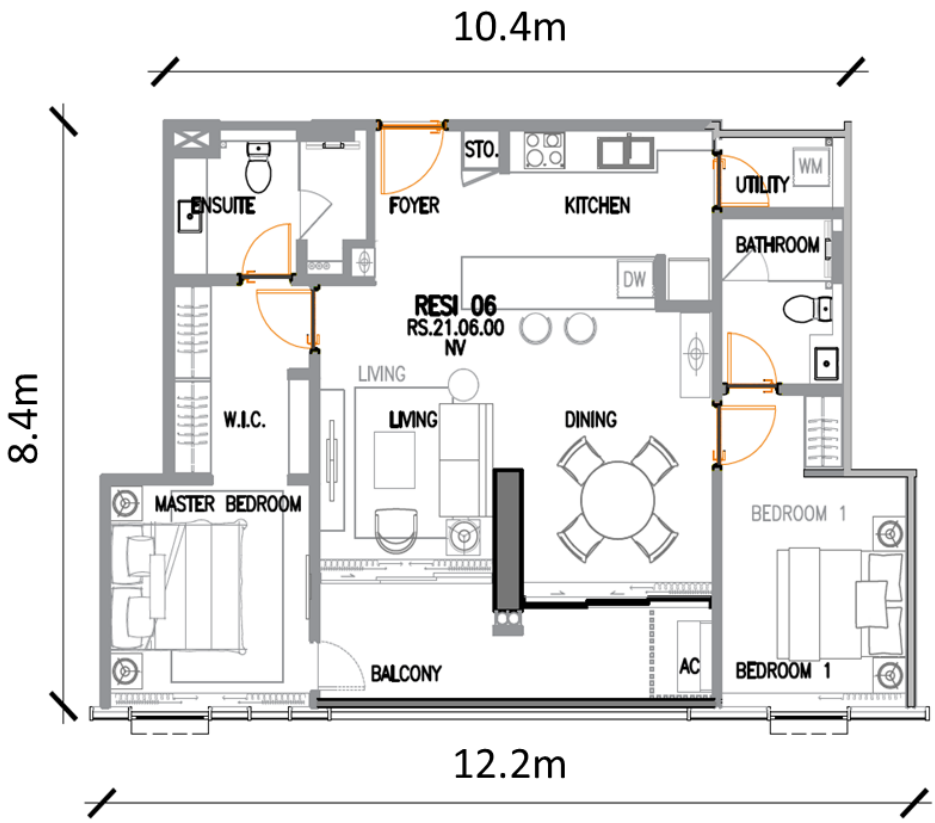

Figure 6.1: Plan view of the apartment considered for the case study

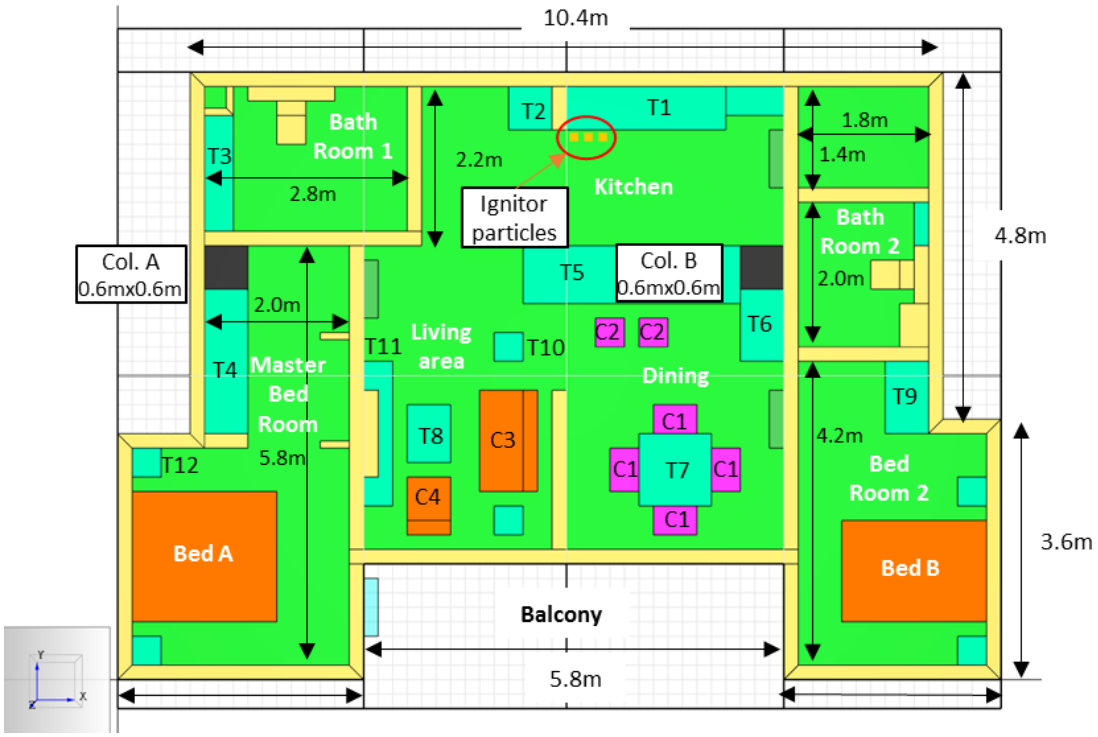

Figure 6.2: Geometry of the developed model in Pyrosim

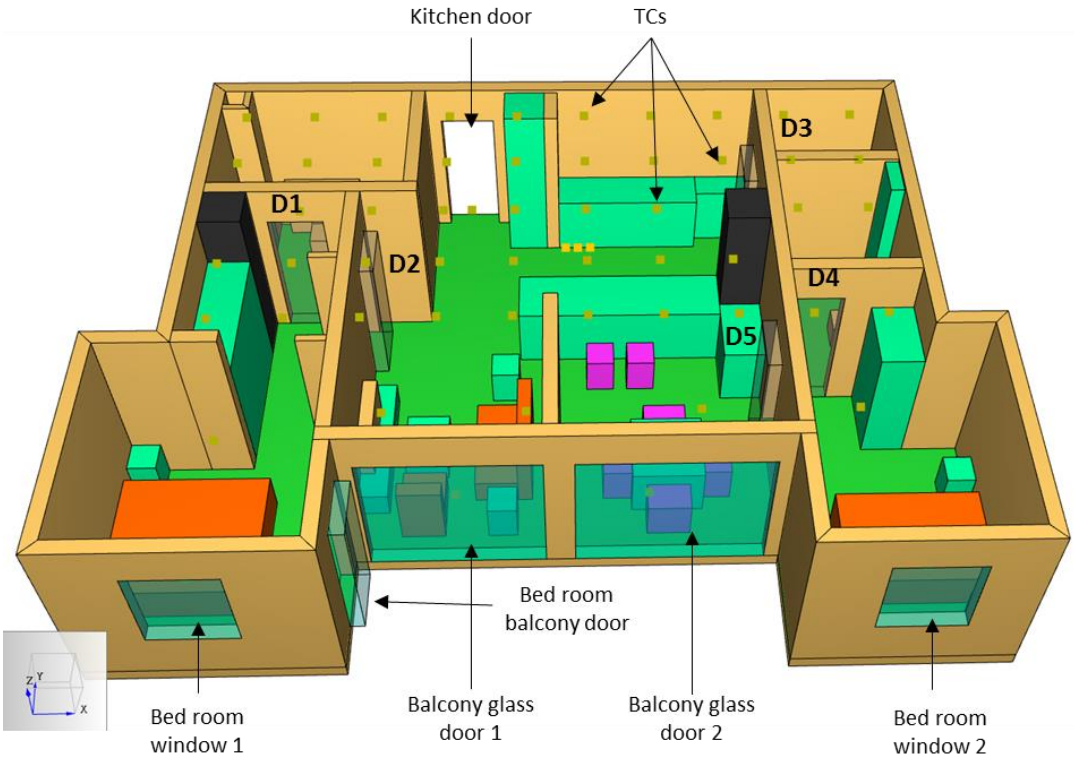

Figure 6.3: Openings in the developed model

Selecting the appropriate mesh size when simulating fire is vital in achieving accurate results. The FDS user manual (McGrattan et al., 2010) proposes the following non-dimensional expression [eqn. (6.5)] to select a size range for simulations involving buoyant plumes.

$\frac{D^*}{\delta x}$ where; D^*- characteristic fire diameter and δx- the nominal size of a mesh cell.

$$D^* = \left(\frac{\dot{Q}}{\rho_\infty c_p T_\infty \sqrt{g}}\right)^{\frac{2}{5}} \tag{6.5}$$

$\dot{Q}$- Heat release rate of fire in kW
ρ_∞- Air density (1.2 kg/m^3)
c_p- Air thermal capacity (1 kJ/kg K)
T_∞- Ambient air temperature (293 K)
g- Gravitational acceleration (9.81 m/s^2)

According to Guillaume et al. (2020), the maximum heat release rate (HRR) that can occur inside a compartment is close to 3.3 MW for the kitchen and bedroom area

and 6.6 MW for living area. As per those values the calculated D^* was 1.55 and 2.05 respectively. The widely accepted ratio for $\frac{D^*}{\delta x}$ ranges from 4 to 16 (US Nuclear Regulatory Commission, 2007). Therefore, a mesh size of 0.2 m was selected which yielded $\frac{D^*}{\delta x}$ ratios of 7.75 and 10.25 respectively and both are within the acceptable range. To ensure that the entire region of interest is simulated, the mesh is made to encompass the entire apartment unit by extending 0.35 m beyond the boundaries of the unit. As running FDS using parallel processing requires a separate mesh for each processor, the meshed region was divided into 8 meshes, enabling the computations to occur on 32 processors simultaneously. Where possible, the meshes were divided along the walls of the unit.

The floor was recreated as a slab obstruction, with the floor slab extending from z = 0 m to z = -0.2m. The walls were recreated as wall obstructions, doors and openings were recreated using holes, while interior furnishing was modelled as simple blocks with details such as legs of tables omitted due to computational constraints. Walls were considered as continuing up to slab bottom level of the upper floor slab. Practically this may not be the case as there will be some space between partition walls and the slab for the building services such as electrical and plumbing. However, a preliminary analysis showed that the fire is more severe when the partitioning walls are at full height. Therefore, they were extended up to the slab-bottom level of the preceding floor. A slab obstruction is placed at z=2.8 m (but not shown in Figure 6.2 as it will obstruct the visualization of the inside arrangement) covering the whole compartment and having an adiabatic surface.

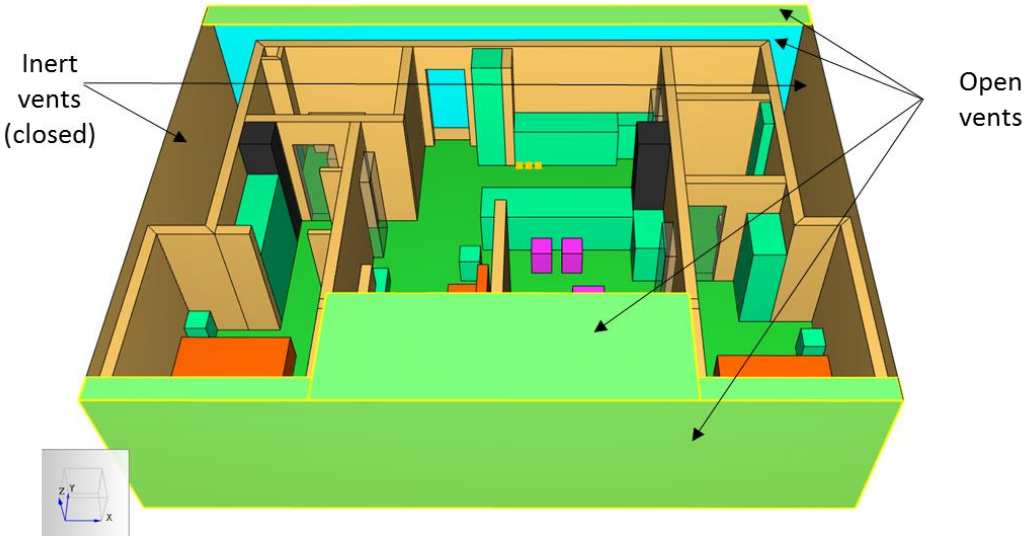

Figure 6.4: Location of vents

Vents are vital components of a fire model as these provide the required airflow for the fire to develop and propagate. For the current apartment, open vents were provided as illustrated in Figure 6.4 to permit movement of air in and out from the model. The remaining sides were inert vents which do not facilitate air movement at their boundary.

Temperature is developed in a structure as a result of heat transfer from the hot gases and flames during a fire. Heat transfer can be two-fold; radiation and conduction combined and called as total heat flux. A real surface would both absorb and emit some heat depending on the gas temperature of the fire and the exposed surface temperature of the solid. According to this phenomenon, the exposed surface temperature of the solid will not be the same as the gas temperature of the fire. The former is the critical input parameter in a structural fire model. In order to overcome this difference Wickström et al. (2007) propose to use the concept of adiabatic surface temperature (AST). AST is defined as the temperature of a perfect insulator which cannot absorb or lose heat to the environment (Wickström, 2011). FDS has the capability of measuring the AST of a solid surface, which is utilized in this analysis to generate the time-temperature histories of the exposed flat slab surface to be implemented in the structural fire model.

A total number of 46 thermocouples were placed on the slab surface around the two columns and span to measure the adiabatic surface temperature due to the fire. The devices are visible as the yellow dots shown above in Figure 6.3. Additionally,

TCs were placed at the mid-height of each external opening (kitchen door, balcony door and windows) to act as triggers to indicate the failure of those openings. As all the doors have glass panels, it was assumed that when the triggering TC reached a value of 300^{o}C, which is the glass breakage temperature (Babrauskas, 2011), the glass in the doors and windows would break and allow flames to penetrate outside.

6.3.4 Simulation parameters

As it is not possible to actually create a fire within an existing building to check the accuracy of the simulation, it is crucial to incorporate accurate material properties which describe the correct combustion behaviour. For the case considered, the combustible materials are identified as the carpet made out of polypropylene fibre, Bed sofas and Chairs that contains Polyurethane form and Tables, Cupboards and benchtop manufactured using Medium Density Fibreboard (MDF). Table 6.2 summarises the input material data utilized in the model along with references indicating from where they were derived.

Table 6.2: Material properties adopted in the fire simulation

	Polypropylene (PP) (Kada et al., 2018)	**Polyurethane (PU) First Reaction (Pau et al., 2014, Wolska et al., 2012)**	**Second Reaction (Wolska et al., 2012)**	**Medium Density Fibreboard (MDF) (Han et al., 2015, Li, 2013, Sonderegger and Niemz, 2009, Zhao et al., 2017)**
ρ, kg/m^3	175	30		660
c, kJ/kg.K	2.16	2.359		1.5
k, W/m.K	0.2	0.05		0.12
Emmisivity	0.97	0.9		0.86
ΔH_c, kj/kg	4.637e4	3.16e4		1.22e4
Reference Temperature, ^{o}C	470	275	375	365
Heating Rate, ^{o}C/min	20	10	10	20
Pyrolysis Range, ^{o}C	75	150	50	140
Heat of Reaction, kJ/kg	875	366	420	360
Char, %	1.4	70 - residue for second reaction	0.72	21.7
Item	Carpet	Bed, Sofa, Chairs		Tables, Cupboards, Benchtop

Values for material properties such as the heat of combustion (ΔHc) were extracted from the SFPE Handbook of Fire Protection Engineering (Hurley et al.,

2015). Information on the reference temperature, heating rate, pyrolysis range, heat of reaction and char percentage were obtained via TGA and DTG. Examples of the calculation method for each parameter are presented in Appendix B.

Studies show that (Ahrens, 2016) most of the fires in high-rise buildings initiate from the kitchen area. Therefore, in this case-study, the fire was assumed to be originating from the kitchen where the cooker is located. Ignitor particles in FDS were utilized to initiate the fire. These are Lagrangian particles which can be positioned on the middle of a cell assigned with a specific diameter and a temperature to maintain for a certain period of time. These particles will increase the temperature of that particular cell. Three ignitor particles having a diameter of 10 mm were placed, as shown in Figure 6.3 in adjacent cells to the carpet. When these cells reach the auto-ignition temperature of the carpet material, the carpet will start to burn. These particles will then no longer participate in the analysis.

As described previously, the ventilation is a critical parameter which defines the spread, growth and suppression of a fire. To simulate different ventilation conditions, it was decided to consider three different scenarios having the following characteristics.

- **Scenario 1** – The kitchen door is always open. Other doors and windows are initially closed, but controllers are assigned to open them when they reach the triggering temperature.
- **Scenario 2** – All doors are open at the start. Windows are initially closed, but controllers are assigned to open them when they reach the triggering temperature.
- **Scenario 3** – Kitchen door is entirely closed, and BR is open at the start. Other doors and windows are initially closed, but controllers are assigned to open them when they reach the triggering temperature.

6.3.5 Results from the fire simulation

Figure 6.5 illustrates the heat release rate for the whole domain. The sudden increase in HRR at t=3.5 to 4.5 min represents the flashover condition. Flashover is defined as the transition to the burning period where the whole room begins to burn after this point. The fire at this point is referred to as a ‘fully developed fire’ and the HRR at this period is usually governed by the available ventilation (Buchanan and

Abu, 2017). It is tough to control a fire when it reaches the flash-over. Eventually, the fuel burns out, and the fire distinguishes. The drop in HRR with the increasing time affirms this kind of behaviour, as shown in Figure 6.5.

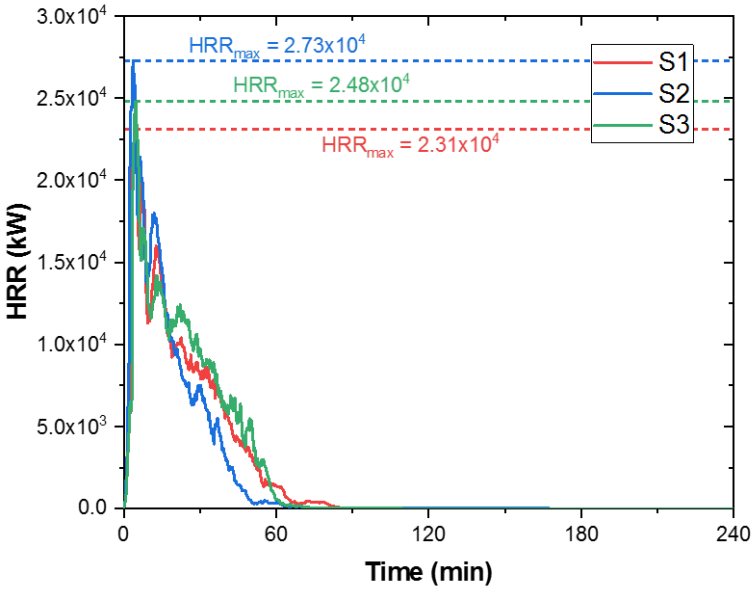

Figure 6.5: Heat Release Rate (HRR)for three scenarios considered

Figure 6.6 further illustrates the spread of fire during the different stages of the fire for scenario 1. As a result of the sudden increase in temperature at flash over the glass panels of the balcony door and bedroom windows break resulting flames ejecting outside the apartment to the external façade. The fire spread within the façade is out of the scope of the study, and therefore, external fire spread is not taken into account in this model. Gradually fire spreads throughout the apartment and material burn away due to fire is also incorporated in the model. Figure 6.6(d) illustrates how certain chairs and part of the mattress in beds gets burned-away during the fire. After the fuel has been consumed in the decay phase, the fire slowly self distinguishes without external fire controls.

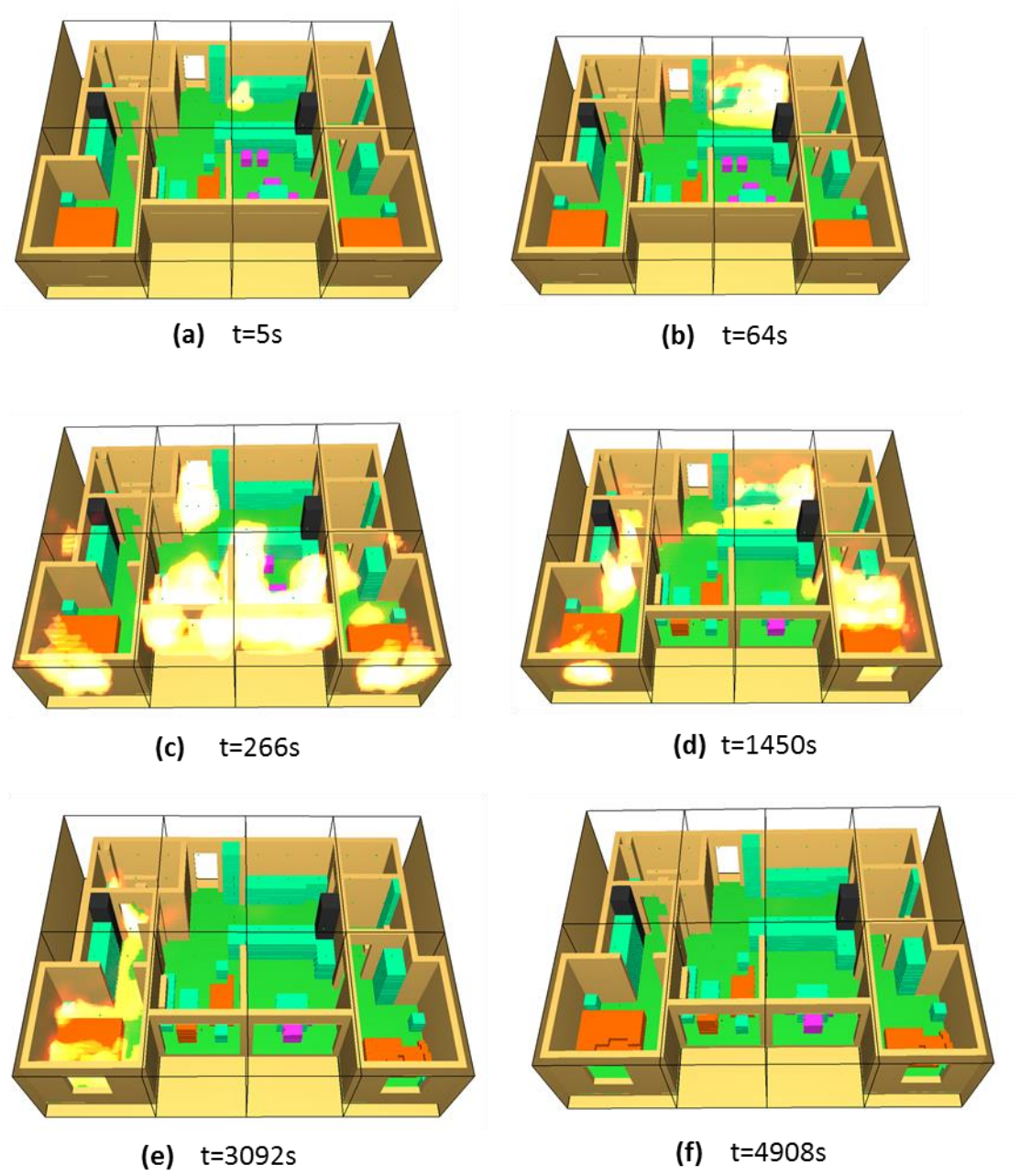

Figure 6.6: Spread of fire at different stages in scenario 1; (a) initiation, (b) initial spread, (c) flashover, (d) burning away of material, (e) gradual decrease of fire, (f) fire self -extinguished

The temperature distribution due to the fire in the kitchen area, which later progresses to other areas of the apartment, is not uniform throughout the whole area. Therefore, to accurately capture the variation of temperature, the area surrounding the two columns are divided into sub-areas, as illustrated in Figure 6.7. TCs were located at each 1m grid to measure the adiabatic surface temperature of the underneath of the slab. The area of one of the sub-areas is approximately 12m^2. Temperatures recorded from all the TCs within that particular sub-area were then averaged to obtain the average temperature variation with time within that sub-area. The average temperature

distribution for a typical sub-area is shown in Figure 6.8. As there was too much noise within the recorded temperature, Savitzky-Golay smoothing (Press and Teukolsky, 1990) was adopted to obtain a smooth time-temperature curve, as shown in Figure 6.8.

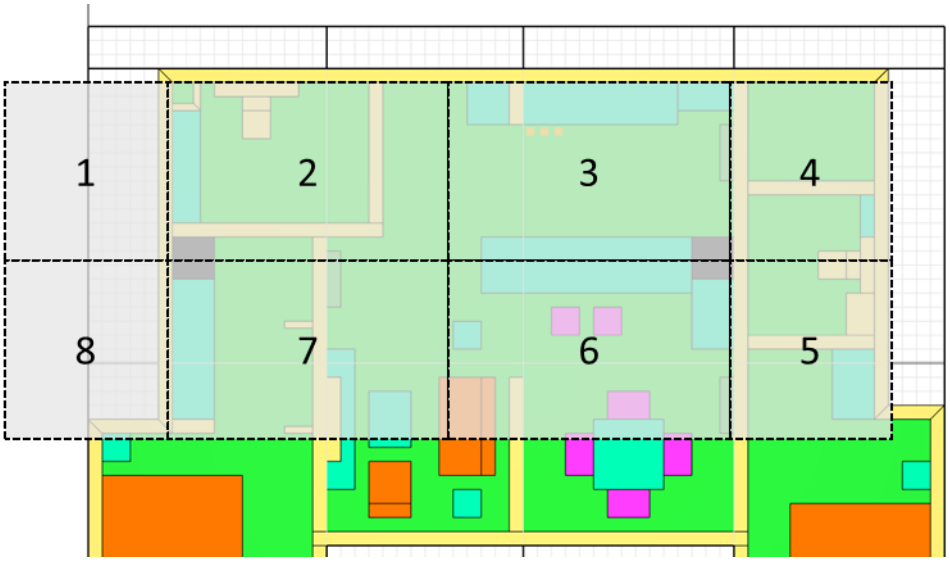

Figure 6.7: Division of sub-areas surrounding the critical area of exposure around the two columns

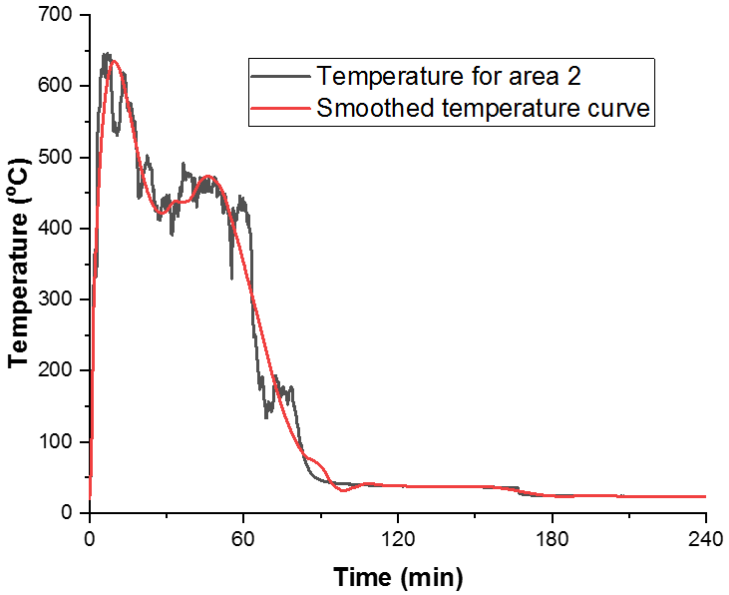

Figure 6.8: Smoothing of time-temperature histories

Figure 6.9 presents the smoothed time-temperature histories for heated areas for 3 scenarios considered. Area 1 and 8 which are at left of column A, are regarded as the extension of the slab which continues to the adjacent apartment. It was assumed that the perimeter walls of the apartment under consideration are preventing the fire from

spreading to the next apartment. Due to that, the temperature of areas 1 and 8 are assumed to be unaffected by the fire, unless the heat is conducted through the slab. This conductive effect is taken into account in the structural model, which will be discussed later. Therefore, only the variation of temperatures in areas 2 to 7 is presented in Figure 6.9.

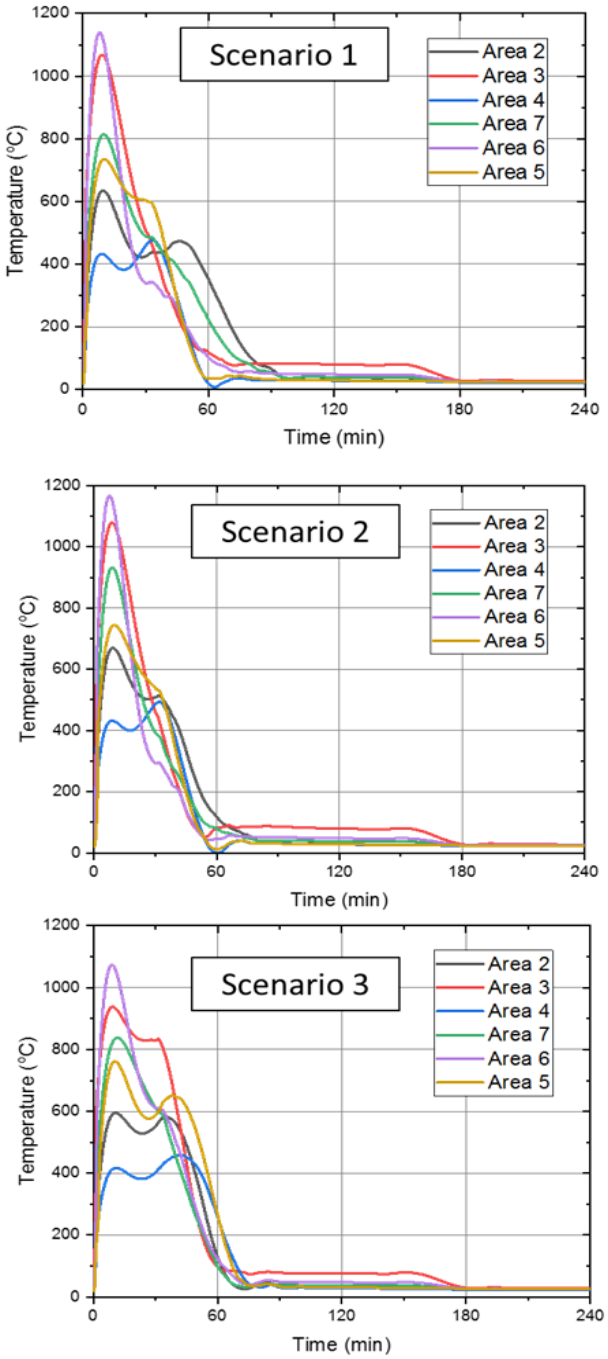

Figure 6.9: Time-temperature histories obtained for different scenarios

The peak temperatures which exceeds 1000^{o}C in all 3 scenarios are reached during the same time as flash-over. The duration of fire in scenarios 1 and 2 are approximately 1 hr, whereas in scenario 3, fire extinguishes at 1 hr and 15 mins. Ventilation in scenario 3 is less than the other two scenarios as the kitchen door, which is closest to the fire source is completely closed from the start. Therefore, flashover, in that case, occurs slightly later than scenario 1 and 2 and the peak temperature also slightly lower than the other two cases. As a result, scenario 3 is having more fuel left after flashover, which explains the slightly higher duration of the fire. It is also important to note that this temperature history has both heating and cooling phases in contrast to the standard fire curve, which consists of only an indefinitely increasing heating phase. To further analyse which scenario is more severe, time-temperature histories were plotted for each sub-area and presented in Figure 6.10.

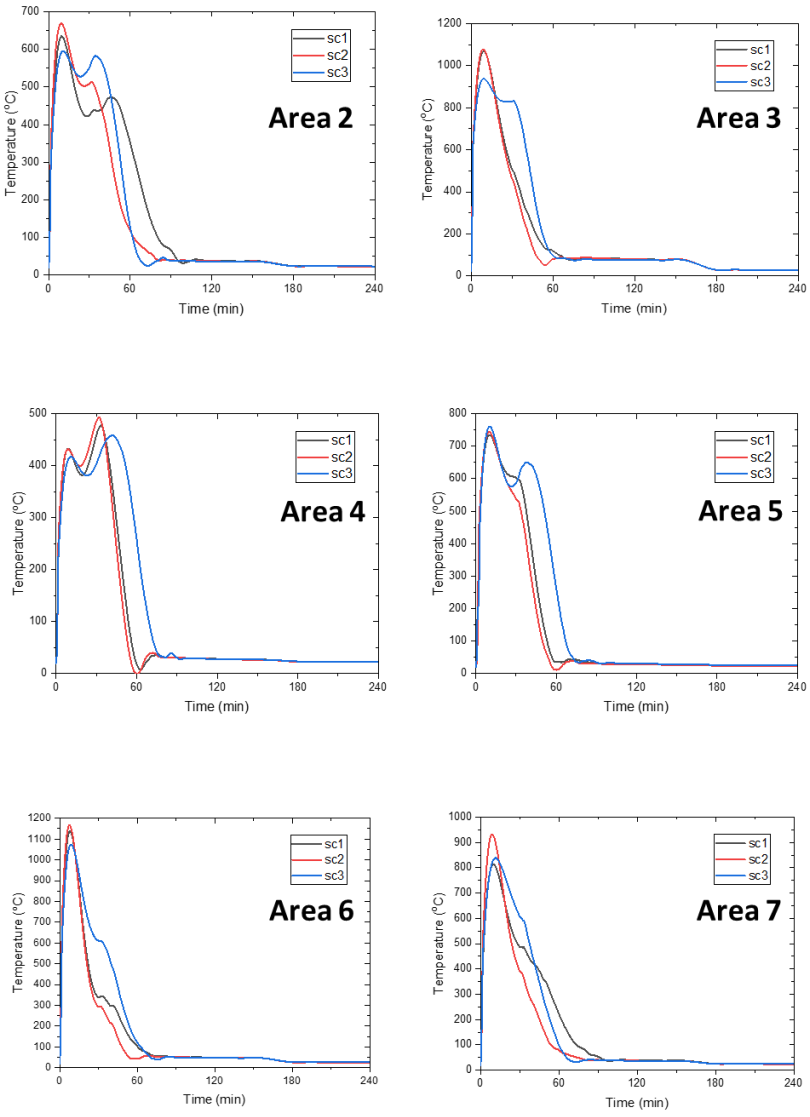

Figure 6.10: Time-temperature histories calculated for each area for different scenarios

Observing the results, it is evident that scenario 2 has caused the maximum temperature in most of the areas. However, the time duration of fire in scenario 3 is slightly more than that of scenario 2. Early attempts to describe the fire severity based on the area under the time-temperature curve has later found to be inadequate in addressing the heat transfer from the fire to the structure (Buchanan and Abu, 2017). Therefore, later it was proposed by Law (1971) and Pettersson (1974) that maximum temperature in a fire will be more critical as it can cause melting or phase change in a material. Based on that concept, it was decided to select scenario 2 as the most severe case for the modelled apartment. Therefore, the time-temperature history depicted by Figure 6.9 (scenario 2) was selected to be applied in the structural model to investigate the FRL.

6.4 APPLICATION OF THE MODELLED FIRE TO THE STRUCTURAL MODEL

According to the plan view of the apartment as presented in Figure 6.1, the span between two columns is taken as 7m. Therefore, slab extensions of 3.5 m were additionally included in the structural model as presented in Figure 6.11 The column size was 600mm x 600mm, and a slab thickness of 180mm was considered. 40 MPa concrete was utilized with heating and cooling phase material properties as described in Chapter 5. Similar properties for reinforcing steel was also adopted in the model. A design fire load of 10 kN/m^2 was applied on to the unexposed surface while reinforcement ratios were 0.85% and 0.4% for the bottom layer and top layer respectively, similar to the values used in Chapter 5. Similar boundary conditions were also utilized in this case, where spring supports represented the continuous action from the adjacent slabs.

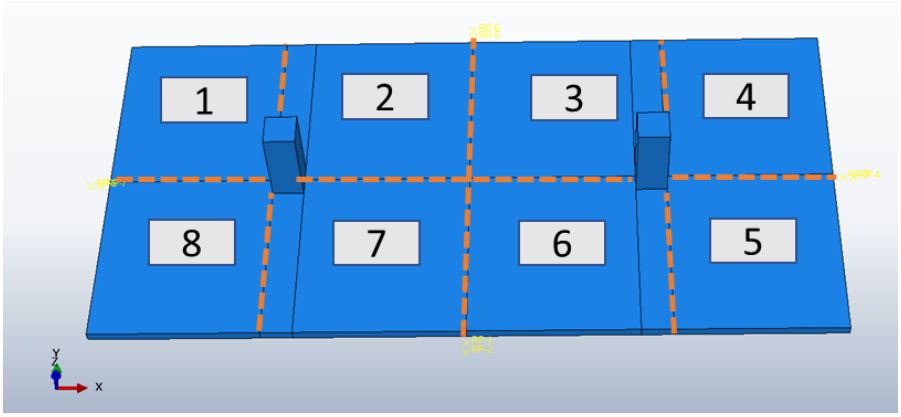

Figure 6.11: Structural model developed in ABAQUS

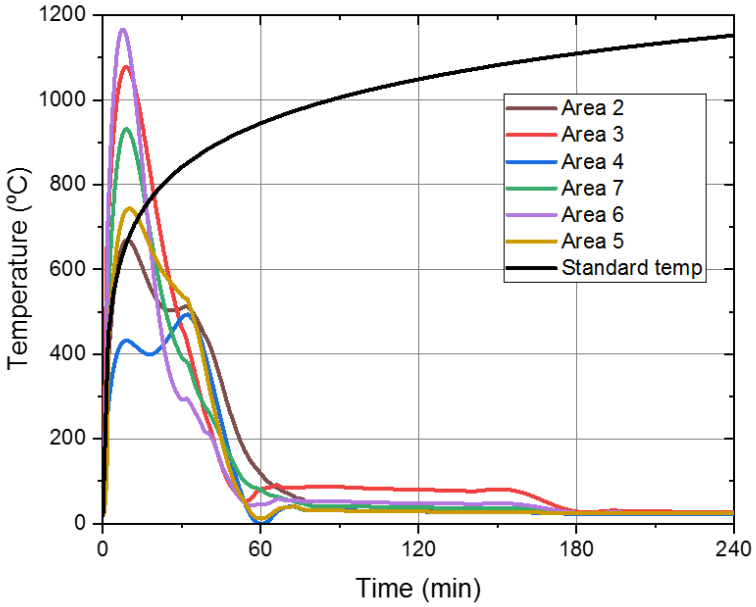

Figure 6.12: Temperature curves applied to the structural model

The exposed surface of the slab was divided into same sub-areas considered in the FDS model for fire development (see Figure 6.11). Two scenarios were considered for the analysis. One where the slab is exposed to the ISO 834 standard time-temperature curve and next the natural fire time-temperature curve determined from the FDS model in the previous section (see Figure 6.12). Areas 1 and 8 belong to the adjacent apartment, and as mentioned earlier, it was assumed that due to the compartmentation effect flames will not spread to adjacent apartments. Therefore, the room temperature was initially applied for those areas while the temperature increased during the analysis as a result of the thermal conductivity of the flat slab. For the remaining areas, the calculated temperatures corresponding to real fire scenario and standard fire are applied while the design load is being maintained. Explicit coupled temperature displacement approach described in Chapter 4 and 5 was utilized for the thermo-mechanical analysis. Field variable was adopted to include the cooling phase material properties. Figure 6.13 and Figure 6.14 present the structural and thermal responses obtained from the FE simulation.

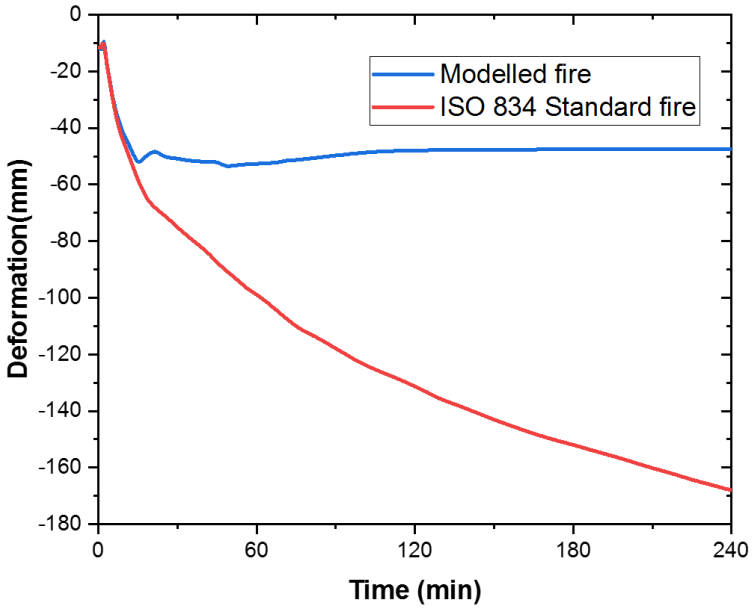

Figure 6.13: Structural response

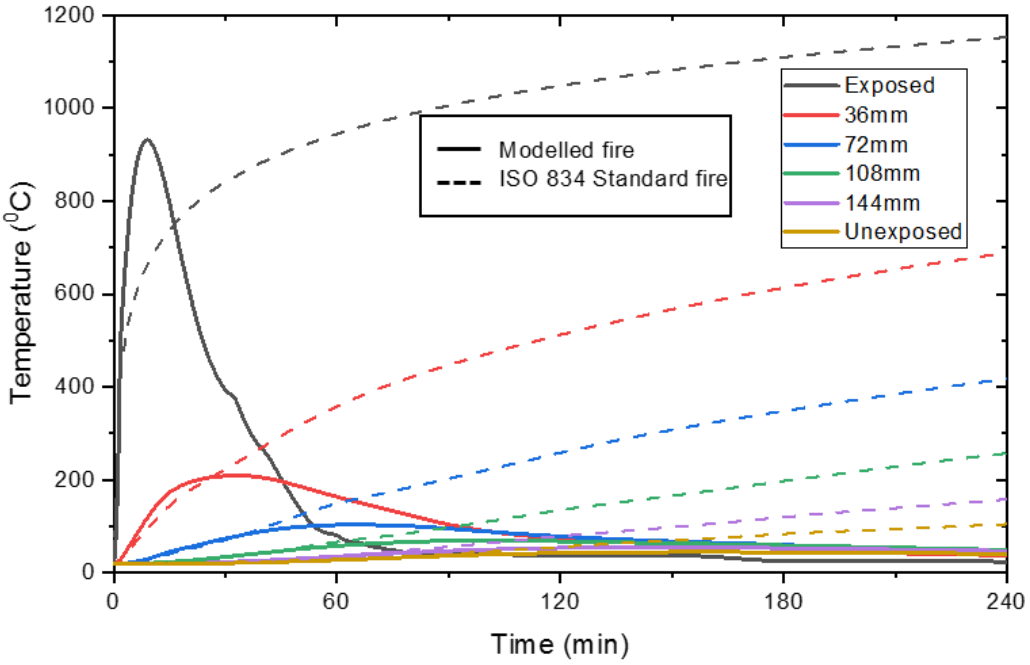

Figure 6.14: Thermal response

It is evident from the results that both the structural and thermal responses are less severe during the modelled fire compared to the standard fire exposure. In the standard fire, the deflection and temperatures continuously increase as it contains an indefinitely increasing heating regime. However, in the modelled fire scenario, the

exposed temperatures decrease when the fire reaches the decaying phase due to a limited amount of fuel. This resulted in significantly less deformation and temperatures across the flat slab. If the fire design is solely based on standards, the FRL for this specific case would have been underestimated. By incorporating the performance-based design approach, more realistic FRL can be predicted, which optimizes the design for fire safety. The importance of using advanced analytical tools to predict the FRLs is further endorsed by this case study.

6.5 SUMMARY

Performance-based fire design is preferred over prescription-based fire design as it yields more optimized solutions on a case by case basis. Numerical simulations of fire scenarios are economical and efficient as practically it is not viable to reconstruct a fire in an actual building. The first step in the performance-based approach is to determine the natural fire curve experienced by the structural element. After comparing different methods available, Fire Dynamics Simulator (FDS), a CFD based fire simulation software was implemented to model an actual fire scenario inside an apartment in a high-rise building.

Combustible characteristics of the different materials inside the apartment were taken into account. Different ventilation conditions were also considered in the fire model. Adiabatic surface temperatures of the overhead flat slab were measured during the full fire duration, from initiation, then flashover, decaying phase and ultimately until self-extinguishment of the fire. Based on the recorded temperatures, the most severe fire scenario was selected to be applied for the structural model.

A structural fire model was created using the FE package ABAQUS for the column and slab arrangement within the apartment. Material properties of concrete and steel at both elevated temperatures and during cooling phase were utilized in the model. The adiabatic surface temperature output for different regions obtained from the fire simulation was assigned as a boundary condition in the structural model. The thermal and structural response of the natural fire scenario was compared with the standard fire exposure. Results indicate that the FRL, when exposed to the natural fire, is significantly higher than when exposed to the standard fire. This highlights the effective use of the performance-based design approach to arrive on an economical yet safe design against fire.

7 Conclusions and Recommendations

7.1 INTRODUCTION

Findings from the experimental and numerical work described in previous chapters are summarised to present the overall conclusions of the research in line with the research questions and objectives highlighted in Chapter 1. Furthermore, the limitations of the investigation and the directions for future research are also presented.

7.2 KEY CONTRIBUTIONS FROM THE RESEARCH

This is the first instance where a large-scale restrained concrete flat slab is tested against standard fire exposure. Although several researchers have suggested that the restrained support conditions could improve the fire resistance level due to the development of membrane forces during fire, it has not been experimentally proved prior to this. Restrained support conditions are crucial as they closely represent the continuity of the flat slab in an actual floor of a building. Moreover, the measurements recorded during the cooling phase is also vital when developing and validating numerical models which include the cooling phase material properties.

The author has introduced the use of coupled temperature-displacement explicit analysis technique with improvisations in order to simulate the thermo-mechanical behaviour of flat slabs in fire. This method eliminates the non-convergence issues encountered when using the standard implicit solver. The ability to couple the thermal and structural response makes this method more efficient than the standard sequential approach where a heat transfer analysis is conducted prior to the structural analysis.

The parametric study conducted by the author based on the validated numerical models developed, investigate the appropriateness of the latest amendments to the Australian fire design guidelines for concrete flat slabs incorporated in the Concrete Structures Standard AS3600-2018. Results of the analysis suggest that while some amendments are in line with the research findings, some rules need to be improved to reduce the risk of failure. This investigation, therefore, can be used as a research basis to evaluate these guidelines. Not only Australian design code but other fire design codes in the world can also make use of these findings.

The author investigated the use of performance-based fire design approach for concrete flat slabs by means of a case study where a fire model was developed for an apartment within a high-rise building. Rather than just relying on the standard prescription-based design principles, moving to a performance-based approach would optimize the solution proposed for fire safety. This has been demonstrated by comparing the fire curve derived from the fire simulation against the standard fire curve. Moreover, the contrasting difference of the thermal and structural response between the simulated fire conditions and the standard fire conditions further highlights the benefit of using a performance-based design approach.

7.3 CONCLUSIONS OF THE FINDINGS

This section summarises the key outcomes and conclusions from each chapter separately.

7.3.1 Conclusions from Literature Review

A comprehensive literature review is presented in Chapter 2, which covers all the aspects of the behaviour of concrete flat slabs in fire. From the critical review of available research data and industry practices, it was evident that the current fire design guidelines related to concrete flat slabs impede the effective use of them in multi-storey buildings—especially the strict thickness requirement which covers the whole floor area. Only Australian concrete code so far has come up with measures to address this issue to a certain extent, but it is unclear whether proposed remedies are based on scientific data or general industry practices. Most design codes are based on the Eurocode flat slab fire design guidelines which are based on a series of fire tests carried out two decades ago. The limitation of these tests is that they were conducted on simply supported specimens which do not take into account the membrane actions developed during fire. Some researchers argue that such an arrangement would have predicted fire resistance levels lower than that with restrained support conditions, which closely represent the actual conditions in a building. However, so far, only one test series was carried out using restrained small-scale specimens, but it was exposed to much lower temperatures than experienced during a building fire.

Numerical modelling was identified as a time saving and cost-effective method to predict the fire behaviour of concrete flat slabs. However, the extent of non-linearities involved both geometrically, and material-wise are causing difficulties to

obtain a reliable solution quickly. Some analytical models have also been developed to assess the flat slabs in fire, which are yet to be simplified to an extent where designers can use them directly for their fire design.

Moving towards the performance-based fire design is found to be the latest trend. It gives the flexibility to the designer to choose a more robust solution depending on the building characteristics rather than relying on the prescription-based design, which considers a general solution for all the cases. Previous studies have demonstrated the use of computational methods to model a natural fire scenario. Such techniques can be adapted to simulate a compartment fire and derive the natural fire time vs temperature curve experienced by a typical concrete flat slab.

7.3.2 Conclusions from the large-scale experiment on restrained flat slab subjected to standard fire

The requirement for a fire test involving large-scale specimen with restrained support conditions was evident through the literature review carried out in Chapter 2. The specimen was subjected to loading and exposed to standard fire simultaneously to observe the thermal and structural response. Measurements were also recorded during the cooling phase, which were later used to validate numerical models. Following conclusions were drawn from the experiment conducted.

- The concrete mix contained poly fibre, and the specimen was cured only for 28 days. No spalling was observed during the total duration of the test.
- The 180mm flat slab specimen did not fail for 3.5 hrs of ISO 834 standard fire exposure in contrast to the fire resistance levels specified by the standards which require a 200mm thickness for an FRL of 90 min or above.
- The use of restrained support conditions which closely represent the actual conditions of a flat slab in a building has increased the fire resistance level. Membrane action developed during fire would have improved the punching shear resistance.
- Data were recorded during the cooling phase as well due to the tendency of failure in the cooling phase, especially in restrained specimens.
- Thermal and Structural response recorded during the heating and cooling phases can be employed in validation studies for numerical models.

7.3.3 Conclusions from the thermo-mechanical modelling of flat slabs in fire

Since real scale fire tests on concrete flat slabs are expensive and time-consuming, the possibility of assessing fire behaviour using numerical modelling is investigated in Chapter 4. The FE element package ABAQUS was chosen for the model development after comparing the capabilities of several commonly used structural fire modelling software.

Among the models developed so far, they all have followed the sequential thermo-mechanical approach, which involves a separate thermal analysis and a structural analysis. The standard implicit solver utilized in the above models has often encountered non-convergence issues due to both geometry and material non-linearities present in the fire models. To overcome this, the author has proposed to use the coupled temperature displacement analysis approach with the explicit solver. Thermal and structural behaviour is combined in this approach which makes it more efficient. The explicit solver is generally used to analyse quick transient events. However, with some improvisations, it can be used to analyse static events while maintaining the quasi-static state. In case of fire, the author has used load factoring to condense the few hours of heating to a few seconds in the analysis. This has been achieved by ensuring that the units which involve a time scale such as conductivity, specific heat and convective heat transfer coefficient were modified in order to be compatible with the load factoring. Whether the analysis remained in the quasi-static state was further verified by observing the kinetic energy and internal energy of the model.

Load induced thermal strain (LITS) or transient creep strains becomes critical, especially when temperatures are beyond 500oC. Therefore, it is important to include these transient creep effect for numerical modelling. Since the author is using the explicit solver, there is no separate creep function in ABAQUS for the explicit solver. Hence, the transient creep is explicitly included in the stress-strain behaviour of concrete.

Incorporating the material properties during the cooling phase is another challenge encountered during thermo-mechanical modelling. To overcome this, the author has used the 'Field Variable' option available in ABAQUS to change the material properties when cooling starts. Adopting such a technique ensures that the structural response takes into account further strength degradation during cooling. This

will also be useful when structures are exposed to natural fires which has a decay phase in contrast to the standard fire curve, which only has a heating phase.

Developed modelling technique and input parameters were validated with the experimental results from the large-scale fire test described in Chapter 3 and two other independent flat slab fire tests.

7.3.4 Conclusions from the parametric study on factors influencing the FRL of concrete flat slabs

A parametric study was conducted using the developed numerical modelling technique to investigate the key influencing factors to the FRL of concrete flat slabs. The focus was on the latest amendments made for the fire design guidelines for concrete flat slabs. Parameters considered were the thickness of the flat slab, the span between the supporting columns and the continuity of top reinforcement within the span.

Australian concrete design code is the first to introduce a limiting distance from the columns where the thickness requirement for flat slabs governs. However, this limit is based on the drop panel dimension limits currently used with flat slabs and not derived from any research evidence. Results from the parametric study indicate that this limit may not be suitable for shorter spans. The author suggests considering the punching angle being developed and the thickness of the slab when specifying this limiting distance.

Another change was the removal of the requirement to have at least 20% of top reinforcement continuing through the full span, to have an FRL of 90 min or more. According to the parametric study, flat slabs not having continuous reinforcement have performed better. Having more reinforcement is beneficial at ambient conditions as it increases the rigidity. However, in case of fire, having more steel reinforcement can increase the risk of failure. More steel increases the overall conductivity of the slab, which accelerates the rate of material degradation at elevated temperatures. Also, steel having more thermal expansion contributes to more deformation of the slab, which increases the risk of failure. Therefore, the decision to remove the top reinforcement continuity requirement can be justified based on the analysis results.

7.3.5 Conclusions from the case-study on performance-based fire design of concrete flat slabs

The effects of a natural fire would be much different from the effects of the standard fire on concrete flat slabs. To test this hypothesis, a case study was conducted on the development of a fire within an apartment selected from an existing high-rise building. At first, the best approach to model a natural fire within a compartment was selected after comparing different fire modelling techniques. Fire dynamics simulator (FDS), which is based on computational fluid dynamics (CFD) was selected to generate the fire model.

Propagation and decay of a natural fire depend on the compartment size, fuel load and ventilation. The outcome of the fire model illustrated different fire behaviours when the ventilation was changed. Unlike the standard fire curve which only has a heating regime, the modelled fire decayed and ultimately extinguished when all the fuel was burned out. Such trends and different scenarios can only be captured by actual fire models. It also provides a case-specific tailor-made time-temperature history instead of a general design fire curve.

The author then described the procedure of employing the generated natural fire temperature field on a structural model. Structural response of the concrete flat slab exposed to natural fire is significantly different from the response to the standard design fire. In the case considered, the standard design fire underestimates the FRL of the flat slab. This highlights the importance of using a performance-based design approach over the code-based prescriptive design approach as the former enhances the flexibility of choosing an optimum design which is suitable for a specific building.

7.4 OVERALL CONCLUSIONS OF THE RESEARCH

Following key points summarise the overall conclusions of the research.

- Among the limited number of fire tests on flat slabs, the vast majority of them were on simply supported small-scale specimens on which the current fire design guidelines are based. 180 mm thick large-scale laterally restrained concrete flat slab tested by the author survived more than 2hrs of standard fire exposure compared to the design code requirements which specifies 200 mm thick slabs for an FRL of 1.5 hrs or more. Laterally restrained support conditions closely represent the actual boundary

conditions of a continuous flat slab in a building, and it enhances the fire resistance due to the membrane action developed during a fire.

- Coupled temperature-displacement analysis step together with explicit solver in FE program ABAQUS can be successfully utilized to model the thermo-mechanical behaviour of concrete flat slabs in fire. This method avoids convergence issues incurred by the standard implicit analysis and also efficiently provides the solution as it does not require to conduct the heat transfer analysis and structural analysis separately.
- Although the general conception about fire relates only to temperature elevation, structural response during the cooling phase is also crucial. Numerical models developed by the author incorporate the material degradation during the cooling phase too, and this is useful primarily to simulate the conditions of structures exposed to natural fires which contain a decaying phase.
- The parametric study conducted by the author using the developed numerical models investigates the latest amendments included in the Australian concrete design code. Analysis suggests that the critical distance (0.16 x span) specified based on the span between columns, should be based on the slab thickness and punching angle instead. Apart from that, the decision to take away the requirement for the continuity of top reinforcement over the span is the correct choice as indicated by the results of the parametric study.
- The time-temperature curve of a natural fire within a compartment having a concrete flat slab needs to be determined in order to follow the performance-based design approach. Fire dynamics simulator (FDS) can be adapted to simulate the actual development of a fire within a compartment. The case-study clearly demonstrates that there is a contrasting difference between the natural fire simulated and the standard time-temperature curve.
- Structural response of the flat slab exposed to the modelled fire is much less severe than when exposed to standard fire in the case considered. Therefore, performance-based approach yields a more case-specific solution and this may be efficient both economically and fire safety-wise when compared to

the prescription-based approach, which provides a general solution for all the scenarios.

Key limitations of the study are;

- The laterally restrained support conditions adapted during the experiment and numerical modelling are valid only for the internal slab panels in a floor. The edge panels could have one or two edges which are not restrained against lateral expansion. Those cases are not considered during the study.
- Structural loading could not be maintained during the cooling phase due to a limitation of the available loading arrangement. It would be interesting to investigate the behaviour during the cooling phase with loading maintained at the same level as during heating.
- Thermo-mechanical modelling utilized the calculated material properties at elevated temperatures based on the measured material properties at ambient conditions. The models used in the study are defined by design codes and also widely used by other researchers. However, the correct material model to calculate the properties at elevated temperatures should be carefully selected and validated with experimental results. Residual material properties and cooling phase properties are also based on code proposed models. Conducting tests on the same structure when it cools down to ambient conditions after the fire would yield more accurate residual material properties.
- The explicit coupled-temperature displacement analysis procedure is validated in this study only for concrete flat slabs. However, the same approach can be extended to model the thermo-mechanical behaviour of other structural concrete elements subjected to fire.
- Since the slabs, in general, are not constructed using high-strength concrete, the numerical modelling did not incorporate the effects of spalling. However, if high-strength concrete structural elements are modelled against fire, spalling will be crucial.

- The study focuses on concrete flat slabs in multi-storey buildings used for residential or business purposes. Therefore, the standard compartment fire models are considered. However, flat slabs which can be found in car park structures can experience much severe fire conditions as the fuel load in such buildings are much higher. A severe fire curve should be applied in such scenarios.
- The accuracy of the compartment fire model developed heavily depends on the accuracy of the combustible material properties considered in the study. There is no way to validate the model experimentally as the actual building constructed cannot be burned. Therefore, when interpreting the results, much focus should be on the characteristics such as fire spread, effects of ventilation and the different phases of fire (growth, flash-over and decay) rather than exact temperature values.

7.5 RECOMMENDATIONS FOR FUTURE WORK

The thesis addressed some of the crucial issues related to the fire resistance of concrete flat slabs. Through large-scale experiments and numerical modelling, it reviewed the major changes to fire design guidelines for concrete flat slabs in Australia and provided a research basis for design codes in other countries of the world to follow. It also introduced a methodology to be adapted in the performance-based fire design of concrete flat slabs. Moreover, this study creates the opportunity for future research in performance-based fire design of concrete structures in general. The recommended future work are as follows.

More fire tests on flat slabs incorporating realistic boundary conditions

The fire test presented in this thesis is the first instance where a large-scale laterally restrained concrete flat slab was tested against standard fire exposure. The results highlighted the importance of boundary conditions that closely represent the actual conditions in a building. Given the limited number of experimental investigations on restrained flat slab specimens in fire, the author suggests conducting more fire tests with realistic boundary conditions subjected to more severe fire conditions such as hydrocarbon fire. If the slab does not fail during the heating phase, it is vital to maintain the same loading and also observe the behaviour during the cooling phase.

Inclusion of spalling of concrete and degradation of the bond between reinforcement and steel in numerical models

The scope of this study is limited to normal grade concrete flat slabs and therefore spalling was assumed to not occur during fire. However, there could be flat slabs constructed using high-strength concrete which is more susceptible to spalling. In such cases, it is important to include a mechanism for spalling of concrete in the numerical models. Another aspect is the bond between reinforcement and concrete at elevated temperatures. The degradation of concrete-reinforcement bond during fire is not yet quantified and therefore not included in numerical models. Hence, the author suggests investigating more on that phenomenon and find a way to incorporate that in the numerical models describing concrete structures in fire.

The difference between intermediate panels and corner & edge panels

The research discussed in this thesis focused on the continuity of the flat slab in all directions. This is valid for an intermediate slab panel which has adjacent slab panels on all four sides. However, in corners and edges, slab panels have one or two edges free to expand. When considering the whole floor area, which consists of all these types of panels, the FRL of the whole floor would depend on fire resistance of all these panels. Therefore, extending the numerical modelling technique developed to simulate a complete floor of a building with different combinations of fire exposed panels would provide more insights into the overall fire behaviour of a building.

Validation and verification of compartment fire models

Burning down an existing building to verify the fire models is not possible. Hence, the accuracy of modelling heavily depends on the accuracy of combustible material properties utilized. Some real scale laboratory recreations of compartment fires are essential, incorporating commonly found material types in residential and office buildings. The outcomes from those studies will immensely contribute to improving the accuracy of computational fire models being developed. Having the capability to model actual fire scenarios in buildings accurately would increase the use of performance-based fire design by the industry.

References

Ahrens, M. (2016) *High-Rise Building Fires*.

Aimin, Y., Yuli, D. & Litang, G. (2013) Behavior of unbonded prestressed continuous concrete slabs with the middle and edge span subjected to fire in sequence. *Fire Safety Journal* **56**:20-29.

Al Hamd, R. K. S., Gillie, M., Warren, H., Torelli, G., Stratford, T. & Wang, Y. (2018) The effect of load-induced thermal strain on flat slab behaviour at elevated temperatures. *Fire Safety Journal* **97**:12-18.

Albrifkani, S. & Wang, Y. C. (2016) Explicit modelling of large deflection behaviour of restrained reinforced concrete beams in fire. *Engineering Structures* **121**:97-119.

Alogla, S. & Kodur, V. (2018) Quantifying transient creep effects on fire response of reinforced concrete columns. *Engineering Structures* **174**:885-895.

American Concrete Institute (2014)Code Requirements for Determining Fire Resistance of Concrete and Masonry Construction Assemblies.

Anderberg, Y., Forsén, N. E., Hietanen, T., Izquierdo, J. M., Le Duff, A., Richter, E., Whittle, R. T., Bossenmayer, H., Litzner, H. U. & J., K. (2004) *Background documents to EN 1992-1-2*.

Anderberg, Y. & Thelandersson, S. (1976) *Stress and deformation characteristics of concrete at high temperatures: experimental investigation and material behaviour model*. Lund Institute of Technology Lund, Sweden.

Annerel, E., Lu, L. & Taerwe, L. (2013a) Punching shear tests on flat concrete slabs exposed to fire. *Fire Safety Journal* **57**:83-95.

Annerel, E. & Taerwe, L. (2015) Design considerations for shear failure of flat concrete slabs exposed to fire. In *fib symposium: Concrete: Innovation and Design*.), pp. 1-13.

Annerel, E., Taerwe, L., Merci, B., Jansen, D., Bamonte, P. & Felicetti, R. (2013b) Thermo-mechanical analysis of an underground car park structure exposed to fire. *Fire Safety Journal* **57**:96-106.

Ansys Inc. (2009) *ANSYS FLUENT 12.0 User's Guide*, See https://www.afs.enea.it/project/neptunius/docs/fluent/html/ug/main_pre.htm.

Ansys Inc. (2011) *ANSYS CFX-Pre User's Guide*. USA.

Ariyanayagam, A. D. & Mahendran, M. (2014) Development of realistic design fire time-temperature curves for the testing of cold-formed steel wall systems. *Frontiers of Structural and Civil Engineering* **8(4)**:427-447.

Arna'ot, F. H., Abid, S. R., Özakça, M. & Tayşi, N. (2017) Review of concrete flat plate-column assemblies under fire conditions. *Fire Safety Journal* **93**:39-52.

Astm International (2016)ASTM E119 : Standard Test Methods for Fire Tests of Building Construction and Materials.

Babrauskas, V. (2011) Glass breakage in fires. *Fire science and technology inc*.

Babrauskas, V. & Williamson, R. B. (1978) The historical basis of fire resistance testing—Part I. *Fire Technology* **14(3)**:184-194.

Bailey, C. G. (2004) Membrane action of slab/beam composite floor systems in fire. *Engineering Structures* **26(12)**:1691-1703.

Bailey, C. G. & Ellobody, E. (2009) Fire tests on bonded post-tensioned concrete slabs. *Engineering Structures* **31(3)**:686-696.

Bailey, C. G. & Toh, W. S. (2007) Behaviour of concrete floor slabs at ambient and elevated temperatures. *Fire Safety Journal* **42(6-7)**:425-436.

Bamonte, P., Felicetti, R. & Gambarova, P. G. (2009) Punching shear in fire-damaged reinforced concrete slabs. *ACI Special Publication* **265**:345-366.

Bamonte, P., Fernández Ruiz, M. & Muttoni, A. (2012) Punching shear strength of R/C slabs subjected to fire. In *Proceedings of the 7th International Conference on Structures in Fire-SiF2012 (Eds. M. Fontana, A. Frangi, M. Knobloch)*.) Proceedings of the 7th International Conference on Structures in Fire …, pp. 689-698.

Barnett, C. (2002) BFD curve: a new empirical model for fire compartment temperatures. *Fire Safety Journal* **37(5)**:437-463.

Bastami, M., Aslani, F. & Esmaeilnia, O. M. (2010) High-temperature mechanical properties of concrete.

Bažant, Z. P. & Cao, Z. (1987) Size effect in punching shear failure of slabs. *ACI Structural Journal* **84(1)**:44-53.

Beitel, J. J. & Iwankiw, N. (2008) *Analysis of needs and existing capabilities for full-scale fire resistance testing.* US Department of Commerce, Technology Administration, National Institute of Standards and Technology.

Belgian Standards Institution (Bin) (1999)NBNB15-002 : Eurocode2: Design of Concrete Structures—Part 1-1: General Rules and Rules for Buildings,.

Binbin, W. (2011) Comparative research on FLUENT and FDS's numerical simulation of smoke spread in subway platform fire. *Procedia Engineering* **26**:1065-1075.

British Standard Institute (1985)BS 8110-1: 1985, Structural Use of Concrete: Part 1: Code of Practice for Design and Construction.

British Standard Institute (1987)BS 476-21:1987 Fire tests on building materials and structures. Methods for determination of the fire resistance of loadbearing elements of construction.

British Standards Institution (1996)Design of concrete structures—Part 1.2: General rules—Structural fire design.

Buchanan, A. H. & Abu, A. K. (2017) *Structural design for fire safety.* John Wiley & Sons.

Burgress, I. W., Dai, X. & Huang, S.-S. (2013) An alternative simplified model of tensile membrane action of slabs in fire. In *Proceedings of International Conference Application of Structural Fire Engineering*) CTU Publishing House, Czech Technical University in Prague, Prague, Czech Republic.

Bwalya, A. C., Benichou, N. & Sultan, M. (2003) *Literature review on design fires.* Institute for Research in Construction, National Research Council Canada.

Canadian Standard Association (2014)CSA A23.1 A23.2: Concrete Materials And Methods Of Concrete Construction/Test Methods And Standard Practices For Concrete.

Chen, S., Zhang, Y. & Ren, A. (2018) A simple method for combining fire and structural models and its application to fire safety evaluation. Automation in Construction 87:39-48.

Chen, Z., Wen, J., Xu, B. & Dembele, S. (2011) Large eddy simulation of fire dynamics with the improved eddy dissipation concept. *Fire Safety Science* **10**:795-808.

Comite Euro-International Du Beton (1993)CEB-FIB model code 1990: Design code, Thomas Telford.

Dassault Systèmes (2014) ABAQUS version 6.14 documentation.

De Boer, J., Hofmeyer, H., Maljaars, J. & Van Herpen, R. (2019) Two-way coupled CFD fire and thermomechanical FE analyses of a self-supporting sandwich panel façade system. Fire Safety Journal 105:154-168.

Diskin, B., Thomas, J. L., Nielsen, E. J., Nishikawa, H. & White, J. A. (2010) Comparison of node-centered and cell-centered unstructured finite-volume discretizations: viscous fluxes. *AIAA journal* **48(7)**:1326-1338.

Dos Santos, C. C. & Rodrigues, J. P. C. (2016) Calcareous and granite aggregate concretes after fire. *Journal of Building Engineering* **8**:231-242.

Drysdale, D. (2011) *An introduction to fire dynamics.* John Wiley & Sons.

Drysdale, D., Schneider, U., Babrauskas, V. & Grayson, S. (1990) Repairability of fire damaged structures", CIB W14 Report. *Fire Safety Journal* **16(4)**:251-336.

Dutta, S., Das, R. & Bhattacharyya, D. (2019a) A multi-physics framework model towards coupled fire-structure interaction for Flax/PP composite beams. Composites Part B: Engineering 157:207-218.

Dutta, S., Kim, N. K., Das, R. & Bhattacharyya, D. (2019b) Effects of sample orientation on the fire reaction properties of natural fibre composites. Composites Part B: Engineering 157:195-206.

Dwaikat, M. B. & Kodur, V. (2009) Hydrothermal model for predicting fire-induced spalling in concrete structural systems. *Fire Safety Journal* **44(3)**:425-434.

Earij, A., Alfano, G., Cashell, K. & Zhou, X. (2017) Nonlinear three–dimensional finite–element modelling of reinforced–concrete beams: Computational challenges and experimental validation. *Engineering Failure Analysis* **82**:92-115.

Ellobody, E. & Bailey, C. G. (2009) Modelling of unbonded post-tensioned concrete slabs under fire conditions. *Fire Safety Journal* **44(2)**:159-167.

European Committee for Standardization (2002)Eurocode 1: Actions on structures - Part 1-2: General actions - Actions on structures exposed to fire

European Committee for Standardization (2004a) EN1992-1-1 Eurocode 2 : Design of Concrete Structures—Part 1-1 : General Rules and Rules for Buildings.

European Committee for Standardization (2004b)Eurocode 2: Design of concrete structures - Part 1-2: General rules -Structural fire design.

European Committee for Standardization (2005a)Eurocode 3: Design of steel structures - Part 1-2: General rules -Structural fire design.

European Committee for Standardization (2005b)Eurocode 4 - Design of composite steel and concrete structures- Part 1-2: General rules - Structural fire design.

Feenstra, J., Hofmeyer, H., Van Herpen, R. & Mahendran, M. (2018) Automated two-way coupling of CFD fire simulations to thermomechanical FE analyses at the overall structural level. Fire Safety Journal 96:165-175.

Fernández Ruiz, M. & Muttoni, A. (2010) Performance and Design of Punching-Shear Reinforcing Systems. In *3rd fib international congress*.) 3rd fib International Congress, vol. 437, pp. 14.

Gales, J., Bisby, L. & Gillie, M. (2011) Unbonded post tensioned concrete slabs in fire-part I-experimental response of unbonded tendons under transient localized heating. *Journal of Structural Fire Engineering* **2(3)**:139-154.

Gasparini, D. A. (2002) Contributions of CAP Turner to development of reinforced concrete flat slabs 1905–1909. *Journal of Structural Engineering* **128(10)**:1243-1252.

Genikomsou, A. S. & Polak, M. A. (2015) Finite element analysis of punching shear of concrete slabs using damaged plasticity model in ABAQUS. *Engineering Structures* **98**:38-48.

Genikomsou, A. S. & Polak, M. A. (2017) 3D finite element investigation of the compressive membrane action effect in reinforced concrete flat slabs. *Engineering Structures* **136**:233-244.

George, S. J. & Tian, Y. (2012) Structural Performance of Reinforced Concrete Flat Plate Buildings Subjected to Fire. *International Journal of Concrete Structures and Materials* **6(2)**:111-121.

Ghoreishi, M., Bagchi, A. & Sultan, M. A. (2015) Punching shear behavior of concrete flat slabs in elevated temperature and fire. *Advances in Structural Engineering* **18(5)**:659-674.

Gillie, M., Usmani, A. & Rotter, M. (2002) Bending and membrane action in concrete slabs In *Proceedings of 2nd International Workshop in Structures in Fire*.

Greenshields, C. (2018) *OpenFOAM v6 User Guide,* See https://cfd.direct/openfoam/user-guide/v6-fvschemes/.

Guillaume, E., Dréan, V., Girardin, B., Koohkan, M. & Fateh, T. (2020) Reconstruction of Grenfell Tower fire. Part 2: A numerical investigation of the fire propagation and behaviour from the initial apartment to the façade. *Fire and Materials* **44(1)**:15-34.

Hadjisophocleous, G. V. & Mehaffey, J. R. (2016) Fire scenarios. In *SFPE Handbook of Fire Protection Engineering*.) Springer, pp. 1262-1288.

Hajiloo, H. & Green, M. F. (2019) GFRP reinforced concrete slabs in fire: Finite element modelling. *Engineering Structures* **183**:1109-1120.

Han, T. U., Kim, Y.-M., Watanabe, C., Teramae, N., Park, Y.-K., Kim, S. & Lee, Y. (2015) Analytical pyrolysis properties of waste medium-density fiberboard and particle board. *Journal of Industrial and Engineering Chemistry* **32**:345-352.

Hawileh, R. & Kodur, V. (2018) Performance of reinforced concrete slabs under hydrocarbon fire exposure. *Tunnelling and Underground Space Technology* **77**:177-187.

Hellenic Cement Industry Association (n.d.) *Concrete in fire conditions,* See http://www.hcia.gr/en/cement-concrete/uses-concrete/mellon_skurodema_purkagia/ (accessed Jan 2020).

Hou, X., Zheng, W. & V.K.R, K. (2013) Response of unbonded prestressed concrete continuous slabs under fire exposure. *Engineering Structures* **56**:2139-2148.

Huang, Z., Burgess, I. W. & Plank, R. J. (1999) Nonlinear analysis of reinforced concrete slabs subjected to fire. *Structural Journal* **96(1)**:127-135.

Hurley, M. J., Gottuk, D. T., Hall Jr, J. R., Harada, K., Kuligowski, E. D., Puchovsky, M., Watts Jr, J. M. & Wieczorek, C. J. (2015) *SFPE handbook of fire protection engineering.* Springer.

Ingason, H., Li, Y. Z. & Lönnermark, A. (2014) *Tunnel fire dynamics.* Springer.

International Organization for Standardization (1999)ISO 834-1 : Fire-resistance tests - Elements of building construction - Part 1: General requirements.

Jain, S., Kumar, S., Kumar, S. & Sharma, T. (2008) Numerical simulation of fire in a tunnel: Comparative study of CFAST and CFX predictions. *Tunnelling and Underground Space Technology* **23(2)**:160-170.

Kada, D., Koubaa, A., Tabak, G., Migneault, S., Garnier, B. & Boudenne, A. (2018) Tensile properties, thermal conductivity, and thermal stability of short carbon

fiber reinforced polypropylene composites. *Polymer Composites* **39(S2)**:E664-E670.

Kalifa, P., Chene, G. & Galle, C. (2001) High-temperature behaviour of HPC with polypropylene fibres: From spalling to microstructure. *Cement and concrete research* **31(10)**:1487-1499.

Kim, N. & Bhattacharyya, D. (2016) Development of fire resistant wool polymer composites: Mechanical performance and fire simulation with design perspectives. Materials & Design 106:391-403.

Kim, N., Dutta, S. & Bhattacharyya, D. (2019) Heat and smoke production of flax fibre reinforced composites under horizontal and vertical orientations. Composites Part B: Engineering 178:107467.

Kirk, A. J. (2010) Collapse investigation of the TU Delft faculty of architecture building: preliminary evaluation of member capacities.).

Kodur, V. (2014) Properties of concrete at elevated temperatures. *ISRN Civil engineering* **2014**.

Kodur, V. & Agrawal, A. (2016) An approach for evaluating residual capacity of reinforced concrete beams exposed to fire. *Engineering Structures* **110**:293-306.

Kodur, V. & Alogla, S. (2017) Effect of high-temperature transient creep on response of reinforced concrete columns in fire. *Materials and Structures* **50(1)**:27.

Kordina, K. (1993) Flat slabs under fire–Redistribution of the internal forces and punching tests. *Institut für Baustoffe, Massivbau und Brandschutz, Technische Universität Braunschweig, Germany, CEN/TC* **250**:1-2.

Law, M. (1971) A relationship between fire grading and building design and contents. *Fire Safety Science* **877**:-1--1.

Lee, J. & Fenves, G. L. (1998) Plastic-damage model for cyclic loading of concrete structures. *Journal of engineering mechanics* **124(8)**:892-900.

Lennon, T. & Moore, D. (2003) The natural fire safety concept—full-scale tests at Cardington. *Fire Safety Journal* **38(7)**:623-643.

Li, K. (2013) On determining density and specific heat of New Zealand medium density fibreboard. *Procedia Engineering* **62**:769-777.

Li, L.-Y. & Purkiss, J. (2005) Stress–strain constitutive equations of concrete material at elevated temperatures. *Fire Safety Journal* **40(7)**:669-686.

Liao, J.-S., Cheng, F.-P. & Chen, C.-C. (2013) Fire resistance of concrete slabs in punching shear. *Journal of Structural Engineering* **140(1)**:04013025.

Lim, L., Buchanan, A., Moss, P. & Franssen, J.-M. (2004) Numerical modelling of two-way reinforced concrete slabs in fire. *Engineering Structures* **26(8)**:1081-1091.

Ma, Z. & Mäkeläinen, P. (2000) Parametric temperature–time curves of medium compartment fires for structural design. *Fire Safety Journal* **34(4)**:361-375.

Maragkos, G., Rauwoens, P. & Merci, B. (2012) Application of FDS and FireFOAM in large eddy simulations of a turbulent buoyant helium plume. *Combustion science and technology* **184(7-8)**:1108-1120.

Mcgrattan, K., Klein, B., Hostikka, S. & Floyd, J. (2010) Fire dynamics simulator (version 5), user's guide. *NIST special publication* **1019(5)**:1-186.

Mcgrattan, K. & Miles, S. (2016) Modeling fires using computational fluid dynamics (CFD). In *SFPE Handbook of Fire Protection Engineering*.) Springer, pp. 1034-1065.

Mcgrattan, K. B. (2005) Fire modeling: where are we? where are we going? *Fire Safety Science* **8**:53-68.

Michael Noblett (n.d.) *Gretzenbach Car Park Fire*, See https://modellingflatslabsinfire.weebly.com/gretzenbach-car-park-fire.html (accessed Jan 2020).

Moss, P. J., Dhakal, R. P., Wang, G. & Buchanan, A. H. (2008) The fire behaviour of multi-bay, two-way reinforced concrete slabs. *Engineering Structures* **30(12)**:3566-3573.

Müller, P., Novák, J. & Holan, J. (2019) Destructive and non-destructive experimental investigation of polypropylene fibre reinforced concrete subjected to high temperature. *Journal of Building Engineering* **26**:100906.

Muttoni, A. (2008) Punching shear strength of reinforced concrete slabs without transverse reinforcement. *ACI Structural Journal* **4(ARTICLE)**:440-450.

Neves, I. C., Rodrigues, J. P. C. & Loureiro, A. D. P. (1996) Mechanical properties of reinforcing and prestressing steels after heating. *Journal of Materials in Civil Engineering* **8(4)**:189-194.

Nguyen, Q., Ngo, T., Mendis, P. & Tran, P. (2013) Composite materials for next generation building façade systems. *Civil Engineering and Architecture* **1(3)**:88-95.

Nguyen, Q. T., Tran, P., Ngo, T. D., Tran, P. A. & Mendis, P. (2014) Experimental and computational investigations on fire resistance of GFRP composite for building façade. *Composites Part B: Engineering* **62**:218-229.

Nielsen, C., Pearce, C. & Bićanić, N. (2002) Theoretical model of high temperature effects on uniaxial concrete member under elastic restraint. *Magazine of Concrete Research* **54(4)**:239-249.

Nyman, J. F. (2002) Equivalent fire resistance ratings of construction elements exposed to realistic fires.

Oliver, J., Oller, S. & Oñate, E. (1989) A plastic-damage model for concrete. *International Journal of solids and structures* **25(3)**.

Opencfd Ltd. (2018) *OpenFOAM: User Guide v1912*, See https://www.openfoam.com/documentation/guides/latest/doc/guide-applications-solvers-combustion-fireFoam.html.

Pau, D., Fleischmann, C., Spearpoint, M. & Li, K. (2014) Thermophysical properties of polyurethane foams and their melts. *Fire and Materials* **38(4)**:433-450.

Pettersson, O. (1974) *The connection between a real fire exposure and the heating conditions according to standard fire resistance tests: with special application to steel structures.* Lund Institute of Technology, Division of Structural Mechanics and Concrete ….

Pierce, J. & Moss, J. (2007) Smoke production, radiation heat transfer and fire growth in a liquid-fuelled compartment fire. *Fire Safety Journal* **42(4)**:310-320.

Portland Cement Association (2005) *An Engineers Guide to: Economical Concrete Floor Systems*.

Press, W. H. & Teukolsky, S. A. (1990) Savitzky-Golay smoothing filters. *Computers in Physics* **4(6)**:669-672.

Quintiere, J. (2006) *Fundamentals of fire phenomena.* Wiley.

Rajendram, A., Khan, F. & Garaniya, V. (2015) Modelling of fire risks in an offshore facility. *Fire Safety Journal* **71**:79-85.

Reddy, D. H. & Ramaswamy, A. (2017) Influence of mineral admixtures and aggregates on properties of different concretes under high temperature conditions I: Experimental study. *Journal of Building Engineering* **14**:103-114.

Sahab, M., Ashour, A. & Toropov, V. (2005) Cost optimisation of reinforced concrete flat slab buildings. *Engineering Structures* **27(3)**:313-322.

Salem, H., Issa, H., Gheith, H. & Farahat, A. (2012) Punching shear strength of reinforced concrete flat slabs subjected to fire on their tension sides. *HBRC Journal* **8(1)**:36-46.

Sangluaia, C., Haridharan, M., Natarajan, C. & Rajaraman, A. (2013) Behaviour of reinforced concrete slab subjected to fire. *International Journal of Computational Engineering Research* **3**:195-206.

Schneider, U. (1986) Modelling of concrete behaviour at high temperatures. *Design of structures against fire*:53-69.

Shakya, A. M. & Kodur, V. K. R. (2015) Response of precast prestressed concrete hollowcore slabs under fire conditions. *Engineering Structures* **87**:126-138.

Smith, H. (2016) Punching shear of flat reinforced-concrete slabs under fire conditions.) The University of Edinburgh.

Smith, H., Stratford, B. & Bisby, L. (2015) Punching shear of reinforced concrete slabs under fire conditions: experiment vs. design. In *The First International Conference on Structural Safety under Fire & Blast CONFAB*.).

Smith, H. K., Stratford, T. J. & Bisby, L. A. (2014) Punching shear of restrained reinforced concrete slabs under fire conditions. In *8th International Conference on Structures in Fire*.), pp. 11-13.

Sonderegger, W. & Niemz, P. (2009) Thermal conductivity and water vapour transmission properties of wood-based materials. *European Journal of Wood and Wood Products* **67(3)**:313-321.

Standards Australia (2002a) AS 1170.0 Structural Design Actions, Part 0: General Principles.) Standards Australia Sydney.

Standards Australia (2002b) AS 1170.1 Structural Design Actions, Part 1: Permanent, imposed and other actions.) Standards Australia Sydney.

Standards Australia (2002c)AS/NZS 1170:Structural design actions Part 0: General principles, Standard, Standards Australia/New Zealand Sydney, Australia/Wellington, New ….

Standards Australia (2009)AS 3600 - Concrete structures.

Standards Australia (2014a)AS 1012.9 Methods of testing concrete. Method 9: Compressive strength tests-Concrete, mortar and grout specimens.

Standards Australia (2014b) AS 1012.10 Methods of testing concrete. Method 10: Determination of indirect tensile strength of concrete cylinders ('Brazil' or splitting test).

Standards Australia (2014c) AS 1012.17 Methods of testing concrete. Method 17: Determination of the static chord modulus od elasticity and Poisson's ratio of concrete specimens.

Standards Australia (2014d) AS 1530.4: Methods for fire tests on building materials, components and structures–Part 4: Fire-resistance test of elements of construction.) Sixth edition edn.

Standards Australia (2018)AS 3600 - Concrete structures.

Standards Council of Canada (2014)Standard Methods of Fire Endurance Tests of Building Construction and Materials.

Standards New Zealand (2006) NZS 3101:Part 1:2006 Concrete Structures Standard.

Sun, E. Q. (2006) Shear locking and hourglassing in MSC Nastran, ABAQUS, and ANSYS. In *Msc software users meeting*.), pp. 1-9.

Tavelli, S., Rota, R. & Derudi, M. (2014) A critical comparison between CFD and zone models for the consequence analysis of fires in congested environments. *Chemical Engineering Transactions* **36**.

Terro, M. J. (1998) Numerical modeling of the behavior of concrete structures in fire. *ACI Structural Journal* **95**:183-193.

The Australian Building Codes Board (2016)National Construction Code: Volume 1.

Theodorakopoulos, D. & Swamy, R. (2002) Ultimate punching shear strength analysis of slab–column connections. *Cement and Concrete Composites* **24(6)**:509-521.

Thomas, G. (2010) Modelling thermal performance of gypsum plasterboard-lined light timber frame walls using SAFIR and TASEF. *Fire and Materials* **34(8)**:385-406.

Thomas, G., Buchanan, A., Carr, A., Fleischmann, C. & Moss, P. (1995) Light timber-framed walls exposed to compartment fires. *Journal of Fire Protection Engineering* **7(1)**:15-25.

Thunderhead Engineering (2014) *Pyrosim User Manual*, See https://www.thunderheadeng.com/wp-content/uploads/downloads/2014/02/PyroSimManual.pdf.

Us Nuclear Regulatory Commission (2007) Verification and validation of selected fire models for nuclear power plant applications. *NUREG-1824*.

Utiskul, Y., Quintiere, J. G., Rangwala, A. S., Ringwelski, B. A., Wakatsuki, K. & Naruse, T. (2005) Compartment fire phenomena under limited ventilation. *Fire Safety Journal* **40(4)**:367-390.

Vecchio, F. & Tang, K. (1990) Membrane action in reinforced concrete slabs. *Canadian Journal of Civil Engineering* **17(5)**:686-697.

Vinocour, M. (1989) An Analysis of Finite-Difference and Finite-Volume Formulation of Conservation Laws. *Journal of Computational Physics* **81**:1-52.

Vyazovkin, S. (2002) Thermogravimetric analysis. *Characterization of Materials*:1-12.

Wahalathantri, B. L., Thambiratnam, D., Chan, T. & Fawzia, S. (2011) A material model for flexural crack simulation in reinforced concrete elements using ABAQUS. In *Proceedings of the first international conference on engineering, designing and developing the built environment for sustainable wellbeing*.) Queensland University of Technology, pp. 260-264.

Wahid, N., Stratford, T. & Bisby, L. (2019a) Calibration of concrete damage plasticity model parameters for high temperature modelling of reinforced concrete flat slabs in fire. *Applications of Structural Fire Engineering 2019, Singapore*.

Wahid, N., Stratford, T. & Bisby, L. (2019b) Modelling the deflection response of reinforced concrete flat slabs during heating.

Walton, W. D., Carpenter, D. J. & Wood, C. B. (2016a) Zone computer fire models for enclosures. In *SFPE handbook of fire protection engineering*.) Springer, pp. 1024-1033.

Walton, W. D., Thomas, P. H. & Ohmiya, Y. (2016b) Estimating temperatures in compartment fires. In *SFPE handbook of fire protection engineering*.) Springer, pp. 996-1023.

Wang, G. (2006) Performance of Reinforced Concrete Flat Slabs Exposed to Fire.), Department of Civil Engineering, University of Canterbury.

Wang, Y., Dong, Y. L., Li, B. & Zhou, G. C. (2013) A fire test on continuous reinforced concrete slabs in a full-scale multi-story steel-framed building. *Fire Safety Journal* **61**:232-242.

Węgrzyński, W. & Konecki, M. (2018) Influence of the fire location and the size of a compartment on the heat and smoke flow out of the compartment. In *AIP Conference Proceedings*.) AIP Publishing, vol. 1922, pp. 110007.

Wickström, U. (2011) The adiabatic surface temperature and the plate thermometer. *Fire Safety Science* **10**:1001-1011.

Wickström, U., Duthinh, D. & Mcgrattan, K. (2007) Adiabatic surface temperature for calculating heat transfer to fire exposed structures. In *Proceedings of the Eleventh International Interflam Conference. Interscience Communications, London*.), vol. 167.

Wolska, A., Goździkiewicz, M. & Ryszkowska, J. (2012) Thermal and mechanical behaviour of flexible polyurethane foams modified with graphite and phosphorous fillers. *Journal of Materials Science* **47(15)**:5627-5634.

Xu, Y., Yuan, H., Zhu, K., He, X. & Chen, G. (2007) Thermogravimetric analysis on the combustion characteristics for blended coals. In *Challenges of Power Engineering and Environment*.) Springer, pp. 153-156.

Yang, R., Khan, F., Yang, M., Kong, D. & Xu, C. (2018) A numerical fire simulation approach for effectiveness analysis of fire safety measures in floating liquefied natural gas facilities. *Ocean Engineering* **157**:219-233.

Yang, Z. N., Dong, Y. L. & Xu, W. J. (2013) Fire tests on two-way concrete slabs in a full-scale multi-storey steel-framed building. *Fire Safety Journal* **58**:38-48.

Yuen, A., Yeoh, G., Alexander, R. & Cook, M. (2014) Fire scene reconstruction of a furnished compartment room in a house fire. *Case Studies in Fire Safety* **1**:29-35.

Zhang, D.-S., Dong, Y.-L. & Fang, Y.-Y. (2014) Behaviour of full-scale two-way simply supported concrete slabs in fire. *Magazine of Concrete Research* **66(16)**:836-844.

Zhao, G., Beji, T., Zeinali, D. & Merci, B. (2017) Numerical study on the influence of in-depth radiation in the pyrolysis of medium density fibreboard. In *15th International Conference Fire and Materials 2017*.) Interscience communications, pp. 863-877.

Zheng, W. Z., Hou, X. M., Shi, D. S. & Xu, M. X. (2010) Experimental study on concrete spalling in prestressed slabs subjected to fire. *Fire Safety Journal* **45(5)**:283-297.

Zhiyin, Y. (2015) Large-eddy simulation: Past, present and the future. *Chinese journal of Aeronautics* **28(1)**:11-24.

Appendix A: Energy and Thermal Outputs of the Parametric Study

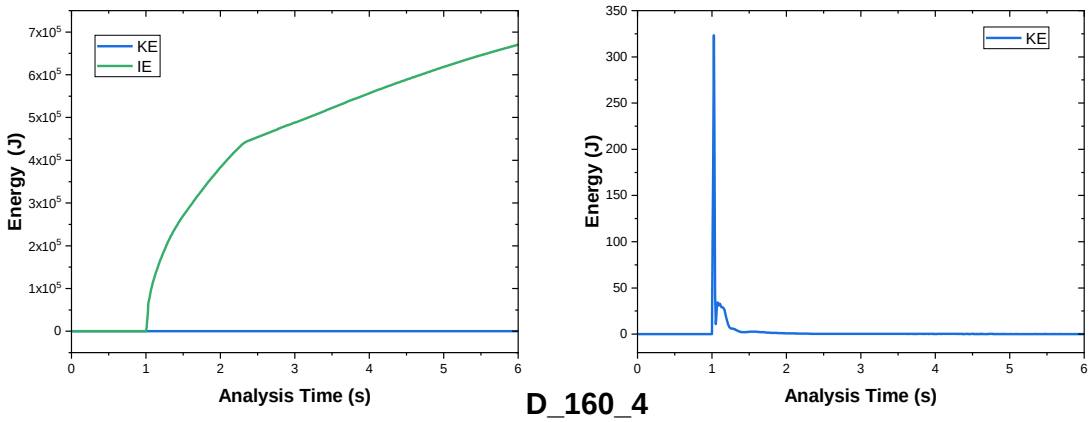

D_160_4

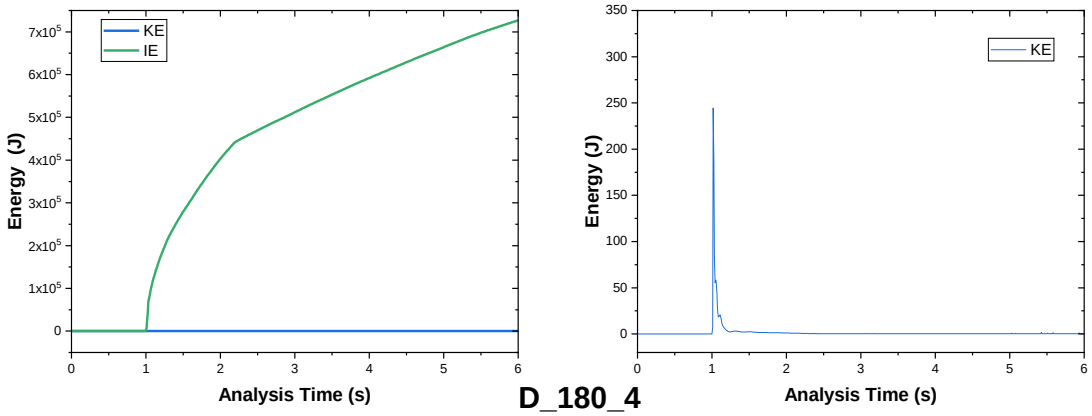

D_180_4

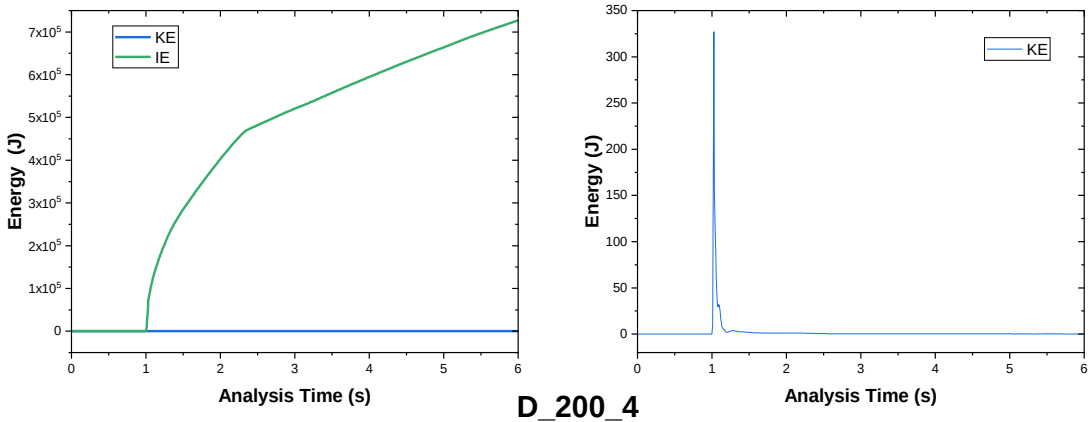

D_200_4

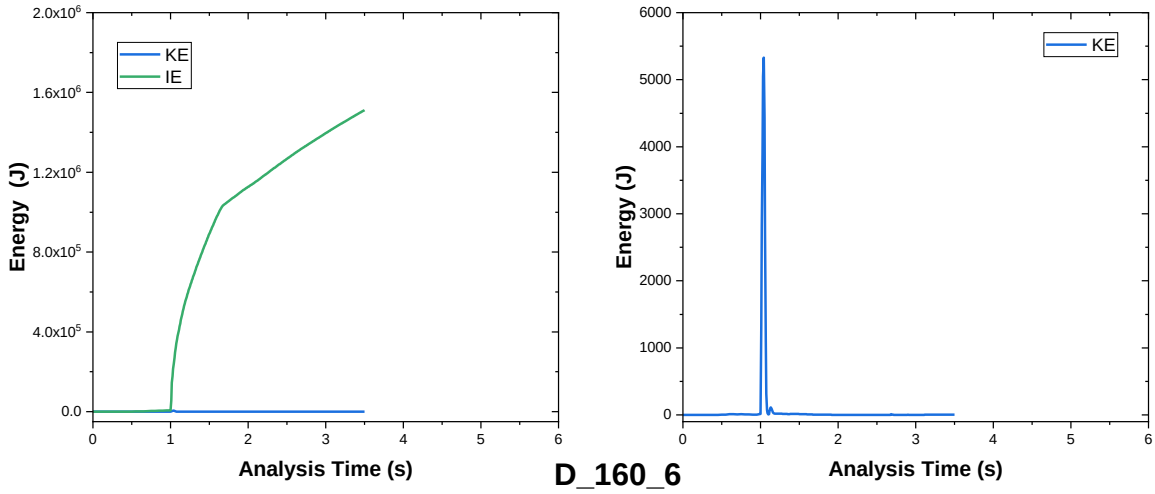

D_160_6

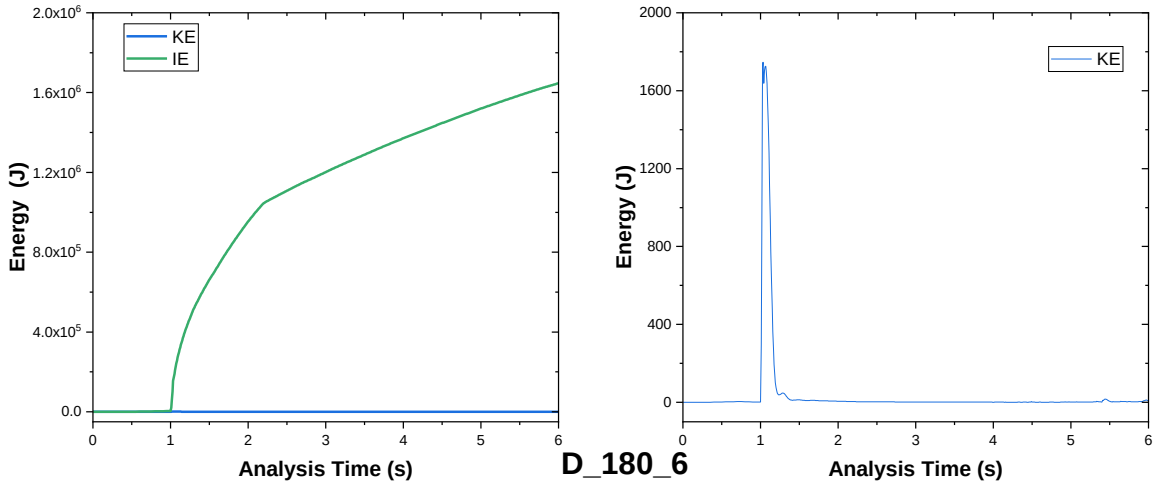

D_180_6

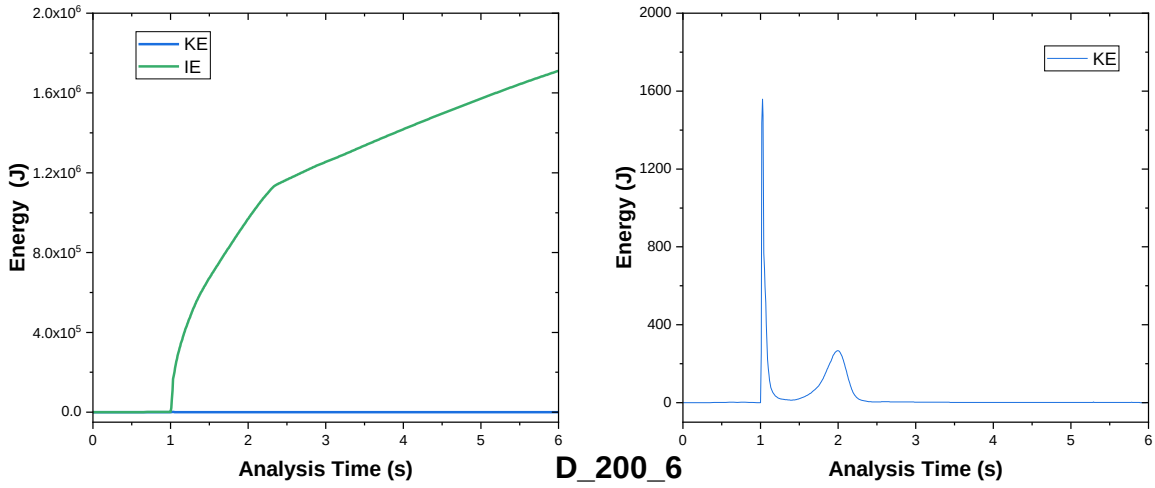

D_200_6

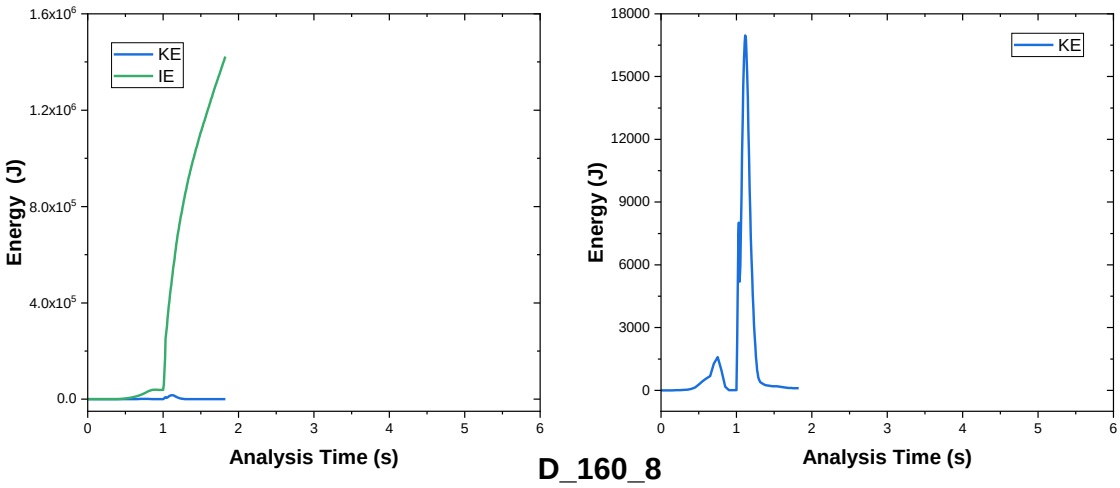

D_160_8

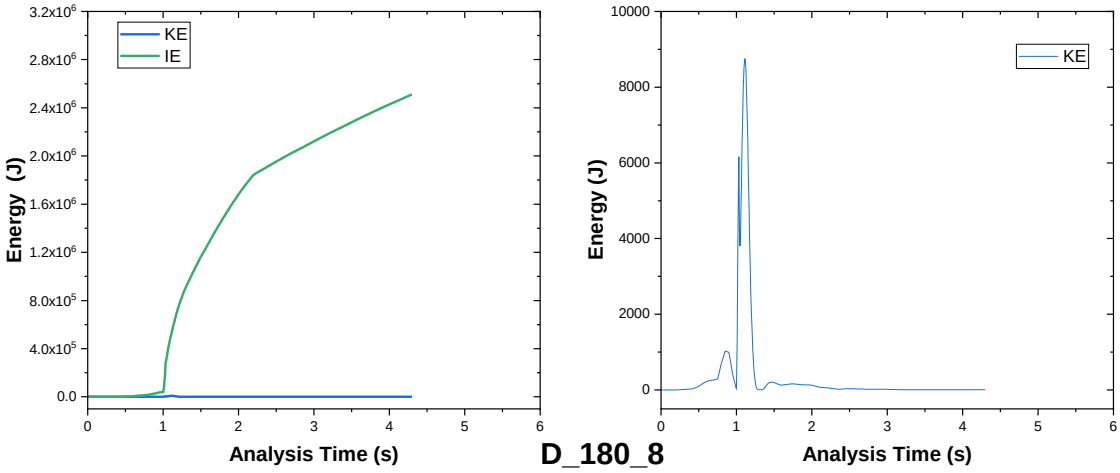

D_180_8

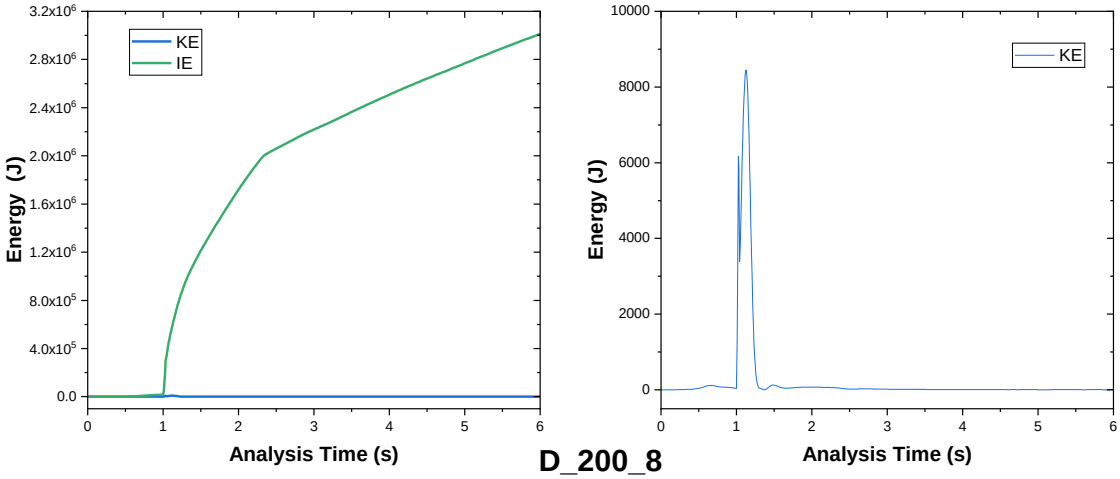

D_200_8

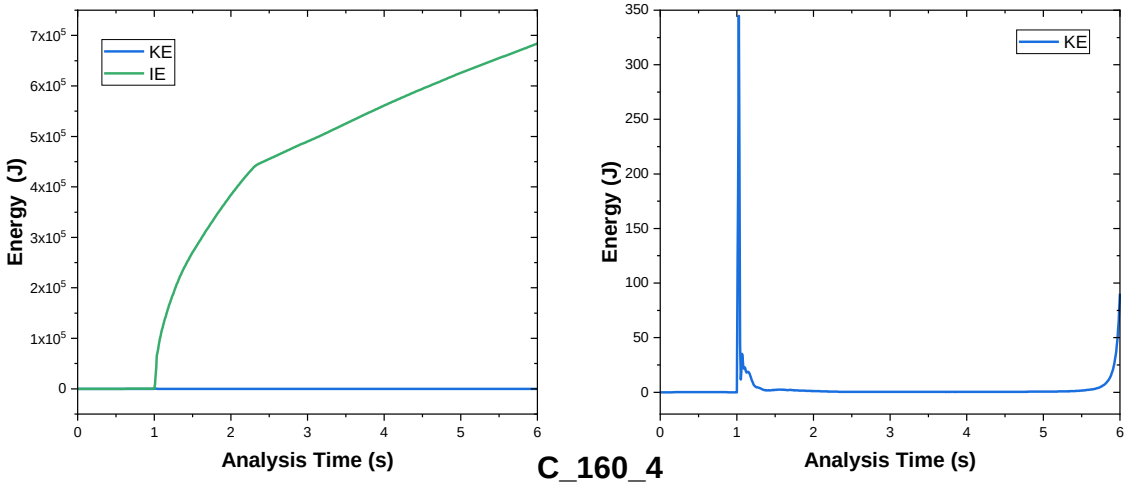

C_160_4

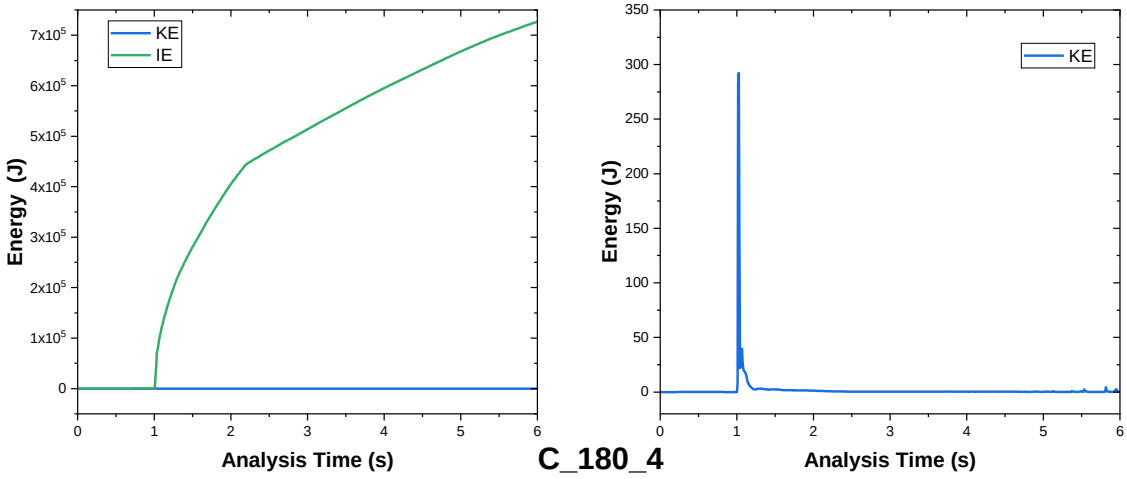

C_180_4

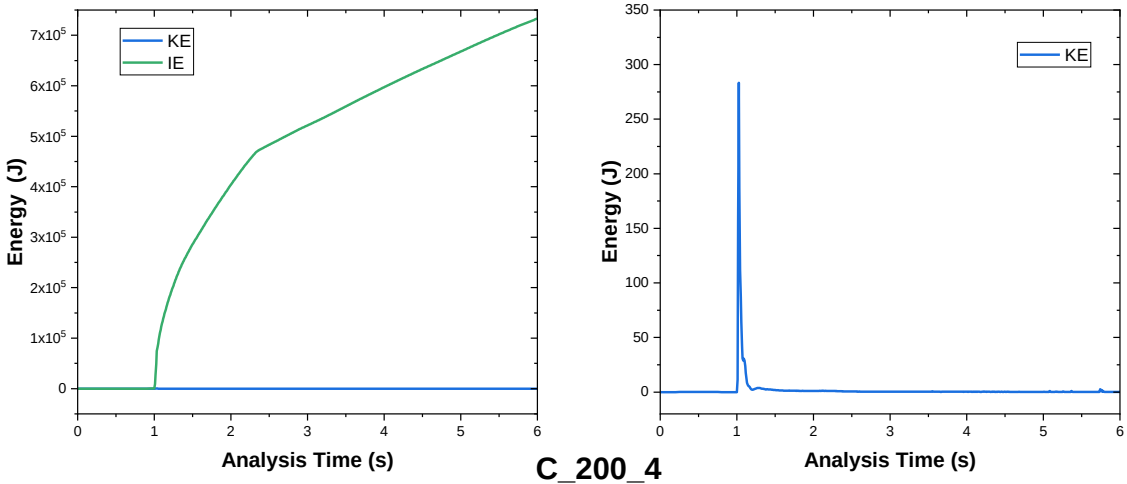

C_200_4

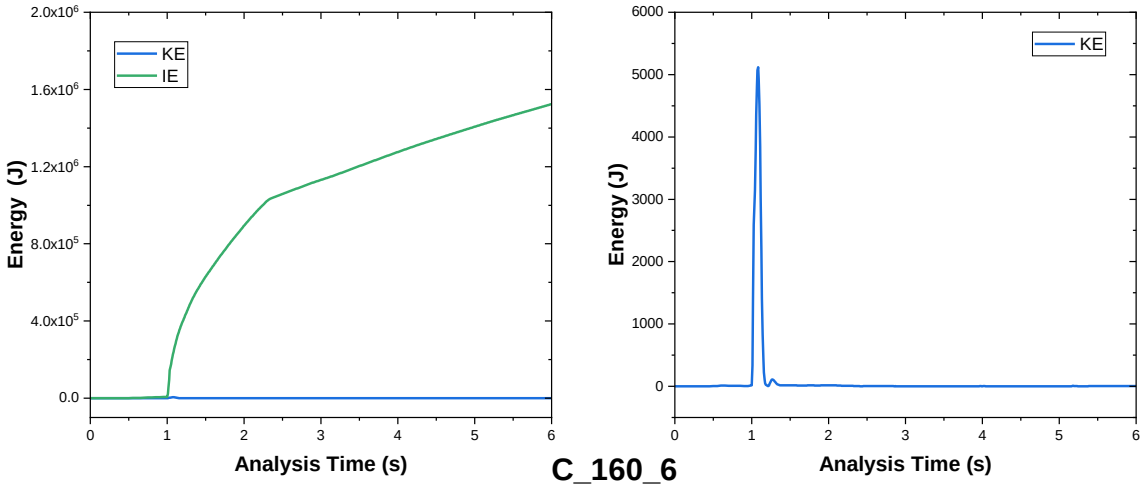

C_160_6

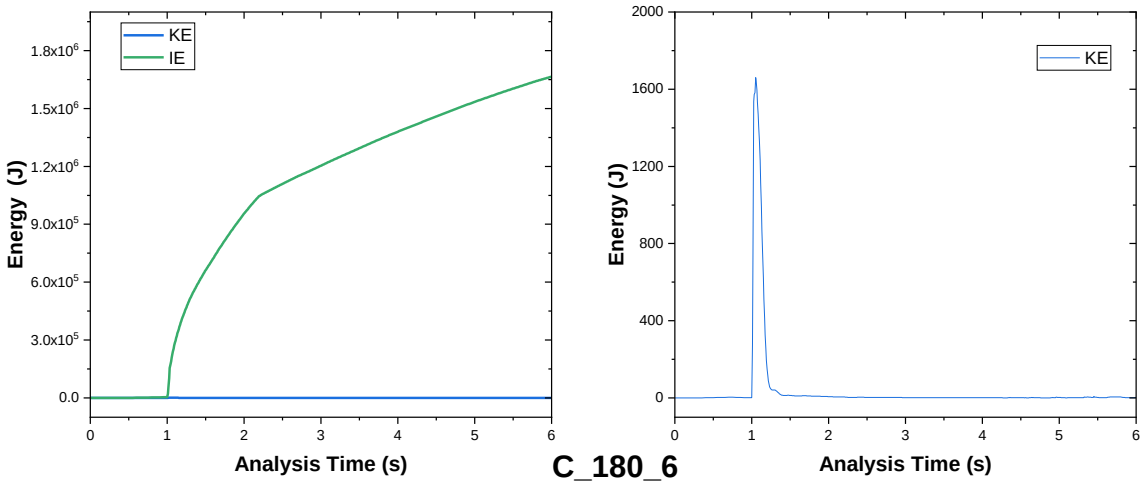

C_180_6

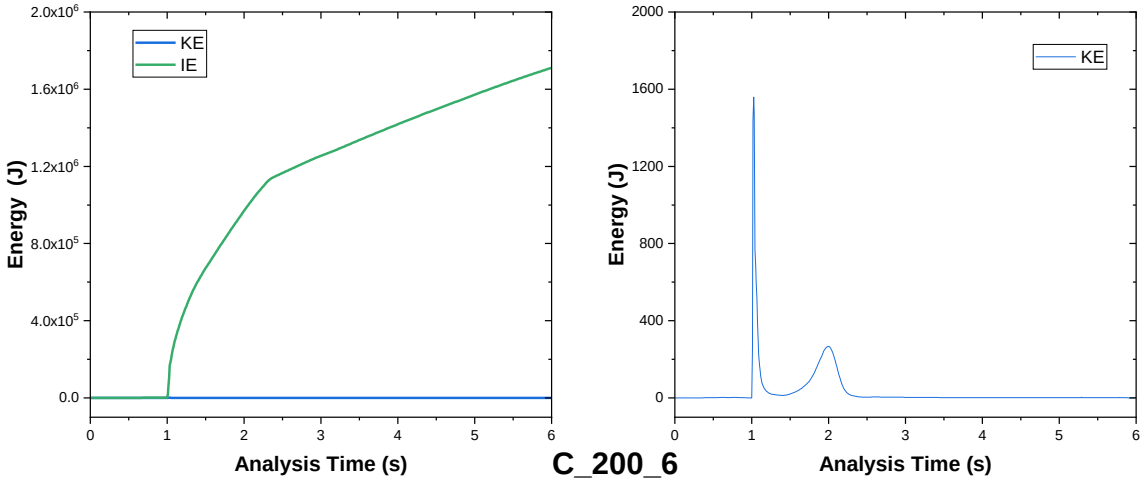

C_200_6

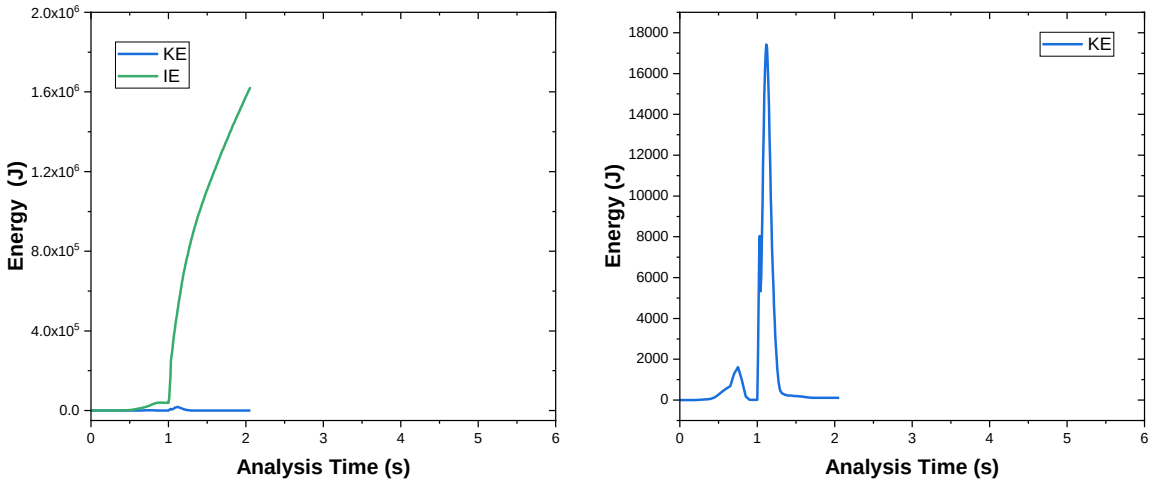

C_160_8

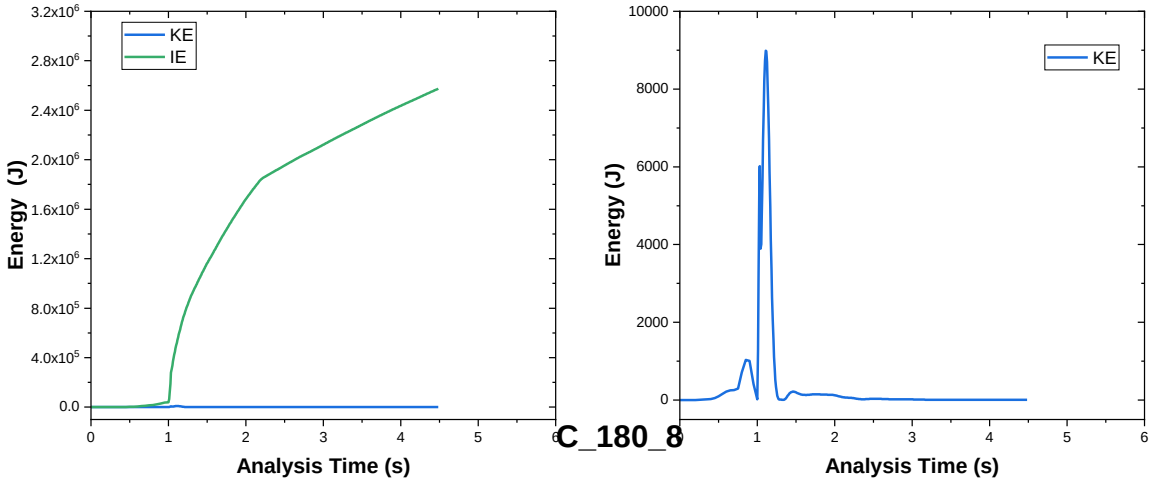

C_180_8

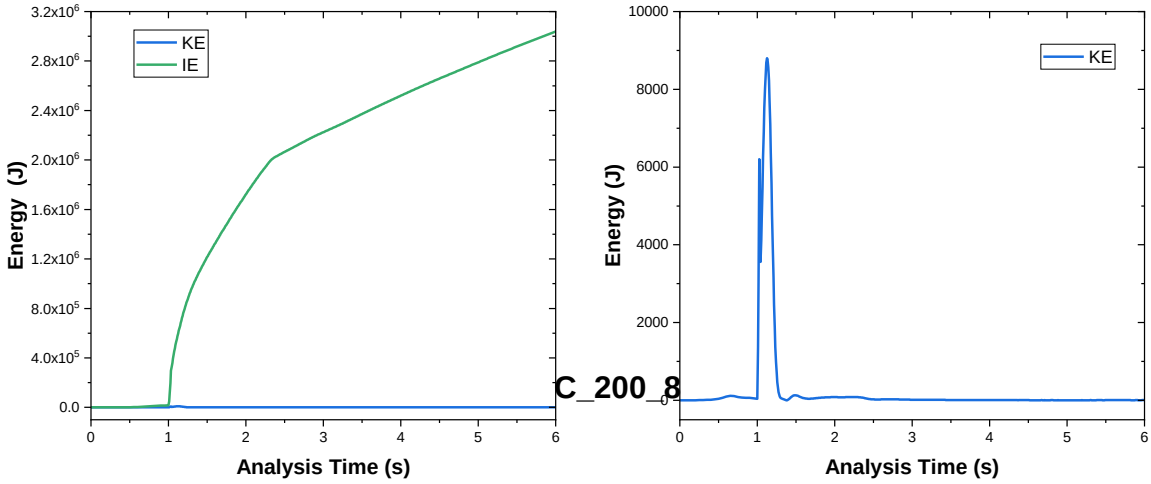

C_200_8

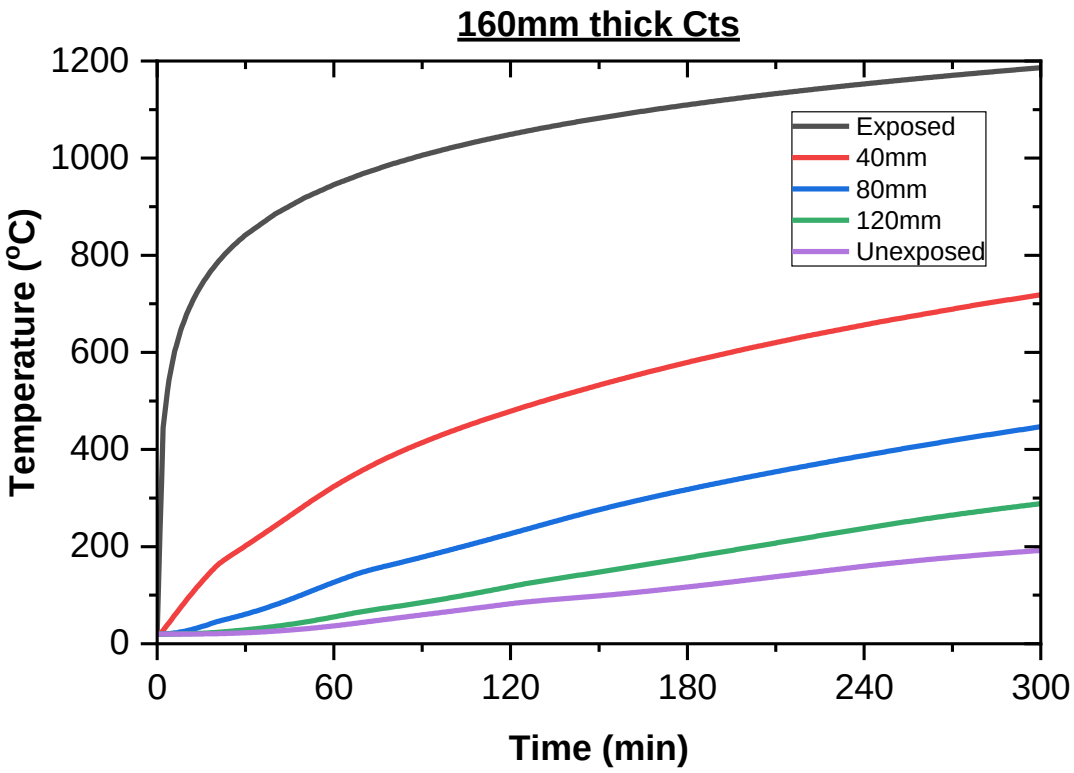

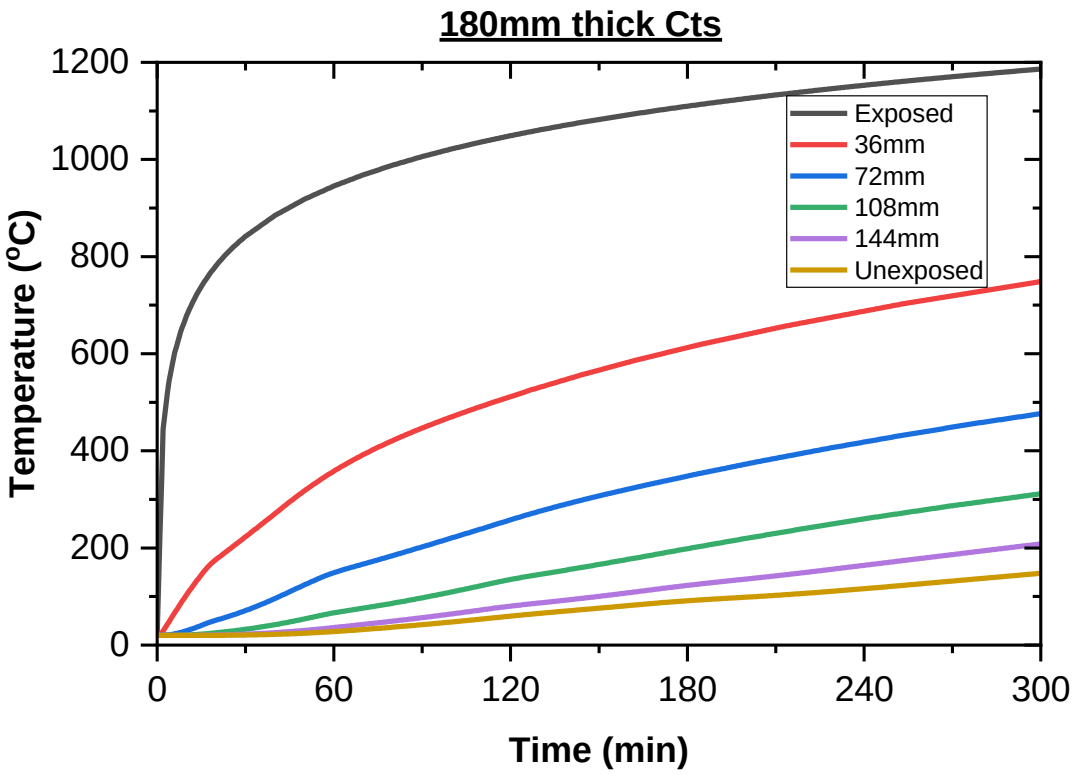

**Cts – 20% of top r/f continuing throughout the complete span
***Dcts – Top r/f does not continue throughout the complete span

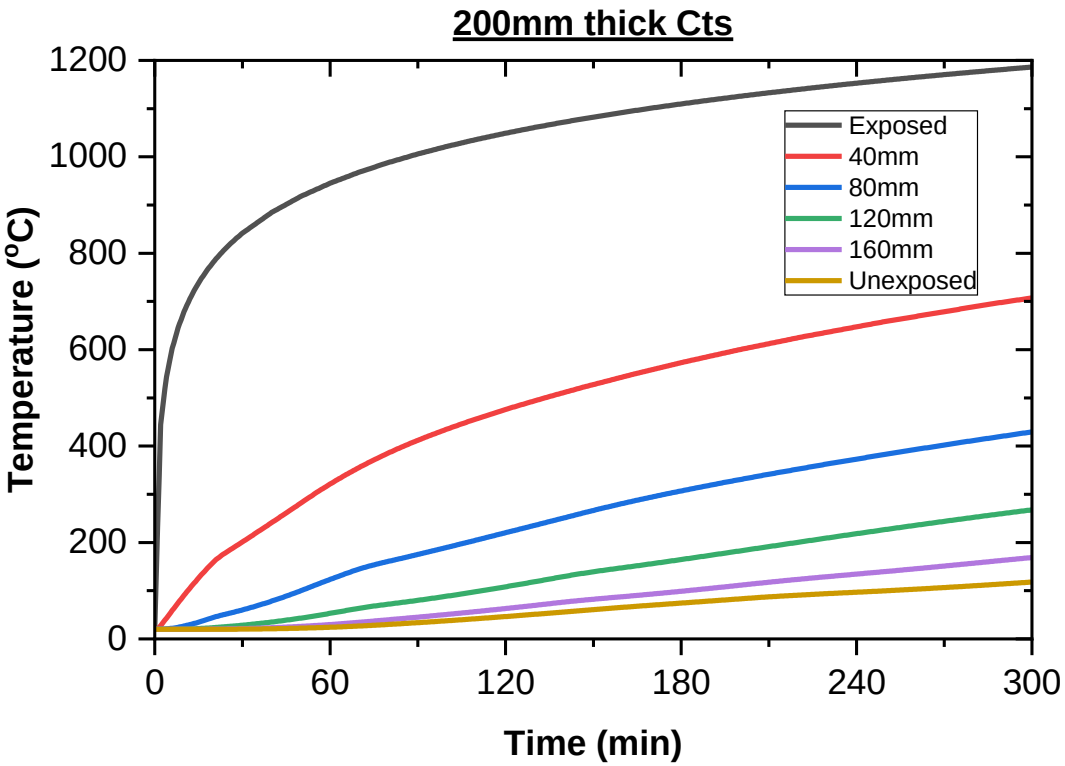
200mm thick Cts
Temperature (°C)
Time (min)
Exposed
40mm
80mm
120mm
160mm
Unexposed
0
200
400
600
800
1000
1200
0
60
120
180
240
300

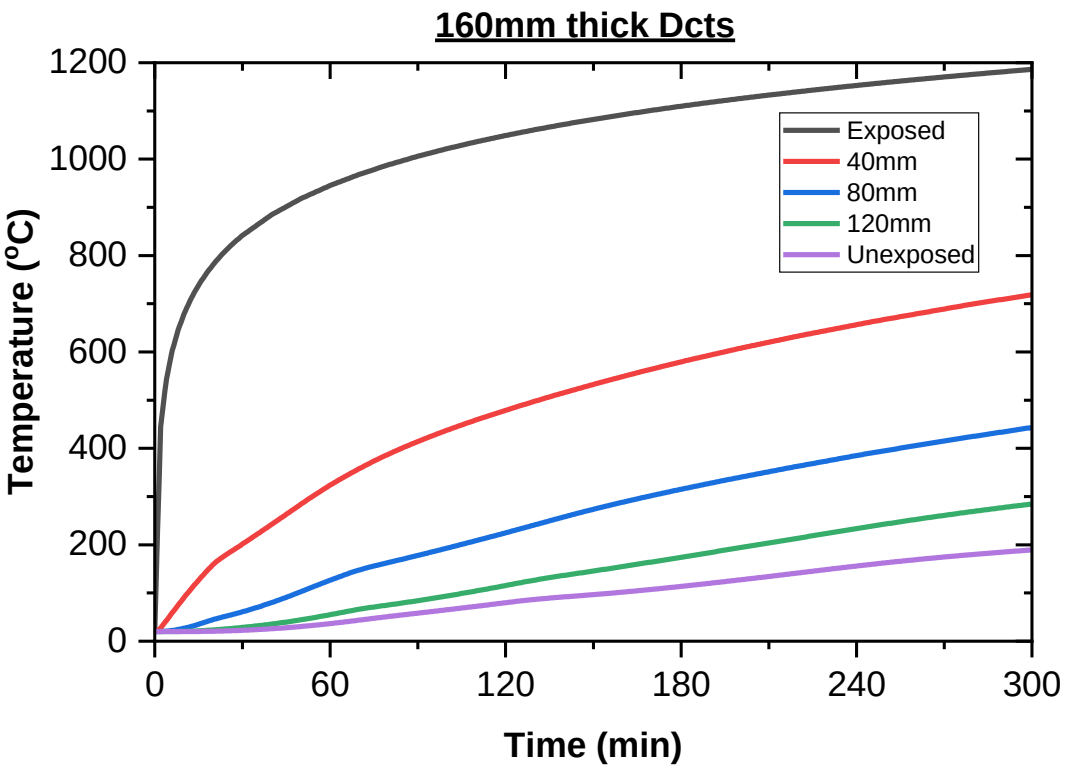
160mm thick Dcts
Temperature (°C)
Time (min)
Exposed
40mm
80mm
120mm
Unexposed
0
200
400
600
800
1000
1200
0
60
120
180
240
300

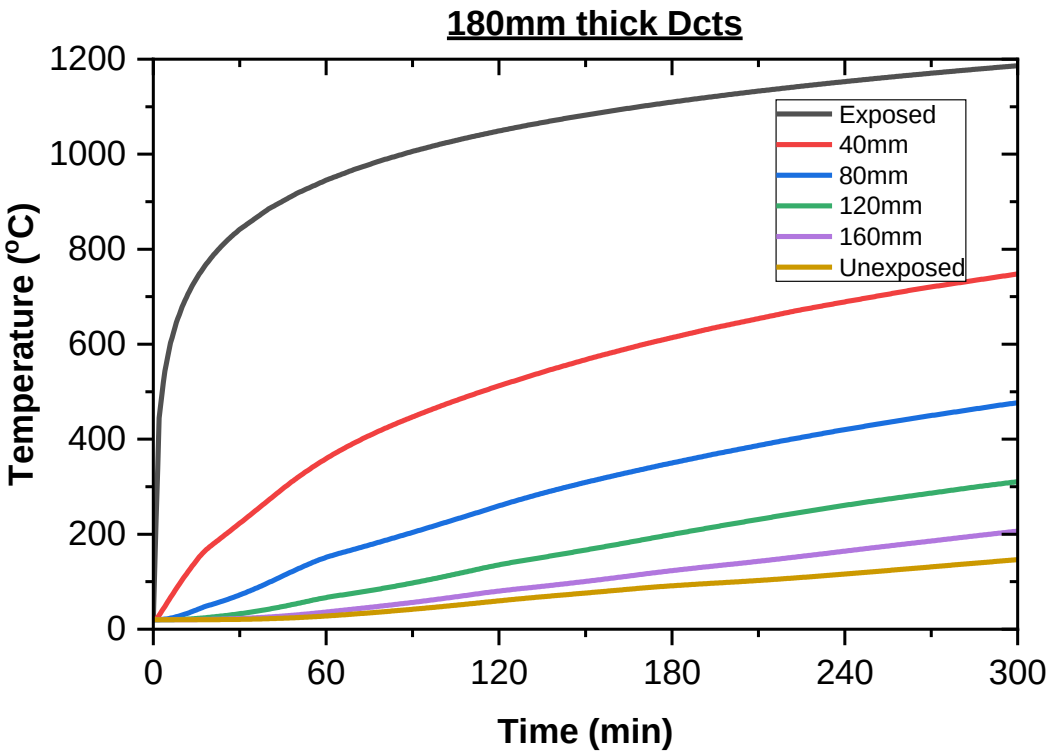
180mm thick Dcts
Temperature (°C)
Time (min)
Exposed
40mm
80mm
120mm
160mm
Unexposed
0
200
400
600
800
1000
1200
0
60
120
180
240
300

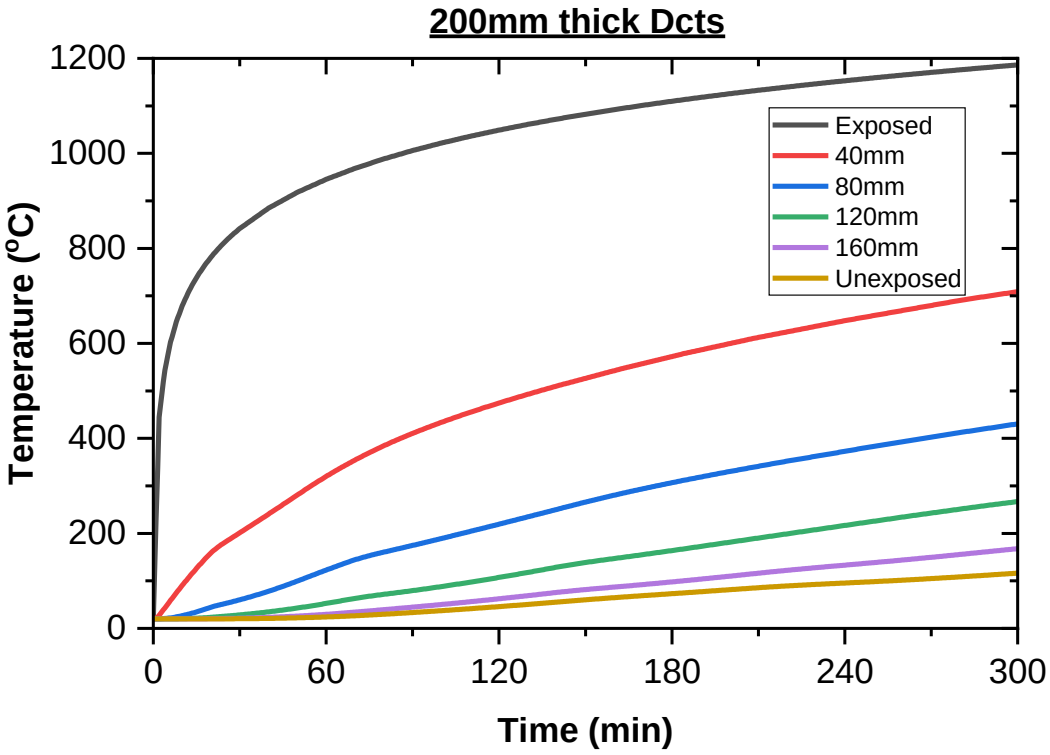
200mm thick Dcts
Temperature (°C)
Time (min)
Exposed
40mm
80mm
120mm
160mm
Unexposed
0
200
400
600
800
1000
1200
0
60
120
180
240
300

Appendix B: Derivation of Material Properties for Fire Simulation using TGA

1) **<u>Polypropylene (PP) [TGA from Kada et al. (2018)]</u>** – Used for Carpet

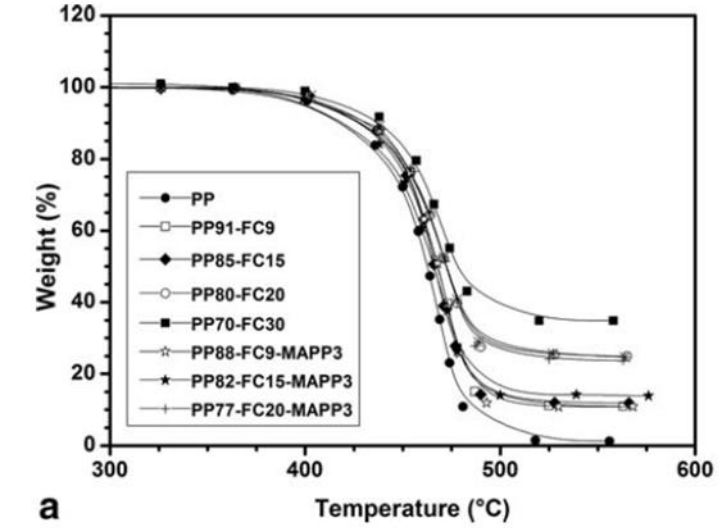

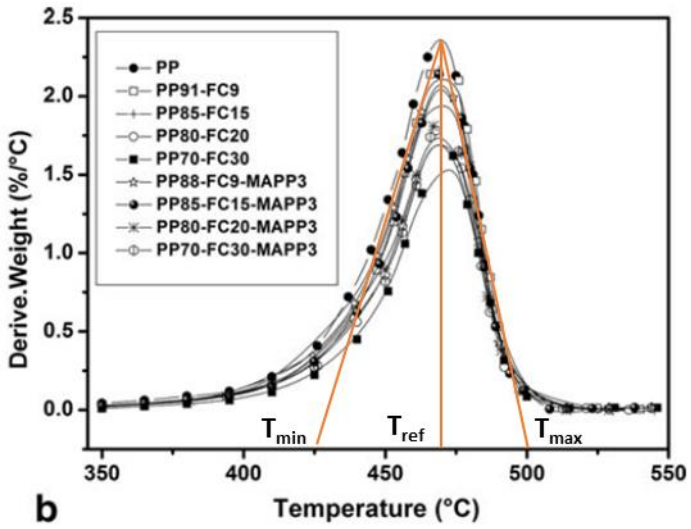

Reference temperature (T_{ref}) = 470°C

Pyrolysis range = T_{max} - -T_{min}

= 500°C – 425°C = 75°C

Heat of reaction = Specific heat capacity x (T_{min} – T_{20})

= 2.16*(425-20) = 875 kJ/kg

2) **<u>Polyurethane Foam (PU) [TGA from Wolska et al. (2012)]</u>** – Used for Bed, Sofa and Chairs

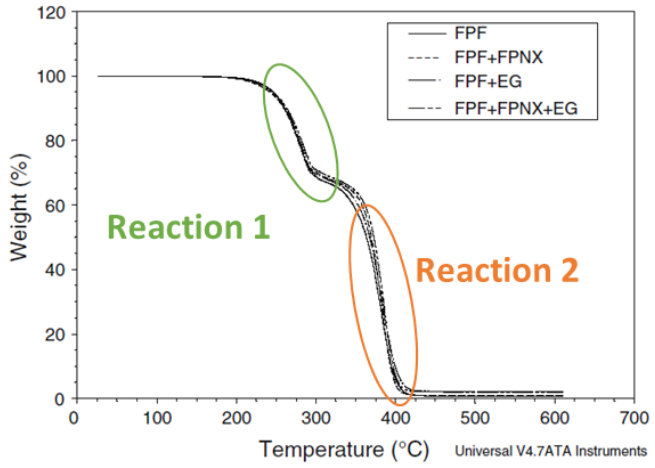

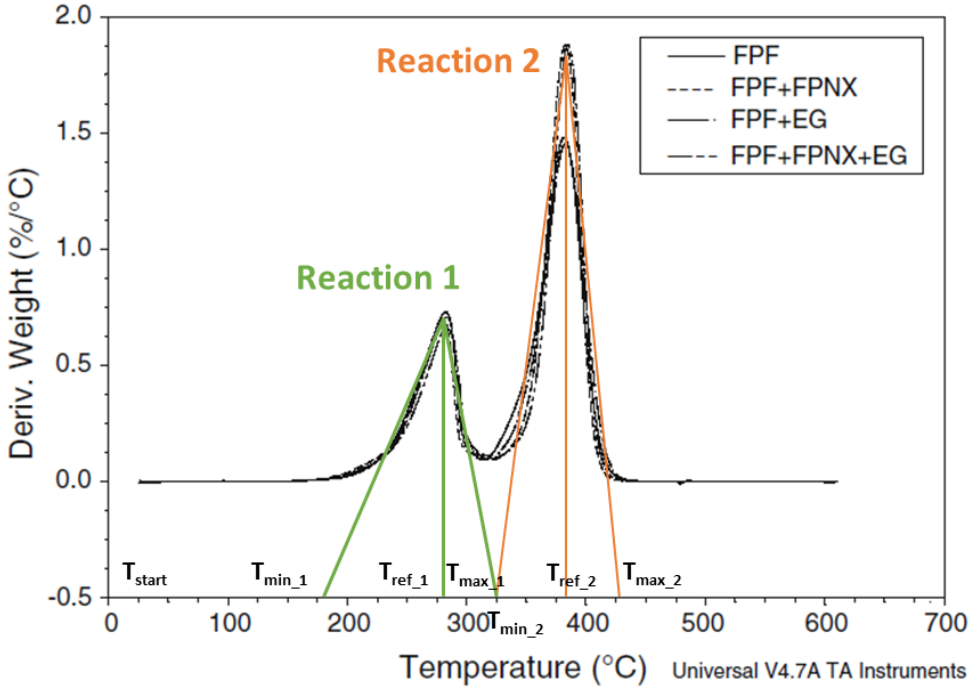

<u>Reaction 1</u>

Reference temperature (T_{ref}) = 275°C

Pyrolysis range = T_{max} - -T_{min}

= 325°C – 175°C = 150°C

Heat of reaction = Specific heat capacity x (T_{min} – T_{20})

= 2.359*(175-20) = 366 kJ/kg

Reaction 2

Reference temperature (T_{ref}) = 375°C

Pyrolysis range = T_{max} - -T_{min}

= 375°C – 325°C = 50°C

Heat of reaction = Specific heat capacity x (T_{min} – T_{20})

= 2.359*(325-20) = 720 kJ/kg

3) **Medium Density Fibreboard (MDF) [TGA from Han et al. (2015)]** – Used for Tables, Cupboards and Benchtop

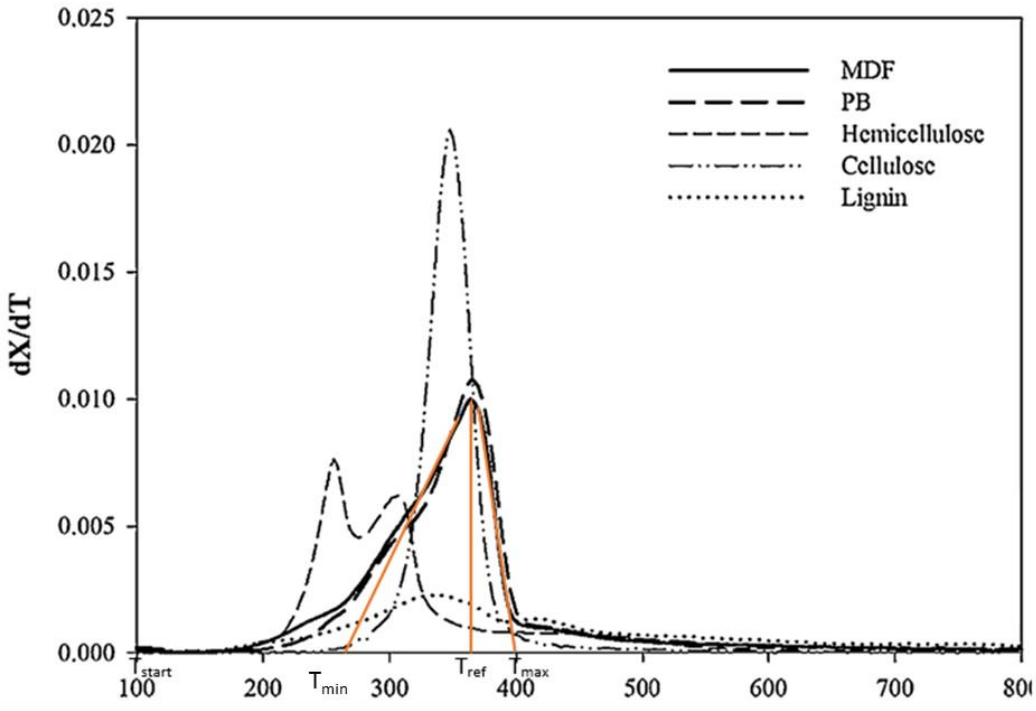

Reference temperature (T_{ref}) = 365°C

Pyrolysis range = T_{max} - -T_{min}

= 400°C – 260°C = 140°C

Heat of reaction = Specific heat capacity x (T_{min} – T_{20})

= 1.5*(260-20) = 360 kJ/kg